UNIVERSITY OF ADELAIDE
20/6/02
LIBRARY

CHARACTERIZATION OF BOVINE INSULIN LIKE GROWTH FACTOR BINDING PROTEIN-2

STRUCTURE AND FUNCTION

By

Francine Ellen Carrick, B.Sc (Hons)

A Thesis submitted to Adelaide University, South Australia in fulfilment of the requirements for the degree of Doctor of Philosophy

Department of Molecular Biosciences
Adelaide University
Adelaide, South Australia.
December, 2001

ACKNOWLEDGEMENTS

I sincerely wish to thank my supervisor, Professor John Wallace, for the support, encouragement and opportunities he generously made available to me throughout my PhD. Thank you also to Dr Briony Forbes who has been there for me throughout my studies as a friend and mentor. Professor Ray Norton was instrumental for the NMR studies conducted in this thesis and I am enormously grateful for his assistance and advice throughout my time in his laboratory. I am also extremely grateful for the generosity and patience of Dr Mark Hinds in teaching me the wonders of NMR spectral analyses.

Throughout my PhD I collaborated with various people whom I sincerely acknowledge. The X-ray crystallography work was done in collaboration with Dr Peter Colman (Walter and Eliza Hall Institute, Parkville, Victoria, Australia) and Ms Patricia Pilling (CSIRO Division of Health Science and Nutrition, Parkville, Victoria, Australia) (both formerly of the Biomolecular Research Institute, Parkville, Victoria, Australia). Mr John Terlet and Dr Marilyn Henderson kindly provided access to the Centre for Electron Microscopy and Microstructure Analysis (CEMMSA) at Adelaide University, South Australia and advised me on the techniques of electron microscopy. I thank Mr Geoff Francis, Mr Adam Tacos and Mr Adam Charlton for access to and assistance with the fermentation suite at GroPep Ltd, Thebarton, South Australia. I am also indebted to Kerrie McNeil for her assistance with the purification of labelled IGF. Thank you also to Dr Grant Booker and Dr Terry Mulhern for their assistance in collecting NMR data in Adelaide.

I was supported throughout my PhD by an Australian Postgraduate Award and a Priority One Scholarship from the CRC for Tissue Growth and Repair. I was also the recipient of generous financial support for conference attendance from the Department of Biochemistry, Adelaide University, the Lorne Protein Conference, Mutual Community, the CRC for Tissue Growth and Repair and the Committee for the 5th International IGF Symposium in Brighton, UK. I was also fortunate enough to travel regularly to the NMR laboratories of the Biomolecular Research Institute

and Walter and Eliza Hall Institute in Parkville, Victoria, which was generously supported by Professor John Wallace and the CRC for Tissue Growth and Repair.

To my friends in the lab for making life colourful; Anne Chapman-Smith, Kerrie McNeil, Denise Miller, Steven Polyak, Sarawut (Yui) Jitrapakdee, Samantha Lien, Teerakul (Gap) Arpornsuwan, Jan Cook, Fiona Whelan, Adam Charlton, Emma Hosszu, and Graham Hobba, thank you. Warm thanks also to Melinda Lucic for her friendship and the many chats and advice she shared with me. To Jessica Roediger for being such a beautiful friend. And to Adam Denley, I never knew sharing a bay could be so much fun! I also sincerely acknowledge Kevin Barnham, Luke Miles, Danielle Smith and David Kaiser for their friendship during my visits to Melbourne.

Thank you to all the people in the department who helped make everything run smoothly, Janis Soltys, Janet Hobbs, Amanda Marshall, Sharon Davy, Jackie Brinkman, Serge Volgin, the ladies in CSU and to Brian Denton for indulging me in the workshop! Thank you also to Jonathan Churchill and Paul Moir for the exceptional job they do managing IT (and my computer problems!). I have made many wonderful friends in the department over the years and I sincerely thank you all.

I wish to thank my parents, Margaret and Brian, and my brothers Andrew, Daniel, Benjamin and Christopher, whose love and support I have always relied on. A special thank you to my Mum for ensuring I was always well nourished. I am sure the boys will be pleased their little sister is finally going to pay some taxes!

The journey throughout my PhD has been complemented by the evolution of a friendship with three very wonderful people whom I will always cherish. Michael Lees, Emma Barry and Tania Dell'Oso, whose generosity of spirit and inner and outer beauty are legendary. I will miss you all enormously!

This thesis is dedicated in loving memory of my Pop, Francis Joseph Neville, whose life inspires me.

ABBREVIATIONS

^{125}I-IGF	radio-iodinated IGF-I tracer
ALS	acid labile subunit
BCIG, X-gal	5-bromo-4-chloro-3-indolyl-β-D-galactopyranoside
BCIP	5-bromo-4-chloro-3-indolyl phosphate
bIGFBP-2	bovine IGFBP-2
β–ME	2-mercaptoethanol
BMRB	BioMagResBank
BSA	bovine serum albumin
Caco	cacodylic acid
cDNA	complementary deoxyribonucleaic acid
CIP	calf intestinal alkaline phosphatase
CPM	counts per minute
CRC	Co-operative Research Centre
CRINEPT	Cross-Correlated Relaxation-Enhanced Polarization Transfer
CSI	chemical shift index
DMEM	Dulbecco's Modified Eagle's Medium
DTT	dithiothreitol
E.coli	*Escherichia coli*
ECM	extracellular matrix
EDC	N-ethyl-N'-[9-dimethylamino)propyl]carbodiimide
EDTA	ethylenediaminetetraacetic acid
ES-MS	electrospray mass spectrometry
FCS	fetal calf serum
FPLC	fast performance liquid chromatography
GAG	glycosaminoglycans
GH	growth hormone
Hepes	4-(2-hydroxyethyl)-1-piperazine-ethanesulphonic acid
HSQC	Heteronuclear Single Quantum Coherence
IGFBP	Insulin-Like Growth Factor Binding Protein
IGF-I	Insulin-Like Growth Factor I

IGF-II	Insulin-Like Growth Factor II
IPTG	isopropyl-β–D-thiogalactopyranoside
ITSS	insulin-transferrin sodium selenite media supplement
JeffM	Jeffamine M-600
LB	Luria broth
MES	2-(N-morpholino)ethanesulfonic acid
NBT	nitroblue tetrazolium
NHS	N-hydroxysuccinimide
NMR	nuclear magnetic resonance
NOE	Nuclear Overhauser Effect
NOESY	Nuclear Overhauser Effect Spectroscopy
PAGE	polyacrylamide gel electrophoresis
PCR	polymerase chain reaction
PDB	Protein Data Bank
PEG	polyethyleneglycol
ppm	parts per million
rpHPLC	reverse phase high performance liquid chromatography
RU	resonance units
SDS	sodium dodecyl sulphate
TFA	trifluoroacetic acid
Tris	2-amino-2-hydroxymethylpropane-1,3-diol
TROSY	Transverse Relaxation Optimized Spectroscopy
UV	ultra-violet

ABSTRACT

Insulin-like growth factor binding proteins (IGFBPs) play an integral role in regulating insulin-like growth factor (IGF) activity as they can both potentiate and inhibit IGF action. When this study commenced, little secondary or tertiary structural data was known for the IGFBPs. Furthermore the mechanism by which IGFBPs interact with IGFs had not been elucidated. The objective of this thesis, therefore, was to increase our understanding of bovine IGFBP-2 (bIGFBP-2) structure and function relationships and to specifically identify and characterise the residues of IGFBP-2 that comprise the IGF binding site.

The initial research goal of this thesis was to define the IGF binding site(s) of bIGFBP-2 using discrete amino-terminal domains (amino acid residues 1-93, 1-104, 1-132 and 1-185) and carboxyl-terminal domains (amino acid residues 96-279, 136-279, 182-284) of bIGFBP-2. The contribution of each domain was investigated on biosensor surfaces involving real time kinetics by BIAcore analysis. Both halves of bIGFBP-2 bound IGF-I and IGF-II in BIAcore studies, albeit with different affinities ($^{1-132}$IGFBP-2: K_D=36.3 nM and 51.8 nM; $^{136-279}$IGFBP-2HIS: K_D=23.8 nM and 16.3 nM respectively). The amino-terminal half appears to contain components responsible for fast association. These results are consistent with a publication by Kalus *et al.*, (1998) that localized a major binding epitope of IGF to residues 40-92 of hIGFBP-5. In contrast, IGF binding by the carboxyl-terminal fragment results in a more stable complex as reflected by its K_D. Furthermore, des(1-3)IGF-I and des(1-6)IGF-II exhibited reduced binding affinity to $^{1-279}$IGFBP-2HIS, $^{1-132}$IGFBP-2 and $^{136-279}$IGFBP-2HIS biosensor surfaces compared with wildtype IGF. A charge reversal at positions 3 and 6 of IGF-I and IGF-II, respectively, affects binding interactions with the amino-terminal fragment and full-length bIGFBP-2 but not the carboxyl-terminal fragment.

The absence of a tertiary structure severely limits the investigation of IGF-IGFBP structure and function relationships. In this study, structure determination of bIGFBP-2 was investigated by X-ray crystallization, NMR spectroscopy and electron microscopy. Attempts to elucidate the structure of IGFBP-2 by NMR analysis were inhibited by size restraints, however amino- and carboxyl-terminal fragments may help to overcome these shortcomings. Crystals were obtained for bIGFBP-2, which continue to be cultivated to diffractable quality. Despite the potential for electron microscopy to provide invaluable insight into the overall conformation of IGFBP-2, NMR or X-ray crystallization studies will offer the greatest information for the structure of IGFBP-2 and the IGF·IGFBP complex.

NMR technology has been used successfully in this study to define one side of the intermolecular interface between ^{15}N- and ^{2}H/^{15}N-labelled IGF-I and IGF-II and unlabelled Trx$^{1-279}$IGFBP-2HIS. Amino acid residues Glu3, Glu9, Leu10, Phe16, Val17, Cys18, Gly19, Asp20, Arg21, Gly22, Phe23, Phe49, Ser51, Leu54, Glu58, Tyr60 and Cys61 of IGF-I were significantly perturbed upon binding of Trx$^{1-279}$IGFBP-2HIS either as a consequence of direct involvement in the binding interaction or due to conformational changes in the molecule. Amino acid residues that were not perturbed in the complex were Leu5-Gly7, Asp12, Leu14-Gln15, Phe25-Lys27, Thr29-Ala38, Gln40-Ile43, Glu46-Cys48, Leu57, Leu64-Lys65, Ala67-Lys68 and Ala70. Furthermore, specific residues of IGF-I were perturbed upon binding of Trx$^{136-279}$IGFBP-2HIS (viz: Gly19, Asp20, Gly22, Phe 23, Tyr24, Phe49 and Leu54), which may constitute the growth factor's binding interface for the high-affinity carboxyl-terminal domain of IGFBP-2.

In conclusion, this thesis has contributed to defining residues of both IGF and IGFBP-2 involved in their high affinity interaction. This study has provided a valuable insight into the binding site for IGFBP-2 that may eventually result in the design and production of IGFBP analogues for therapeutic applications.

STATEMENT OF ORIGINALITY

This thesis contains no material that has been accepted for the award of any other degree or diploma in any University. To the best of my knowledge and belief it contains no material that has previously been published by any other person except where due reference is made. The author consents to this thesis being made available for photocopy and loan.

Francine Ellen Carrick

TABLE OF CONTENTS

ACKNOWLEDGEMENTS i
ABBREVIATIONS iii
ABSTRACT v
STATEMENT OF ORIGINALITY vii
TABLE OF CONTENTS viii
LIST OF FIGURES xvi
LIST OF TABLES xxi
LIST OF PUBLICATIONS xxii

CHAPTER 1
INTRODUCTION AND LITERATURE REVIEW 1

1.1 AN INTRODUCTION TO THE IGF SYSTEM 2
1.2 IGF STRUCTURE 6
1.3 IGFBP STRUCTURE 12
1.3.1 IGFBP Primary Structure *12*
1.3.2 The Disulfide Bonds of IGFBPs Maintain Structural Integrity *14*
1.3.3 IGFBP Secondary and Tertiary Structure *16*
1.4 IGF RESIDUES INVOLVED IN IGFBP BINDING 20
1.4.1 Summary of the IGFBP binding site on IGF *24*
1.5 IGFBP RESIDUES INVOLVED IN IGF BINDING 24
1.5.1 IGF binding by residues in the amino-terminal region *26*
1.5.2 IGF binding by residues in the carboxyl-terminal region *29*
1.5.3 IGF binding by residues in the central region *32*
1.5.4 Summary of the IGF binding site on IGFBPs *32*
1.6 FUNCTIONAL CONSEQUENCES OF THE IGF-IGFBP INTERACTION 34
1.6.1 IGF-dependent actions of IGFBPs *34*
1.6.2 IGF-independent actions of IGFBPs *35*
1.6.3 Functional Consequences of Loss of IGFBP *36*
1.7 MODIFICATIONS OF IGFBPS THAT INFLUENCE IGF BINDING 37
1.7.1 Phosphorylation of IGFBPs *37*
1.7.2 Glycosylation of IGFBPs *38*
1.7.3 Proteolysis of IGFBPs *39*
1.7.4 Cell association by IGFBPs *41*
1.8 AIMS AND EXPERIMENTAL STRATEGY 43

CHAPTER 2
GENERATION OF VECTORS FOR THE EXPRESSION OF TRUNCATED bIGFBP-2 FRAGMENTS **44**

2.1 INTRODUCTION 45

2.2 MATERIALS 50

2.2.1 Bacterial Culture Media and Solutions *50*

2.2.2 Bacterial Growth Media and Buffers *50*

2.2.3 Bacterial Strains *50*

2.2.4 Materials for Molecular Biology *51*

2.2.5 Solutions for DNA Procedures *51*

2.2.6 Kits for Molecular Biology *52*

2.2.7 Vectors and Oligonucleotides *52*

2.2.7.1 Vectors 53

2.2.7.2 Oligonucleotides: 53

2.3 METHODS 58

2.3.1 Mini Preparation of Plasmid DNA (Small-Scale) *58*

2.3.2 Midi Preparation of Plasmid DNA (Large-Scale) *59*

2.3.3 Agarose Gel Electrophoresis of DNA Samples *59*

2.3.4 Amplification of DNA by Polymerase Chain Reaction (PCR) *60*

2.3.5 Restriction Endonuclease Digestion of DNA *60*

2.3.6 QuikChange Site Directed Mutagenesis of Plasmid DNA *61*

2.3.7 Muta-Gene Phagemid In Vitro Mutagenesis *61*

2.3.7.1 Synthesis of Uracil-Containing Single Stranded DNA 62

2.3.7.2 Phosphorylation of the Mutagenic Oligonucleotides 62

2.3.7.3 In Vitro Mutagenesis 63

2.3.8 Isolation and Purification of DNA from Agarose Gels *63*

2.3.9 DNA Ligation *64*

2.3.10 Preparation of Competent Cells *64*

2.3.11 Bacterial Transformation *65*

2.3.12 ^{T7}DNA Squencing *65*

2.3.13 Dye Terminator DNA Sequencing *66*

2.3.14 fmol DNA Cycle Sequencing *66*

2.4 RESULTS AND DISCUSSION 67

2.4.1 Strategy for Expression Vector Generation *67*

2.4.2 Vectors for Mammalian Expression *68*
2.4.2.1 N-Terminal Expression Constructs *68*
2.4.2.2 C-Terminal Expression Constructs 74
2.4.2.3 Introduction of the Apa I Restriction Site by Site-Directed Mutagenesis 74
2.4.2.4 Cloning of C-Terminal Expression Constructs 75
2.4.3 Vectors for E.coli expression *81*
2.4.3.1 $^{1\text{-}279}$IGFBP-2HIS Expression Constructs 81
2.4.3.2 N-Terminal Expression Constructs 83
2.4.3.3 C-Terminal Expression Constructs 83
2.4.4 Confirmation of the Expression Systems Constructed *83*
2.5 SUMMARY 87

CHAPTER 3
EXPRESSION, PURIFICATION AND CHARACTERISATION OF RECOMBINANT IGFBP-2 TRUNCATED PROTEINS **89**

3.1 INTRODUCTION 90
3.2 MATERIALS 91
3.2.1 Tissue Culture Materials *91*
3.2.2 Tissue Culture Media and Buffers *91*
3.2.3 E. coli Protein Expression Media and Buffers *92*
3.2.4 Materials for Protein Detection and Purification *92*
3.2.4.1 Protein Electrophoresis, Transfer and Ligand Blot Buffers 94
3.2.4.2 Chromatography Buffers 94
3.2.4.3 HPLC Buffers 95
3.2.4.4 Nickel Chromatography Buffers 95
3.2.4.5 Charcoal Binding Assay Buffers 96
3.2.5 Antibodies and Protein Standards *96*
3.3 METHODS 96
3.3.1 Expression of bIGFBP-2 and bIGFBP-2 Truncations from Mammalian COS-1 Cells *96*
3.3.1.1 FPLC Purification of DNA for Mammalian Cell Transfections 96
3.3.1.2 Transfection of COS-1 Cells 97
3.3.1.3 Collection of Cell Lysates 98
3.3.2 Expression of bIGFBP-2 and Truncations from E. coli BL21 Cells *98*

3.3.3 IGF-Affinity Chromatography *99*
3.3.4 Ni-Affinity Chromatography *100*
3.3.5 Enterokinase Cleavage *101*
3.3.6 General Methods for Protein Expression and Detection *101*
3.3.6.1 SDS Polyacrylamide Gel Electrophoresis 101
3.3.6.2 Coomassie Blue Staining of SDS Polyacrylamide Gels 102
3.3.6.3 Immunoblotting of Nitrocellulose Filters 102
3.3.6.4 Western Ligand Blots 103
3.3.6.5 Mass Spectroscopy and N-terminal Sequencing 104
3.3.6.6 Solution binding assays 104
3.3.6.7 Biosensor Analyses 105
3.4 RESULTS 105
3.4.1 Protein Expression *105*
3.4.1.1 Expression of $^{1-132}$IGFBP-2, $^{1-185}$IGFBP-2, $^{96-284}$IGFBP-2, $^{96-279}$IGFBP-2HIS and $^{137-279}$IGFBP-2HIS from Mammalian COS-1 Cells 105
3.4.1.2 Expression of $^{1-93}$IGFBP-2, $^{1-104}$IGFBP-2 and $^{182-284}$IGFBP-2 From Mammalian COS-1 Cells 106
3.4.1.3 Expression of Trx$^{1-279}$IGFBP-2HIS, Trx$^{1-132}$IGFBP-2, Trx$^{1-185}$IGFBP-2 and Trx$^{136-279}$IGFBP-2HIS from *E. coli* Cells 109
3.4.2 Purification of Protein *112*
3.4.2.1 IGF-Affinity Chormatography 112
3.4.2.2 Ni-Affinity Chromatography 115
3.4.2.3 Enterokinase Digestion of Thioredoxin IGFBPs 118
3.4.3 Preliminary Binding Assays and Protein Integrity *127*
3.4.3.1 Mass Spectroscopy and N-Terminal Sequencing 127
3.4.3.2 Solution Binding Assays 127
3.4.3.3 Comparison of the Binding Kinetics of bIGFBP-2 and $^{1-279}$IGFBP-2HIS with IGF-I and IGF-II 129
3.4.3.4 Comparison of Mammalian and *E. coli* Expressed IGFBPs 130
3.4.3.5 Integrity of the IGFBP-2 Truncations 133
3.5 DISCUSSION 135
3.5.1 Expression of $^{1-93}$IGFBP-2, $^{1-104}$IGFBP-2 and $^{182-284}$IGFBP-2 ..... *136*
3.5.2 Expression of $^{1-132}$IGFBP-2, $^{1-185}$IGFBP-2, $^{96-279}$IGFBP-2HIS, $^{96-284}$IGFBP-2, $^{136-279}$IGFBP-2HIS, $^{137-279}$IGFBP-2HIS and $^{1-279}$IGFBP-2HIS *137*

3.5.3 How do the purification protocols compare? *140*

3.5.4 How do mammalian and E. coli expressed proteins compare? *141*

3.5.5 Concluding Remarks *141*

CHAPTER 4
BIACORE ANALYSIS OF AMINO- AND CARBOXYL-TERMINAL bIGFBP-2 FRAGMENTS **143**

4.1 INTRODUCTION 144

4.2 MATERIALS 148

4.2.1 Solutions for BIAcore *148*

4.3 METHODS 148

4.3.1 Biosensor Surface Preparation *148*

4.3.2 Acquisition of Kinetic Binding Data *149*

4.3.3 Evaluation of Kinetic Binding Data *150*

4.4 RESULTS 153

4.4.1 Do The Amino- and Carboxyl-Terminal Domain Fragments Bind IGF-I and IGF-II? *153*

4.4.2 Can the Amino- and Carboxyl-Terminal Domain Fragments Reconstitute The High Affinity IGF:IGFBP Interaction? *158*

4.4.3 How Are The IGF-IGFBP Molecules Orientated In The High Affinity Complex? ... *159*

4.5 DISCUSSION 163

CHAPTER 5
PREPARATION OF PROTEIN FOR STRUCTURAL STUDIES **169**

5.1 INTRODUCTION 170

5.2 MATERIALS 172

5.2.1 Materials for Protein Expression, Purification and Characterization *172*

5.2.2 Bacterial Strains *172*

5.2.3 Vectors for Protein Expression *172*

5.2.4 Fermentation Medium *174*

5.2.5 Buffers for Protein Purification *174*

5.2.6 Materials for Gel Filtration *175*

5.2.7 Gel Filtration Buffers *175*

5.2.8 McIlvaine's Citric Acid Phosphate Buffer *175*

5.3 METHODS 176

5.3.1 Fermentation of IGF-I and IGF-II *176*
5.3.2 Purification of IGF-I and IGF-II Ligands *177*
5.3.2.1 Purification of Labelled IGF-I 178
5.3.2.2 Purification of Labelled IGF-II 179
5.3.3 Glucose Trials for ^{13}C IGF-I Fermentations *180*
5.3.4 Large Scale Expression of Trx^{1-279}IGFBP-2HIS, Trx^{1-132}IGFBP-2 and $Trx^{136-279}$IGFBP-2HIS *181*
5.3.5 BIAcore analysis *182*
5.3.6 Gel Filtration *182*
5.4 RESULTS AND DISCUSSION 183
5.4.1 IGF Fermentations and Purification *183*
5.4.2 Fermentation of $^{13}C/^{15}N/^{2}H$ IGF-I *187*
5.4.3 Large-Scale Expression of Trx^{1-279}IGFBP-2HIS, Trx^{1-132}IGFBP-2 and $Trx^{136-279}$IGFBP-2HIS *190*
5.4.4 Comparison of the IGF Binding Activity of Trx^{1-279}IGFBP-2HIS and bIGFBP-2 by BIAcore Analysis *190*
5.4.5 Investigation of the Effect of pH on the IGF·IGFBP Interaction by BIAcore analysis *193*
5.4.6 Gel Filtration Experiments *196*
5.5 SUMMARY 198

CHAPTER 6
IGFBP-2 STRUCTURE DETERMINATION: X-RAY CRYSTALLOGRAPHY, NMR AND ATOMIC FORCE MICROSCOPY **200**

6.1 INTRODUCTION 201
6.2 X-RAY CRYSTALLOGRAPHY STUDIES 203
6.2.1 MATERIALS *204*
6.2.2 METHODS *204*
6.2.2.1 Hanging Drop Method of Crystallization 204
6.2.3 RESULTS AND DISCUSSION *206*
6.3 NMR SPECTROSCOPY ANALYSIS 212
6.3.1 MATERIALS *213*
6.3.1.1 NMR BUFFERS 213
6.3.2 METHODS *213*
6.3.2.1 NMR Spectroscopy 213

6.3.3 RESULTS AND DISCUSSION *214*

6.4 ELECTRON MICROSCOPY ANALYSIS 219

6.4.1 MATERIALS *220*

6.4.2 METHODS *220*

6.4.2.1 Sample Preparation for Atomic Force Microscopy (AFM) 220

6.4.3 RESULTS AND DISCUSSION *220*

6.5 CONCLUDING REMARKS 221

CHAPTER 7
IDENTIFICATION OF SPECIFIC IGF-I AND IGF-II RESIDUES INVOLVED IN BINDING BIGFBP-2 BY HETERONUCLEAR NMR SPECTROSCOPY **222**

7.1 INTRODUCTION 223

7.1.1 IGFBP binding site on IGFs *223*

7.1.2 NMR as a tool for defining binding interfaces *226*

7.1.3 NMR Spectroscopy *227*

7.2 MATERIALS 230

7.2.1 NMR Buffers *230*

7.3 METHODS 230

7.3.1 Sample Preparation *230*

7.3.2 NMR spectroscopy *231*

7.3.3 Chemical Shift Assignments *231*

7.4 RESULTS 232

7.4.1 Comparison of deuterated and protonated samples *233*

7.4.2 Comparison of HSQC vs TROSY spectra *233*

7.4.3 Identification ofIGF-I Chemical shift Perturbation Upon Interaction With Trx^{1-279}IGFBP-2HIS *235*

7.4.3.1 IGF-I Chemical Shift Assignments 235

7.4.3.2 Chemical Shift Assignments of IGF-I Complexed to Trx^{1-279}IGFBP-2HIS 250

7.4.3.3 Chemical shift perturbations upon binding of Trx^{1-132}IGFBP-2 or $Trx^{136-279}$IGFBP-2HIS 258

7.4.3.4 Tertiary Model of IGF-I Residues Perturbed Upon Binding of Trx^{1-279}IGFBP-2HIS 261

7.4.4 Identification ofIGF-II Chemical shift Perturbations Upon InteractionWith Trx^{1-279}IGFBP-2HIS *263*

7.4.4.1 IGF-II Chemical Shift Assignments 263
7.4.4.2 Spectral Analysis of IGF-II Complexed to IGFBP-2 268
7.5 DISCUSSION 273
7.5.1 Implications for IGFBP binding *277*
7.5.2 Implications of IGF receptor binding *278*
7.6 CONCLUDING REMARKS 280

CHAPTER 8
FINAL DISCUSSION 281

8.1 SUMMARY OF FINDINGS 282
8.2 FUTURE DIRECTIONS 285
8.2.1 Structure determination *285*
8.2.2 Design of IGF and IGFBP mimics *288*
8.3 CONCLUSION 289

REFERENCES 290

LIST OF FIGURES

CHAPTER 1

1.1 Schematic representation of the IGF system 3

1.2 Schematic representation of the inhibition and potentiation of IGF by IGFBPs 5

1.3 Comparative sequence data of the insulin-like growth factors 7

1.4 Schematic representation of the structural homology between insulin, IGF-I and IGF-II 9

1.5 Crystal structure of the interface of IGF-I complexed to mini-IGFBP-5 complex 11

1.6 Sequence alignments of the six IGFBPs 13

1.7 Alignment of IGFBP-2 protein sequences 15

1.8 Schematic representation of the disulfide bonds of IGFBPs 17

1.9 NMR structure of mini-IGFBP-5 19

1.10 Surface representation of IGF-I with residues involved in binding IGFBPs highlighted 25

1.11a IGF binding studies targeting the N-terminal region of IGFBPs 27

1.11b IGF binding studies targeting the C-terminal region of IGFBPs 30

1.11c IGF binding studies targeting the central region of IGFBPs 33

1.12 Sites of post-translational modification of IGFBPs 38

CHAPTER 2

2.1 Amino acid sequence and schematic representation of wildtype bIGFBP-2 and the truncated constructs 46

2.2 pGF8 expression vector 54

2.3 pET32a (+) expression vector 55

2.4 cDNA encoding the bigfbp-2 insert in the pxmt2 expression vector 57

2.5 Cloning of cDNA encoding the N-terminal fragments into pGF8 69

2.6 Polymerase chain reaction (PCR) of cDNA encoding bIGFBP-2 70

2.7 Expression vector pGF8*Apa*I 76

2.8 Cloning of cDNA encoding the C-terminal fragments into pGF8 77

2.9 Cloning of cDNA encoding the C-terminal fragment (96-284) into pGF8 79

2.10 Expression vector pGF8HIS 80

2.11 Cloning of cDNA encoding Wildtype and N-terminal fragments into pET32a (+) 82

2.12 Cloning of cDNA encoding the C-terminal fragments into pET32a (+) 84

2.13 DNA sequencing of the pGF8(1-185) expression vector 85

2.14 Dye terminator DNA sequencing to confirm incorporation of the hexahistidine-tag 86

CHAPTER 3

3.1 Antibody and ^{125}I-IGF-II Western blot analysis of recombinant bIGFBP-2 and truncated IGFBP-2s 107

3.2 Coomassie stained gel of the *E.coli* expressed proteinsTrx$^{1-279}$IGFBP-2HIS, Trx$^{1-132}$IGFBP-2, Trx$^{1-185}$IGFBP-2 and Trx$^{136-279}$IGFBP-2HIS 111

3.3 IGF-affinity and cation exchange chromatograms of the purification of $^{1-185}$IGFBP-2 from COS-1 cell conditioned medium 113

3.4 IGF-affinity chromatogram of the purification of $^{96-284}$IGFBP-2 from COS-1 cell conditioned medium 114

3.5 Purification of $^{96-279}$IGFBP-2HIS by Ni-affinity chromatography and rpHPLC 117

3.6 Purification of COS-1 derived bIGFBP-2 and $^{1-279}$IGFBP-2HIS by rpHPLC 119

3.7 Analysis of the IGF-affinity purification of Trx$^{1-279}$IGFBP-2HIS 120

3.8 Optimisation of the Enterokinase cleavage of Trx$^{1-279}$IGFBP-2HIS 122

3.9 Reverse phase HPLC of the Enterokinase cleavage of TrxIGFBP-2s 123

3.10 SDS PAGE analysis of bIGFBP-2HIS and truncated mutants 124

3.11 Purification of $^{1-279}$IGFBP-2HIS 125

3.12 Reverse phase HPLC purification of the Enterokinase digested TrxIGFBP-2 truncations 126

3.13 Analysis of the $^{1-185}$IGFBP-2 binding properties by solution binding assays 128

3.14 Comparison of the IGF Binding Properties of bIGFBP-2 and $^{1-279}$IGFBP-2HIS 131

3.15 Comparison of the IGF binding properties of *E.coli* and mammalian derived proteins 132

3.16 Tryptophan fluorescence spectroscopy of bIGFBP-2 and $^{136-279}$IGFBP-2HIS 134

CHAPTER 4

4.1 BIAcore analysis of the interaction between IGF and IGFBP-2 147

4.2 Comparison of the goodness of fit for the 1:1 Langmuir and Two State (Conformational Change) Reaction binding models 152

4.3 BIAcore analysis of $^{1-279}$IGFBP-2HIS and truncated fragments over IGF biosensor surfaces 154

4.4 BIAcore analysis of IGF-I and IGF-II ligands over IGFBP biosensor surfaces 155

4.5 BIAcore analysis of preincubated $^{1-132}$IGFBP-2 and $^{136-279}$IGFBP-2HIS analogues over IGF biosensor surfaces 160

4.6 BIAcore analysis of the sequential injection of IGF and bIGFBP-2 mutants across $^{1-279}$IGFBP-2HIS, $^{1-132}$IGFBP-2 and $^{136-279}$IGFBP-2HIS biosensor surfaces 161

4.7 BIAcore analysis of IGF mutant analogues across bIGFBP-2 biosensor surfaces 162

4.8 Model of the orientation of the IGF-IGFBP-2 interaction 168

CHAPTER 5

5.1 IGF expression vectors and fusion proteins 174

5.2 Coomassie stained tricine gel of labelled IGF ferments 185

5.3 HPLC chromatograms of the purified labelled IGF-I and IGF-II ligands 186

5.4 IGF-I expressions with various glucose concentrations 189

5.5 BIAcore comparison of bIGFBP-2 and TrxIGFBP-2HIS over IGF biosensor surfaces 191

5.6 BIAcore analysis of Trx^{1-132}IGFBP-2, Trx^{1-185}IGFBP-2 and $Trx^{136-279}$IGFBP-2HIS over IGF biosensor surfaces 192

5.7 BIAcore analysis of the effect of pH on the IGF-IGFBP interaction 195

5.8 Gel filtration of bIGFBP-2 and Trx^{1-279}IGFBP-2HIS 197

CHAPTER 6

6.1 Crystals of bIGFBP-2 209

6.2 ^{1}H NMR spectrum of Trx^{1-279}IGFBP-2HIS 215

6.3 ^{1}H NMR spectrum of Trx^{1-279}IGFBP-2HIS 216

6.4 Sequence alignment of amino-terminal binding fragments of IGFBP-2, IGFBP-5 and IGFBP-6 218

CHAPTER 7

7.1 Surface representation of IGF-I with residues involved in binding IGFBPs highlighted 224

7.2 HSQC and TROSY spectral quality improved with deuterated ^{15}N IGF-I 234

7.3 TROSY spectrum of ^{2}H/^{15}N IGF-I with chemical shift assignments 236

7.4 Differences in published proton chemical shift assignments for IGF-I 238

7.5 Differences in published proton chemical shift assignments for IGF-I 239

7.6 Correlation of nuclei in 3D HNCA experiments 241

7.7 Strip plot of ^{2}H/^{15}N/^{13}C IGF-I 3D HNCA experiment 242

7.8 $^{13}C_{\alpha}$ chemical shift index plot of IGF-I chemical shift assignments 246

7.9 Comparison of chemical shift assignments of IGF-I with values in the literature 247

7.10 Temperature and pH titration of ^{15}N IGF-I 249

7.11 TROSY Spectra of Free IGF-I and IGF-I complexed to Trx^{1-279}IGFBP-2HIS 251

7.12 pH titration of ^{2}H/^{15}N IGF-I complexed to Trx^{1-279}IGFBP-2HIS 252

7.13 TROSY of free ligand overlayed with HNCA of IGF-I complexed with Trx^{1-279}IGFBP-2HIS 253

7.14 Strip plot of $^{2}H/^{15}N/^{13}C$ IGF-I bound to Trx1-279IGFBP-2HIS 3D HNCA experiment 254

7.15 Amino acid residues that were perturbed insignificantly upon binding of Trx^{1-279}IGFBP-2HIS 256

7.16 Identification of significantly perturbed IGF-I residues 257

7.17 Comparison of Free $^{2}H/^{15}N$ IGF-I and Trx^{1-132}IGFBP-2 bound $^{2}H/^{15}N$ IGF-I 259

7.18 Chemical Shift Perturbations of IGF-I upon complex formation with $Trx^{136-279}$IGFBP-2HIS 260

7.19 Surface representation of IGF-I with significantly perturbed residues highlighted 262

7.20 Labelled TROSY spectrum of $^{2}H/^{15}N$ IGF-II 264

7.21 Comparison of IGF-II chemical shift assignments with values in the literature 265

7.22 Temperature and pH titration of ^{15}N IGF-II 266

7.23 TROSY Spectra of Free IGF-II ligand and IGF-II complexed to Trx^{1-279}IGFBP2-HIS 269

7.24 Comparison of the free and Trx^{1-279}IGFBP-2HIS bound spectra of IGF-I and IGF-II 270

7.25 Comparison of free $^{2}H/^{15}N$ IGF-II and Trx^{1-132}IGFBP-2 bound $^{2}H/^{15}N$ IGF-II 272

LIST OF TABLES

2.1 Vectors constructed for the expression of full-length and truncated IGFBP-2 49

2.2 GC content of the PCR fragments 71

2.3 GC content and dissociation temperatures (tm) of the oligonucleotide primers 72

3.1 Protein quantities purified by IGF-affinity and Ni-affinity chromatography protocols 110

3.2 Comparison of the kinetics of the interaction between bIGFBP-2 and $^{1-279}$IGFBP-2HIS with IGF-I and IGF-II using the 1:1 Langmuir binding model 130

4.1 Kinetic analysis of bIGFBP-2 mutants interactions with IGF biosensor surfaces using the 1:1 Langmuir binding model 156

4.2 Kinetic analysis of IGF-II analogues across wildtype and mutant bIGFBP-2 biosensor surfaces using the Two State (conformational change) model 163

5.1 Optical density of cell cultures grown in deuterium oxide 187

5.2 Summary of the IGF-I and IGF-II fermentations and purification 188

5.3 Comparison of the kinetics of the interaction between bIGFBP-2 and Trx$^{1-279}$IGFBP-2HIS with IGF-I and IGF-II using the 1:1 Langmuir binding model 193

6.1 Screens for the analysis of optimal conditions for crystal growth 205

7.1 Chemical shift assignments for IGF-I 243

7.2 Chemical shift assignments for IGF-II 267

LIST OF PUBLICATIONS

This thesis is based on the following publications:

Carrick, F.E., Forbes, B.E. and Wallace, J.C.

BIAcore analysis of Bovine Insulin Like Growth Factor Binding Protein-2 (bIGFBP-2) Identifies Major IGF Binding Site Determinants in Both the Amino- and Carboxy-Terminal Domains

J Biol Chem. 276(29):27120-27128

Carrick, F.E., Forbes, B.E. and Wallace, J.C.

Insulin-like Growth Factor Binding Proteins – Structure and Function Relationships

Manuscript in preparation.

Carrick, F.E., McNeil, K., Forbes, B.E., Wallace, J.C. and Norton, R.S.

Identification of specific IGF-I and IGF-II residues involved in binding bIGFBP-2 by heteronuclear NMR

Manuscript in preparation.

And conference proceedings:

Carrick, F.E., Forbes, B.E. and Wallace, J.C. (1998). Characterisation of the IGF Binding Site on Bovine IGFBP-2. Proceedings of the 23rd Annual Lorne Protein Conference. (Lorne, Victoria, Audtralia). Poster.

Carrick, F.E., Forbes, B.E. and Wallace, J.C. (1998). Localisation of the IGF binding site of Bovine IGFBP-2 by BIAcore analysis. Proceedings of the 42nd Annual ASBMB - 38th Annual ASPP and 20th Annual NZSPP Conferences. (Adelaide, South Australia). Poster.*

Carrick, F.E., Hobba, G.D., Forbes, B.E. and Wallace, J.C. (1999). Investigating the IGF Binding Site on bIGFBP-2 by Truncation Studies and BIAcore Analysis. Proceedings of the 24th Annual Lorne Protein Conference. (Lorne, Victoria, Australia). Poster.

Carrick, F.E., Hobba, G.D., Forbes, B.E. and Wallace, J.C. (1999). Defining the Ligand Binding Site on Bovine IGFBP-2 by BIAcore Analysis. Proceedings of the 2nd Annual BIAcore Symposium. (Lorne, Victoria, Australia). Oral.

Carrick, F.E., Forbes, B.E. and Wallace, J.C. (1999). Recreating a High Affinity Insulin-Like Growth Factor Binding Protein Using Discrete N- and C-Terminal Domain Fragments. Proceedings of the 5th International Symposium on Insulin-Like Growth Factors. (Brighton, United Kingdom). Oral.*

Carrick, F.E., McNeil, K.A., Forbes, B.E., Wallace J.C and Norton R.S. (2000). NMRAnalysis of the Structure and Function Relationships Between bIGFBP-2 and IGF. *Abstract in:* "Growth Hormone and IGF Research: 10:4" 4th International IGFBP Symposium (Terrigal NSW, Australia).

Forbes, B.E., Parkinson, E.J., Carrick, F.E., Lucic M. R. and Wallace, J.C. (2000). Understanding IGFBP-2 Structural Change upon IGF Binding. Abstract in: *Growth Hormone and IGF Research.* **10**(4). 4th International IGFBP Symposium (Terrigal NSW, Australia).

Wallace, J.C., Lucic, M.R., Carrick, F. E. and Forbes, B. E. (2000). IGFBP Evolution and Structure. Abstract in: *Growth Hormone and IGF Research.* **10**(4). 4th International IGFBP Symposium (Terrigal NSW, Australia).

Carrick, F.E., Forbes, B.E., Lucic, M.R. and Wallace, J.C. (2001). Interactions of Insulin-like Growth Factors With Their Binding Proteins. Proceedings of the 4th Australian Peptide Conference – From Discovery to Therapeutics (Lindeman Island, Queensland, Australia).

* Awarded an Australian Society for Biochemists and Molecular Biologists (ASBMB) Student Poster Prize

CHAPTER 1

INTRODUCTION AND LITERATURE REVIEW

1.1 AN INTRODUCTION TO THE IGF SYSTEM

The insulin-like growth factor (IGF) growth regulatory system is a complex network involving the IGFs, IGF receptors, IGF binding proteins (IGFBPs) and an extended array of molecules and enzymes that act to influence the activities of the IGF system components (Figure 1.1). The actions of IGFs are mediated by interaction with the insulin and IGF receptors, but are also modulated by interaction with a second class of protein, the insulin-like growth factor binding proteins (IGFBPs). Indeed, the post-translational control of IGF activity by IGFBPs appears to be a critical component of this system and thus will be the focus of this review.

IGFs (IGF-I and IGF-II) are the major growth factors present in serum (reviewed by Humbel, 1990) and are produced by most tissues of the body. The liver, and to a lesser extent bone, are the major sources of circulating IGF. IGFs have diverse biological actions including decreasing serum glucose levels and stimulation of cellular proliferation, resulting from their increasing DNA, protein and carbohydrate synthesis (Rechler, 1993; Muller *et al.*, 1994). Furthermore, IGFs exhibit potent anti-apoptotic effects that have been shown to stimulate terminal differentiation in some cell types. IGFs are developmentally regulated and are essential for prenatal growth (DeChiara *et al.*, 1990; Carr *et al.*, 1995). Disruption of the gene for either IGF-I or IGF-II causes growth retardation and in some cases lethality (DeChiara *et al.*, 1990). Not only are IGFs endocrine hormones required for normal systemic growth and development, but localised growth regulation by IGFs also implies both autocrine and paracrine actions (D'Ercole *et al.*, 1984; Lund *et al.*, 1986; Ooi and Herington, 1988). It appears that IGFs synthesised locally are important for developmental states such as embryogenesis and also for the progression of disease states such as osteoporosis, osteoarthritis, atherosclerosis, diabetic nephropathy and retinopathy (Jones *et al.*, 1991; LeRoith *et al.*, 1995). High levels of IGF-I and IGF-II have also been linked to cancerous states (reviewed by Holly *et al.*, 1999; Yu and Rohan, 2000).

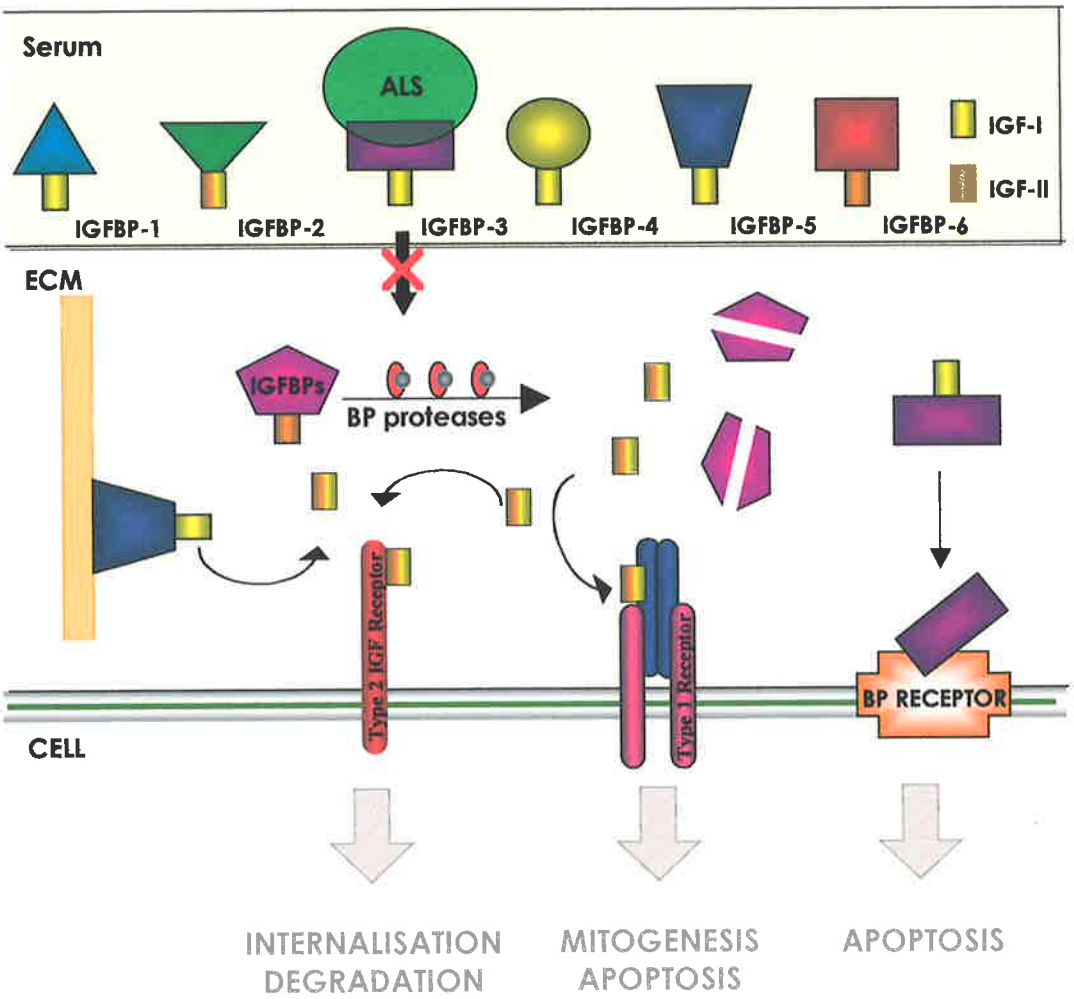

Figure 1.1 Schematic representation of the IGF system
IGFBPs are synthesised in the liver and other organs and secreted into the circulation where they form complexes with IGFBPs (1-6). Each IGFBP binds IGF-I and IGF-II although IGFBP-6 has a marked preference for IGF-II over IGF-I ligand. IGFBPs increase the IGF circulating half-life and up to 70 % of the IGF is found with IGFBP-3 and the acid labile subunit (ALS) in a ternary complex which can not cross the vascular wall. Binary complexes however cross the vascular wall and influence tissue distribution. Furthermore, IGFBPs regulate the availability of IGFs to interact with the Type 1 and Type 2 IGF receptors. Post-translational modifications including proteolysis, phosphorylation and associations with cell surfaces/ECM and cell surface receptors influence the IGFBP affinity for IGFs and hence IGF bioavailability. IGFBPs also exhibit IGF-independent actions and IGFBP specific receptors have been identified.

The biological roles of the IGFs on their target cells are mediated via specific cell surface receptors, the type-I IGF receptor and type-II IGF receptor (reviewed by Ward *et al.*, 2001; Rother and Accili, 2000). IGF-I and IGF-II bind to the type-I IGF receptor, the type-II IGF receptor and the insulin receptor (IR) with varying affinities. While the type-I receptor binds IGF-I, IGF-II and to a lesser extent insulin, the type-II IGF receptor primarily binds IGF-II. It binds IGF-I with an affinity 100-times lower than for IGF-II, and does not bind insulin at all (reviewed in Braulke, 1999). The type-I IGF receptor is a tyrosine kinase receptor (Nissley and Lopaczynski, 1991) through which the metabolic, mitogenic and anti-apoptotic effects of IGFs are exerted (reviewed by Baker *et al.*, 1993; Baserga *et al.*, 1997; Sepp-Lorenzino, 1998). The role of the type-II IGF receptor is less clearly understood. The type-II IGF receptor, also known as the mannose-6-phosphate receptor, appears to be involved in endosomal trafficking and hence the sequestration of IGF-II for removal and degradation (Sohar *et al.*, 1998). The type-II IGF receptor therefore appears to be a primary control of IGF-II bioavailability.

IGF bioavailability and activity are also modulated through binding high affinity IGFBPs (reviewed by Rajaram *et al.*, 1997; Hwa *et al.*, 1999; Baxter, 2000). As IGFBPs are more abundant than IGF receptors and exhibit higher affinity for IGF, all of the IGFs, whether in circulation or in the extracellular space, are associated with one of six IGFBPs (IGFBP-1 to -6). The ternary complex of IGFBP-3, IGF and the acid labile subunit (ALS) is the most abundant in circulation (reviewed by Rajaram *et al.*, 1997) (Figure 1.2). IGFBPs have diverse biological functions including transportation of IGF from the vasculature to specific tissues, storage of IGFs in an inert complex to increase circulating half-life and inhibit ligand clearance; tissue localisation and modulation of IGF interactions with the receptors. In fact, IGFBPs have been shown to both stimulate and inhibit IGF action (reviewed by Baxter, 2000). The IGF·IGFBP complex is a latent one that cannot activate the type-I receptor. However, this association is reversible and indeed, the IGFBPs can also potentiate IGF activity by co-localising IGFs to receptor-rich cell surfaces and extracellular matrix sites where IGFs are subsequently released (Rechler, 1993).

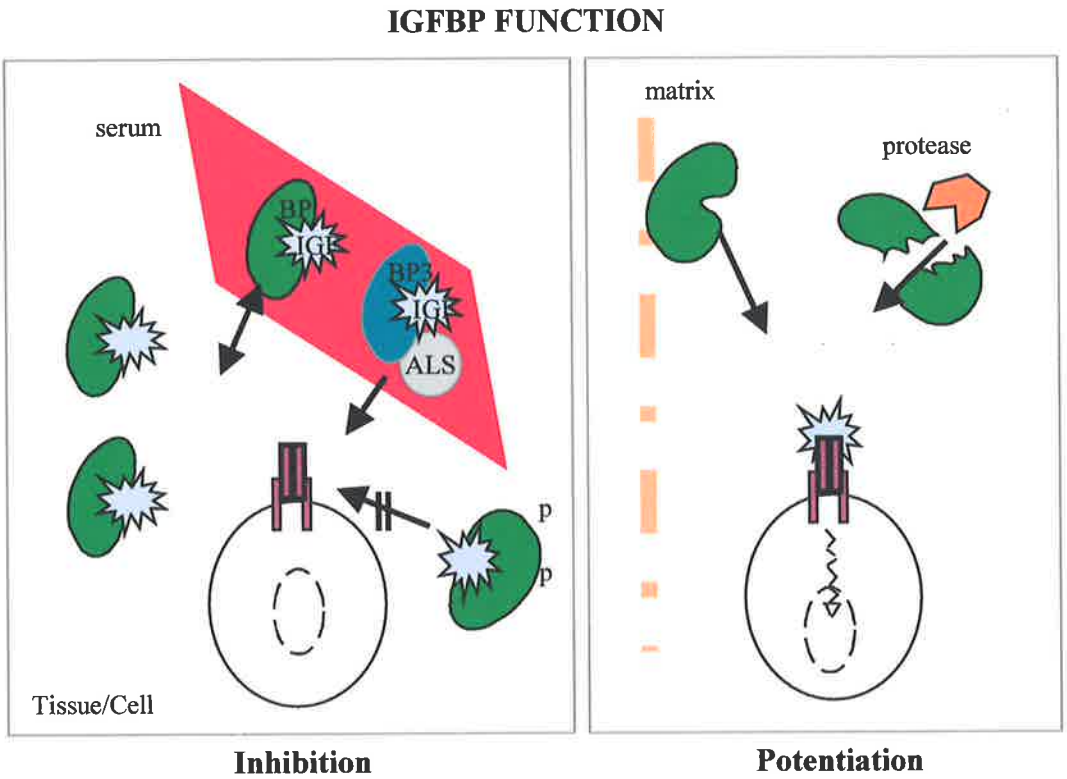

Figure 1.2 Schematic representation of the inhibition and potentiation of IGF by IGFBPs IGF ligands are held in a latent complex with IGFBPs such that they can no longer interact with the IGF receptors and elicit mitogenic and metabolic effects. Indeed, the ternary complex of IGFBP-3, the ALS and IGF cannot cross the vascular wall. Binary complexes however cross the vascular wall and influence tissue distribution and IGF bioactivity. IGFBPs however can also promote interactions between IGF and IGF receptors. Post-translational modifications including proteolysis, phosphorylation and associations with cell surfaces/ECM and cell surface receptors have been shown to decrease the affinity of IGFBPs for IGF thus increasing IGF bioavailability.

Although the IGF system components have been extensively investigated, our understanding of the integrated network of molecular mechanisms involved is limited. To date, there is limited tertiary structural information for protein components of the IGF network, in particular the IGFBPs. Furthermore, the regulation of IGFs by IGFBPs continues to be explored, yet a comprehensive model of the protein-protein interactions and modulatory consequences of such associations is insufficiently understood. Indeed, the recent discovery of IGF independent properties of the IGFBPs has not been exhaustively characterised nor understood. This is a review of our current understanding of the molecular structures and mechanisms of the IGF-IGFBP component of the IGF system.

1.2 IGF STRUCTURE

IGFs are related at both primary and tertiary structural levels to insulin, and appear to have been extensively conserved throughout vertebrate evolution, as highlighted by the recent cloning of IGF cDNA from the Atlantic Hagfish (Upton *et al.*, 1997) and from lamprey (Moriyama *et al.,* 2000)(Figures 1.3 and 1.4). IGF-I and IGF-II are single polypeptide hormones consisting of 70 and 67 amino acid residues respectively. The structures of IGFs reveal four domains designated B, C, A and D from the N-terminus (Rotwein, 1991). Amino acid residues Gly1 to Thr29, Gly30 to Thr41, Gly42 to Cys62 and Ala63 to Ala70 of IGF-I and Ala1 to Phe28, Ser29 to Arg40, Gly41 to Ala61 and Thr62 to Glu67 of IGF-II, correspond to domains B, C, A and D respectively. The primary structure conservation between IGF-I and IGF-II is striking (Rotwein, 1991). In fact, 70 % of residues of the B and A domains of human IGF-I and IGF-II are identical to each other and 50 % of the residues are identical to the corresponding residues of insulin (Rotwein, 1991). The C domain of IGFs is analogous to the C domain of mammalian proinsulin however IGFs have an additional D domain at their carboxyl-terminus that has no insulin counterpart (Torres *et al.*, 1995). The prepropeptides of IGFs contain an N-terminal signal sequence. Two alternative forms of a C-terminal E domain

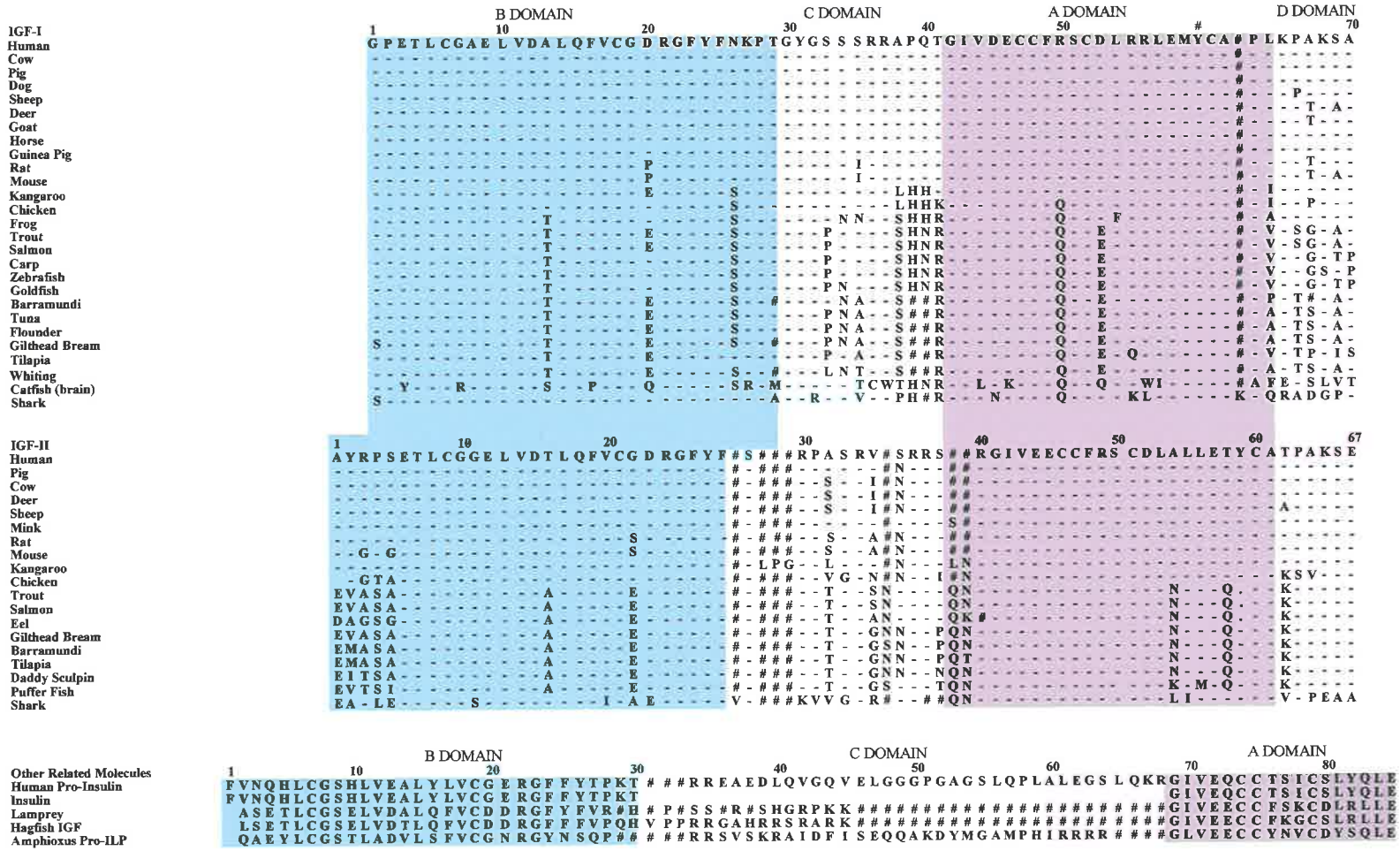

Figure 1.3 Comparative Sequence Data of the Insulin-like Growth Factors

Known amino acid sequences of different IGF-I and IGF-II species. Dashed lines represent identical sequences compared to human counterparts and # was used to frame shift peptides for maximal alignment between sequences. Complete amino acid sequences are given for IGF related molecules. (Adpated from a leaflet produced by GroPep Ltd., Thebarton, SA, Australia.)

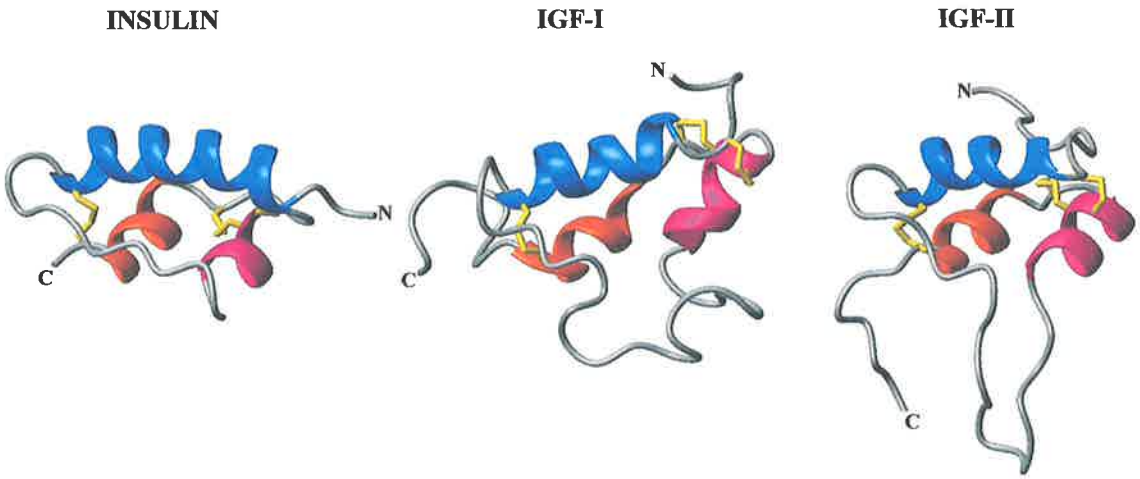

Figure 1.4 Schematic representation of the structural homology between insulin, IGF-I and IGF-II
Insulin (Bentley *et al.*, 1976), IGF-I (Sato *et al.*, 1992) and IGF-II (Torres *et al.*, 1995) are structurally similar (described in Section 1.2). The structures have been aligned along the first helix (blue) of the B-domain. The second (magneta) and third (orange) helices comprise the A-domain of the molecules. Insulin does not contain a C-domain and both IGF-I and IGF-II have an additional D-domain at their C-terminus. The three disulfide bonds are depicted in gold.

result from alternative splicing of the mRNA (Daughaday and Rotwein, 1989). Both are cleaved post translationally (de Pagter-Holthuizen *et al.*, 1986).

IGFs were originally classified according to their ability to exhibit similar mitogenic actions to that of insulin and indeed they share a high degree of sequence homology with pro-insulin (Rinderknecht and Humbel, 1978a; Rinderknecht and Humbel, 1978b; Blundell *et al.*, 1983). Hence it is not surprising that the first molecular models of IGF were based on the crystal structure of insulin (Blundell *et al.*, 1978; Blundell *et al.*, 1983). Since then, the structures of IGF-I (Cooke *et al.*, 1991; Sato *et al.*, 1993) and IGF-II (Terasawa *et al.*, 1994; Torres *et al.*, 1995) have been determined through nuclear magnetic resonance (NMR) studies and recently, a crystal structure of IGF-I complexed to an N-terminal fragment of IGFBP-5 has been reported (Żesławski *et al.*, 2001)(Figure 1.5). The general fold of the IGF-I molecule is preserved in the free and IGFBP-5-bound states, although the N-terminal residues appear to become fixed upon complex formation (Żesławski *et al.*, 2001). Both the NMR and crystal structures are in strong agreement with the predicted structure modelled on insulin.

The IGF molecules are extremely stable, forming compact globular structures with a hydrophobic core. The secondary structure is predominantly helical, stabilised by three disulfide bonds that are essential for the integrity of the molecule (Hober *et al.*, 1992; Milner *et al.*, 1995). The IGF secondary structure begins with the B-domain that comprises a short flexible stretch of residues preceding the first α-helix (B1) (IGF-I: Ala8-Cys18 and IGF-II: Gly11-Cys21), β-turn (IGF-I: Gly19-Gly22 and IGF-II: Gly22-Gly25) and extended loop of 4 amino acid residues (IGF-I: Phe23-Asn26 and IGF-II: Phe26-Phe28). The C-domain is a 13 amino acid region of high mobility, connecting the B and A domains. This region is not removed proteolytically after translation as it is from pro-insulin. The A domain contains two α-helices, the A1-helix (IGF-I: Gly42-Cys48 and IGF-II: Ile42-Arg49) and A2-helix (IGF-I: Leu54-Cys61 and IGF-II: Leu53-Tyr59). These α-helices are separated by a loop structure and are maintained in an antiparallel orientation to each other by disulfide bonds (IGF-I: Cys47:Cys52 and IGF-II: Cys46:Cys51). Furthermore, the A1 and A2 helices are stabilised in

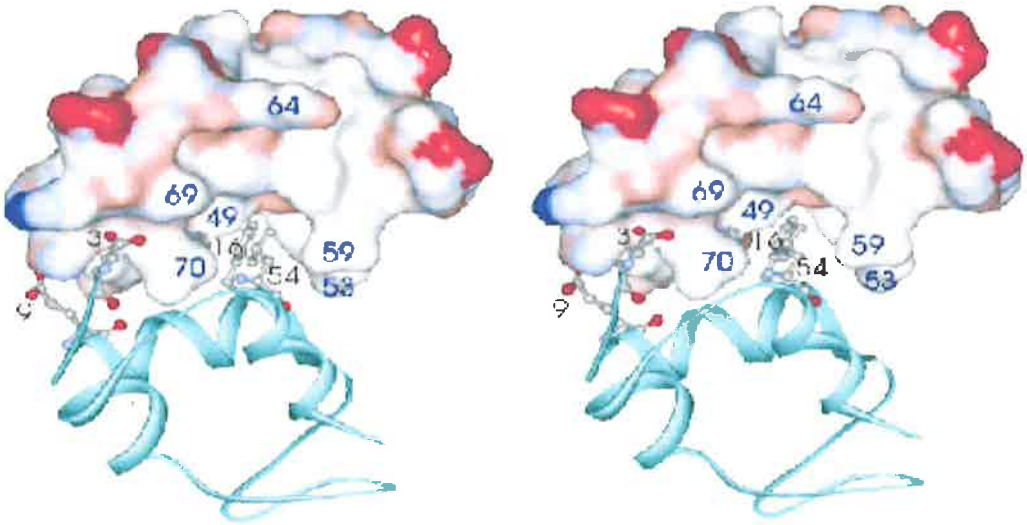

Figure 1.5 Crystal structure of the interface of IGF-I complexed to mini-IGFBP-5 complex The crystal structure of IGF-I (blue ribbon diagram) complexed with mini-IGFBP-5 (surface plot) has been determined. The side chains of the IGF-I residues involved in the binding interaction with mini-IGFBP-5 have been indicated and the charged residues of mini-IGFBP-5 have been coloured red -positively charged; blue -negatively charged and white –neutral. This figure has been replicated from Żesławski *et al.,* 2001 (Figure 2.B).

a planar orientation over the B helix by two disulfide bonds that link the beginning of the B-helix to the C-terminal end of the A1-helix (IGF-I: Cys6:Cys48 and IGF-II: Cys9:Cys47) and the C-terminal end of the B-helix to the C-terminal end of the A2-helix (IGF-I: Cys18:Cys61 and IGF-II: Cys21:Cys60). Residues 26-28 also appear to participate in intermolecular β-sheet formation. The D-domain, extending from the A2 helix is a flexible stretch of residues that comprise the C-terminus of the molecule.

The structures of IGF-I, IGF-II and insulin are similar in the well-defined regions. NMR has also investigated disulfide isomers and variants of IGF, which contain the helical segments, and hydrophobic core common to the IGF molecules (De Wolf *et al.*, 1996; Gill *et al*, 1996; Laajoki *et al.*, 2000; Sato *et al.*, 2000). Interestingly, the tertiary fold of both mini-IGF and Long-[Arg-3]-IGF-I did not differ substantially from the native molecule although slight variations in the orientation of the axes of the helices was reported (Laajoki *et al.*, 2000). Furthermore, naturally occurring disulfide isomers of IGF exhibit local similarities but global differences compared to the native molecule (Sato *et al.*, 2000). Interestingly, significant differences between IGF-I and IGF-II occur at the start of the third helix, which has been shown to be important for the modulation of type-2 receptor activity, and at the C-terminus. These differences might attribute unique functions to IGF-I and IGF-II.

1.3 IGFBP STRUCTURE

1.3.1 IGFBP PRIMARY STRUCTURE

Whilst the structures of IGF-I and IGF-II are well characterised, our structural knowledge of the IGFBP molecules is less extensive. Much of the information we have to date has been inferred from cDNA sequence analyses. The primary amino acid sequences for all six high affinity IGFBPs however, have been determined for a wide range of species as shown in Figure 1.6. The characteristic feature of the IGFBP amino acid alignment is the conserved

```
IGFBP-1  1   --------APWQCAPCSAEKLALCPPVSA---------------SCSEVTRS--A--GCGCCPMCALPLGAACGVATARCARGLSCRALPGEQQP
IGFBP-2  1   -------EVLFRCPPCTPERLAACGPPPVAPPAAVAAVAGGARMPCAELVRE--P--GCGCCSVCARLEGEACGVYTPRCGQGLRCYPHPGSELP
IGFBP-3  1   GASSGGLGPVVRCEPCDARALAQCAPPPA---------------VCAELVRE--P--GCGCCLTCALSEGQPCGIYTERCGSGLRCQPSPDEARP
IGFBP-4  1   -------DEAIHCPPCSEEKLARCRPP----------------VGCEELVRE--P--GCGCCATCALGLGMPCGVYTPRCGSGLRCYPPRGVEKP
IGFBP-5  1   ------LGSFVHCEPCDEKALSMCPPSP---------------LGCE-LVKE--P--GCGCCMTCALAEGQSCGVYTERCAQGLRCLPRQDEEKP
IGFBP-6  1   --------ALARCPGCGQGVQAGCP-----------------GGCVEEEDGGSPAEGCAEAEGCLRREGQECGVYTPNCAPGLQCHPPKDDEAP

IGFBP-1  69  LHALTRGQGACVQESDAS------------------- ---APHAAEAG-SPESPESTEITEEELLDNFHLMAPSEEDHSILWDAISTYDGSK--
IGFBP-2  85  LQALVMGEGTCEKRRDAEYGASPEQVADNGDDHSEGGLVENHVDSTMNMLGGGGSAGRKPLKSGMKELAVFREKVTEQHRQMGKGGKHHLGLEE-
IGFBP-3  77  LQALLDGRGLCVNASAVSRLRAYLLPAPPAPGNASESEEDRSAGSVESPSVSSTHRVSDPKFHPLHSKIIIIKKGHAKDSQRYKVDYESQSTDTQ
IGFBP-4  69  LHTLMHGQGVCMELAEIEA-------------------------IQESLQPSDKDEGDHPNNSFSPCSAHDRRCLQKHFAKIRDRSTSGGKMKVN
IGFBP-5  70  LHALLHGRGVCLNEKSYR------EQVKIER-DSREHEEPTTSEMAEETYSPKIFRPKHTRISELKAEAVKKDRRKKLTQSKFVGGAENTAHPRI
IGFBP-6  70  LRALLLGRGRCLPARAPA-------------------------VAEE----------NPKESKPQAGTARPQDVNRRDQQRNPGTSTTPSQP--

IGFBP-1  138 -ALHVTNIKKWKEPCRIELYRVVESLAKAQETSGEE----ISKFYLPNCNKNGFYHSRQCETSMDGEAGLCWCVYPWNGKRIPGSPEI-RGDPNC
IGFBP-2  179 --PKKLRPPPARTPCQQELDQVLERISTMRLPDERGPLEHLYSLHIPNCDKHGLYNLKQCKMSLNGQRGECWCVNPNT-GKLIQGAPTIRGDPEC
IGFBP-3  172 NFSSESKRETEYGPCRREMEDTLNHLKFLNVLSPRG-------VHIPNCDKKGFY KKQCRPSKGRKRGFCWCVDKYG-QPLPGYTTKGKEDVHC
IGFBP-4  139 GAPREDARPVPQGSCQSELHRALERLAASQSRTHED----LYIIPIPNCDRNGNFHPKQCHPALDGQRGKCWCVDRKTGVKLPGGLEP-KGELDC
IGFBP-5  158 ISAPEMRQESEQGPCRRHMEASLQELKASPRMVPRA-------VYLPNCDRKGFYKRKQCKPSRGRKRGICWCVDKYG-MKLPGMEYV-DGDFQC
IGFBP-6  127 --NSAGVQDTEMGPCRRHLDSVLQQLQTEVYRGAQT-------LYVPNCDHRGFYRKRQCRSSQGQRRGPCWCVDRMG-KSLPGSPDGNG-SSSC

IGFBP-1  227 QIYFNVQN-----------
IGFBP-2  271 HLFYNEQQEARGVHTQRMQ
IGFBP-3  259 YSMQSK-------------
IGFBP-4  229 HQLADSFRE----------
IGFBP-5  244 HTFDSSNVE----------
IGFBP-6  211 PTGSSG-------------
```

Figure 1.6 Sequence alignment of the six IGFBPs.
Amino acid sequences of human IGFBP-1 to –6 were aligned using a Clustal algorithm. Conserved cysteine residues are highlighted in black and all other conserved residues are highlighted in grey. Conservative substitutions are indicated by open boxes. Numbering is of the mature peptides/

pattern of cysteine residues in both the amino- and carboxyl-terminal thirds of the protein, which exhibit extensive residue homology (Landale *et al.*, 1995). In fact, the distinct regions of amino acid sequence homology suggest that the IGFBPs consist of three domains of approximately equal length (Rechler, 1993; Baxter, 1994; Jones and Clemmons, 1995), highly conserved cysteine-rich amino- and carboxyl-termini, joined by a linker domain unique to each IGFBP species. This has been shown for IGFBP-2 in Figure 1.7. The susceptibility of the central region of IGFBPs to proteolysis both *in vitro* and *in vivo*, suggests this region is not intimately involved in secondary structure though it may contain determinants to confer specific biological functions to each of the IGFBPs. Whilst there is limited information regarding the specific residues that comprise the IGF binding site, the proposed IGF binding site on the IGFBPs is believed to be located within the highly conserved amino- and carboxyl-terminal domains. Indeed, several studies have shown that the amino- and carboxyl-terminal regions of IGFBPs contain residues important for IGF binding (reviewed by Hwa *et al.*, 1999; Baxter, 2000).

1.3.2 THE DISULFIDE BONDS OF IGFBPS MAINTAIN STRUCTURAL INTEGRITY

The most prominent feature of the IGFBPs is the conservation of 16 cysteine residues; ten distributed throughout the amino-terminal domain (twelve for IGFBP-1 through –5) and a further six throughout the carboxyl-terminal domain. Disruption of these cysteine residues has been shown to severely reduce the affinity of the IGFBPs for IGF (Sommer *et al.*, 1991; Brinkman *et al.*, 1991a; Brinkman *et al.*, 1991b). The absence of interdomain disulfide bonds suggests the highly conserved amino- and carboxyl-terminal regions of IGFBPs exist as independent structural domains (Forbes *et al.*, 1998; Neumann *et al.*, 1998). This was recently found to be true for hIGFBP-6, a unique IGFBP that lacks two of the twelve N-terminal cysteine residues and exhibits significant IGF-II preferential binding (Neumann and Bach, 1999). The

```
bovine     1   EVLFRCPPCTPESLAACKPPPGAAAGPAGDAR----VPC-ELVREPGCGCCSVCARLEGERCGVYTPRCGQGLRCYPNPGSELPLRALVHGEGTC
ovine      1   EVLFRCPPCTPESLAACKPPPGAAAGPAGDAR----VPC-ELVREPGCGCCSVCARLEGERCGVYTPRCGQGLRCYPNPGSELPLRALVHGEGTC
human      1   EVLFRCPPCTPERLAACGPPPVAPPAAVAAVAGGARMPCAELVREPGCGCCSVCARLEGEACGVYTPRCGQGLRCYPHPGSELPLQALVMGEGTC
mouse      1   EVLFRCPPCTPEALAACGPPPD--------------APCAELVREPGCGCCSVCARQEGEACGVYIPRCAQTLRCYPNPGSELPLKALVTGAGTC
rat        1   EVLFRCPPCTPERLAACGPPPD--------------APCAELVREPGCGCCSVCARQEGEACGVYIPRCAQTLRCYPNPGSELPLKALVTGAGTC
chicken    1   EVLFRCPPCTAERLAACSPAAR--------------PPCPELVREPGCGCCPVCARLEDEACGVYTPRCAAGLRCYPDPGAELPPQALVQGQGTC
zebrafish  1   EMVFRCPSCTAERQAACPMLT---------------ETCGEIVREPGCGCCPVCARQEGEQCGVYTPRCSSGLRCYPKPDSELPLELLVQGLGRC

bovine     91  EKHGD-AEYSASPEQVADNGEEHSEGGLVENHVDGNVNLMGGGGGAGRKPLKSGMKELAVFREKVTEQHRQMGKGGKHHLGLEEPKKLRPPPART
ovine      91  EKHGD-AEYSASPEQVADNGEEHSEGGQVENHVDGNVNLMGGGGGAGRKPLKFRMKELAVFREKVTEQHRQMGKGGKHHLGLEEPKKLRPPPART
human      96  EKRRD-AEYGASPEQVADNGDDHSEGGLVENHVDSTMNMLGGGGSAGRKPLKSGMKELAVFREKVTEQHRQMGKGGKHHLGLEEPKKLRPPPART
mouse      82  EKRR----VGTTPQQVADSDDDHSEGGLVENHVDGTMNMLGGGSSAGRKPLKSGMKELAVFREKVNEQHRQMGKG-AKHLSLEEPKKLRPPPART
rat        82  EKRR----VGATPQQVADSEDDHSEGGLVENHVDGTMNMLGG-SSAGRKPPKSGMKELAVFREKVNEQHRQMGKG-AKHLSLEEPKKLRPPPART
chicken    82  ARPPDTDEYGASTEPPADNGDDRSESILAENHVDSTGGMMSG--ASSRKPLKTGMKEMPVMREKVNEQQRQMGKVGKAHHNHEDSKKSRMPTGRT
zebrafish  81  GRKVD--------TEPTGSAEPREVSGEVQDPLDIGLTEVPP----IRKPTKD-----SPWKESAVLQHRQQLKSKMKYHKVEDPK--APHAKQS

bovine     185 PCQQELDQVLERISTMRLPDERGPLEHLYSLHIPNCDKHGLYNLKQCKMSLNGQRGECWCVNPNTGKLIQGAPTIRGDPECHLFYNEQ-QGARGV
ovine      185 PCQQELDQVLERISTMRLPDERGPLEHLYSLHIPNCDKHGLYNLKQCKMSLNGQRGECWCVNPNTGKLIQGAPTIRGDPECHLFYNEQ-QGARGV
human      190 PCQQELDQVLERISTMRLPDERGPLEHLYSLHIPNCDKHGLYNLKQCKMSLNGQRGECWCVNPNTGKLIQGAPTIRGDPECHLFYNEQ-QEARGV
mouse      172 PCQQELDQVLERISTMRLPDDRGPLEHLYSLHIPNCDKHGRYNLKQCKMSLNGQRGECWCVNPNTGKPIQGAPTIRGDPECHLFYNEQ-QETGGA
rat        171 PCQQELDQVLERISTMRLPDDRGPLEHLYSLHIPNCDKHGLYNLKQCKMSLNGQRGECWCVNPNTGKPIQGAPTIRGDPECHLFYNEQ-QENDGV
chicken    175 PCQQELDQVLERISTMRLPDERGPLEHLYSLHIPNCDKHGLYNLKQCKMSVNGQRGECWCVDPIHGKVIQGAPTIRGDPECHLFYTAHEQEDRGA
zebrafish  157 QCQQELDQVLERISKITFKDNRTPLEDLYSLHIPNCDKRGQYNLKQCKMSVNGYRGECWCVNPHTGRPMPTSPLIRGDPNCNQYLDGQ-EMDPSV

bovine     279 HTQRMQ
ovine      279 HTQRMQ
human      284 HTQRMQ
mouse      266 HAQSVQ
rat        265 HAQRVQ
chicken    270 HALRSQ
zebrafish  251 DPPN--
```

Figure 1.7 Alignment of IGFBP-2 Protein Sequences

IGFBP-2 protein sequences for bovine (Upton *et al., 1990; Bourner et al.,* 1992), ovine (Delhanty and Han, 1992), human (Binkert *et al.,* 1989), mouse (Landwher *et al.*, 1993), Rat (Brown *et al.*, 1990), chicken (Schoen *et al.,* 1995) and zebrafish (Duan *et al.*, 1999). Conserved cysteine residues are boxed in black and all other conserved residues are highlighted in grey. The alignment was created using ClustalW1.8 (Thompson *et al.*, 1994).

amino-terminal disulfide bonds of hIGFBP-6 are arranged in two sub-domains. The first sub-domain consisted of the consecutive disulfides bonded residues Cys29-Cys32, Cys40-Cys44 and Cys57-Cys63, while the second sub-domain contains the remaining four cysteine residues Cys71-Cys84, Cys78-Cys104. Analogous residues to the second subdomain in IGFBP-1 (Neuman and Bach, 1999), IGFBP-2 (B.Forbes; *unpublished*), IGFBP-3 (Hashimoto *et al.*, 1997), IGFBP-4 (Chelius *et al.*, 2001) and hIGFBP-5 (Kalus *et al.*, 1998) have also been shown to form disulfide bonds. Indeed, Kalus and co-workers concluded residues Ala40-Ile92 was not only a sub-domain of hIGFBP-5, but also possessed the major IGF binding site determinant. The disulfide bonds formed consecutively within the C-terminal domain of hIGFBP-6, Cys163-Cys190, Cys201-Cys212, Cys214-Cys234, were identical to those of bIGFBP-2 (Forbes *et al.*, 1998) and hIGFBP-4 (Standker *et al.*, 2000). The known disulfide bonds have been summarised schematically in Figure 1.8.

Despite the high degree of sequence homology, Chelius and co-workers reported a differing cysteine pairing in the amino terminus of IGFBP-4 compared to hIGFBP-6. In contrast to IGFBP-6, the first two cysteine residues of IGFBP-1 (Neuman and Bach, 1999) and IGFBP-4 (Chelius *et al.,* 2001) are not linked, nor are cysteine residues 3 and 4. Chelius and co-workers further identified disulfide bonds between cysteine residues 3-8, 4-7, 9-11 and 10-12 (and between the two cysteine residues in the central domain). By inference, this would also be true for the remaining IGFBPs, which also have an additional two adjacent cysteine residues in the N-terminal motif: Gly-Cys-Gly-Cys-Cys-(2X)-Cys-Ala-(6X)-Cys (Bairoch, 1991).

1.3.3 IGFBP SECONDARY AND TERTIARY STRUCTURE

To date, there is limited secondary and tertiary structure information for the IGFBPs, and the absence of sequence homology with proteins of known tertiary structure severely limits the molecular modelling of variant IGFBPs and IGFs for therapeutic applications. The molecular mass of the IGFBPs has, until recent advances in technology, limited structure

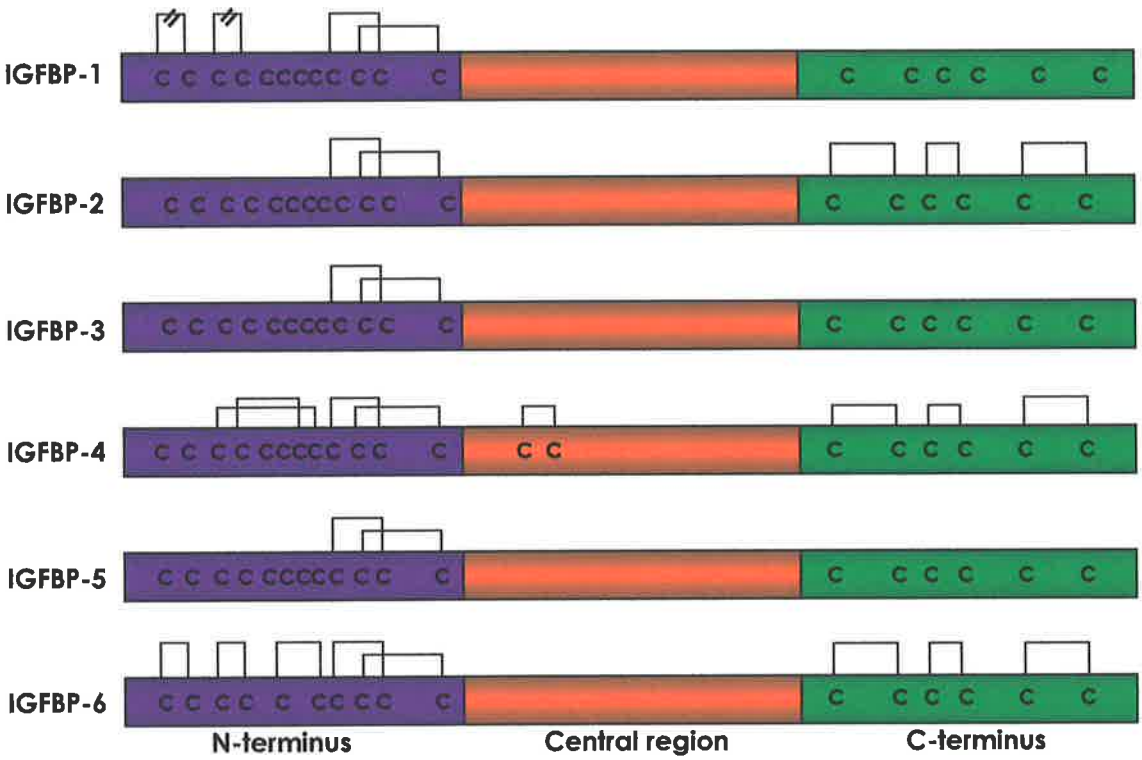

Figure 1.8 Schematic representation of the disulfide bonds of IGFBPs
The complete disulfide bonding pattern for IGFBP-6 has been determined (Neumann *et al.*, 1998; Neumann and Bach, 1999). Cysteine residues are marked (C) and known disulfide bonds indicated by black lines. IGFBP-1 through –5 have an additional two amino-terminal cysteine residues as indicated and IGFBP-4 contain two unique cysteine residues in the central region. Amino-terminal disulfide bonds are also shown for IGFBP-1 (Neumann and Bach, 1999), IGFBP-2 (B.Forbes, *unpublished*), IGFBP-3 (Hashimoto *et al.*, 1997), IGFBP-4 (Standker *et al.*, 2000; Chelius *et al.,* 2001) and IGFBP-5 (Kalus *et al.*, 1998). Amino-terminal disulfide bonds of IGFBP-1 (Neumann and Bach, 1999) and IGFBP-4 (Chelius *et al.*, 2001) differ from those reported for IGFBP-6. The carboxyl terminal disulfide bonds are conserved in IGFBP-2 (Forbes *et al.*, 1998) and IGFBP-4 (Standker *et al.*; 2000).

determination studies. IGFBPs are relatively large proteins ranging in molecular weight form 24-55 kDa, which is approaching the upper limit of resolution by NMR spectroscopy. Structural determination of IGFBPs has therefore relied heavily on sequence analysis and has been confined to predictions based on computer modelling (IGFBP-3, (Spencer and Chan, 1995) IGFBP-4, (Landale *et al.*, 1995). Landale and co-workers used mathematical algorithms and comparison of other IGFBP family members to predict the secondary structural content of human IGFBP-4 (Landale *et al.*, 1995). Consequently, the amino terminal region of IGFBPs was predicted to comprise predominantly β-strands and β-turn while the central and carboxyl-terminal cysteine rich domains were predicted to contain mostly helical secondary structural elements.

An NMR structure of a fragment of hIGFBP-5 (Ala40 to Ile92; mini-IGFBP-5) provided great insight into the structure of the IGFBP molecule (Kalus *et al.*, 1998) (Figure 1.9). The NMR structure was in good agreement with the prediction algorithm (Landale *et al.*, 1995) as it contained three short antiparallel β-strands (residues 46-47, 59-61, 78-82) in a compact arrangement (Kalus *et al.*, 1998). In contrast, a C-terminal fragment of hIGFBP-5 (residues 135-246), was estimated to contain approximately 40 % random coil conformation while the remaining unconserved central region of IGFBP-5 was relatively unstructured (Kalus *et al.*, 1998).

IGF-I has recently been crystallised in complex with mini-IGFBP-5 providing a spatial understanding of the interacting molecules (Żesławski *et al.,* 2001)(Figure 1.5). Interestingly, the fold of mini-IGFBP-5 was conserved in complex with IGF-I. Two regions of mini-IGFBP-5 remain poorly defined including the five C-terminal residues and the solvent exposed loop (Pro62-Pro69), which was rigidified in the presence of ligand. The binding interface and the specific interacting residues of both IGF-I and mini-IGFBP-5 will be discussed in the following sections.

Based on the high degree of sequence homology and the conserved pattern of cysteine residues throughout the IGFBP family, the IGFBPs may possess a common structure. Hence,

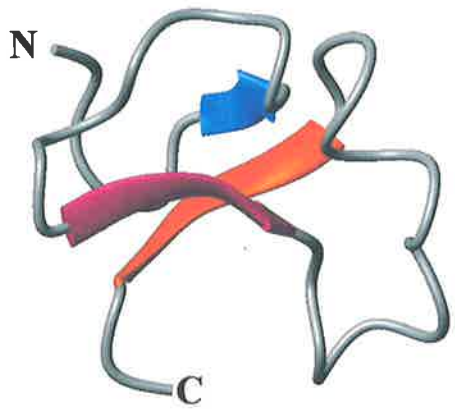

Figure 1.9 NMR structure of mini-IGFBP-5
The NMR structure of mini-IGFBP-5 (Ala40 to Ile92) contains three short antiparallel β-strands (residues 46-47, 59-61, 78-82) in a compact arrangement (Kalus *et al.*, 1998). This figure was constructed using MOLMOL (Koradi *et al.*, 1996).

the information obtained for hIGFBP-5 has provided a basis for the determination of the structure of the remaining IGFBPs. The complete structure of the IGFBPs and the spatial arrangement of the amino- and carboxyl-terminal domains, relative to one another, will provide the ultimate insight into the IGFBP structure-function paradigm.

1.4 IGF RESIDUES INVOLVED IN IGFBP BINDING

Given the diverse biological effects of IGFs and the central role of IGFBPs in the regulation of IGF activity, the molecular interactions between the IGFs and IGFBPs are of particular interest. High-resolution NMR structures of both IGF-I and IGF-II have been published (Cooke *et al.*, 1991; Sato *et al.*, 1993; Terasawa *et al.*, 1994; Torres *et al.*, 1995) which has enabled detailed correlation of IGF structure-function relationships to be made. In addition, numerous studies have provided insight into the specific residues of IGF involved in the IGFBP binding interaction (Bayne *et al.*, 1988; Bagley et al., 1989; Cascieri *et al.*, 1989; Moss *et al.*, 1991, Bach *et al.*, 1993; Francis et al., 1993; Oh *et al.*, 1993; Magee et al., 1999). Various techniques have been used to investigate the residues of IGF involved in both binding protein and receptor interactions including amino acid deletions or mutations and substitution of homologous residues of the insulin molecule. NMR and deuterium exchange studies have also been used to probe the structural binding epitopes on IGF-I required for interaction with IGFBP-1 (Jansson *et al.*, 1998, Ehring, 1999).

Naturally occurring variants of IGFs have provided insight into the critical residues involved in IGF interactions with IGFBPs. A variant form of IGF-I lacking the first three amino acid residues, des(1-3) IGF-I, has been isolated from bovine colostrum (Francis *et al.*, 1988) and shown to have reduced ability to interact with IGFBP (Szabo *et al.*, 1988) and a 5- to 10-fold increased potency, compared with native IGF-I, toward stimulating protein synthesis in L6 rat myoblasts (Ballard *et al.*, 1987). In addition, sequential deletions from the amino-terminal end of IGF-I confirmed the importance of Glu3 in the IGFBP binding interaction (Bagley *et al.*, 1989) and a charge reversal of Glu3 to either a lysine or arginine residue had the greatest impact

on IGFBP interaction (Wallace *et al.*, 1989). The corresponding residue in IGF-II, Glu6, has been shown to be equally important in the high affinity interaction (Francis *et al.*, 1993). Interestingly, a study by Ho and Baxter (1997), showed des(1-6) IGF-II was incapable of displacing IGF ligand from a C-terminal IGFBP-2 fragment isolated from human milk suggesting the amino hexapeptide of IGF-II is required for interaction with the C-terminal region of IGFBP-2.

Homologue domain swapping of IGF residues with the corresponding residues of insulin has provided information regarding specific residues involved in the interaction with IGFBP. Insulin is incapable of interacting with IGFBPs, however substitution of the B-domain with that of IGF-I conferred IGFBP binding ability to insulin (De Vroede *et al.*, 1985). Likewise, substituting the IGF-I B-domain with that of insulin reduced the affinity of IGF-I for serum IGFBPs (Bayne *et al.*, 1988). Substitution of amino acid residues Phe49, Arg50, and Ser51 in IGF-I (Clemmons *et al.*, 1992; Oh *et al.*, 1993), and Phe48, Arg49 and Ser50 in IGF-II (Bach *et al.*, 1993) with the corresponding insulin residues affected IGFBP binding. Furthermore, substitution of IGF-II residue Phe26 with Ser or Leu, decreased binding to the type-I IGF and insulin receptors, IGFBP-1 and IGFBP-6 (up to 80-fold), but affected the remaining binding proteins to a lesser extent (Sakano *et al.*, 1991; Bach *et al.*, 1993). Alanine substitutions of IGF-I residues Ile43, Val44 or Leu54 reduced binding to IGFBP-1 up to 4-fold, but did not affect binding to IGFBP-3 (Dubaquie` and Lowman, 1999).

IGF residues involved in the IGFBP interaction have also been identified by alanine scanning and point mutation analysis. IGF-I residues Gln15 and Phe16 are involved in the binding interaction and when mutated in combination with Glu3 and Thr4, binding to serum IGFBP is decreased up to 600-fold (Ballard *et al.*, 1987; Bayne *et al.*, 1988; Francis *et al.*, 1992; King *et al.*, 1992; Oh *et al.*, 1993). Alanine substitution of Gln15 and Phe16 showed these residues were important for structural integrity of the molecule (Jansson *et al.*, 1997). However, mutants with alternative substitutions that did not grossly affect the structure of IGF (Glu15Gln, Glu9Lys and Phe16Ser), also exhibited reduced affinity for IGFBPs (Magee *et al.*, 1999). Interestingly, the binding affinities of mutants Phe16Ser and Glu9Lys IGF-I varied for each of

the six binding proteins (Magee *et al.*, 1999). Alanine mutagenesis across the entire IGF-I molecule identified additional residues involved in the IGFBP interaction, including Gly7, Leu10 and Phe25 (Dubaquie` and Lowman, 1999). Indeed, NMR studies by Jansson and co-workers (1998) revealed Gly7 of IGF-I exhibited chemical shift perturbations upon interaction with IGFBP-1.

Chemical iodination and NMR approaches have also been used to investigate the specific residues of IGF involved in the IGFBP interaction. The binding domain of IGFs was probed by chemical iodination of tyrosine residues in hIGF-I and oIGF-II (Moss *et al.*, 1991). The accessibility of these tyrosine residues to iodination was compared in the presence and absence of IGFBP-2. Iodination of Tyr60 and Tyr59 of IGF-I and IGF-II respectively, were decreased 2- and 6-fold respectively when IGF was bound to IGFBP-2, while iodination of Tyr24 and Tyr31 in IGF-I and Tyr2 and Tyr27 in IGF-II were not inhibited by complexing with IGFBP-2. Recent analysis of backbone chemical shifts by NMR spectroscopy provided additional information about the residues of IGF and IGFBPs involved in the interaction. IGF-I residues perturbed in the presence of IGFBP-1 were Pro2, Glu3, Cys6, Gly7, Gly19, Pro28-Gly30, Gly32, Arg36, Arg37, Gln40-Gly42, Pro63, Lys65, Pro66, Lys68-Ala70 (Jansson *et al.*, 1998). These residues also appear to form the major IGF-binding site of the N-terminal fragment of IGFBP-5 (Ala40-Ile92) (Kalus *et al.*, 1998). Indeed, subsequent alanine substitution of arginine residues Arg36, Arg37 and Arg50 of IGF-I affected IGFBP-1 binding (Jansson *et al.*, 1998).

To date, the crystal structure of IGF-I complexed with mini-IGFBP-5 has provided greatest insight into the binding interface of both molecules (Żesławski *et al.*, 2001). The interaction is principally hydrophobic involving protruding side chains of IGF-I and solvent exposed hydrophobic side chains of the mini-IGFBP-5. As shown in Figure 1.5, side chains of IGF-I Glu3, Phe16 and Leu54 are inserted deep into a cleft on the mini-IGFBP-5 molecule. Phe16 makes direct contact with the backbone and side chain of Val49 and with Cys60 of mini-IGFBP-5. Other residues identified by mutagenesis (Glu3, Thr4, Gln15, Phe16, Phe49, Arg50 and Ser51) are located within or near the mini-IGFBP-5 binding site including Gln15, which

neighbours the important Phe16, and residues Phe48, Arg49 and Ser50, which are within three residues of the interface.

Clearly, IGF analogues affect binding to each IGFBP family member to varying degrees (Clemmons *et al.*, 1992; Bach *et al.*, 1993; Magee *et al.*, 1999). The critical residues of IGFs involved in binding to IGFBP-1 and IGFBP-2 differ (Clemmons *et al.*, 1990). The A chain residues at positions 49-51 of IGF-I and 48-50 of IGF-II are most detrimental to IGFBP-2 binding of IGFs while optimal binding of IGF-I and IGF-II to IGFBP-1 is also dependent on residues 3 and 4 of IGF-I and residues 6 and 7 of IGF-II at the N-terminus of the B-domain. Dramatic loss of IGF affinity for IGFBP-3 is observed upon extensive B-chain substitution. Charge reversal of Glu9Lys, a residue located in the B-domain α-helix in IGF-I, decreased to varying degrees the affinity for each of the six binding proteins, without affecting the overall structure of the molecule (Magee *et al.*, 1999). It is interesting to note that IGFBP-1 and IGFBP-6 are most sensitive to changes in residues 26 and 48-50 in IGF-II although they have markedly different preferences for IGF-II. Furthermore, the residues of IGF-I required to bind both IGFBP-1 and IGFBP-3 are similar, although the A domain is not involved in IGFBP-3 binding (Clemmons *et al.*, 1990). These results suggest that while the IGFBP-binding sites overlap in some parts of the IGF molecule, the binding sites vary. Indeed, the IGFBP-3 binding site on IGF-I may be smaller than that of IGFBP-1 and IGFBP-2. In addition, the binding site of IGFBP-4 was predicted to be larger than the binding sites for IGFBPs 1-3 as the N-terminal α-helix and the C-terminus of the B region, the 2 α-helices of the A region and additional determinants in the D region of IGF-I are all involved in IGFBP-4 interactions (Clemmons *et al.*, 1992). The differences in amino acid residues involved in binding the various IGFBPs may be reflective of the requirements for interaction with either the amino acid side chains or amino acid backbone residues (Dubaquie` and Lowman, 1999).

1.4.1 SUMMARY OF THE IGFBP BINDING SITE ON IGF

Specific residues of IGF peptides involved in binding to IGFBPs include Glu3, Thr4, Gln15, Phe16, Phe49, Arg50 and Ser51 of IGF-I, and Glu6, Phe48, Arg49 and Ser50 of IGF-II (Figure 1.10). IGF-I analogues with insulin-like substitutions at specific positions in the A and B domain helical regions of IGF have reduced affinity for binding proteins. The B chain of both IGF-I and IGF-II appears to be the major region involved in the IGFBP binding interaction suggesting that a common binding site exists on IGFBPs (Clemmons *et al.*, 1992). This is further supported by the extensive sequence conservation between and within IGFBP species. Different residues in the binding site of IGFBPs may determine the relative binding affinities of IGFBPs for IGFs (Clemmons *et al.*, 1992). Structure determination studies will ultimately provide a comprehensive insight in to the molecular dynamics of the binding interaction, which will provide invaluable information regarding the docking of IGFBPs and IGF molecules for the design of IGFBPs with altered IGF binding specificity for therapeutic application.

1.5 IGFBP RESIDUES INVOLVED IN IGF BINDING

Whilst some of the residues of IGF-I and IGF-II involved in the interaction with IGFBPs have been identified, the exact mechanism of interaction and the IGF binding site(s) on the IGFBPs have yet to be elucidated. Some information about the IGF binding site(s) has been derived from IGFBP proteolysis occurring either during purification strategies or by specific IGFBP proteases. Furthermore, studies of recombinantly modified IGFBPs have also contributed to defining the IGF binding site. The proposed IGF binding site on the IGFBPs is believed to be located within the highly conserved amino- and carboxyl-terminal domains as studies have shown both contain residues important for IGF binding (reviewed by Hwa *et al.*, 1999; Baxter, 2000). Published data will be presented to support the hypothesis that residues in both the amino- and carboxyl-terminal domains form the IGF binding site (Figure 1.11).

A. Mutagenesis Studies

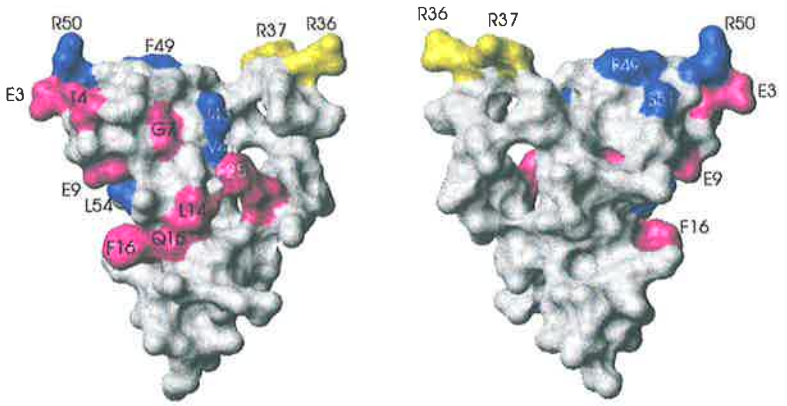

B. NMR with IGFBP-1 - Jansson *et al.*, 1998

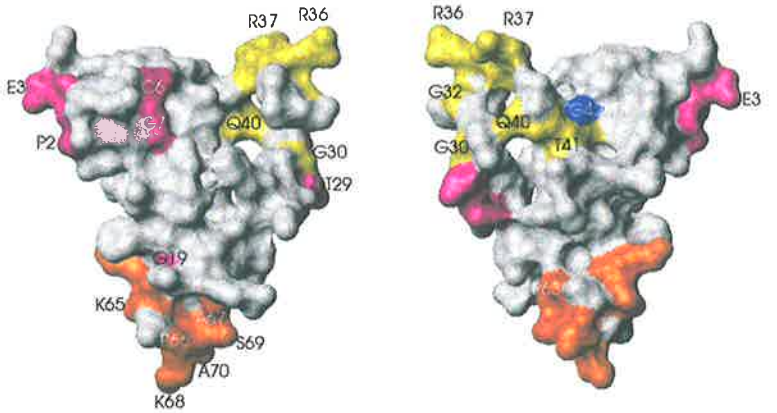

C. Crystal Structure - Zesławski *et al.*, 2001

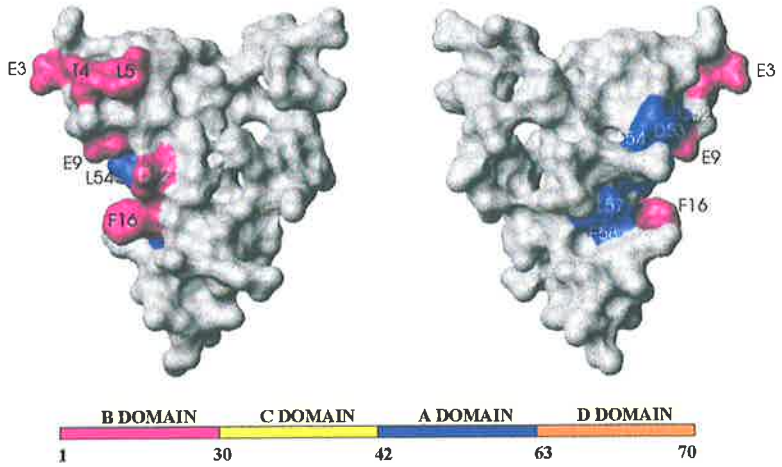

Figure 1.10 Surface representation of IGF-I with residues involved in binding IGFBPs highlighted

The residues of IGF-I identified to be important for binding IGFBPs by mutagenesis (A. as discussed in Section 1.5) and by heteronuclear NMR experiments (B. Jansson *et al.*, 1998) are highlighted with respect to their domains (pink: B-domain; yellow: C-domain; blue: A-domain and orange: D-domain. The residues which were within 5 Å of mini-IGFBP-5 in the crystal structure are also highlighted (C. Zesławski *et al.*, 2001). IGF-I has been presented in two orientations with rotation of 180° about the vertical axis.

1.5.1 IGF BINDING BY RESIDUES IN THE AMINO-TERMINAL REGION

Earliest insights into IGF binding regions of IGFBPs arose from observations that proteolysed fragments often retained residual affinity for IGFs. IGF binding activity has been reported for amino-terminal fragments of IGFBP-1 (Huhtala *et al.*, 1986), IGFBP-3 (Sommer *et al.*, 1991; Lalou *et al.*, 1997; Kubler *et al.*, 1999), IGFBP-4 (Chernausek *et al.*, 1995; Standker *et al.*, 1999) and IGFBP–5 (Huhtala *et al.*, 1986; Andress *et al.*, 1993; Chernausek *et al.*, 1995; Kubler *et al.*, 1999; Standker *et al.*, 2000) (Figure 1.11a). Although these fragments demonstrate IGF binding properties, there is a distinct loss of affinity, suggesting a requirement for additional components. Interestingly, IGFBP related proteins (IGFBPrPs), which share sequence similarities with the N-terminal domain of the high affinity IGFBPs, have also been reported to bind IGF-I, IGF-II and insulin (Bork, 1993; Oh *et al.*, 1996; Kim *et al.*, 1997; Hwa *et al.*, 1999).

Several recombinant N-terminal fragments of IGFBPs including IGFBP-3 (Hashimoto *et al.*, 1997; Vorwerk *et al.*, 1998), IGFBP-4 (Qin *et al.*, 1998) and IGFBP-5 (Andress *et al.*, 1993) have also been produced which provide further support for an IGF binding site located within the N-terminal domain. Hashimoto and co-workers expressed a fragment of IGFBP-3 (amino acid residues 1-93) which retained 4.2% IGF binding and showed that addition of linker peptide residues (94-186) restored IGF binding to 12% of native rIGFBP-3 for IGF (Hashimoto *et al.*, 1997). Interestingly, the central linker region appeared to contribute to the structural integrity and hence IGF binding potential of these amino-terminal fragments.

Chemical iodination studies of bIGFBP-2 by Hobba and co-workers, showed conclusively that residue Tyr60 in the N-terminal domain contributed to IGF binding (Hobba *et al.*, 1996). Furthermore, the loss of IGF binding observed upon iodination of bIGFBP-2 was shown through alanine scanning mutagenesis to be a consequence of altering the normal function of the Tyr60 side chain. Substitution of Val59Ala also altered the bIGFBP-2 binding characteristics while alanine substitution for Thr61, Pro62 and Arg63 had no effect (Hobba *et al.*, 1998). Imai and co-workers confirmed the importance of corresponding amino-terminal

```
IGFBP-1   1   ---- ----APWQCAPCSAEKLALC PPVSA- ------ ---- ----SC SEVTRS--A- -CCGCC PMCALPLGAACGVATARCARGLSC RALPGE QQP
IGFBP-2   1   ---- ---EVLFRCPPCTPERLAAC GPPPVA PPAAVA AVAG GARMPC AELVRE--P- -CCGCC SVCARLEGEACGVYTPRCGQGLRC YPHPGS ELP
IGFBP-3   1   GASS GGLGPVVRCEPCDARALAQC APPPA- ------ ---- ----VC AELVRE--P- -CCGCC LTCALSEGQPCGIYTERCGSGLRC QPSPDE ARP
IGFBP-4   1   ---- ---DEAIHCPPCSEEKLARC RPP--- ------ ---- ---VGC EELVRE--P- -CCGCC ATCALGLGMPCGVYTPRCGSGLRC YPPRGV EKP
IGFBP-5   1   ---- --LGSFVHCEPCDEKALSMC PPSP-- ------ ---- ---LGC E-LVKE--P- -CCGCC MTCALAEGQSCGVYTERCAQGLRC LPRQDE EKP
IGFBP-6   1   ---- ----ALARCPGCGQGVQAGC P----- ------ ---- ---GGC VEEEDGGSPAEGCAEAEGCL RREGQECGVYTPNCAPGLQC HPPKDD EAP

IGFBP-1  69   LHAL TRGQGACVQE SDAS-- ---- ------ ------ ---- -APHAA EAG- SPESPE STEITE EELL DNFHLMAPSE EDHSIL WDAI STYDGS K--
IGFBP-2  85   LQAL VMGEGTCEKR RDAEYG ASPE QVADNG DDHSEG GLVE NHVDST MNML GGGGSA GRKPLK SGMK ELAVFR EKVT EQHRQM GKGG KHHLGL EE-
IGFBP-3  77   LQAL LDGRGLCVNA SAVSRL RAYL LPAPPA PGNASE SEED RSAGSV ESPS VSSTHR VSDPKF HPLH SKIIII KKGH AKDSQR YKVD YESQST DTQ
IGFBP-4  69   LHTL MHGQGVCMEL AETEA- ---- ------ ------ ---- ----IQ ESLQ PSDKDE GDHPNN SFSPCSAHDR RCLQ KHFAKI RDRS TSGGKM KVN
IGFBP-5  70   LHAL LHGRGVCLNE KSYR-- ---- ---- EQVKIE R-DSRE HEEP TTSEMA EETY SPKIFR PKHTRI SELK AEAVKK DRRK KLTQSK FVGG AENTAH PRI
IGFBP-6  70   LRAL LLGRGRCLPA RAPA-- ---- ------ ------ ---- ----VA EE-- ------ --NPKE SKPQ AGTARP QDVN RRDQQR NPGT STTPSQ P--

IGFBP-1 138   -ALH V TNIKK WKEPCRIELY RVVE SLAKAQ ETSGEE ---- ISKFYL PNCN KNGFYH SRQCET SMDG EAGLCW CVYP WNGKRI PGSP EI-RGD PNC
IGFBP-2 179   --PK KLRPPP ARTPCQQELD QVLE RISTMR LPDERG PLEH LYSLHI PNCD KHGLYN LKQCKM SLNG QRGECW CVNP NT-GKL IQGA PTIRGD PEC
IGFBP-3 172   NFSS ESKRET EYGPCRREME DTLN HLKFLN VLSPRG ---- ---VHI PNCD KKGFYK KKQCRP SKGR KRGFCW CVDK YG-QPL PGYT TKGKED VHC
IGFBP-4 139   GAPR EDARPV PQGSCQSELH RALE RLAASQ SRTHED ---- LYIIPI PNCD RNGNFH PKQCHP ALDG QRGKCW CVDR KTGVKL PGGL EP-KGE LDC
IGFBP-5 158   ISAP EMRQES EQGPCRRHME ASLQ ELKASP RMVPRA ---- ---VYL PNCD RKGFYK RKQCKP SRGR KRGICW CVDK YG-MKL PGME YV-DGD FQC
IGFBP-6 127   --NS AGVQDT EMGPCRRHLD SVLQ QLQTEV YRGAQT ---- ---LYV PNCD HRGFYR KRQCRS SQGQ RRGPCW CVDR MG-KSL PGSP DGNG-S SSC

IGFBP-1 227   QIYF NVQN-- ---- -----
IGFBP-2 271   HLFY NEQQEA RGVH TQRMQ
IGFBP-3 259   YSMQ SK---- ---- -----
IGFBP-4 229   HQLA DSFRE- ---- -----
IGFBP-5 244   HTFD SSNVE- ---- -----
IGFBP-6 211   PTGS SG---- ---- -----
```

Figure 1.11a IGF binding studies targeting the N-terminal region of IGFBP.
Details of the studies can be found in Section 1.5.1. Residues from different IGFBPs that were targeted have been mapped on to the human IGFBP sequences. (PM)=point mutation, (F)=fragment, (Del)=deletion.
IGFBP-1: (Del) Brinkman et al 1991a; IGFBP-2: (PM) Hobba et al., 1998; IGFBP-3: (F) Hashimoto et al., 1997;
IGFBP-4: (Del) Qin et al., 1998; IGFBP-5: (F) Kalus et al., 1998.

residues in IGFBP-3 (Imai *et al.*, 2000) and Qin *et al.* for IGFBP-4 (Imai *et al.*, 1997; Qin *et al.*, 1998). NMR analysis of the binding interaction between an N-terminal fragment of hIGFBP-5 (amino acid residues Ala40-Ile92) and IGF-II, implicated the equivalent residues, Val49, Tyr50, Pro62 and Lys68 to Leu74, in the interaction (Kalus *et al.*, 1998).

Crystallisation of mini-IGFBP-5 with IGF-I conclusively defined the IGF binding site on this IGFBP fragment. As discussed in Section 1.4, mini-IGFBP-5 forms a cleft into which side chains of IGF-I insert (viz: Glu 3, Phe16 and Leu54). The cleft is formed by side chains of Arg53 and Arg59 on the solvent exposed side of the molecule and of Val49, Leu70 and Leu74 on the opposite inner side. Residues Cys60 and Leu61 form the base of the cleft (Figure 1.5). A network of hydrogen bonds including Glu3 and Glu9 of IGF-I and His71 and Tyr50 of mini-IGFBP-5 encloses the hydrophobic cluster on the solvent side of the molecule. Furthermore, Arg59 of mini-IGFBP-5 makes hydrogen bonds with Glu58 of IGF-I.

Amino-terminal fragments of hIGFBP-5 (amino acid residues 1-94 and 40-92) exhibited 200-fold reduced affinity for IGF compared to wildtype IGFBP-5 by BIAcore analysis. This was shown to be due to increased dissociation kinetics. Similarly, a fragment of rIGFBP-3 encompassing amino acid residues Glu52-Ala92 exhibited only 0.008% of the binding affinity of the full-length protein for IGF-II (Hashimoto *et al.*, 1997). Addition of amino acid residues (1-51) increased the affinity of the fragment (1-92) to only approximately 4% of the full-length protein (Hashimoto *et al.*, 1997). As amino acid residues 1-39 of hIGFBP-5 did not contribute to maintaining the complex, it was concluded that additional components required for stability would be derived from the C-terminal residues of IGFBPs. It is feasible therefore, that the IGF binding sites located in the amino- and carboxyl-terminal domains of IGFBPs, combine with each other to create one high affinity-binding site.

1.5.2 IGF BINDING BY RESIDUES IN THE CARBOXYL-TERMINAL REGION

Amino-terminal fragments of IGFBPs clearly retain IGF binding activity however additional components are necessary for high affinity binding. Naturally occurring carboxyl-terminal fragments of IGFBP-2 (Wang *et al.*, 1988; Ho and Baxter, 1997), IGFBP-3 (Sommer *et al.*, 1991; Spencer and Chan, 1995) and IGFBP-5 (Standker *et al.*, 1998) have also been shown to possess residual IGF binding activity (Figure 1.11b). Like the amino-terminal fragments of IGFBPs, the carboxyl terminal domains only retain partial IGF binding and hence it would appear that both the N- and C-terminal domains are required for high affinity binding, or perhaps at least for maintenance of the correct tertiary fold for IGF binding to occur.

Wang and co-workers (1988) provided the first evidence of IGF binding activity in the carboxyl-terminal domain of IGFBPs. Both native IGFBP-2 (33kDa) and a 21kDa IGFBP fragment were purified from the BRL-3A rat liver cell line and shown to possess differing N-termini. The 21kDa fragment of rIGFBP-2 (270 amino acids) has as its N-terminus amino acid residue 148. No mass spectroscopy data were obtained for this fragment. Although the 21kDa carboxyl-terminal fragment bound ^{125}I-IGF-I by affinity cross-linking, it bound with 5- to 15-fold lower affinity than the 33kDa protein and was not recognised by polyclonal antibodies to native IGFBP-2.

Recently, Ho and Baxter (1997) isolated from human milk a C-terminal fragment of IGFBP-2 ($^{169\text{-}289}$IGFBP-2) that demonstrated less than 10 % binding to ^{125}I-IGF-I and 25 % binding to ^{125}I-IGF-II compared with wildtype hIGFBP-2 in solution binding assays. These results indicate the C-terminal domain of hIGFBP-2 contains at least one of the determinants for IGF binding. Horney and co-workers (2001) have complemented these studies using photoaffinity labelled rhIGFBP-2 to confirm that C-terminal residues 212-227 and 266-287 are involved in IGF-I interactions.

Carboxyl-terminal deletion and chemical modification studies have highlighted the importance of these residues in IGF binding. Progressive C-terminal truncations have been

```
IGFBP-1   1   --------APWQCAPCSAEKLALCPPVSA---------------SCSEVTRS--A--GCGCCPMCALPLGAACGVATARCARGLSCRALPGEQQP
IGFBP-2   1   -------EVLFRCPPCTPERLAACGPPPVAPPAAVAAVAGGARMPCAELVRE--P--GCGCCSVCARLEGEACGVYTPRCGQGLRCYPHPGSELP
IGFBP-3   1   GASSGGLGPVVRCEPCDARALAQCAPPPA---------------VCAELVRE--P--GCGCCLTCALSEGQPCGIYTERCGSGLRCQPSPDEARP
IGFBP-4   1   -------DEAIHCPPCSEEKLARCRPP----------------VGCEELVRE--P--GCGCCATCALGLGMPCGVYTPRCGSGLRCYPPRGVEKP
IGFBP-5   1   ------LGSFVHCEPCDEKALSMCPPSP---------------LGCE-LVKE--P--GCGCCMTCALAEGQSCGVYTERCAQGLRCLPRQDEEKP
IGFBP-6   1   --------ALARCPGCGQGVQAGCP------------------GGCVEEEDGGSPAEGCAEAEGCLRREGQECGVYTPNCAPGLQCHPPKDDEAP

IGFBP-1  69   LHALTRGQGACVQESDAS----------------------APHAAEAG-SPESPESTEITEEELLDNFHLMAPSEEDHSILWDAISTYDGSK--
IGFBP-2  85   LQALVMGEGTCEKRRDAEYGASPEQVADNGDDHSEGGLVENHVDSTMNMLGGGGSAGRKPLKSGMKELAVFREKVTEQHRQMGKGGKHHLGLEE-
IGFBP-3  77   LQALLDGRGLCVNASAVSRLRAYLLPAPPAPGNASESEEDRSAGSVESPSVSSTHRVSDPKFHPLHSKIIIIKKGHAKDSQRYKVDYESQSTDTQ
IGFBP-4  69   LHTLMHGQGVCMELAEIEA------------------------IQESLQPSDKDEGDHPNNSFSPCSAHDRRCLQKHFAKIRDRSTSGGKMKVN
IGFBP-5  70   LHALLHGRGVCLNEKSYR------EQVKIER-DSREHEEPTTSEMAEETYSPKIFRPKHTRISELKAEAVKKDRRKKLTQSKFVGGAENTAHPRI
IGFBP-6  70   LRALLLGRGRCLPARAPA-------------------------VAEE----------NPKESKPQAGTARPQDVNRRDQQRNPGTSTTPSQP--

                                                                                  *****                  **
IGFBP-1 138   -ALHVTNIKKWKEPCRIELYRVVESLAKAQETSGEE----ISKFYLPNCNKNGFYHSRQCETSMDGEAGLCWCVYPWNGKRIPGSPEI-RGDPNC
IGFBP-2 179   --PKKLRPPPARTPCQQELDQVLERISTMRLPDERGPLEHLYSLHIPNCDKHGLYNLKQCKMSLNGQRGECWCVNPNT-GKLIQGAPTIRGDPEC
IGFBP-3 172   NFSSESKRETEYGPCRREMEDTLNHLKFLNVLSPRG-------VHIPNCDKKGFYKKKQCRPSKGRKRGFCWCVDKYG-QPLPGYTTKGKEDVHC
IGFBP-4 139   GAPREDARPVPQGSCQSELHRALERLAASQSRTHED----LYIIPIPNCDRNGNFHPKQCHPALDGQRGKCWCVDRKTGVKLPGGLEP-KGELDC
IGFBP-5 158   ISAPEMRQESEQGPCRRHMEASLQELKASPRMVPRA-------VYLPNCDRKGFYKRKQCKPSRGRKRGICWCVDKYG-MKLPGMEYV-DGDFQC
IGFBP-6 127   --NSAGVQDTEMGPCRRHLDSVLQQLQTEVYRGAQT-------LYVPNCDHRGFYRKRQCRSSQGQRRGPCWCVDRMG-KSLPGSPDGNG-SSSC

IGFBP-1 227   QIYFNVQN-----------
IGFBP-2 271   HLFYNEQQEARGVHTQRMQ
IGFBP-3 259   YSMQSK-------------
IGFBP-4 229   HQLADSFRE----------
IGFBP-5 244   HTFDSSNVE----------
IGFBP-6 211   PTGSSG-------------
```

Figure 1.11b IGF binding studies targeting the C-terminal region of IGFBP

Details of the studies can be found in Section 1.5.2. Residues from different IGFBPs were targeted and have been mapped to the human IGFBP sequence. (PM)=point mutation, (F)=fragment, (Del)=deletion.

IGFBP-1: (PM) Jones *et al.*, 1993a; (PM) Brinkman *et al.*, 1991b; IGFBP-2: (Del) Forbes *et al.*, 1998;
IGFBP-3: (F) Spencer and Chan, 1995; (Del) Firth *et al.*, 1998., (PM) Firth *et al.*, 1998; IGFBP-4: (residues 121-237) Qin *et al.*, 1998;
IGFBP-5: Kalus *et al.*, 1998; Arai *et al.*, 1996a; Bramani *et al.*, 1999 and Song *et al.*, 2000.

generated for IGFBP-1 (Brinkman *et al.*, 1991b), IGFBP-2 (Forbes *et al.*, 1998) and IGFBP-3 (Hashimoto *et al.*, 1997; Firth *et al.*, 1998). Early truncation studies by Brinkman and co-workers were somewhat compromised by a lack of structural knowledge in the absence of disulfide bonding patterns, and hence disruption of IGF binding may have been attributable to lack of structural integrity reflected by the formation of disulfide linked multimers due to the presence of unpaired cysteine residues (Brinkman *et al.*, 1991b). A more recent deletion study, in which the disulfide bonds were considered, has shown that up to 48 residues of the C-terminus of IGFBP-2 (Δ236-284 bIGFBP-2) could be removed before a dramatic loss in IGF binding was observed (Forbes *et al.*, 1998). Deletion of His223 to Gln284 of bIGFBP-2 resulted in an 80-fold loss of IGF affinity when compared to native bIGFBP-2 in solution binding assays. Substitution of conserved amino acid residues in a corresponding region of hIGFBP-5 (Gly203Lys and Gln209Ala) resulted in approximately 8- and 6-fold reduction in affinity for IGF-I respectively (Bramani *et al.*, 1999). Furthermore, C-terminal residues 222-236 of bIGFBP-2 were shown in mutation studies to be important for normal IGF binding activity (Lucic 2000; *unpublished*).

Despite the evidence of carboxyl-terminal fragments binding IGF, other carboxyl-terminal fragments have been reported not to bind IGF (IGFBP-4: Qin *et al.*, 1998; IGFBP-5: Kalus *et al.*, 1998). Differences may arise from variations in the sensitivity of the binding assay performed. Furthermore, it is possible that harsh treatments involving guanidine and urea during isolation and analysis compromised the structural integrity and hence IGF binding ability of these fragments. The deletion studies by Forbes and co-workers (1998) provided evidence that the entire C-terminal domain of bIGFBP-2 is not essential for IGF binding.

1.5.3 IGF BINDING BY RESIDUES IN THE CENTRAL REGION

The central region of IGFBPs does not appear to be directly involved in binding IGFs (Figure 1.11c). Although the IGFBP-5 fragment 95-134 did not exhibit detectable binding affinity for IGF by BIAcore analysis (Kalus *et al.*, 1998), deletion of amino acid residues 89-184 of hIGFBP-3 reduced IGF binding 40-fold (Firth *et al.*, 1998). Conversely, deletion of amino acid residues 94-119 and 121-141 of hIGFBP-4 did not alter IGF binding activity (Qin *et al.*, 1998). Site directed mutagenesis to target proteolytic cleavage sites within the central linker domain has shown mutations to Lys120Asn, His121Asn (Rees *et al.*, 1998), Lys134Gln, Lys136Gln, Met135Leu and Met135Glu (Conover *et al.*, 1995) of IGFBP-4 and Lys138Asn, Lys139Asn of IGFBP-5 (Imai *et al.*, 1997) did not affect IGF binding. In addition, mutagenesis of sites important for phosphorylation of IGFBP-1, Ser98Ala and Ser101Ala, did not affect the affinity of the molecule for IGF-I (Jones *et al.*, 1993c).

1.5.4 SUMMARY OF THE IGF BINDING SITE ON IGFBPS

Clearly, both the amino- and carboxyl-terminal domains of IGFBPs possess the ability to bind IGF. Interestingly, none of the fragments reported in the literature to date retain full IGF binding activity. It is apparent that critical IGF binding determinants are absent from these fragments and in order to establish a high affinity-binding complex, both N- and C-terminal domains need to be present. A comprehensive knowledge of the residues involved in the IGF·IGFBP interaction will ultimately allow researchers to develop a comprehensive insight into the molecular dynamics of the binding interaction making it possible to produce mutant binding proteins for therapeutic applications.

1.6 FUNCTIONAL CONSEQUENCES OF THE IGF-IGFBP INTERACTION

The classical role of the IGFBPs has been to indirectly modulate IGF activity. IGFBPs are multi-functional proteins; they increase the circulating half-life of IGF ligands, they store IGF in an inert form at tissue specific locations; release IGFs when physiologically appropriate and facilitate the movement of IGFs out of circulation. Recently however, IGFBPs have been attributed their own functions, independent of the IGFs, which include influencing both apoptosis and growth.

1.6.1 IGF-DEPENDENT ACTIONS OF IGFBPS

IGFBPs modulate IGF activity by determining the amount of IGF available to interact with the IGF receptors and indeed, can exert both inhibitory and stimulating control over the interaction. The inhibition of IGF by IGFBPs has been well documented for all IGFBPs at all levels of growth. Because IGF interacts with either IGFBPs or the Type 1 IGF receptor exclusively, IGFs must be released from the IGFBP complex before association with and subsequent activation of the receptor can occur. The release of IGF from the IGFBP complex for interaction with the receptor is achieved primarily through reducing IGFBP affinity for IGFs. As discussed in Section 1.7 below, post-translational modifications including proteolysis, alterations in phosphorylation status (of IGFBP-1) and through conformational change upon binding to the ECM, cell surfaces and cell surface receptors all contribute to reducing IGF affinity. Investigations of IGF release mechanisms and subsequent effect on IGF bioactivity, have most commonly involved the generation of recombinant mutated forms of IGFBPs.

In addition to inhibiting the interaction between IGF and IGF receptors, IGFBPs play a major role in sequestering IGF for storage and potential endocrine function (Guler *et al.*, 1989). In contrast to the relatively short half-life of free IGF (10 to12 minutes), association with IGFBPs increases the circulating half-life of IGF to approximately 15 hours in humans. When

complexed, IGFBPs also influence the tissue distribution and localisation of IGFs through interactions with various cell surface proteins and ECM.

1.6.2 IGF-INDEPENDENT ACTIONS OF IGFBPS

IGFBPs have been classified and characterised according to their ability to interact with and modulate IGF activity. However, it has become apparent that IGFBPs have additional functions that are independent of both binding of the IGFs and activation or inhibition of the Type 1 IGF-receptor. IGF independent actions are well established for IGFBP-3 and IGFBP-5 (Schedlich *et al.*, 1998), and recently, IGFBP-1 and IGFBP-2 have also been attributed with IGF independent roles (Jones *et al.*, 1993a; Oh *et al.*, 1998; Cohen, 2000).

Following years of investigating IGFBP modulation of IGF cellular growth functions, IGFBP-3 and IGFBP-5 were themselves shown to possess specific growth regulatory functions. Both IGFBP-3 and IGFBP-5 can be translocated to and localised within the nucleus, through a nuclear localisation signal located in the basic carboxyl-terminal domain of the IGFBPs (Schedlich *et al.*, 1998). Although the biological significance has not been determined, the binding proteins are suggested to possess a transcriptional regulatory role. Upon entering the nucleus, the IGFBP-3 can bind to the retinoid receptor RXR-alpha (Liu *et al.*, 2000).

Interestingly, IGFBP-3 has been shown to induce apoptosis independent of the Type I IGF receptor and p53, as the apoptotic effect is observed in the p53-negative prostate carcinoma cell line PC-3 (Rajah *et al.*, 1997).

IGFBPs have also been shown to associate with specific cell surface receptors (not IGF receptors). IGFBP-1 and IGFBP-2 contain α5β1 integrin binding motifs (Arg-Gly-Asp) in their carboxyl-terminal domains. The integrins are a family of cell surface receptors that are principally involved in the attachment of cells to the extracellular matrix and are a structural feature of such proteins as fibronectin, fibrinogen and vitronectin (reviewed by Hynes *et al.*, 1987). IGFBP-1 has been shown to specifically bind to α5β1integrin receptors to modulate

FAK (focal adhesion kinase) activity, stimulate cell migration and apoptosis (Perks *et al.*, 1999). Indeed, high concentrations of IGFBP-1 *in vitro* stimulated cell migration in an IGF-independent manner (Jones *et al.*, 1993a) and stimulated re-epithelialization of dermal ulcers in rabbits when co-administered with IGF-I (Galiano *et al.*, 1996). IGFBP-3 has also been shown to associate specifically with cell surface receptors and subsequently inhibit growth in breast cancer cells (Oh *et al.*, 1993). As yet, the IGFBP-3 receptor has not been identified although the type V TGFβ receptor could be a putative IGFBP-3 receptor (Leal *et al.*, 1997; Leal *et al.*, 1999). IGFBP-4 and –5 may also interact with this receptor. Recently, an IGFBP-5 membrane receptor has been purified from osteoblast cells (Andress, 1998) although it remains unidentified at this time.

It may be that the IGFs modulate the function of the binding proteins (Rechler, 1997), a view that continues to be explored.

1.6.3 FUNCTIONAL CONSEQUENCES OF LOSS OF IGFBP

Investigations of the specific roles of the IGF system components have often involved non-physiological conditions and it is thus difficult to attribute consequences as direct or secondary involvement. Knockout and transgenic mice have provided unique information about the IGFs, IGF receptors and the IGFBPs. IGF-I and IGF-II knockout mice have reduced offspring size and an increased incidence of neonatal death (reviewed in Won and Powell-Braxton, 1998; Jones and Clemmons, 1995). In humans, a partial IGF-I gene deletion resulted in severe prenatal and postnatal growth failure (Camacho-Hubner *et al.,* 1999). IGF-I receptor knockout mice exhibit phenotypes culminating in postnatal death (Liu *et al.*, 1993). In contrast to the extreme consequences of IGF and receptor knockouts, disruption of IGFBPs had no major physiological aberrations. Gene knockouts have been reported for IGFBP-2 (Wood *et al.*, 1993), IGFBP-3 (Pintar *et al.*, 1999), IGFBP-4 (Pintar *et al.*, 1998), IGFBP-5 (Pintar *et al.*, 1999) and IGFBP–6 (Pintar *et al.*, 1998). The most significant effects were reported for mice

lacking IGFBP-2, which had a smaller spleen mass (Pintar *et al.*, 1996), and IGFBP-4 deficient mice, which were smaller than their littermates (Pintar *et al.*, 1998). Combinatorial knockouts of up to three of the binding proteins have failed to affect murine viability and hence it appears that other IGFBPs counteract the loss of function (Pintar *et al.*, 1996; Pintar *et al.*, 1999). This apparent functional redundancy further contributes to the complexity of the IGFBP system.

1.7 MODIFICATIONS OF IGFBPS THAT INFLUENCE IGF BINDING

Posttranslational modifications of IGFBPs, including phosphorylation, glycosylation, proteolysis and associations with cell surfaces and cell surface receptors, have been shown to influence IGFBP availability and bioactivity. Interestingly, these modifications occur almost exclusively within the non-conserved central region of IGFBPs as summarised in Figure 1.12.

1.7.1 PHOSPHORYLATION OF IGFBPS

IGFBP-1, IGFBP-3 and IGFBP-5 have been shown to be serine-phosphorylated at multiple sites in their central domains (reviewed by Coverley and Baxter, 1997). Phosphorylation of hIGFBP-1 at serine residues 101, 119 and 169 increases its affinity for IGF-I 6-fold compared to the non-phosphorylated form (Jones *et al.*, 1991; Jones *et al.*, 1993c) however the mechanism by which phosphorylation of hIGFBP-1 increases IGF binding affinity is not known. Interestingly, this was not observed for rIGFBP-1 (Peterkofsky *et al.*, 1998). In contrast to IGFBP-1, phosphorylation of IGFBP-3 did not influence its IGF affinity in competition assays (Hoeck and Mukku, 1994) though it may increase the affinity of IGFBP-3 for ALS and cell surfaces (Coverley and Baxter, 1997). The functional significance of IGFBP-5 phosphorylation is yet to be determined.

```
IGFBP-1   1   --------APWQCAPCSAEKLALCPPVSA---------------SCSEVTRS--A--GCGCCPMCALPLGAACGVATARCARGLSCRALPGEQQP
IGFBP-2   1   -------EVLFRCPPCTPERLAACGPPPVAPPAAVAAVAGGARMPCAELVRE--P--GCGCCSVCARLEGEACGVYTPRCGQGLRCYPHPGSELP
IGFBP-3   1   GASSGGLGPVVRCEPCDARALAQCAPPPA---------------VCAELVRE--P--GCGCCLTCALSEGQPCGIYTERCGSGLRCQPSPDEARP
IGFBP-4   1   -------DEAIHCPPCSEEKLARCRPP----------------VGCEELVRE--P--GCGCCATCALGLGMPCGVYTPRCGSGLRCYPPRGVEKP
IGFBP-5   1   ------LGSFVHCEPCDEKALSMCPPSP---------------LGCE-LVKE--P--GCGCCMTCALAEGQSCGVYTERCAQGLRCLPRQDEEKP
IGFBP-6   1   --------ALARCPGCGQGVQAGCP-----------------GGCVEEEDGGSPAEGCAEAEGCLRREGQECGVYTPNCAPGLQCHPPKDDEAP

IGFBP-1  69   LHALTRGQGACVQESDAS------------------- ---APHAAEAG-SPESPESTEITEEELLDNFHLMAPSEEDHSILWDAISTYDGSK--
IGFBP-2  85   LQALVMGEGTCEKRRDAEYGASPEQVADNGDDHSEGGLVENHVDSTMNMLGGGGSAGRKPLKSGMKELAVFREKVTEQHRQMGKGGKHHLGLEE-
IGFBP-3  77   LQALLDGRGLCVNASAVSRLRAYLLPAPPAPGNASESEEDRSAGSVESPSVSSTHRVSDPKFHPLHSKIIIIKKGHAKDSQRYKVDYESQSTDTQ
IGFBP-4  69   LHTLMHGQGVCMELAEIEA-------------------------IQESLQPSDKDEGDHPNNSFSPCSAHDRRCLQKHEAKIRDRSTSGGKMKVN
IGFBP-5  70   LHALLHGRGVCLNEKSYR------EQVKIER-DSREHEEPTTSEMAEETYSPKIFRPKHTRISELKAEAVKKDRRKKLTQSKFVGGAENTAHPRI
IGFBP-6  70   LRALLLGRGRCLPARAPA--------------------------VAEE----------NPKESKPQAGTARPQDVNRRDQQRNPGTSTTPSQP--

IGFBP-1 138   -AIHVTNIKKWKEPCRIELYRVVESLAKAQETSGEE----ISKFYLPNCNKNGFYHSRQCETSMDGEAGLCWCVYPWNGKRIPGSPEI-RGDPNC
IGFBP-2 179   --PKKLRPPPARTPCQQELDQVLERISTMRLPDERGPLEHLYSLHIPNCDKHGLYNLKQCKMSLNGQRGECWCVNPNT-GKLIQGAPTIRGDPEC
IGFBP-3 172   NFSSESKRETEYGPCRREMEDTLNHLKFLNVLSPRG-------VHIPNCDKKGFYKKKQCRPSKGRKRGFCWCVDKYG-QPLPGYTTKGKEDVHC
IGFBP-4 139   GAPREDARPVPQGSCQSELHRALERLAASQSRTHED----LYIIPIPNCDRNGNFHPKQCHPALDGQRGKCWCVDRKTGVKLPGGLEP-KGELDC
IGFBP-5 158   ISAPEMRQESEQGPCRRHMEASLQELKASPRMVPRA-------VYLPNCDRKGFYKRKQCKPSRGRKRGICWCVDKYG-MKLPGMEYV-DGDFQC
IGFBP-6 127   --NSAGVQDTEMGPCRRHLDSVLQQLQTEVYRGAQT-------LYVPNCDHRGFYRKRQCRSSQGQRRGPCWCVDRMG-KSLPGSPDGNG-SSSC

IGFBP-1 227   QIYFNVQN-----------
IGFBP-2 271   HLFYNEQQEARGVHTQRMQ
IGFBP-3 259   YSMQSK-------------
IGFBP-4 229   HQLADSFRE----------
IGFBP-5 244   HTFDSSNVE----------
IGFBP-6 211   PTGSSG-------------
```

Figure 1.12 Sites of post-translational modifications on IGFBPs

Details of the studies can be found in Section 1. All residues have been mapped to human IGFBPs. Heparin ( ) and RGD ( ) binding motifs are sites of IGFBP localisation to cell surfaces/ECM and cell surface receptors. Potential N-glycosylation ☐ and O-glycosylation sites ☐ are indicated. Sites of proteolytic cleavage are found predominantly in the central region of IGFBPs. Potential cleavage sites are boxed ☐ and experimentally determined cleavage sites are indicated as follows:

IGFBP-2: Wang *et al.*, 1988; Ho and Baxter, 1997; IGFBP-3 Binoux *et al.*, 1988; Okabe *et al* 1999;
IGFBP-4: Chernausek *et al.*, 1995, Standker *et al.*, 1999; Byun *et al.*, 2000;
IGFBP-5: Standker *et al.*, 1999.

1.7.2 GLYCOSYLATION OF IGFBPS

The oligosaccharide moieties of glycoproteins are well known sites for cell surface and extracellular matrix interactions, and have been proposed to both retard the rate of clearance of a protein from the circulation and offer protection against proteolysis (reviewed by Varki, 1993). Whilst glycosylation has been observed for IGFBP-3 (Zapf *et al.*, 1988), IGFBP-4 (Ceda *et al.*, 1991), IGFBP-5 (Conover and Kiefer, 1993), and IGFBP-6 (Bach *et al.*, 1992), it appears to bear no influence on the affinity of IGF interactions (Conover, 1991; Sommer *et al.*, 1991; Firth and Baxter, 1995; Neumann *et al.*, 1998). Glycosylation did however reduce the association of IGFBP-3 with cell surfaces (Firth and Baxter, 1999) and increased the resistance of IGFBP-6 to proteolytic cleavage by chymotrypsin and trypsin (Neumann *et al.*, 1998). Interestingly, the glycosylation sites of IGFBP-3 and IGFBP-6 as well as the putative glycosylation site of IGFBP-4 all occur in the connecting domain of the IGFBPs.

1.7.3 PROTEOLYSIS OF IGFBPS

IGFBPs' biological actions are greatly influenced by proteolysis, a regulatory mechanism of protein function (reviewed by Rajah *et al.*, 1995; Fowlkes *et al.*, 1997). In fact, degradation of the IGFBP is believed to be a key component in the regulation of differentiation of specific cell types. The specific cleavage of IGFBPs by proteases dramatically reduces the affinity of IGFBPs for IGF molecules, releasing the ligand for subsequent interaction with the IGF receptor and signalling. Indeed, proteolytic fragments with significantly reduced affinity for IGFs have been reported for IGFBP-1 (Huhtala *et al.*, 1986), IGFBP-2 (Wang *et al.*, 1988; Cohick and Clemmons, 1993; Gockerman and Clemmons, 1995; Ho and Baxter, 1997), IGFBP-3 (Baxter and Skriver, 1993; Lassarre and Binoux, 1994; Lalou *et al.*, 1995), IGFBP-4 (Conover and Kiefer, 1993; Durham *et al.*, 1995) and IGFBP-5 (Andress *et al.*, 1993; Nam *et al.*, 1994; Thrailkill *et al.*, 1995). Interestingly, no protease specific cleavage of IGFBP-6 has been reported in the literature to date. Furthermore, IGFBP-4 and IGFBP-5 have been made

protease resistant by specific site directed mutagenesis of protease sensitive sites (Conover *et al.*, 1995).

IGFBP proteolysis is prominent in pregnancy and in response to trauma (reviewed by Maile and Holly, 1999). During pregnancy, IGFBP proteases degrade IGFBP-3 into smaller fragments that often display reduced affinity for IGF (Muller *et al.*, 1994). While the partially proteolysed IGFBP-3 fragments remain in the 150kDa complex, their decreased affinity for IGF results in an increased availability of free ligand essential for foetal development (Suikkari and Baxter, 1991). In addition, children with solid tumours or leukaemia had significantly higher IGFBP-3 protease activity in serum than control or remissive patients (Muller *et al.*, 1994). Proteolysis of IGFBP-3 reduces the amount of functional IGFBP available for mediating IGF function; hence proteolysis may contribute to tumour progression and metastasis. Indeed, IGFBP fragments resulting from proteolysis can themselves modulate IGF activity (Andress *et al.*, 1993; Lalou *et al.*, 1997; Zadeh and Binoux, 1997).

Investigations have revealed that specific proteases exist for each of the IGFBPs and that IGFBP cleavage is predominantly localized to the unique central region (Wang *et al.*, 1988; Chernausek *et al.*, 1995; Conover *et al.*, 1995; Ho and Baxter, 1997; Lalou *et al.*, 1997). Some of the proteases implicated so far include plasmin for IGFBP-2 (Menouny *et al.*, 1997) and cathepsin D (Conover and De Leon, 1994), prostate specific antigen in seminal plasma (Cohen *et al.*, 1992) and matrix metalloproteinase-9 (Manes *et al.*, 1999) for IGFBP-3. Pregnancy-associated plasma protein-A, purified from human fibroblast conditioned medium, was shown to be an IGF-dependent protease for IGFBP-4 (Lawrence *et al.*, 1999). Interestingly, IGFBP-4 proteolysis is dramatically enhanced through binding to IGF (Fowlkes and Freemark, 1992; Conover *et al.*, 1993; Byun *et al.*, 2000), while IGF reduces IGFBP-5 proteolysis in human osteoblast cell conditioned medium (Conover and Kiefer, 1993). IGFBP-5 proteolysis has also been attributed to complement secreted by fibroblasts and smooth muscle cells (Clemmons *et al.,* 1999). Cancer proteases secreted from prostate and breast cancer cell lines have been proposed to act as growth stimulators by increasing local IGF bioavailability (Conover *et al.*, 1995; Salahifar *et al.*, 1997).

1.7.4 CELL ASSOCIATION BY IGFBPS

IGFBPs associate with extracellular matrix (ECM) and cell surfaces through glycosaminoglycans such as heparin. Binding of IGF/IGFBP complexes to the ECMs facilitates localisation of IGF in close proximity to receptors for subsequent cellular signalling. Indeed the IGF-II:IGFBP-2 complex stimulates cell proliferation in human osteoblast cell cultures rich in ECM, however normal IGF-II activity is inhibited by this complex in cell cultures where little ECM exists (Khosla *et al.*, 1998). Interestingly, patients with hepatitis-C associated osteosclerosis produce increased levels of IGFBP-2 and subsequently exhibit an increase in bone mass (Khosla *et al.*, 1998).

One consequence of the interaction with ECM and cell surfaces is the reduction in IGF binding affinity (Jones *et al.*, 1993c; Arai *et al.*, 1994). Arai and co-workers (1994) observed a 17-fold decrease in affinity of IGFBP-5 for IGF-I upon incubation with glycosaminoglycans. Furthermore, IGFBP-5 associated with a cell culture derived matrix was shown to potentiate the biological actions of IGF-I (Jones *et al.*, 1993b). Hence, binding of the IGF:IGFBP complex to the ECM may be a mechanism to both localise and release IGF to sites where it is required, through altering the IGFBP affinity for the IGF ligand.

IGFBPs have been shown to associate with a number of extracellular components including heparin. A heparin consensus sequence exists in the C-terminal cysteine-rich domains of all IGFBPs with the exception of IGFBP-4 (Cardin and Weintraub, 1989; Hodgkinson *et al.*, 1994; Booth *et al.*, 1996; Fowlkes and Serra, 1996; Firth *et al.*, 1998). Synthetic peptides corresponding to the heparin-binding motif inhibited the ability of both IGFBP-3 and IGFBP-5 to associate with the extracellular matrix and endothelial cell surfaces (Booth *et al.*, 1995; Parker *et al.*, 1996). Furthermore, the mutagenic disruption of this site in IGFBP-3 (Firth *et al.*, 1998) and IGFBP-5 (Arai *et al.*, 1996b) led to a reduction in heparin affinity and abolished cell surface binding. IGFBP-5 is also able to bind types-III and -IV collagen, laminin and fibronectin (Jones *et al.*, 1993b). IGFBP-2, in contrast to the other high affinity binding proteins, binds ECM better in the presence of IGF ligand (Arai *et al.*, 1996a). Presumably this

is a consequence of an altered conformational state that exposes a glycosaminoglycan-binding site. Russo and co-workers used rat brain cells from the olfactory bulb to confirm that IGFBP-2 binds to components of the extracellular matrix, which include the glycosaminoglycans chondroitin -4 and -6 sulfate, keratin sulfate and heparin (Russo *et al.*, 1997).

Heparin inhibits the formation of IGFBP-3 and IGFBP-5 complexes with IGF-I and also disrupts pre-formed complexes (Arai *et al.*, 1996a). Site directed mutagenesis of the residues Arg201, Lys202, Lys206 and Arg214 of rIGFBP-5 affected heparin- but not IGF-binding while mutation of residues Gly203 and Glu209 produced a 3-fold reduction in the affinity for IGF (Song *et al.*, 2000). These results suggest that while differing residues are involved in IGF- and heparin-binding, these sites overlap in the region 201-214 of rIGFBP-5. Interestingly, the heparin-binding motif of IGFBP-3 (residues 228-232) also contributes to ALS binding. Indeed, co-incubation of IGFBP-3 with heparin inhibited the association of ALS with IGFBP-3 (Baxter, 1990; Firth *et al.*, 1998).

1.8 AIMS AND EXPERIMENTAL STRATEGY

IGFBPs play an integral role in regulating IGF activity as they can both potentiate and inhibit IGF action. The structural and functional properties of the IGFBPs however, remain poorly defined at the time this project commenced and the IGF binding site on IGFBPs had not been determined. In addition, there is limited secondary and tertiary structural information regarding the IGFBPs, thereby severely limiting the investigation of IGF-IGFBP structure and function relationships. The aim of this research therefore, is to increase the understanding of bIGFBP-2 structure and to specifically identify and characterise the residues of IGFBP-2 that comprise the IGF binding site. Novel insight into the IGF binding site of IGFBP-2 will enable the design and production of IGFBP analogs with altered IGF affinity or specificity for therapeutic applications.

The systematic identification of an IGF-binding motif on IGFBPs has recently become a priority of IGF research. As discussed in Section 1.7, there is increasing evidence to suggest that both the amino- and carboxyl-terminal domains of IGFBPs contain information pertinent for IGF binding. Many of these studies however, are incompletely defined and inhibited by a lack of structural knowledge, mass spectroscopy data and binding assay sensitivity. Thus, the initial research goal of this thesis was to identify the IGF binding site(s) of bIGFBP-2. The strategy involved generating discrete modules of bIGFBP-2 encompassing the amino-terminal and carboxyl-terminal domains and assessing their IGF binding properties by BIAcore analysis. These fragments were generated on the basis of sequence alignments, exon coding regions (Landale *et al.*, 1995) and naturally occurring IGFBP fragments (Huhtala *et al.*, 1986; Wang *et al.*, 1988; Hashimoto *et al.*, 1997; Ho and Baxter, 1997; Kalus *et al.*, 1998; Standker *et al.*, 1998).

The amino- and carboxyl-terminal fragments of bIGFBP-2 enabled investigation of the roles of these domains in IGF binding. Three key experiments were performed. Firstly, the kinetics of the interaction between IGF and IGFBP-2 fragments were assessed in straightforward kinetic experiments. Secondly, the possibility of reconstituting the high affinity

interaction was investigated using a variety of approaches including pre-incubation and sequential injection of amino- and carboxyl-terminal fragments across biosensor surfaces. Finally, IGF analogues were used to define the orientation of the molecule in the binding complex.

The second major goal of this thesis was to further define the structure of the bIGFBP-2 molecule. To date, structure studies have been inhibited by molecular size constraints and the absence of a large-scale production system for IGFBP. In this study, structure determination techniques involved analysis by NMR, X-ray crystallization and electron microscopy. In addition to structure determination, NMR was also used to investigate the specific residues of IGF involved in binding IGFBP-2 by analysing backbone chemical shifts in the presence and absence of the binding protein. A similar strategy has been used previously to define residues of IGF-I involved in binding IGFBP-1 (Jansson *et al.*, 1998). Furthermore, the amino- and carboxyl-terminal fragments generated in this study were important tools to specifically define the IGFBP binding site on both IGF-I and IGF-II. Such structure determination studies will ultimately provide a comprehensive insight into the molecular dynamics of the binding interaction.

CHAPTER 2

GENERATION OF VECTORS FOR THE EXPRESSION OF TRUNCATED bIGFBP-2 FRAGMENTS

2.1 INTRODUCTION

Whilst the role of the IGFBPs in modulating IGF activity is widely accepted, the exact mechanism of interaction and the IGF binding sites on the IGFBPs have yet to be elucidated. The proposed IGF binding site on the IGFBPs is believed to be located within the highly conserved regions of IGFBPs and indeed both the amino-and carboxyl-terminal domains of IGFBPs have been shown to bind IGF (reviewed by Hwa *et al.*, 1999; Baxter, 2000). Insight into the IGF binding site of IGFBPs has been derived from naturally occurring and recombinant fragments of IGFBPs, deletion and chemical modification studies and NMR analysis (as discussed in Chapter 1). Many of the IGFBP fragments used in these studies have been poorly defined and in some cases, the sensitivity of binding assay used may not reflect the true binding properties of the IGFBP fragments or truncations being investigated. None of the IGFBP fragments reported to date retain wildtype IGF binding affinity. It is unclear therefore, where the major IGF binding site resides.

One of the objectives of the current thesis is to define the IGF binding site of bovine IGFBP-2 (bIGFBP-2). The strategy involved targeting the highly conserved amino- and carboxyl-terminal domains of bIGFBP-2 by expressing various truncations and characterising their IGF binding properties by BIAcore analysis. Amino-terminal fragments encoding amino acid residues 1-93, 1-104, 1-132 and 1-185 and carboxyl-terminal fragments encoding amino acid residues 96-279, 136-279, 182-284 were generated in this study as outlined in Figure 2.1. Concomitant availability of amino- and carboxyl-terminal fragments will permit direct comparison of their contribution to IGF binding and provide a comprehensive understanding of the molecular interactions involved. The objective is to answer some of the many questions about the IGF binding site on IGFBPs and the function of naturally occurring IGFBP fragments. What are the smallest amino- and carboxyl-terminal fragments capable of binding IGF and which of these most resemble wildtype IGFBP binding? What are the IGF binding characteristics of the two highly conserved domains and what are the biological and

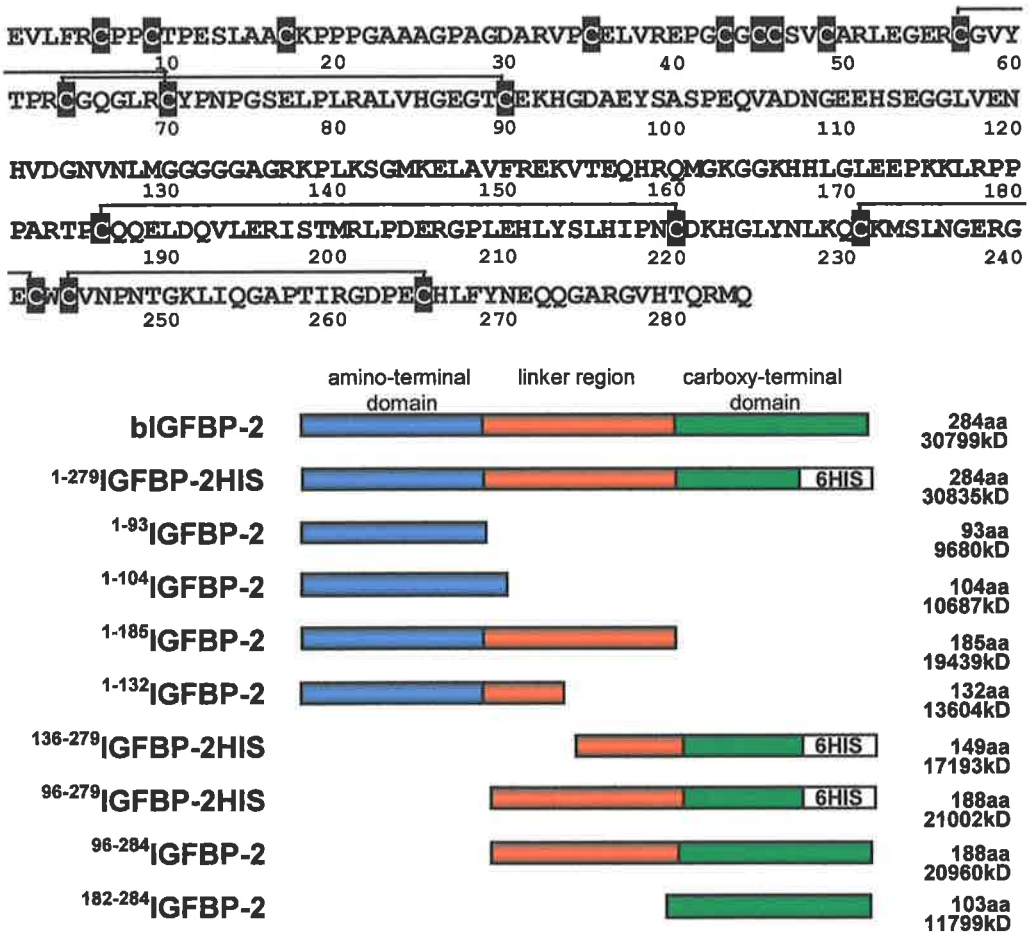

Figure 2.1 Amino acid sequence and schematic representation of wildtype bIGFBP-2 and the truncated constructs

The amino acid sequence of bIGFBP-2 is shown in the single letter code. Conserved cysteine residues are boxed and known disulfide bonds are indicated with connecting lines. Wildtype bIGFBP-2 and truncated analogues are represented as boxes and the proposed amino-, carboxyl- and linker-domains are indicated. The predicted peptide masses and residue lengths are shown to the right of the figure and the inclusion of hexahistidine-tags is indicated as open boxes.

physiological consequences of the interactions? Can the high affinity binding interaction between IGF and IGFBP be reconstituted using the truncated amino- and carboxyl-terminal fragments?

Identifying the specific residues of IGFBP-2 involved in the IGF binding interaction will contribute significantly to our understanding of the molecular interaction. However, the absence of a tertiary structure severely limits the investigation of IGF-IGFBP structure and function relationships. Structure determination studies will ultimately provide a comprehensive insight into the molecular dynamics of the binding interaction making it possible to produce mutant binding proteins specific for a particular IGF for therapeutic applications. Structure determination studies have been inhibited to date by the inability to obtain IGFBP crystals and by the fact that the molecular masses of the IGFBPs are at the upper limit of resolution for nuclear magnetic resonance (NMR) spectroscopy analysis. Hence, generation of discrete amino- and carboxyl-terminal modules of the native protein will contribute greatly to the elucidation of the structure of bIGFBP-2.

The studies presented in this thesis required the recombinant expression of full-length and truncated IGFBP-2 fragments. Furthermore, large quantities of protein are essential for structure determination studies. The cDNA encoding bIGFBP-2 was originally isolated from Madin Darby bovine kidney (MDBK) cells in this laboratory (Upton et al., 1990). The cDNA for the signal sequence and bIGFBP-2 were inserted into the expression vector pXMT2 (Rathjen *et al.*, 1990) to yield pGF8 (Forbes *et al.*, 1998). Bovine IGFBP-2 has since been routinely expressed in, and secreted from, COS-1 cells. This system provided the cellular machinery required for the correct processing and expression of bIGFBP-2 and hence was anticipated to similarly process and express the truncated forms of bIGFBP-2. Although this system was capable of generating active bIGFBP-2, an *E. coli* expression system for large-scale production of native and truncated IGFBP-2 was also established.

On the basis of sequence alignments, exon coding regions (Landale *et al.*, 1995) and naturally occurring IGFBP fragments (Huhtala *et al.*, 1986; Wang *et al.*, 1988; Hashimoto *et*

al., 1997; Ho and Baxter, 1997; Kalus *et al.*, 1998; Standker *et al.*, 1998), discrete modules of the native protein encompassing the amino-terminal domain (amino acid residues 1-93, 1-104, 1-132 and 1-185) and carboxyl-terminal domain (amino acid residues 96-279, 136-279, 182-284) of bIGFBP-2 were targeted for investigation (Figure 2.1). This chapter describes the construction of mammalian and *E. coli* expression vectors encoding truncated bIGFBP-2 sequences as summarized in Table 2.1.

TABLE 2.1 VECTORS CONSTRUCTED FOR THE EXPRESSION OF FULL-LENGTH AND TRUNCATED IGFBP-2

Vectors for mammalian cell expression in the vector pXMT2		*Protein*
pGF8*Apa*I	An *Apa* I restriction site was introduced at the 3' end of the cDNA encoding the leader sequence for subsequent cloning of C-terminal constructs.	bIGFBP-2
pGF8HIS	The cDNA encoding a hexahistidine tag was introduced at the 3' end of the bIGFBP-2 gene corresponding to amino acid residues 279-284.	$^{1-279}$IGFBP-2HIS
pGF8(1-93)	N-terminal construct encoding amino acid residues 1-93.	$^{1-93}$IGFBP-2
pGF8(1-104)	N-terminal construct encoding amino acid residues 1-104	$^{1-104}$IGFBP-2
pGF8(1-132)	N-terminal construct encoding amino acid residues 1-132	$^{1-132}$IGFBP-2
pGF8(1-185)	N-terminal construct encoding amino acid residues 1-185	$^{1-185}$IGFBP-2
pGF8(96-279HIS)	C-terminal construct encoding amino acid residues 96-279HIS.	$^{96-279}$IGFBP-2HIS
pGF8(96-284)	C-terminal construct encoding amino acid residues 96-284, and incorporating the 3' UTR.	$^{96-284}$IGFBP-2
pGF8(137-279HIS)	C-terminal construct encoding amino acid residues 137-279HIS.	$^{137-279}$IGFBP-2HIS
pGF8(185-279HIS)	C-terminal construct encoding amino acid residues 185-279HIS.	$^{185-279}$IGFBP-2HIS
pGF8(185-284)	C-terminal construct encoding amino acid residues 185-284, and incorporating the 3' UTR.	$^{185-284}$IGFBP-2

Vectors for E. coli cell expression in the vector pET32a		*Protein*
pET$^{1-279}$IGFBP-2HIS	The cDNA encoding bIGFBP-2 with a C-terminal histidine tag was introduced into the *E. coli* expression vector pET32a (+) from Novagen.	Trx$^{1-279}$IGFBP-2HIS
pET$^{1-132}$IGFBP-2	N-terminal construct encoding amino acid residues 1-132.	Trx$^{1-132}$IGFBP-2
pET$^{1-185}$IGFBP-2	N-terminal construct encoding amino acid residues 1-185.	Trx$^{1-185}$IGFBP-2
pET$^{136-279}$IGFBP-2HIS	C-terminal construct encoding amino acid residues 136-279 and a six-histidine tag.	Trx$^{136-279}$IGFBP-2HIS

2.2 MATERIALS

2.2.1 BACTERIAL CULTURE MEDIA AND SOLUTIONS

Mrs. J. Brinkman (Central Services Unit, Department of Biochemistry, Adelaide University) prepared the following media and solutions using methods described by Sambrook *et al.*, 1989. All solutions were made in redistilled water using the Milli-Q Ultra Pure Water System (Millipore Pty Ltd, North Ryde, NSW, Australia). Solutions and media were sterilised by autoclave.

2.2.2 BACTERIAL GROWTH MEDIA AND BUFFERS

Luria-Bertani Medium (LB)
1 % (w/v) bacto®tryptone, 0.5 % (w/v) bacto®yeast extract, 0.17 M NaCl pH 7.0

Luria-Bertani Plates (L plates)
LB + 1.5 % (w/v) bacto-agar

2YT
1.6 % (w/v) Bacto tryptone, 1 % (w/v) Bacto yeast extract, 0.5 % (w/v) NaCl
-Adjusted to pH 7.0 with NaOH

Transformation Buffer 1 (TB1)
30 mM KAc, 100 mM RbCl, 10 mM $CaCl_2$ ($2H_2O$), 50 mM $MnCl_2$ ($4H_2O$), 15% glycerol
-Adjusted to pH 5.8 and filter sterilised

Transformation Buffer 2 (TB2)
10 mM 3-N-morpholinopropanesulfonic acid (MOPs), 10 mM RbCl, 75 mM $CaCl_2$ ($2H_2O$), 15 % glycerol
-Adjusted to pH 6.5 and filter sterilised

2.2.3 BACTERIAL STRAINS

***E. coli* DH5-α:** supE44, ΔlacU169, hsdR17, recA1, endA1, gyrA96, λ^-, relA1, [ϕ80lacZΔM15]
***E. coli* BL21:** *E. coli* B F^-dcm ompT hsdS ($r_B^- m_B^-$) gal (DE3)
***E. coli* CJ236:** *dut*$^-$, *ung*$^-$, *thi*$^-$, *rel*A1; pCJ105 (Cm^r)

2.2.4 MATERIALS FOR MOLECULAR BIOLOGY

Bacto®tryptone and bacto®yeast extract were purchased from DIFCO Laboratories, MI, USA. Ammonium persulphate, ampicillin, chloramphenicol, ethidium bromide, kanamycin, lithium chloride, lysozyme, polyethylene glycol (PEG) 6000, proteinase K and ribonuclease A (RNase A) were obtained from Sigma Chemical Co. MO, USA. Special grade phenol was purchased from Wako Pure Chemicals Industries Limited, Osaka, Japan. Chloroform and ammonium acetate were from BDH Chemicals Australia Pty. Ltd., Kilsyth, Victoria, Australia. SPP1 and pUC 19 DNA molecular weight markers and restriction endonucleases *Apa* I and *Pst* I were obtained from Geneworks, Thebarton, South Australia, Australia. *Dpn* I, *Nco* I, *Not* I and *Sma* I were obtained from New England Biolabs, Beverly, MA, USA, while *Eco*R I and the universal restriction endonuclease buffer, One Phorall Plus Buffer, were from Pharmacia Biotechnology International, AB, Sweden. Pwo DNA polymerase, T4 DNA ligase, T4 polynucleotide kinase, calf intestinal phosphatase (CIP) and CIP buffer were obtained from Boehringer Mannheim Australia, Sydney, NSW, Australia. All reagents used were of analytical grade.

2.2.5 SOLUTIONS FOR DNA PROCEDURES

PCR reaction Buffer
50 mM Tris-HCl pH 9.0, 20 mM $(NH_4)_2SO_4$, 0.005 % BSA, 0.25 mM dNTPs, 3 mM $MgCl_2$

Tris Borate EDTA (TBE)
0.09 M Tris, 0.09 M boric acid, 2.5 mM EDTA

Ethidium Bromide Stain (working stock)
0.1 mg/ml ethidium bromide prepared in distilled water

10 x DNA loading dye
50 % (v/v) glycerol, 0.25 % (w/v) bromophenol blue, 0.25 % (w/v) xylene cyanol FF

Tris EDTA (TE)
10 mM Tris, pH 7.5, 0.1 mM EDTA

2.2.6 KITS FOR MOLECULAR BIOLOGY

The GENECLEAN Kit for clean DNA was obtained from Bio 101 La Jolla, CA, USA. The Geneworks Gel extraction kit and the Geneworks Plasmid DNA kit were obtained from Geneworks, Thebarton, SA, Australia. The QuikChange Site Directed Mutagenesis Kit was obtained from Stratagene, CA, USA; while the Muta-Gene Phagemid Kit was obtained from Bio-Rad Pty. Ltd., North Ryde, NSW, Australia. The ^{T7}Sequencing Kit was purchased from Amrad Pharmacia Biotech, Boronia, Victoria, Australia. The ABI PRISM Dye Terminator Cycle Sequencing Ready Reaction Kit with AmpliTaq DNA polymerase was obtained from Perkin Elmer, Norwalk, CT, USA while the *fmol* DNA Cycle Sequencing System was obtained from Promega Pty. Madison, WI, USA. The ABI PRISM Dye Terminator Cycle Sequencing Ready Reaction Kit was obtained from Perkin Elmer, Norwalk, USA.

2.2.7 VECTORS AND OLIGONUCLEOTIDES

The cDNA for bIGFBP-2 was previously cloned into the multiple cloning site of the pXMT2 expression system (Rathjen *et al.*, 1990) in this laboratory (Forbes *et al.*, 1998) and was subsequently designated pGF8 (Figure 2.2). The pXMT2 vector has routinely been used in the transfection of COS-1 cells. pGF8 was the expression system of choice for the expression of truncated bIGFBP-2 constructs in the present investigation.

The *Pst* I-*Sma* I insert (base pairs 1-331) encoding the leader sequence and first 75 amino acid residues of bIGFBP-2 was previously cloned into the pBluescript-II (KS$^-$) vector (Stratagene, CA, USA) yielding pGDH-1 (Hobba *et al.*, 1996). This vector was used as the template for the introduction of an *Apa* I restriction site at the 3' end of DNA encoding the leader sequence.

2.2.7.1 Vectors

pXMT2	Rathjen *et al.*, 1990.	
pGF8	Forbes *et al.*, 1998.	Figure 2.2
pGF14	Lucic *et al.*, 1998.	Figure 2.11
pKS$^-$	Stratagene, CA, USA	
pGDH1	Hobba *et al.*, 1996.	
pET32a (+)	Novagen, Madison, USA.	Figure 2.3

Oligonucleotides were designed using Oligo™ 4.0s and Amplify software and were synthesised by Geneworks Pty. Ltd., Thebarton, SA, Australia, except where indicated otherwise. Restriction enzyme sites are underlined.

2.2.7.2 Oligonucleotides:

1:2BP-2:	**ttt agc ttg aat tct tat cca cct ccc atc aag tt** *Oligonucleotide introduces an EcoR I restriction site at the 5' terminus.*
2:2BP-2:	**aaa ggt acc cca tgg ggt cgg aag ccc ctc aag** *Oligonucleotide introduces an Nco I restriction site at the 5' terminus.*
2:2*Apa*IBP-2:	**aaa aat tgg gcc cgg aag ccc ctc aag tcc ggc atg** *Oligonucleotide is complementary to a sequence within IGFBP-2 corresponding to amino acid residues 137-144 and also introduces an Apa I restriction site at the 5' terminus.*
bp2*Apa*Ifor:	**cga ctg cgg ggc ccg cgc cga ggt g** *Oligonucleotide introduces a single base pair change resulting in an Apa I restriction site without changing the amino acid sequence.*
bp2*Apa*Irev:	**cac ctc ggc gcg ggc ccc gca gtc g** *Oligonucleotide introduces a single base pair change resulting in an Apa I restriction site without changing the amino acid sequence.*
LCHIS:	**ttt aag ctt gaa ttc tta gtg gtg gtg gtg gtg gtg cac ccc tcg agc ccc ctg ctg ctc gtt gta** *Oligonucleotide replaces amino acid residues 280-284 with histidine residues and has an engineered EcoR I restriction site at the 5' terminus.*
LongC*Apa*I:	**ttt ttt ggg gcc cgc gcc gct gag tac agc gcc agc** *Oligonucleotide has an engineered Apa I restriction site at the 5' terminus.*
LongN:	**ttt aag ctt gaa ttc tta ggg ggt cct ggc agg** *Oligonucleotide has an engineered EcoR I restriction site at the 5' terminus.*

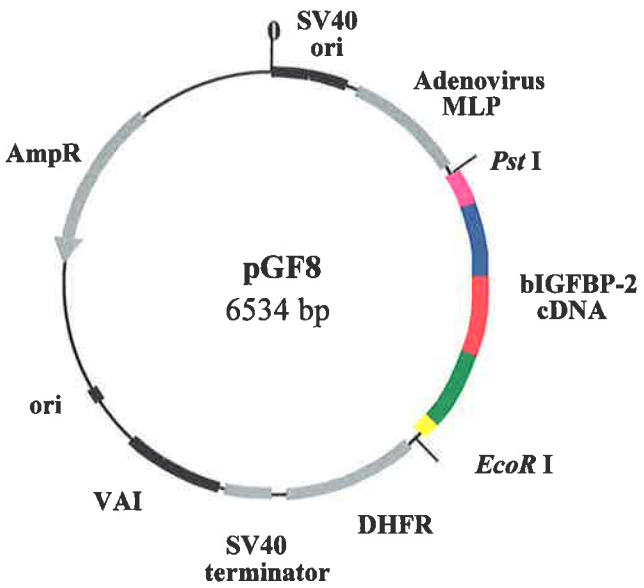

Figure 2.2 pGF8 expression vector
The bovine IGFBP-2 expression vector, pGF8, was constructed from the mammalian expression vector pXMT2 (Rathjen *et al.*, 1990). The bIGFBP-2 insert is 1425 base pairs in length and was cloned using the *Pst* I and *Eco*R I restriction sites. The pXMT2 vector contains the simian virus origin of replication (SV40 ori) and transcriptional enhancer, the adenovirus major late promoter (MLP), the dihydrofolate reductase (DHFR) coding region, the SV40 polyadenylation site (SV40 terminator), the adenovirus VAI gene, the colicin E1 origin of replication (ori) and the β-lactamase ampicillin resistance gene (AmpR).

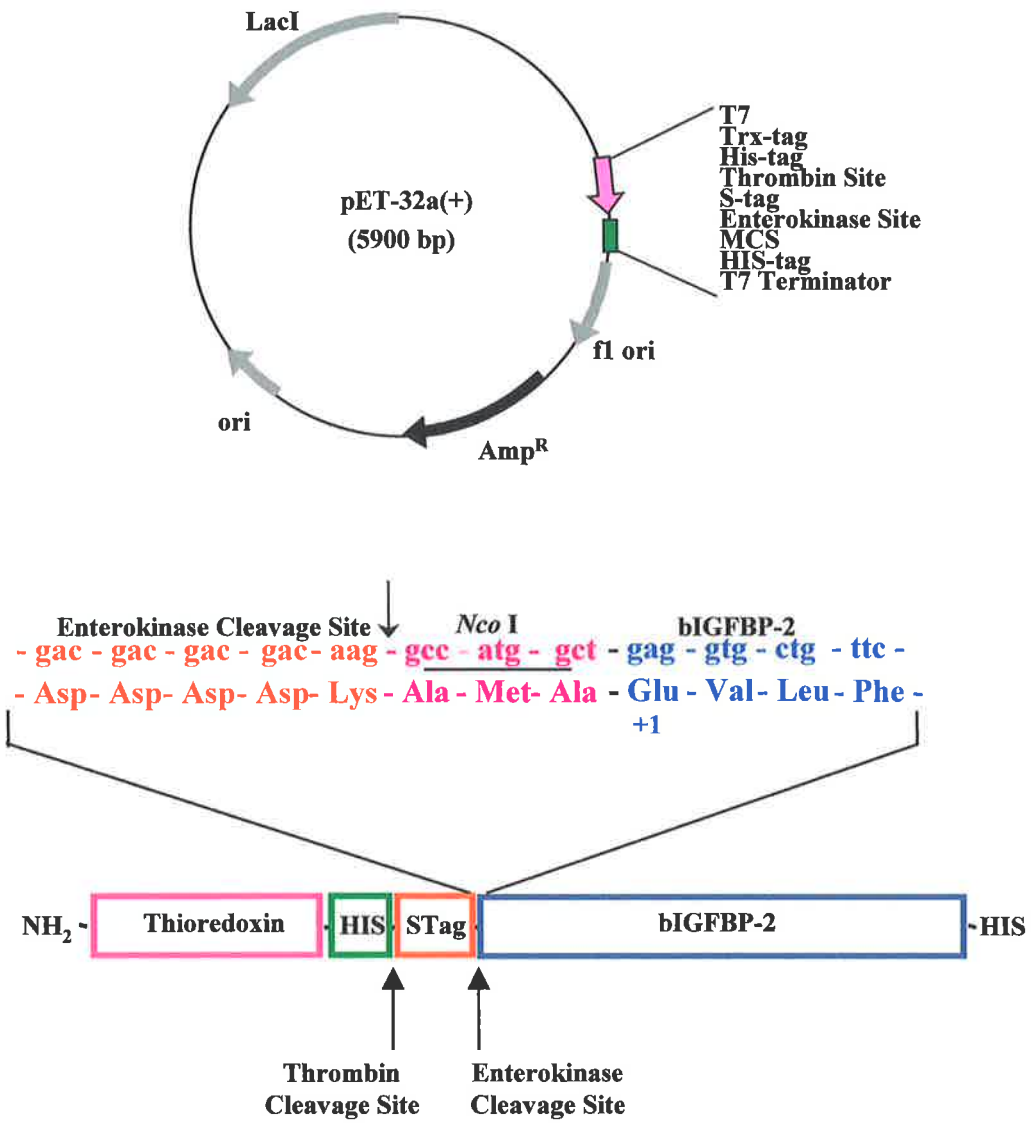

Figure 2.3 pET32a (+) expression vector
The pET32a (+) expression vector (Novagen, Madison, USA) is a high level expression vector designed for the production of protein fused with a 109 amino acid thioredoxin tag. The resultant protein also contains cleavable HIS-tag and S-tag sequences for detection and purification. The pET32a (+) plasmid is under T7 transcriptional regulation and contains the β-lactamase ampicillin resistance gene (AmpR). Cleavage of the resultant fusion protein with enterokinase results in the addition of Ala-Met-Ala at the N-terminus of the bIGFBP-2 sequence.

Oligonucleotides (continued)

Primer 1 (Sigma®):	**gtg aac ttg atg gga ggt gga ggt gat gat gac gat aag ccc ctc aag tcc ggc atg** Oligonucleotide mutates DNA encoding residues 135-138 to encode amino acid residues DDDD.
Primer 2 (Sigma®):	**cat gcc gga ctt gag ggg ctt atc gtc atc atc acc tcc acc tcc cat caa gtt cac** Oligonucleotide mutates DNA encoding residues 135-138 to encode amino acid residues DDDD.
ShortC-2:	**ttt ttt ggg gcc cgc gcc ggc agg ggt ggc aaa cat cac** *Oligonucleotide has an engineered Apa* I *restriction site at the 5' terminus.*
ShortC*Apa*I:	**ttt ttt ggg gcc cgc gcc gcc agg acc ccc tgc cag** *Oligonucleotide has an engineered Apa* I *restriction site at the 5' terminus.*
ShortN:	**ttt aag ctt gaa ttc tta gtg ctt ttc gca agt gcc ctc gcc gtg gac** *Oligonucleotide has an engineered Eco*R I *restriction site at the 5' terminus.*
SJH-5:	**tac gaa ttc tta ctt gtc aca gtt ggg gat gtg tag gga** *Oligonucleotide is complementary to a sequence within IGFBP-2 corresponding to amino acid residues 214-222.*
SN-2	**ttg aat tct tac tgc tcg ggg ctg g** *Oligonucleotide has an engineered Eco*R I *restriction site at the 5' terminus.*
Vic1ex:	**ttg aga tct ggc cat aca ctt gag** *Oligonucleotide is directly complementary to a sequence 5' of IGFBP-2 in the pXMT2 expression vector.*
Vic2:	**gcc ttc aca cgc tag gat t** *Oligonucleotide is directly complementary to a sequence 3' of IGFBP-2 in the pXMT2 expression vector.*

The positions of the oligonucleotide sequences in the pGF8 template are shown in Figure 2.4.

(-156/-52) Vic1ex
TGC CTT TGA GGG TGG CCG CGT CCA TCT GGT GAG AAA AGA CAA TCT TTT TGT TGT CAA GCT TGA GGT GTG GCA GGC TTG AGA TCT GGC CAT
CYS LEU OPA GLY TRP PRO ARG PRO SER GLY GLN LYS ARG GLN SER PHE CYS CYS GLN ALA OPA GLY VAL ALA GLY LEU ARG SER GLY HIS
(-66/-22) *Pst* I
ACA CTT GAG TGA CGG TGA CAT CCA CTT TGC CTT TCT CTC CAC AGG TGT CCA CTC CCA GGT CCA ACT gca ggc cat atg cag ccg aga ctg
THR LEU GLU OPA GLN OPA HIS PRO LEU CYS LEU SER LEU HIS ARG CYS PRO LEU PRO GLY PRO THR ala gly his met gln pro arg leu
Apa I bp2Apa1 rev
(25/9) bp2Apa1 for gcc
ggc ggc ccc gcg ctg ctg ctg ctg ccg ccg ctg ctg ctg ctg ctg ctg ctg ggc gcg ggc ggc ggc gac tgc ggg gcg cgc gcc gag gtg
gly gly pro ala leu leu leu leu pro pro leu leu leu leu leu leu leu gly ala gly glu gly asp cys gly ala arg ala glu val
(115/39) A
ctg ttc cgc tgc ccg ccc tgc acg ccc gag agc ctg gcc gcc tgc aag ccc ccg ccc ggc gcc gcg gcc ggg ccg gcc ggc gac gcc cgc
leu phe arg cys pro pro cys thr pro glu ser leu ala ala cys lys pro pro pro gly ala ala ala gly pro ala gly asp ala arg
(205/69)
gtg ccc tgc gag ctg gtc cgc gag ccg ggc tgc ggc tgc tgc tcc gtg tgc gcc cgg ctg gag gga gag cgg tgc ggc ctc tac acc ccc
val pro cys glu leu val arg glu pro gly cys gly cys cys ser val cys ala arg leu glu gly glu arg cys gly val tyr thr pro
Short N
(295/99) *Sma* I NTERM-3
cgc tgc ggt cag ggg ctg cgc tgc tat ccc aac ccg ggc tcc gag ctg ccc ctg agg gcg ctg gtc cac ggc gag ggc act tgc gaa aag
arg cys gly gln gly leu arg cys tyr pro asn pro gly ser glu leu pro leu arg ala leu val his gly glu gly thr cys glu lys
Long C *Apa* I
(385/129) SN-2
cac ggc gat gct gag tac agc gcc agc ccc gag cag gtt gca gac aac ggc gag gag cac tct gag gga ggc ctg gtc gag aac cac gtg
his gly asp ala glu tyr ser ala ser pro glu gln val ala asp asn gly glu glu his ser glu gly gly leu val glu asn his val
1:2BP-2 2:2apaBP-2
(475/159) primer 1 (sigma) 2:2BP-2 primer 2 (sigma)
gac ggg aac gtg aac ttg atg gga ggt gga ggt ggt gcc ggt cgg aag ccc ctc aag tcc ggc atg aag gag ctg gcc gtg ttc cgg gag
asp gly asn val asn leu met gly gly gly gly gly ala gly arg lys pro leu lys ser gly met lys glu leu ala val phe arg glu
D D D D
(565/189) *Not I*
aag gtc acg gag cag cac cgg cag atg ggc aag ggt ggc aaa cat cac ctc ggc ctg gag gag ccc aag aag ctg cgg ccg cca cct gcc
lys val thr glu gln his arg gln met gly lys gly gly lys his his leu gly leu glu glu pro lys lys leu arg pro pro pro ala
Short C *Apa* I
(655/209) Long N
agg acc ccc tgc cag cag gaa tgg gac cag gtc ctg gag cgg atc tcc acc atg cgc ctt ccg gat gag cgg ggt ccc ctg gag cac ctc
arg thr pro cys gln gln glu leu asp gln val leu glu arg ile ser thr met arg leu pro asp glu arg gly pro leu glu his leu
(745/239) SJH-5
tac tcc cta cac atc ccc aac tgt gac aag cat ggc ctg tac aac ctc aaa cag tgc aag atg tct ctg aac ggg cag cgt ggg gag tgc
tyr ser leu his ile pro asn cys asp lys his gly leu tyr asn leu lys gln cys lys met ser leu asn gly gln arg gly glu cys
(835/269)
tgg tgt gtg aac cct aac acc ggg aag ctg atc cag gga gcc ccc acc atc cgg gga gac ccc gag tgt cat ctc ttc tac aac gcg acg
trp cys val asn pro asn thr gly lys leu ile gln gly ala pro thr ile arg gly asp pro glu cys his leu phe tyr asn glu gln
(925/299) H H H H H LCHIS
cag ggg gct cga ggg gtg cac acc cag cgg atg cag TAA ACC ATA GCC AGC CGG TGC CTG GCA CCC CCA CCA TCC GGG GAG ACC CGA GTG
gln gly ala arg gly val his thr gln arg met gln OCH THR ILE ALA SER ARG CYS LEU ALA PRO PRO PRO SER GLY GLU THR ARG VAL
(1015/329)
TCA CTC TCT TCT ACA ACG AGC AGC AGG GGG CTC GAG GGG TGC ACA CCA GAG GAT GCA GTA AAC CAT AGC CAG CCG GTC CTG GCA CCC CCC
SER LEU SER SER THR THR SER SER ARG GLY LEU GLU GLY CYS THR PRO ALA ASP ALA VAL ASN HIS SER GLN PRO VAL LEU ALA PRO PRO
(1105/359)
ACC TCT TCG GAG CGG GCA GAG CAT GGA GAG CGC ATG CGT GGT GGG TGG CGG GGC AGA GCT TCC AGG AGT TCT GAC ATG TGT ATT TAT ATT
THR SER SER GLU ARG ALA GLU HIS GLY GLU ARG MET ARG GLY GLY TRP ARG GLY ARG ALA SER ARG SER SER ASP MET CYS ILE TYR ILE
(1195/389)
TGG AAA GAG ACC GGC ACC GAG CTC GGC ACA CAC CCC CCC ACC CCC TTC CCC ACC TTC CCC CTC CCC AGC CGG AGA TGC CTG CAC CCT CCC
TRP LYS GLU THR GLY THR GLU LEU GLY THR HIS PRO PRO THR PRO PHE PRO THR PHE PRO LEU PRO SER ARG ARG CYS LEU HIS PRO PRO
(1285/409)
TGC TCG AGG CTT GCT GGG CAG GAA GGG GAT GGT TGC AGT GGC AGA GCT GGG GTA AAT GTT TGG GAG AGG GAA AAA AAG AAA TTT TTA TTT
CYS SER ARG PRO ALA GLY GLN GLU GLY ASP GLY CYS SER GLY ARG ALA GLY VAL ASN VAL TRP GLU ARG GLU LYS LYS LYS PHE LEU PHE
(1375/439) *EcoR* I
TTG AAC CCC TGT GTC TCT TTT GCT TAA GAT TAA AGG AAG GAA AAA TAA GGA ATT CCG GGG GGG GGG GGG GGG GGG ACA GCT CAG GGC TGC
LEU ASN PRO CYS VAL SER PHE ALA OCH ASP OCH ARG LYS GLU LYS OCH GLY ILE PRO GLY GLY GLY GLY GLY GLY THR ALA GLN GLY CYS
(1465/465) Vic2
GAT TTC GCG CCA AAC TTG ACG GCA ATG CTA GCG TGA AGG CTG GTA
ASP PHE ALA PRO ASN LEU THR ALA ILE LEU ALA OPA ARG LEU VAL

↔	Mutagenic oligonucleotides	D	Residues mutated to Aspartate
→	PCR oligonucleotides, direction shown	H	Residues mutated to Histidine
▭	bIGFBP-2 leader sequence	▭	3' non-coding region

Figure 2.4 cDNA encoding the bIGFBP-2 insert in the pXMT2 expression vector
The cDNA encoding bIGFBP-2 was cloned in to pXMT2 by *Pst* I and *Eco*R I restriction sites. The numbering on the left hand side of each line defines the base/amino acid position of the sequence in the pXMT2 vector beginning at the *Pst* I site. The coding region of bIGFBP-2 is presented in lower case and the amino acid residues are numbered below the sequence. The 3' non-coding region is coloured green and the sequence of the pXMT2 vector is in upper case. The leader sequence of bIGFBP-2 is boxed in yellow. Restriction sites are highlighted in coloured font. Arrows positioned above the sequence indicate oligonucleotide primer locations and directions. Where a mutation has been introduced, the amino acid it codes for is defined in the single letter code.

2.3 METHODS

Molecular biology procedures were generally performed as described by Sambrook *et al.*, 1989; and are detailed in this section.

2.3.1 MINI PREPARATION OF PLASMID DNA (SMALL-SCALE)

Plasmid DNA was propagated in the *E. coli* strain DH5-α. LB (5 ml), supplemented with the appropriate antibiotic(s), was inoculated with a single colony containing the plasmid of interest. Following overnight growth at 37 °C with shaking, the cells were recovered by centrifugation at 3200 x g for 10 minutes at room temperature. The cell pellet was resuspended in 100 µl TEG lysis buffer (25 mM Tris-HCl pH 8.0, 10 mM EDTA, 50 mM glucose) and incubated on ice for 5 minutes. Cell rupture was achieved by the addition of 200 µl 0.2 M NaOH, 1 % SDS and incubated on ice with 150 µl 3 M sodium acetate (NaAc) pH 5.2 for 5 minutes. Cellular debris was removed by centrifugation at 13200 x g for 10 minutes at 4 °C. Plasmid DNA in the supernatant was removed to a fresh Eppendorf tube and treated with RNase A (10 µl 2 mg/ml) at 45 °C for 30 minutes. Plasmid preparations were further purified by phenol-chloroform and chloroform extraction. This involved the addition of 0.5 volume of special grade phenol (saturated with 0.1 M Tris HCl pH 8.0) and 0.5 volume of chloroform to the aqueous plasmid preparation. The sample was mixed vigorously by vortex and the aqueous phase recovered upon centrifugation at 13000 x g for 5 minutes. The chloroform extraction is as described above but with one volume of chloroform only. Plasmid DNA recovered in the aqueous phase was precipitated by the addition of 2.5 volumes ice-cold RNase-free ethanol, 0.3 M NaAc pH 5.2 and incubation at -20 °C for 30 minutes. The DNA was recovered as a pellet by centrifugation at 13000 x g for 10 minutes at 4 °C. The pellet was washed with 70 % ethanol, lyophilised under vacuum (Speed-Vac, Savant) and dissolved in a desired quantity of water.

2.3.2 MIDI PREPARATION OF PLASMID DNA (LARGE-SCALE)

E. coli DH5-α cells containing the mutant DNA in the appropriate bIGFBP-2 expression construct were grown overnight from a single colony at 37 °C in 50 ml of LB supplemented with 100 μg/ml ampicillin. After overnight growth the cells were pelleted at 5000 x g, for 5 minutes at 4 °C. The drained pellet was resuspended in 3 ml of TEG lysis buffer. The suspension was incubated on ice for 5 minutes with 3 mg lysozyme. The cells were allowed to lyse on ice for 5 minutes in 6ml of 0.2 M NaOH, 1 % SDS. Chromosomal DNA was precipitated on ice for 15 minutes in 4.5 ml 3 M NaAc pH 5.2. The cell debris was pelleted at 10000 x g, for 5 minutes at 4 °C and the supernatant collected. The DNA was precipitated in 8 ml ice-cold isopropanol for 5 minutes at room temperature before being centrifuged at 10000 x g, 5 minutes at 4 °C. The supernatant was removed and the DNA pellet resuspended in 1 ml of H_2O and 2.5 ml 4 M LiCl, incubated on ice for 15 minutes prior to centrifugation at 10000 x g, 4 °C for 5 minutes. The supernatant was again collected and the DNA precipitated in ice-cold RNase-free ethanol at -20 °C for 30 minutes. The DNA was pelleted at 10000 x g, for 5 minutes at 4 °C, resuspended in 400 μl TE and transferred to a 1.5 ml Eppendorf tube to be treated with 20 μg RNase A at 45 °C for 30 minutes. The DNA preparation was then treated with 8 μl 10 % SDS and 50 μg proteinase K for 15 minutes at 37 °C prior to phenol/chloroform extraction (as described in Section 2.3.1) and precipitated in 2.5 volumes ice-cold RNase-free ethanol.

2.3.3 AGAROSE GEL ELECTROPHORESIS OF DNA SAMPLES

DNA samples were assessed by separation on agarose gels submerged in TBE running buffer (100 mM Tris-borate, pH 8.3, 2.5 mM EDTA). Agarose gels varied in concentration from 1-2 % depending on the size of the DNA sample being electrophoresed. Samples were diluted in loading buffer (1x: 2 % glycerol, 0.04 % bromophenol blue, 0.04 % xylene cyanol in

1 x TBE) loaded into the wells of the agarose gel and electrophoresed at 150 V. The gels were subsequently stained with 1 μg/ml ethidium bromide in TBE for 10 minutes followed by destaining in H_2O for 5 minutes. The DNA was visualised under long or short wave UV light as appropriate. A photographic record was obtained.

2.3.4 AMPLIFICATION OF DNA BY POLYMERASE CHAIN REACTION (PCR)

Polymerase chain reactions (PCR) were performed to amplify specific segments of DNA. The PCR and control reactions were usually assembled in the laminar flow unit to prevent contamination. The reaction was performed in 1 x PCR buffer (100 mM Tris-HCl, pH 8.85 (20 °C), 250 mM KCl, 50 mM $(NH_4)_2SO_4$, 20 mM $MgSO_4$) with 5 mM deoxynucleotide triphosphates, 10 % DMSO, 2 units of Pwo DNA polymerase, 100 ng of oligonucleotide primers and 10 ng of template plasmid. A 20 μl reaction was assembled and overlayed with 30 μl of paraffin oil. All PCR reactions were performed in a Perkin Elmer Cetus Thermal Cycler (Norwalk, CT, USA) using the following profile unless otherwise stated: initial denaturation at 94 °C for 3 minutes; followed by 30 cycles of denaturation: 94 °C, 1 minute; annealing: 60 °C, 1 minute and extension: 72 °C, 1.5 minutes. A final extension cycle at 72 °C for 10 minutes was performed before terminating the reaction by lowering the temperature to 4 °C. PCR products were identified on 1-2 % agarose gels against molecular weight markers.

2.3.5 RESTRICTION ENDONUCLEASE DIGESTION OF DNA

Plasmids were treated with specific restriction endonucleases under conditions recommended by the supplier of the enzyme. Digestion was terminated by the addition of agarose gel electrophoresis buffer or by freeze storage.

2.3.6 QUIKCHANGE SITE DIRECTED MUTAGENESIS OF PLASMID DNA

QuikChange site-directed mutagenesis was performed as recommended by the manufacturer (Stratagene, CA, USA). Briefly, the mutagenesis reaction was performed with 125 ng of the mutagenic oligonucleotides, BP2*Apa*Ifor and BP2*Apa*Irev, 30 or 60 ng of double stranded pGF8, 10 mM dNTP mix (2.5 mM each dNTP) in reaction buffer (1x: 10 mM KCl, 6 mM $(NH_4)SO_4$, 20 mM Tris-HCl pH 8.0, 2 mM $MgCl_2$, 0.1% Triton X-100, 10 μg/ml nuclease-free BSA) in a final volume of 50 μl. *Pfu* DNA polymerase (2.5 units) catalysed the reaction which proceeded under the following cycling parameters in the Perkin Elmer Cetus Thermal Cycler: denaturation, 95 °C, 30 seconds; 12 cycles denaturation, 95 °C, 30 seconds; annealing, 55 °C, 1 minute; extension, 68 °C, 12 minutes. Following PCR, the samples were incubated on ice for 2 minutes prior to digestion of the parental strand with 10 units *Dpn* I restriction enzyme at 37 °C for 1 hour. One microlitre of the mutagenesis reaction was then transformed into 50 μl of *Epicurian Coli* XL1-Blue supercompetent cells (Stratagene, CA, USA) as described in Section 2.3.11. Antibiotic resistance was established in 0.5 ml preheated (42 °C) NZY + Broth at 37 °C for 1 hour on the rolling drum. The transformation reactions were then plated on LB plus ampicillin plates (100 μg/ml) at 37 °C overnight.

2.3.7 MUTA-GENE PHAGEMID *IN VITRO* MUTAGENESIS

The protocol described is from the manual for the Bio-Rad *In Vitro* Mutagenesis Kit with noted adaptations. Prior to mutagenesis, single stranded DNA was generated and the mutagenic oligonucleotides phosphorylated as discussed in the following sections.

2.3.7.1 Synthesis of Uracil-Containing Single Stranded DNA

E. coli CJ236 cells harbouring pGDH-1 were obtained from G.Hobba. A single colony was picked and grown overnight at 37 °C in 2 ml of 2YT, supplemented with 15 μg/ml chloramphenicol and 100 μg/ml ampicillin. A fresh 2 ml of 2YT was inoculated with 200 μl of overnight culture and incubated at 37 °C with shaking for 3 hours. M13K07 helper phage (5 x 10^8 p.f.u; Bio-Rad, Richmond, CA, USA) were added to the culture and grown for 1 hour prior to the addition of kanamycin (14 μg/ml) and overnight growth. The phagemids were collected by centrifugation of 1.5 ml of the culture at 13200 x g for 5 minutes at 4 °C. One millilitre of the supernatant was removed to a fresh Eppendorf and treated with 200 μg RNase A at room temperature for 30 minutes. Finally, the phagemids were precipitated on ice for 30 minutes in 20% PEG/2.5 M NaCl and centrifuged at 4 °C for 15 minutes. The pellet was drained, resuspended in 200 μl of Tris-EDTA and extracted twice with an equal volume of phenol. The upper aqueous phase (180 μl) was transferred to a fresh tube and the single strand uracil containing DNA precipitated with ice-cold RNase-free ethanol.

2.3.7.2 Phosphorylation of the Mutagenic Oligonucleotides

The Muta-Gene Phagemid *In Vitro* Mutagenesis protocol required phosphorylation of the oligonucleotides to be used in the reaction. The following reaction was assembled in a microcentrifuge tube: 200 pmol oligonucleotide, 100 mM Tris-HCl pH 8.0, 10 mM $MgCl_2$, 5 mM DTT and 0.4 mM ATP pH 7.0 in a final volume of 30 μl. The reaction was mixed well and incubated at 37 °C for 45 minutes with 4.5 units of T4 polynucleotide kinase. Heating at 65 °C for 10 minutes terminated the reaction.

2.3.7.3 In Vitro Mutagenesis

The phosphorylated mutagenic oligonucleotide (6 pmol) was annealed to uracil-containing single-stranded DNA (200 ng) in annealing buffer (1x: 20 mM Tris-HCl pH 7.4, 2 mM $MgCl_2$, 50 mM NaCl) in a final reaction volume of 10 µl. The reaction was heated to 65°C for 2 minutes and allowed to cool at a rate of 1 °C per minute over 30 minutes before incubation on ice. The reaction was supplemented with synthesis buffer (0.4 mM each dNTP, 0.75 mM ATP, 17.5 mM Tris-HCl pH 7.4, 3.75 mM $MgCl_2$, 1.5 mM DTT), 3 units T4 DNA ligase and 0.5 units T7 DNA polymerase. The reactions were incubated on ice for 5 minutes, at room temperature for 5 minutes and finally at 37 °C for 30 minutes to allow T4 DNA polymerase extension. The reaction was stopped by the addition of stop buffer (10 mM Tris-HCl pH 8.0, 10 mM EDTA). Synthesis of the complementary strand was assessed by visualisation on a 1 % agarose gel. The mutagenic DNA (5 µl) was transformed into DH5-α competent cells (see Section 2.3.11).

2.3.8 ISOLATION AND PURIFICATION OF DNA FROM AGAROSE GELS

The restriction endonuclease digest reactions were electrophoresed at 150 V on an agarose gel and the desired DNA fragment excised from the gel under long wave UV light. The DNA was then isolated from the agarose and purified using the GENECLEAN Kit (Bio 101 Inc, CA, USA). The gel slice was dissolved in 25 µl TBE modifier and 225 µl 6 M NaI in a 1.5 ml Eppendorf tube at 65 °C. Glassmilk (5 µl; GENECLEAN Kit) was added to the suspension and incubated for 5 minutes at 65 °C for smaller fragments (300 bp) or at room temperature for larger fragments. The silica matrix with bound DNA was pelleted at 13200 x g for 5 seconds and the supernatant removed. The pellet was washed 3 times by resuspension in 200 µl New Wash (GENECLEAN Kit) followed by pelleting at 13200 x g for 5 seconds. DNA was eluted from the silica matrix in 10 µl H_2O at 65°C for 3 minutes, pelleted at 13200 x g for 30 seconds

and the DNA which eluted into the supernatant was removed to a fresh Eppendorf tube. The DNA was eluted twice from the Glassmilk. DNA was also extracted from agarose gels using the Geneworks Gel Extraction kit as recommended by the manufacturer (Geneworks, Thebarton, South Australia).

2.3.9 DNA LIGATION

The restriction endonuclease-digested vector was generally treated with 1 unit of Calf Intestinal Phosphatase (CIP) at 37 °C for 30 minutes in dephosphorylation buffer in a final volume of 50 µl. The DNA was extracted with phenol/chloroform (Section 2.3.1) and precipitated in 2.5 volumes RNase-free ethanol and 0.3 M NaAc pH 5.2. The digested PCR product and dephosphorylated vector were ligated at a molar excess of 3:1 respectively in ligase buffer (66 mM Tris-HCl pH 7.6, 6.6 mM $MgCl_2$, 66 µM ATP) with 1 unit of T4 DNA ligase at 14 °C overnight in a total volume of 10 µl.

2.3.10 PREPARATION OF COMPETENT CELLS

Competent cell preparation was performed as described by Sambrook *et* al., (1989). Briefly, a single colony of the *E. coli* bacterial strain, DH5-α or BL21, was grown overnight in 5 ml of LB at 37 °C with shaking. Fresh LB (50 ml) was inoculated with the overnight culture (500 µl) and grown at 37 °C to an A_{600} of 0.6. The culture was incubated on ice for 30 minutes prior to pelleting the cells at 3200 x g for 10 minutes at room temperature. The pellet was drained and left to incubate on ice for 30 minutes in ice cold 50 mM $CaCl_2$, 50 mM $MgCl_2$. The suspension was then centrifuged at 3200 x g for 5 minutes and resuspended in a final volume of 3 ml 80 mM $CaCl_2$. Cells were left on ice for at least 1-2 hours before use. Competent cells were stored at -80 °C in 200 µl aliquots.

Alternatively, competent *E. coli* cells were prepared as described by CLONTECH Laboratories, Inc (Palo Alto, CA, USA). Fresh LB (5 ml) was inoculated with a single colony and grown overnight at 37 °C with shaking. A fresh 10 ml of LB was inoculated with the overnight culture (330 µl) and grown to an A_{600} of approximately 0.6 before subculturing 5 ml into fresh LB (100 ml). This culture was grown to an A_{600} of 0.6 then incubated on ice for 5 minutes. The cells were pelleted (4000 x g) for 5 minutes at 4°C and resuspended in ice cold TB1 (4 ml) on ice for 5 minutes. The cells were pelleted (4000 x g) for 5 minutes at 4 °C and resuspended in TB2 (4 ml). The cells were incubated on ice for 15 minutes prior to use or aliquoted and stored at -80 °C in 200 µl aliquots.

2.3.11 BACTERIAL TRANSFORMATION

The ligation reaction (5-10 µl) was added to 200 µl of competent cells and incubated on ice for 30 minutes. The cells were heat-shocked for 90 seconds at 42 °C, allowed to recover on ice for 5 minutes and at room temperature for 5 minutes. The mixture was then incubated in 1 ml LB at 37 °C for 30 minutes to permit expression of antibiotic resistance. The cells were then centrifuged at 6500 x g for 2 minutes, resuspended in 100 µl LB and spread on LB plates containing the appropriate antibiotic(s) and incubated overnight at 37 °C. Transformation controls included no DNA and vector only.

2.3.12 ^{T7}DNA SQUENCING

Methods for ^{T7}DNA sequencing were as described by the manufacturer (Amrad Pharmacia Biotech). DNA polymerase extension can be terminated by dideoxynucleotides to yield fragments of various lengths; identification of the terminated nucleotide facilitates sequence analysis (Sanger *et al.*, 1977). Briefly, the protocol involved annealing primer (0.5 pmol) to template DNA (1 µg) in Sequenase reaction buffer (1 M Tris-HCl pH 7.6, 100 mM

$MgCl_2$, 160 mM DTT) in a final volume of 10 μl. The reactions were heated to 65 °C for 2 minutes and allowed to cool to room temperature over 30 minutes. The annealed primer and template were labelled with α-[^{32}P]-dATP (5 μCi) in a reaction mix containing 0.1 M DTT, labelling nucleotide mix and 3.25 units ^{T7}Sequenase enzyme and incubated at room temperature for 5 minutes. The appropriate dideoxy termination mixture was added to Eppendorf tubes containing dATP, dCTP, dGTP or dTTP and incubated at 37 °C for 5 minutes. The reactions were subsequently electrophoresed on a 6 % polyacrylamide gel and the sequence of the template deduced by the location of the primer extension product terminated by the particular dideoxynucleotide present in the reaction. The chain terminated fragments in each reaction represent the occurrence of the corresponding deoxynucleotide in the sequence.

2.3.13 DYE TERMINATOR DNA SEQUENCING

The ABI PRISM Dye Terminator Cycle Sequencing Ready Reaction Kit involves amplification of the DNA to be sequenced with a terminator premix of fluorescently-labelled dideoxynucleotides (A-dye terminator, C-dye terminator, G-dye terminator, T-dye terminator, dATP, dCTP, dGTT, dTTP, Tris-HCl, $MgCl_2$, thermal stable pyrophosphatase, AmpliTaq DNA polymerase) and an appropriate primer. The dideoxynucleotides result in the termination of the DNA polymerase extension, yielding fragments of various lengths. The terminal base in each fragment was identified by fluorescence using a model 373 Perkin Elmer sequencing machine.

2.3.14 *fmol* DNA CYCLE SEQUENCING

The *fmol* DNA cycle sequencing kit from Promega (Madison, WI, USA) was used for PCR sequencing. Oligonucleotide (100ng) was labelled using γ-[^{32}P]-ATP in a reaction mix containing T4 polynucleotide kinase buffer and T4 polynucleotide kinase in a final volume of 10 μl. Radiolabelled primer (1.5 μl) was then used in the extension/termination reaction with

approximately 1μg of template DNA in *fmol* sequencing buffer. Sequencing grade *Taq* DNA polymerase (5 units) was added and the mix aliquoted to deoxy- and dideoxy-NTPs in the appropriate microcentrifuge tubes. The reactions were placed into a Perkin Elmer thermal cycler under the following cycle parameters: 95 °C, 2 minutes for 1 cycle and then: 95 °C, 30 seconds (denaturation); 55 °C, 30 seconds (annealing); 70 °C, 1 minute (extension) for a total of 30 cycles. The reactions were stopped with *fmol* sequencing stop solution and denatured at 100 °C for 2 minutes prior to loading on a 6 % polyacrylamide sequencing gel. The results were visualised by autoradiography.

2.4 RESULTS AND DISCUSSION

2.4.1 STRATEGY FOR EXPRESSION VECTOR GENERATION

Investigation of the function and structure of the highly conserved amino- and carboxyl-terminal domains of bIGFBP-2 required establishment of expression vectors encoding truncated bIGFBP-2 sequences. Expression vectors for mammalian protein expression were generated using the vector pGF8 as a template for PCR amplification. These vectors comprised cDNA encoding the bIGFBP-2 truncations 1-93, 1-104, 1-132, 1-185, 96-279, 96-284, 137-279, and 182-284 (Figure 2.1). Bovine IGFBP-2 truncations were therefore produced in an established expression system capable of generating and correctly processing IGFBPs.

Structure determination studies require large quantities of protein (possibly labelled with ^{15}N, ^{13}C or ^{2}H) and hence it was also important to generate an expression system capable of large-scale protein production in economically viable *E. coli* cells. The cDNA for bIGFBP-2 and the truncations $^{1\text{-}132}$IGFBP-2, $^{1\text{-}185}$IGFBP-2 and $^{136\text{-}279}$IGFBP-2HIS were therefore cloned into the pET32a (+) vector for expression in *E. coli* BL21 cells.

2.4.2 VECTORS FOR MAMMALIAN EXPRESSION

2.4.2.1 N-Terminal Expression Constructs

Generation of the N-terminal constructs was achieved by the introduction of stop codons in the wildtype bIGFBP-2 cDNA expression vector, pGF8, by PCR. PCR used the common forward primer Vic1ex, located 5' of the *Pst* I restriction site and the reverse primers Nterm3 ($^{1-93}$IGFBP-2), SN-2 ($^{1-104}$IGFBP-2), 1:2BP-2 ($^{1-132}$IGFBP-2) and LongN ($^{1-185}$IGFBP-2) to introduce stop codons after residues His93, Gln104, Gly132 and Pro185, respectively. The reverse primers also introduced an *Eco*R I restriction site at the 3' end to facilitate re-ligation of the PCR product into the parent vector, pXMT2. Oligonucleotide primers are listed in Section 2.2.7.2 and the cloning strategy for the amino-terminal constructs is outlined in Figure 2.5. PCR reactions were performed routinely with 10 % DMSO as described by Sun *et al.*, 1993, to overcome secondary structure formation as a consequence of the high GC rich content of the bIGFBP-2 cDNA.

Amplification of the parent vector pGF8 was greatly influenced by template strand re-annealing and secondary structure formation. Prior to use of DMSO, PCR reactions had often failed to generate a fragment of the desired size whilst in other attempts multiple non-specific bands were evident on analytical gels (Figure 2.6A). This was due to the high GC content of full-length bIGFBP-2 cDNA, particularly in the regions to be targeted for amplification by PCR (Table 2.2). Furthermore, oligonucleotide primers exhibited high denaturing temperatures for PCR reactions as a consequence of their GC content (Table 2.3). Particular difficulties have been reported during PCR of GC rich DNA templates due to high denaturing temperatures (Tm) (Varadaraj and Skinner, 1994). If template Tm exceeds the primer annealing temperature, the primer-template DNA complex may be less favoured, resulting in decreased synthesis of the complementary strand. Conversely, if the template Tm is considerably lower than the primer annealing temperature, non-specific DNA fragments may be amplified resulting in extra bands

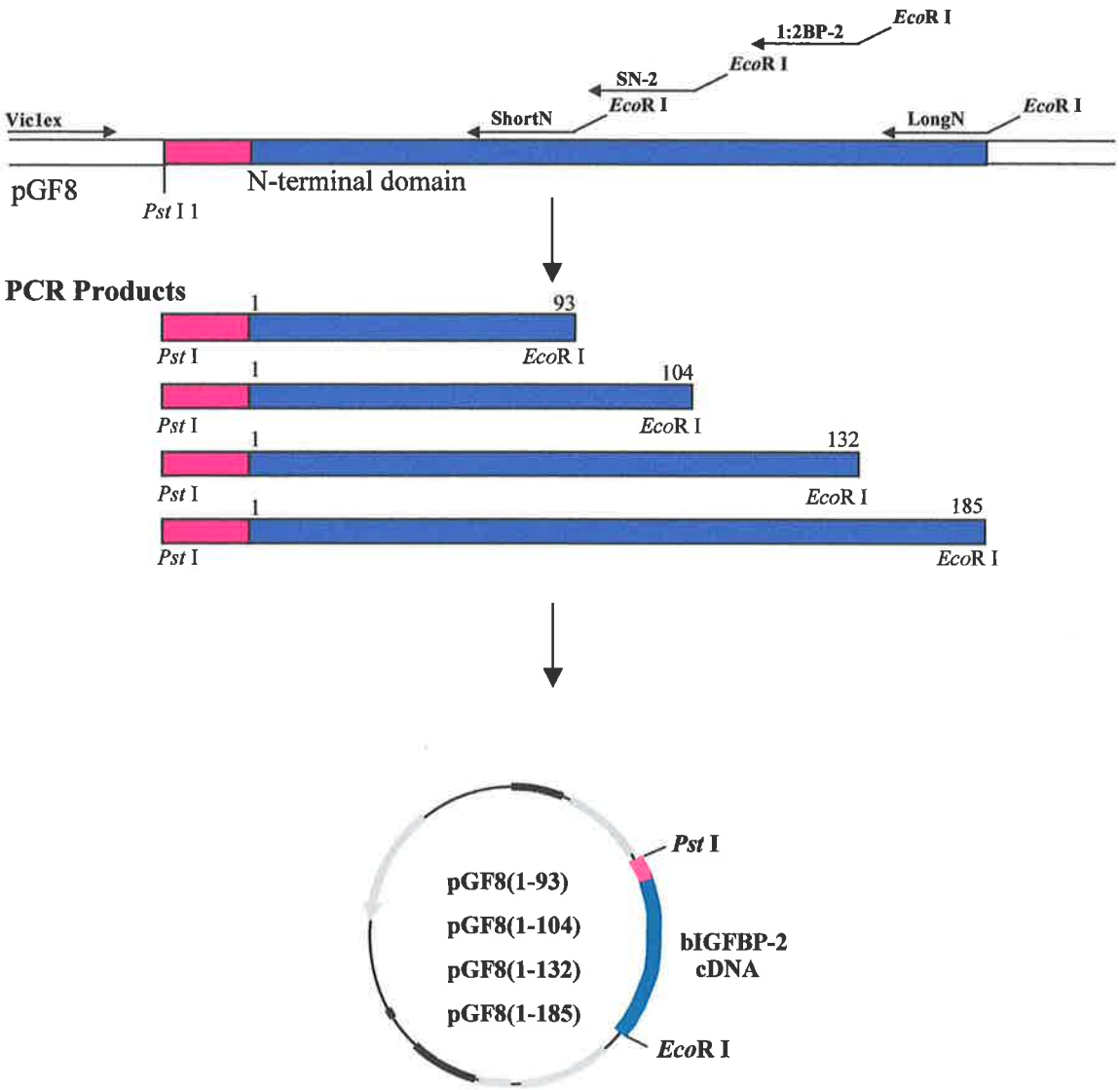

Figure 2.5 Cloning of cDNA encoding the N-terminal fragments into pGF8
Specific regions of bIGFBP-2 were amplified from the pGF8 template by PCR. The oligonucleotide primers are schematically represented as arrows above the bIGFBP-2 cDNA. The forward primer Vic1ex (located 5' of the cDNA encoding the leader sequence) and the reverse primers ShortN, SN-2, 1:2BP-2 and LongN were used to generate the mammalian expression vectors pGF8(1-93), pGF8(1-104), pGF8(1-132), pGF8(1-185), respectively (Section 2.4.2.1). Numbering refers to the corresponding amino acid residue in bIGFBP-2. Restriction enzyme sites for cloning are indicated.

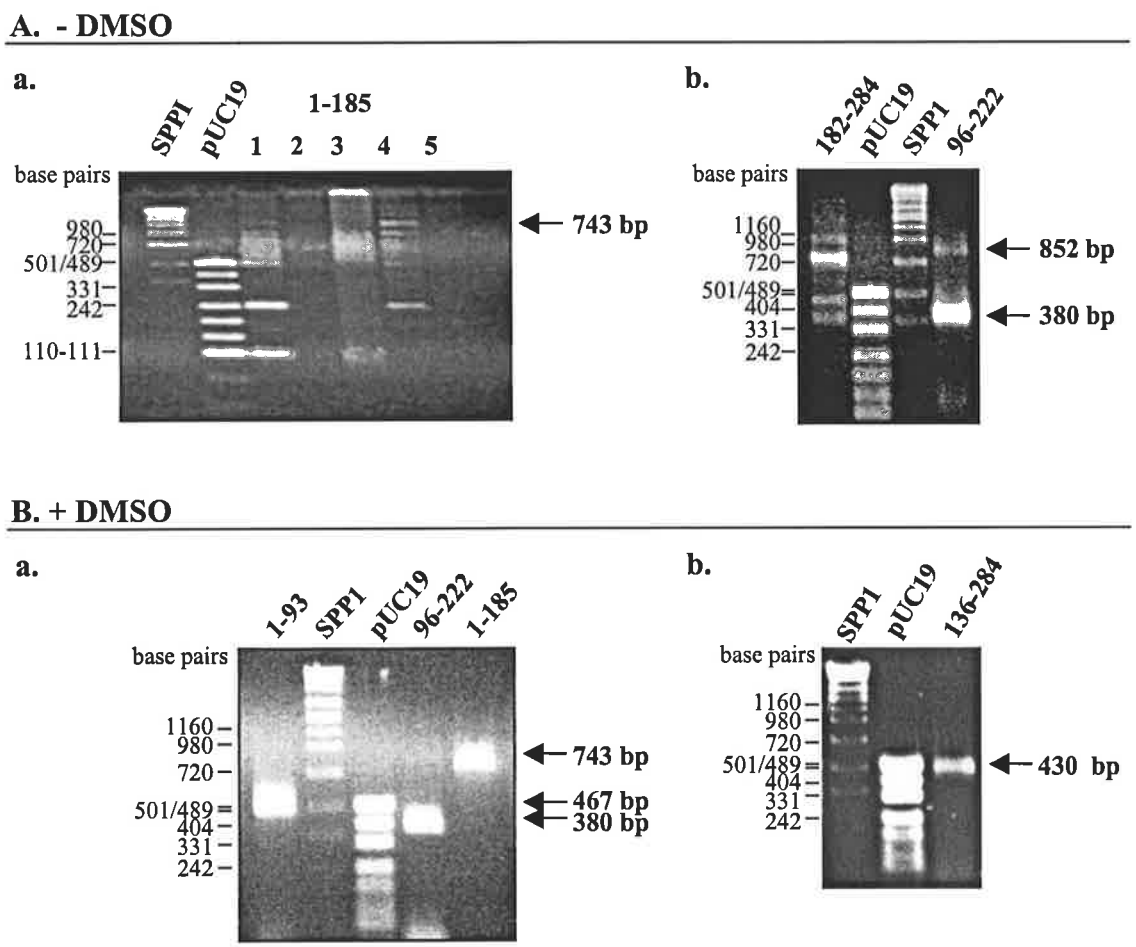

Figure 2.6 Polymerase chain reaction (PCR) of cDNA encoding bIGFBP-2
PCR reactions were analysed on 1.5% agarose gels with 500 ng of molecular weight markers SPP1 and pUC19. Molecular weight sizes (base pairs) are indicated on the left of the gels. The desired PCR fragments are shown with arrows on the right. 4 µl of the 30 µl reaction were loaded onto the gel.

A: PCR reactions were performed with 1 unit of Pwo DNA polymerase as described in Section 2.3.4. The 1-185 PCR product was amplified from template pGF8 using the primers Vic1ex and LongN (a). Lane 1-5 contain: 1) pGF8 template + primers; 2) pGF8, no primer control; 3) no template control; 4) pGF8 and Vic1ex; 5) pGF8 and LongN. The 182-284 and 96-222 PCR fragments were amplified with primers ShortC*Apa*I and Vic2; and LongC*Apa*I and SJH5, respectively (b).

B: PCR reactions were performed with 2 units of Pwo and 10% DMSO as described in Section 2.3.4. The PCR products 1-93, 96-222 and 1-185 were amplified using the primers Vic1ex and ShortN, LongC*Apa*I and SJH-5, and Viclex and LongN, respectively (a). The PCR fragment 136-279HIS was amplified with primers 2:2BP-2 and LCHIS (b).

TABLE 2.2 GC CONTENT OF THE PCR FRAGMENTS

FRAGMENT	OLIGONUCLEOTIDES	LENGTH base pairs	GC CONTENT
1-93	Vic1ex and ShortN	467	73%
1-104	Vic1ex and SN-2	501	73%
1-132	Vic1ex and 1:2BP-2	585	71%
1-185	Vic1ex and LongN	744	70%
96-221	LongCApaI and SJH5	380	65%
96-279HIS	LongCApaI and LCHIS	566	63%
136-279HIS	2:2BP-2 and LCHIS	447	63%
137-279HIS	2:2apaBP-2 and LCHIS	444	63%
182-279HIS	ShortCApaI and LCHIS	309	62%
182-284 + UTR	Vic2 and ShortCApaI	846	60%
pGF8 *Pst* I - *Sma* I	-	332	79%
pGF14 *Nco* I - *Not* I	-	539	71%
pGF8 *Not* I - *Eco*R I	-	1251	64%
bIGFBP-2	-	1425	65%

The base pair length and the GC content of the cDNA encoding IGFBP fragments are listed. The oligonucleotide primers used to generate the various PCR fragments are listed. Alternatively, fragments were generated by endonuclease restriction digest as indicated.

TABLE 2.3 GC CONTENT AND DISSOCIATION TEMPERATURES TM OF THE OLIGONUCLEOTIDE PRIMERS

PRIMER	SEQUENCE	SIZE	GC CONTENT	TM
ShortN	**ttt aag ctt gaa ttc tta gtg ctt ttc gca agt gcc ctc gcc gtg gac**	48mer	48%	87°C
SN-2	**ttg aat tct tac tgc tcg ggg ctg g**	25mer	52%	76°C
LongN	**ttt aag ctt gaa ttc tta ggg ggt cct ggc agg**	33mer	49%	81°C
bp2*Apa*Ifor	**cga ctg cgg ggc ccg cgc cga ggt g**	25mer	84%	89°C
bp2*Apa*Irev	**cac ctc ggc gcg ggc ccc gca gtc g**	25mer	84%	89°C
ShortC*Apa*I	**ttt ttt ggg gcc cgc gcc gcc agg acc ccc tgc cag**	36mer	72%	92°C
ShortC-2	**ttt ttt ggg gcc cgc gcc ggc agg ggt ggc aaa cat cac**	39mer	64%	91°C
LongC*Apa*I	**ttt ttt ggg gcc cgc gcc gct gag tac agc gcc agc**	36mer	67%	90°C
SJH-5	**tac gaa ttc tta ctt gtc aca gtt ggg gat gtg tag gga**	39mer	44%	82°C
Vic1ex	**ttg aga tct ggc cat aca ctt gag**	24mer	46%	72°C
LCHIS	**ttt aag ctt gaa ttc tta gtg gtg gtg gtg gtg gtg cac ccc tcg agc ccc ctg ctg ctc gtt gta**	66mer	55%	94°C
Vic2	**gcc ttc aca cgc tag gat t**	19mer	53%	68°C
1:2BP-2	**ttt agc ttg aat tct tat cca cct ccc atc aag tt**	35mer	37%	77°C
2:2apaBP-2	**aaa aat tgg gcc cgg aag ccc ctc aag tcc ggc atg**	36mer	58%	87°C
2:2BP-2	**Aaa ggt acc cca tgg ggt cgg aag ccc ctc aag**	33mer	61%	86°C
Primer 1 (Sigma®)	**gtg aac ttg atg gga ggt gga ggt gat gat gac gat aag ccc ctc aag tcc ggc atg**	57mer	54%	92°C
Primer 2 (Sigma®)	**cat gcc gga ctt gag ggg ctt atc gtc atc atc acc tcc acc tcc cat caa gtt cac**	57mer	54%	92°C

Oligonucleotide primers are listed. The denaturing temperature was calculated using the % GC method.

on analytical gels. This is due to denaturation of the template at a temperature insufficient for disruption of non-specific primer interactions.

Prior to successful optimisation of the PCR conditions, several avenues were investigated. Primers were generated on the basis of results obtained by software for primer analysis: Oligo™ 4.05 and Amplify 1.0. These programs aid in choosing optimal primers for PCR by calculating Tm, detecting hairpin loop structures and binding palindromes. PCR parameters including magnesium sulphate and enzyme concentrations, primer concentration and length, and the parent template concentrations were varied. Cycling parameters, in particular the annealing temperatures, were also altered. None of these factors contributed to the successful amplification of bIGFBP-2.

The generation of non-specific products by PCR may have been a consequence of the inability of the DNA template to denature sufficiently for specific primer annealing and fragment amplification. Sun and co-workers (1993) proposed that the high GC content of DNA causes the rapid renaturation of the template thereby preventing single strand amplification. Stable secondary structures in the template DNA may also contribute to the interference of primer extension resulting in additional satellite bands (Varadaraj and Skinner, 1994). Varadaraj and Skinner (1994) showed that dimethyl sulfoxide (DMSO) and some non-ionic detergents decreased inter- and intra-strand re-annealing in GC-rich templates and subsequently improved PCR sequencing of DNA. They also showed that concentrations of DMSO in excess of 2 % inhibited activity of DNA Taq Polymerase while concentrations greater than 5 % significantly decreased the activity of engineered enzymes. Similarly, Sun and co-workers (1993) showed a 47 % inhibition of Taq DNA polymerase by 10 % DMSO and suggested the use of 2-fold concentrations of enzymes in such reactions. Therefore, these conditions were adopted for the PCR amplification of the mutant bIGFBP-2 constructs. The desired fragments of bIGFBP-2 were amplified by PCR in the presence of 10 % DMSO and 2 units Pwo DNA polymerase as described in Section 2.3.4. Notably amplification of the N-terminal regions was

achieved with 10 % DMSO (Figure 2.6B). Interestingly, 3 % DMSO did reduce non-specific priming but did not yield the correct PCR fragment (results not shown).

2.4.2.2 C-Terminal Expression Constructs

2.4.2.3 Introduction of the Apa I Restriction Site by Site-Directed Mutagenesis

In vivo, bIGFBP-2 is expressed with an amino-terminal leader peptide that permits secretion of the mature protein from cells. To enable the secretion of C-terminal domains expressed in mammalian cells, an *Apa*I restriction site was introduced at the 3' end of the sequence encoding the bIGFBP-2 leader peptide in pGF8 (amino acids MQPRLGGPALLLLP). An *Apa* I restriction site was the most suitable as only a single base needed to be altered (G 102 C) which did not alter the amino acid sequence (Figure 2.7). The *Apa* I restriction site was generated by a site-directed mutagenesis approach by Kunkel (1985), using the Bio-Rad™ *in vitro* Mutagenesis Kit and mutagenic oligonucleotide bp2*Apa*Irev. The subsequent vector was designated pGF8*Apa*I (Figure 2.7).

Briefly, the *Pst* I-*Sma* I fragment of bIGFBP-2, cloned into pBluescript-II (KS$^-$), (pGDH-1, Hobba *et al.*, 1996), had been previously transformed into *E. coli* CJ236. Upon infection of this strain with the helper phage M13K07, the non-coding strand was selectively packaged in phagemids and secreted from the cell as a single strand viral particle. This single stranded DNA acted as the template for site-directed mutagenesis by PCR. Of the colonies obtained by this method, 10% contained the introduced *Apa* I restriction site. The *Pst* I-*Sma* I fragment containing the newly synthesised *Apa* I restriction site was cloned back into pGF8 to produce pGF8*Apa*I.

Prior to the generation of this mutant vector, site directed mutagenesis was also attempted using the QuikChange Mutagenesis kit (Section 2.3.6). In brief, this approach involved amplification of double stranded template DNA by PCR using complementary

mutagenic oligonucleotide primers, bp2*Apa*Ifor and bp2*Apa*Irev (see Section 2.2.7.2). The methylated template DNA was subsequently digested by *Dpn* I restriction enzyme leaving the mutagenic strand for replication *in vivo*. This method, however, failed to generate the desired mutation. This could be attributed to the same difficulties encountered during the amplification of bIGFBP-2 sequences by PCR. Presumably, rapid renaturation of the GC-rich DNA template and extensive secondary structure prevent the extension of the oligonucleotide primers and the synthesis of the complementary strand. Inter-strand re-annealing was immediately eliminated by generation of single strand DNA in the site-directed mutagenesis approach by Kunkel (1985). The low efficiency of this system however, may also be due to secondary structure formation within the single stranded template DNA.

2.4.2.4 Cloning of C-Terminal Expression Constructs

PCR products encoding the C-terminal domain of bIGFBP-2 to be cloned into the pGF8*Apa*I vector were generated using the forward primers ShortC*Apa*I ($^{182-284}$IGFBP-2), 2:2apaBP-2 ($^{136-279}$IGFBP-2HIS) and LongC*Apa*I ($^{96-279}$IGFBP-2HIS) which all incorporated 5' *Apa* I restriction sites to facilitate ligation downstream of the signal sequence in pGF8*Apa*I. The reverse primer Vic2, located 3' of the *Eco*R I cloning site in pGF8 and complementary to the pXMT2 vector, was used to generate the C-terminal construct $^{182-284}$IGFBP-2. The reverse primer LCHIS was used to introduce a 6-histidine tag at the end of the C-terminal constructs $^{96-279}$IGFBP-2HIS and $^{136-279}$IGFBP-2HIS and eliminated the extensive 3' untranslated region (Figure 2.8). This was achieved by replacing the cDNA encoding the five C-terminal amino acid residues of bIGFBP-2 with cDNA encoding histidine residues. Forbes *et al.*, (1998) showed deletion of these residues did not affect IGF binding. All reverse primers introduced a 3' *Eco*R I restriction site for ligation into the pGF8*Apa*I vector. The cloning strategy for the production of C-terminal constructs is shown in Figure 2.8.

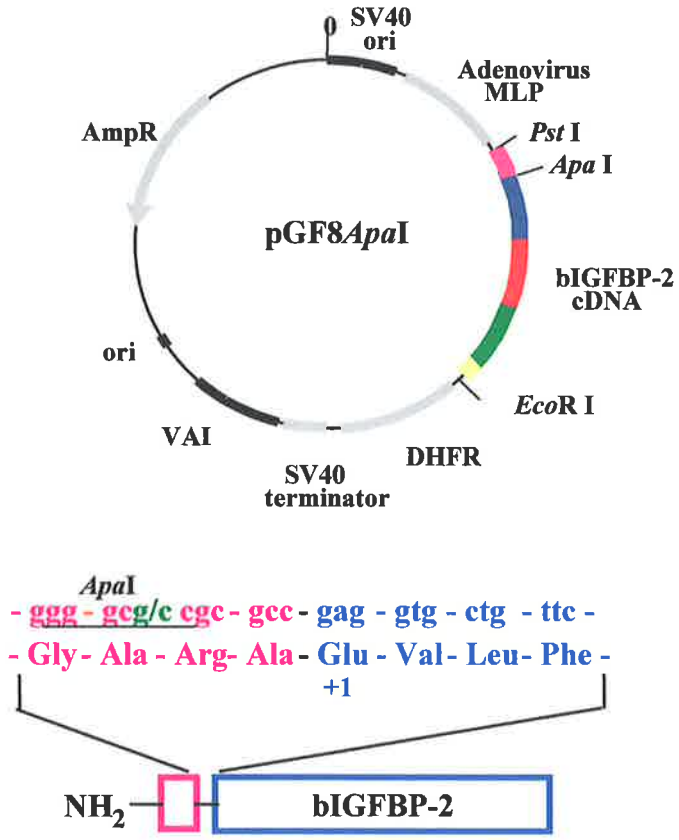

Figure 2.7 Expression vector pGF8*Apa*I
The bIGFBP-2 expression vector for mammalian expression (pGF8) was modified to facilitate cloning of the C-terminal constructs. An *Apa* I restriction site (gggccc) was introduced immediately downstream of the cDNA encoding the leader sequence by QuikChange mutagenesis (described in Section 2.3.6) using the oligonucleotide primers bp2*Apa*Ifor and bp2*Apa*Irev.

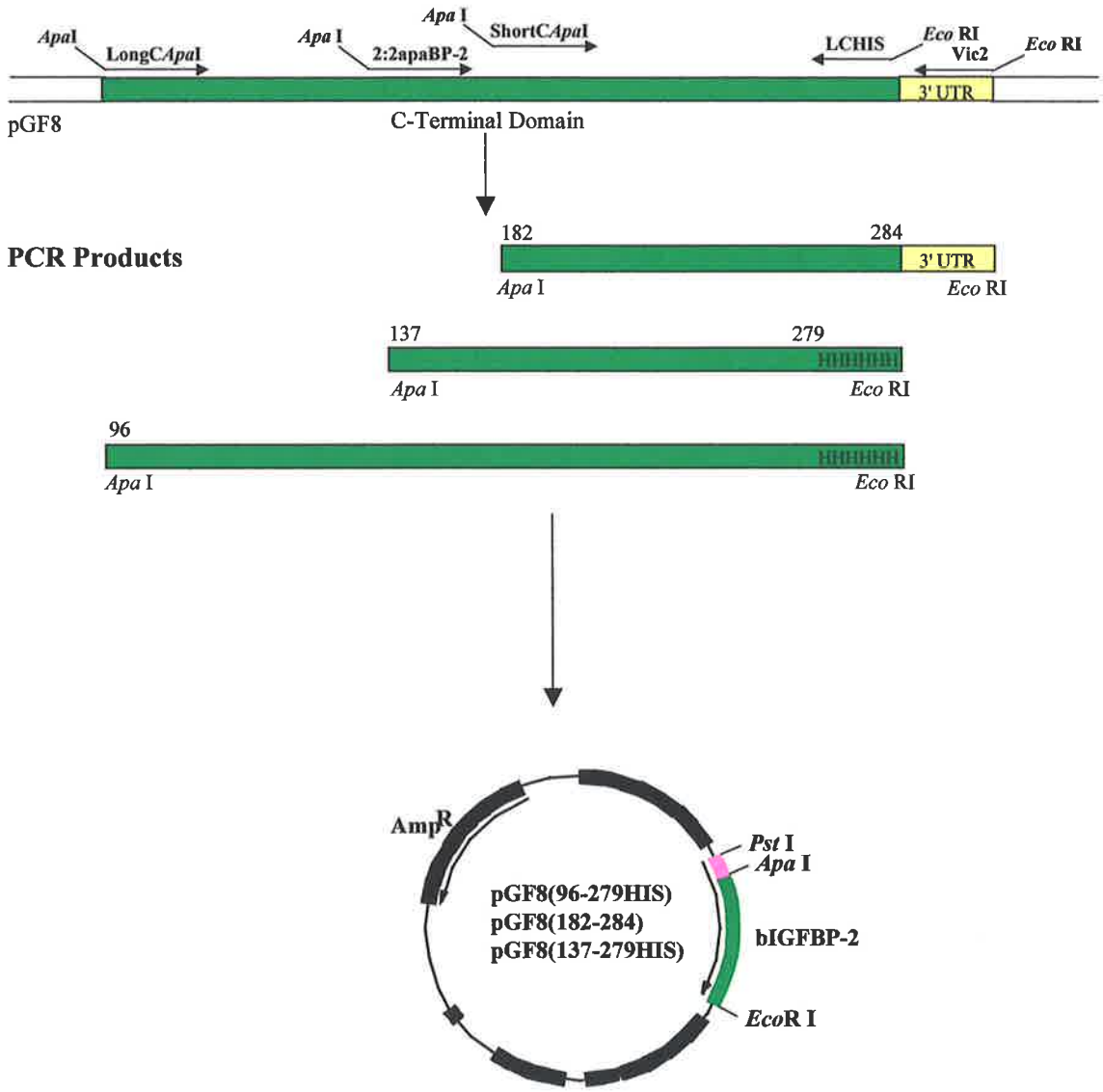

Figure 2.8 Cloning of cDNA encoding the C-terminal fragments into pGF8
Specific regions of bIGFBP-2 were amplified from the pGF8 template by PCR. The oligonucleotide primers are schematically represented as arrows above the bIGFBP-2 cDNA. The forward primers Long*CApa*I and Short*CApa*I and the reverse primer Vic2 (located 3' of the *Eco*R I restriction site in the pXMT2 vector) were used to generate the mammalian expression vector pGF8(182-284). These constructs contained the 3' non-coding region. Oligonucleotides Long*CApa*I and 2:2*Apa*BP-2 together with the reverse primer LCHIS, generated pGF8(182-279HIS) and pGF8(137-279HIS), respectively (Section 2.4.2.4). Numbering refers to the corresponding amino acid residue in bIGFBP-2. Restriction enzyme sites for cloning are indicated.

In addition to the construct pGF8(96-279HIS) generated by PCR as described above, a C-terminal construct pGF8(96-284) was generated using the forward primer, LongC*Apa*I, located at the 5' end of the DNA coding for the non-conserved central domain, and the reverse primer, SJH-5, located 3' of the unique *Not* I restriction site (Figure 2.9). The resultant PCR product was digested with *Apa* I and *Not* I and subsequently cloned into template vector pGF8*Apa*I. This construct contained the 3' UTR and did not encode the C-terminal hexahistidine tag for enhanced purification. This proved to be limiting during the purification of the expressed truncated mutant. Hence a hexahistidine tag was introduced by PCR amplification using the LCHIS oligonucleotide (pGF8(96-279HIS)). A hexahistidine tag was also incorporated into the full-length bIGFBP-2 clone (pGF8HIS) (Figure 2.10) to directly compare the effect of the histidine tag on IGFBP function.

While considerable difficulties were encountered during the amplification of the N-terminal fragments, generation of the C-terminal PCR products was easier. Analytical gels of cDNA encoding amino acid residues 96-222 and 182-284 indicate the successful generation of the correct size fragments by PCR although additional satellite bands were present (Figure 2.6A). The ability to produce the C-terminal fragments may reflect the lower GC content of this portion of bIGFBP-2 cDNA (Table 2.2). Sufficient PCR product was obtained for the successful construction of the C-terminal expression vectors, however it was noted that co-generation of the multiple non-specific products observed did decrease the yield of the desired product. The yield of the C-terminal PCR fragment encoding amino acid residues 96-222, was increased by the addition of 10 % DMSO, with a concomitant elimination of non-specific priming. Interestingly, 10 % DMSO did not improve the PCR reaction for the short C-terminal region of bIGFBP-2 (results not shown), which had the lowest GC content of the domains amplified.

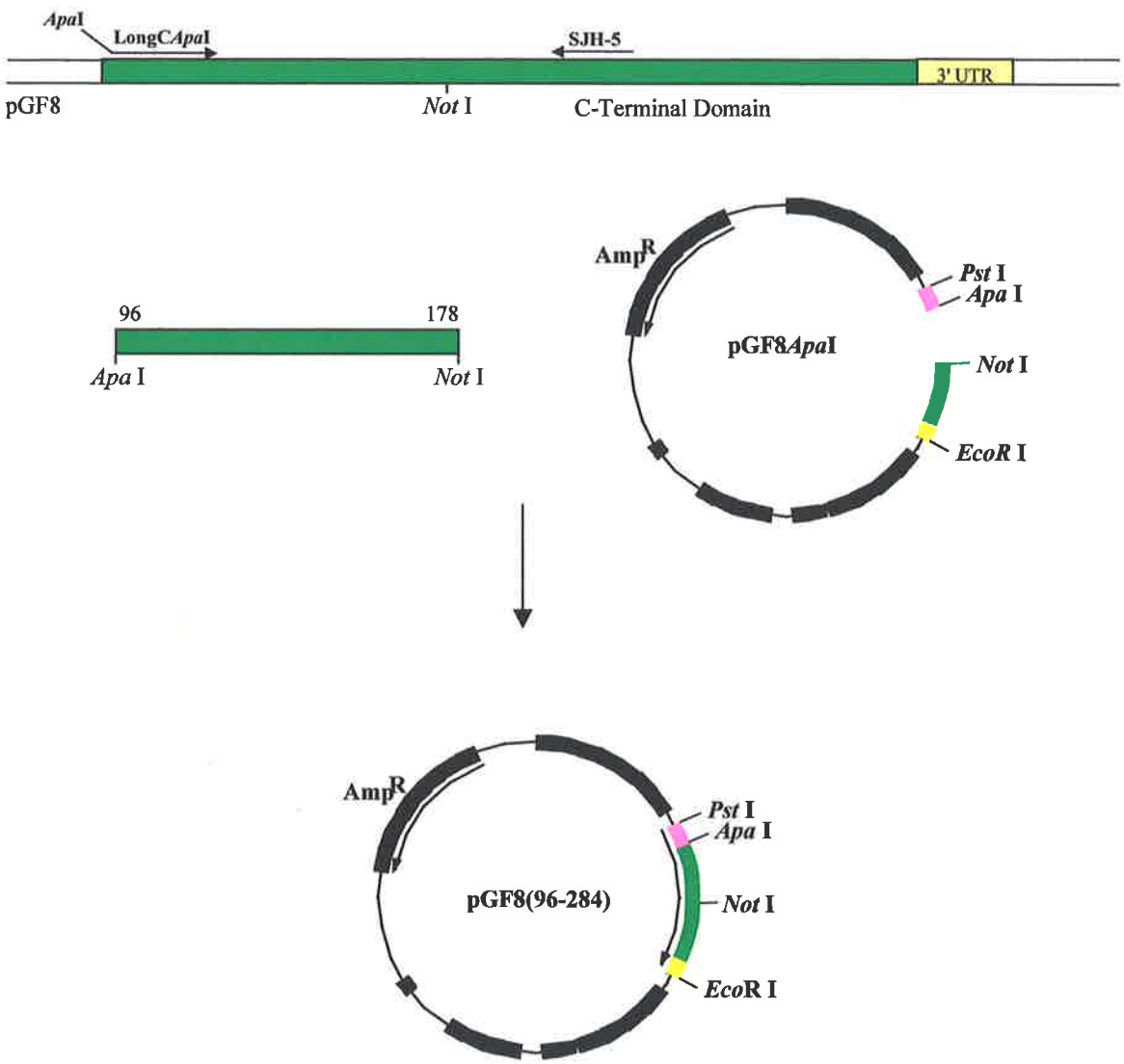

Figure 2.9 Cloning of cDNA encoding the C-terminal fragment (96-284) into pGF8
The cDNA encoding amino acid residues 96-284 of bIGFBP-2 was amplified by PCR, using the forward primer LongC*Apa*I and the reverse primer SJH-5, which is located 3' of the unique *Not* I restriction site in pGF8. The resultant PCR product was digested and cloned into the pGF8*Apa*I expression vector using the *Apa* I - *Not* I restriction sites to yield expression vector pGF8(96-284).

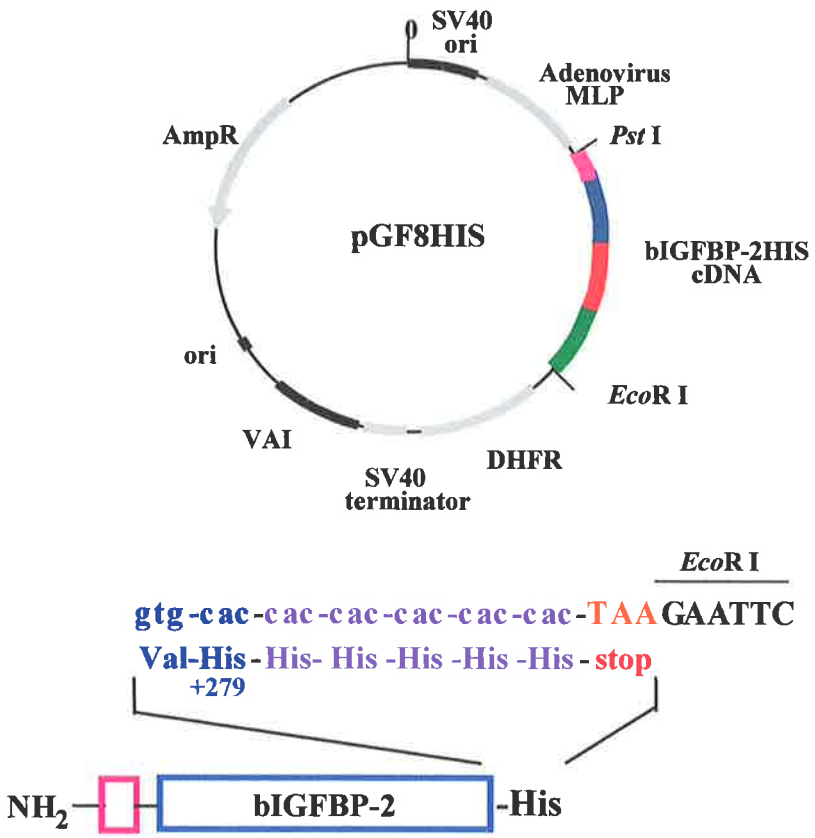

Figure 2.10 Expression vector pGF8HIS
The bIGFBP-2 expression vector for mammalian expression (pGF8) was modified to facilitate cloning (*Apa* I restriction site) and subsequent purification of the C-terminal constructs. The cDNA encoding the last five amino acid residues of the bIGFBP-2 gene was also replaced to encode histidine residues for enhanced purification of the expressed protein. This was achieved by PCR using the oligonucleotide LCHIS as described in Section 2.4.2.4.

2.4.3 VECTORS FOR *E. COLI* EXPRESSION

2.4.3.1 $^{1-279}$IGFBP-2HIS Expression Constructs

An *E. coli* expression system for bIGFBP-2 did not exist prior to this study. Establishment of a large-scale expression system, such as those commonly achieved in *E. coli,* was essential for the structure determination studies of both wildtype IGFBP-2 and the truncated, functional amino- and carboxyl-terminal domains. Hence bIGFBP-2 was cloned into the pET32a (+) expression vector (Figure 2.3). This vector encodes a thioredoxin-tag for enhanced solubility of the recombinant protein, an S-tag for antibody detection and both N- and C-terminal histidine-tags as purification probes. In addition, these tags could be removed with conveniently placed thrombin and enterokinase cleavage sites.

The cDNA encoding bIGFBP-2 was cloned into pET32a (+) using the restriction enzyme sites *Nco* I and *Eco*R I. This was achieved by a two step ligation of the *Nco* I-*Not* I fragment of pGF14 (a vector containing the bIGFBP-2 gene in Bluescript KS$^-$; Lucic *et al.*, 1997) and the *Not* I-*Eco*R I fragment of pGF8HIS with the parent vector pET32a (+) as shown in Figure 2.11. The subsequent expression vector was designated pET$^{1-279}$IGFBP-2HIS. An additional three amino acid residues (A-M-A-) were introduced at the N-terminus of IGFBP-2 after cleavage by enterokinase as a consequence of the cloning strategy (as indicated in Figure 2.3). Subsequent analysis of AMA-IGFBP-2HIS showed identical activity to bIGFBP-2 (discussed in Chapter 3). Interestingly, an N-terminal variant of bIGFBP-2 (GARA-IGFBP-2) is routinely co-expressed and purified from COS-1 preparations that exhibits near native binding properties.

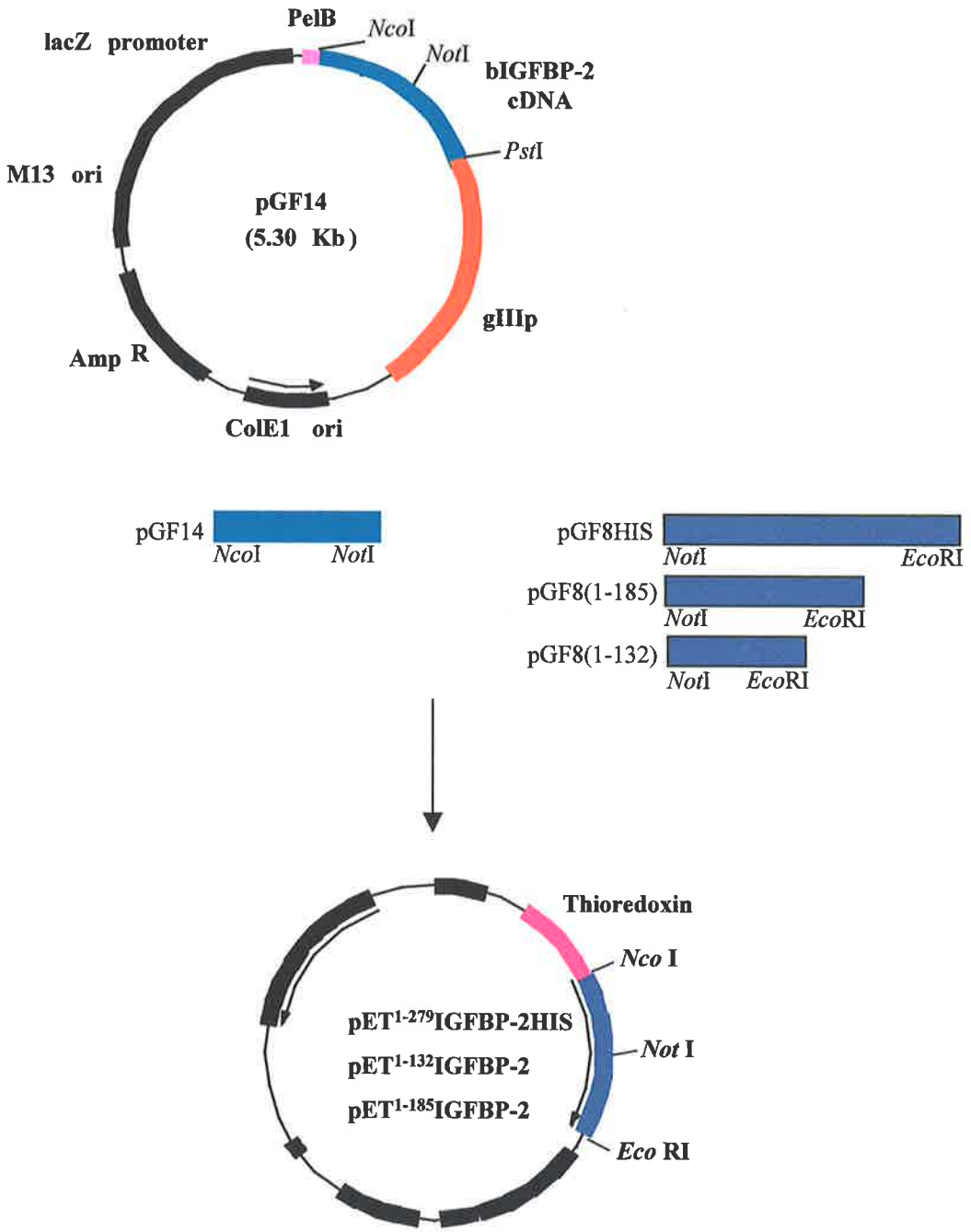

Figure 2.11 Cloning of cDNA encoding wildtype and N-terminal fragments into pET32a (+) The cDNA encoding amino acid residues 1-279HIS, 1-132 and 1-185 of IGFBP-2 were introduced into the pET32a (+) expression vector (Novagen) by a three-fragment ligation as described in Sections 2.4.4.1 and 2.4.4.2. The *Nco* I-*Not* I fragment of pGF14 and the *Not* I-*Eco*R I fragment from pGF8HIS, pGF8(1-132) and pGF8(1-185) were cloned into pET32a (+), digested with *Nco* I-*Eco*R I. The resultant *E. coli* expression vectors were designated pET^{1-279}IGFBP-2HIS, pET^{1-132}IGFBP-2 and pET^{1-185}IGFBP-2 respectively.

2.4.3.2 N-Terminal Expression Constructs

The cDNA encoding the N-terminal fragments $^{1\text{-}132}$IGFBP-2 and $^{1\text{-}185}$IGFBP-2 were also cloned into the pET32a (+) expression vector (pET$^{1\text{-}132}$IGFBP-2 and pET$^{1\text{-}185}$IGFBP-2); in the same way that the full-length cDNA was introduced (Figure 2.11).

2.4.3.3 C-Terminal Expression Constructs

The cDNA encoding $^{136\text{-}279}$IGFBP-2HIS was amplified by PCR and introduced into the pET32a (+) vector (pET$^{136\text{-}279}$IGFBP-2HIS). The PCR reaction involved primers 2:2BP-2, which introduced an *Nco*I restriction site at the 5' end of the construct, and LCHIS, which introduced both an *Eco*R I restriction site and cDNA encoding a hexahistidine tag at the 3' end of the construct (Figure 2.12). The PCR reaction was performed with 10 % DMSO.

2.4.4 CONFIRMATION OF THE EXPRESSION SYSTEMS CONSTRUCTED

The presence of the correct bIGFBP-2 cDNA insert in mammalian expression vectors was confirmed by digestion with *Pst* I and *Eco*R I restriction enzymes while newly generated *E. coli* vectors were checked by digestion with *Nco* I and *Eco*R I restriction enzymes. The entire subcloned cDNA of each construct was subsequently sequenced to ensure correct incorporation of the restriction enzyme site (*Apa* I) and that no errors were introduced during PCR. *fm*ol DNA cycle sequencing and ABI PRISM Dye Terminator Cycle Sequencing confirmed generation of correct cDNA clones (Figure 2.13 and 2.14). Automated sequencing was performed at the Institute of Medical and Veterinary Science Sequencing Centre, Adelaide, SA, Australia; and required at least 1 μg of DNA to obtain successful sequences. Initial attempts to sequence the newly generated vectors by ^{T7} DNA Sequencing, automated Dye Terminator DNA

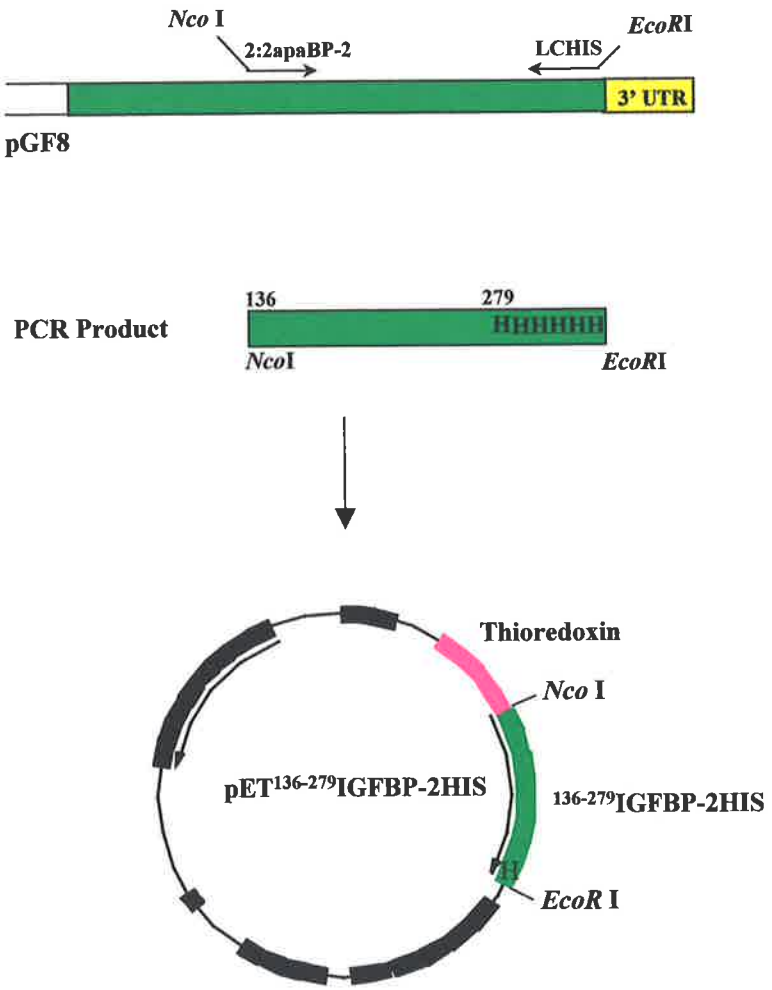

Figure 2.12 Cloning of cDNA encoding the C-terminal fragments into pET32a (+)
The cDNA encoding amino acid residues 136-279 of bIGFBP-2 was amplified by PCR, using the forward primer 2:2BP-2 and the reverse primer LCHIS, which encodes a hexahistidine tag. The resultant PCR product was cloned into the pET32a (+) expression vector (Novagen) using the *Nco* I-*Eco*R I restriction sites. This produced the *E. coli* expression vector: pET$^{136-279}$IGFBP-2HIS.

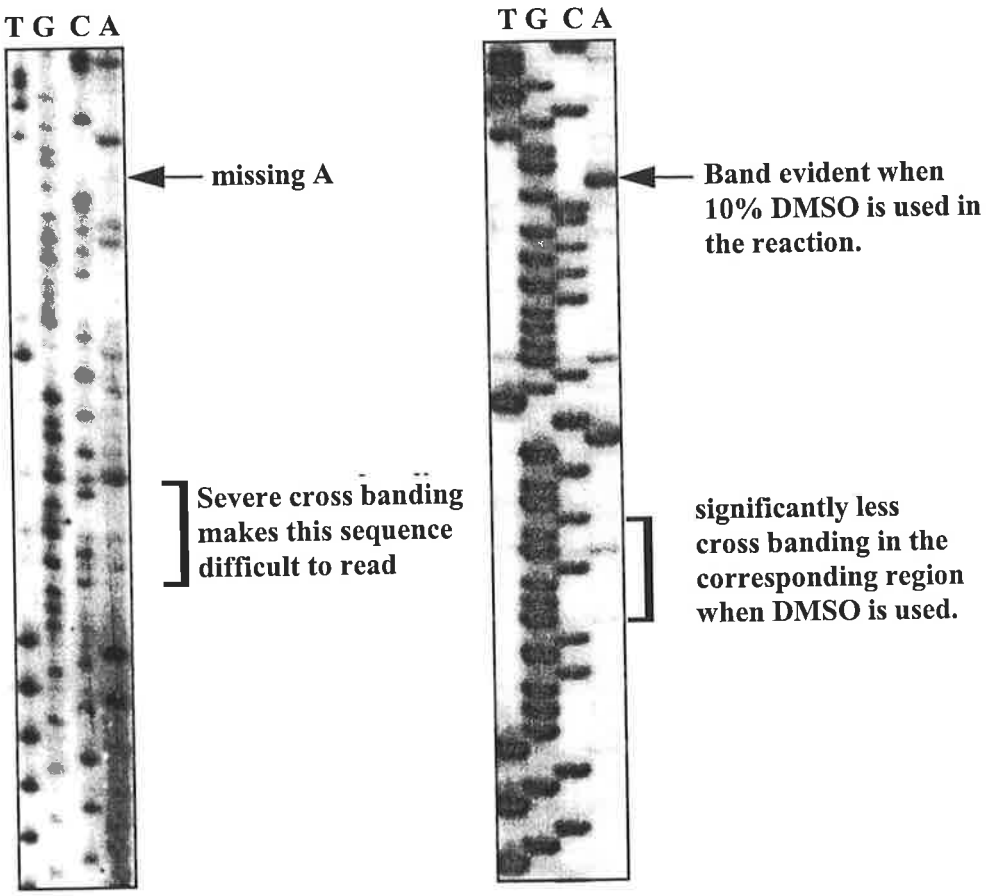

Figure 2.13 DNA sequencing of the pGF8(1-185) expression vector

a) DNA sequencing of the mutant expression vector pGF8(1-185) was performed by *fmol* DNA cycle sequencing as described by the manufacturer and in Section 2.3.14. Resultant sequences, both for pGF8(1-185) and the other expression vectors constructed (not shown), could not be read successfully.

b) The same region of pGF8(1-185) was sequenced with the addition of 10 % DMSO to the reaction. This greatly improved the quality of the sequence. Note the reduction in cross banding and the greater definition of the di-deoxynucleotide terminated bands.

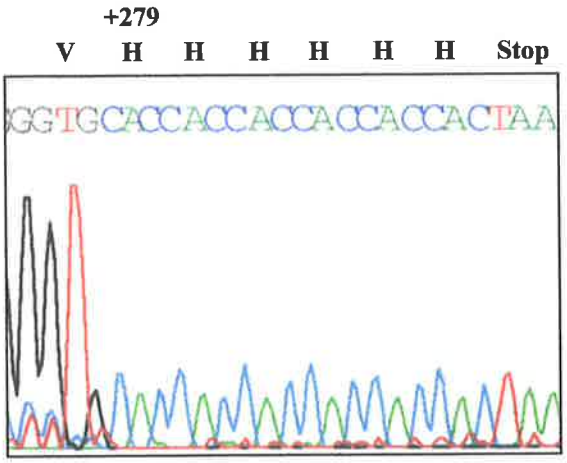

Figure 2.14 Dye terminator DNA sequencing to confirm incorporation of the hexahistidine-tag
Automated dye-terminator DNA sequencing confirmed the successful incorporation of the cDNA encoding the hexahistidine-tag into pGF8 to produce pGF8HIS. The DNA sequence was obtained using an internal forward primer, ShortC*Apa*I (Section 2.2.9), and the method described in Section 2.3.13. The single letter amino acid codes above the DNA sequence data highlight the residues that were changed (TQRMQ→HHHHH).

Sequencing and *fmol* DNA Cycle Sequencing was not successful. ^{T7} DNA Sequencing and automated Dye Terminator DNA Sequencing failed to generate a DNA sequence beyond the first few base pairs. *fmol* DNA Cycle sequencing did yield a sequence which extended a considerable length through the targeted region however both extensive cross banding and poor quality prevented confident analysis of the sequence. This was believed to be due to the same re-annealing problems experienced during the amplification of the PCR fragments. The addition of 10 % DMSO to the *fmol* DNA Cycle Sequencing reaction resulted in successful sequencing and verification of the mutant expression constructs. A comparison of the quality of sequencing obtained in the presence and absence of 10 % DMSO is presented in Figure 2.13.

2.5 SUMMARY

As summarised in Table 2.1, expression vectors were successfully established for the production of wildtype bIGFBP-2 and amino- and carboxyl-terminal fragments in both mammalian and *E. coli* cells.

Generation of bIGFBP-2 Expression Vectors

Two variant forms of the wildtype bIGFBP-2 expression vector were generated in this study, pGF8HIS and pGF8(*Apa*I). pGF8HIS incorporated a histidine-tag at the 3' end of the cDNA encoding bIGFBP-2 to facilitate purification of the expressed protein, while the introduction of an *Apa* I restriction site at the 3' end of the cDNA encoding the leader sequence, producing pGF8(*Apa*I), facilitated cloning of the C-terminal contructs.

Generation of N-Terminal Expression Vectors

Stop codons were strategically introduced into the cDNA of bIGFBP-2 in pGF8 to generate amino-terminal fragments of varying lengths. Expression vectors now exist for the production of $^{1\text{-}93}$IGFBP-2, $^{1\text{-}104}$IGFBP-2, $^{1\text{-}132}$IGFBP-2 and $^{1\text{-}185}$IGFBP-2 in COS-1 monkey kidney cells

(pGF(1-93), pGF8(1-104), pGF8(1-132) and pGF8(1-185)). The cDNAs for wildtype bIGFBP-2, $^{1-132}$IGFBP-2 and $^{1-185}$IGFBP-2 were also cloned into the pET32a (+) expression vector to enable the large-scale production of protein achievable in *E. coli* cells (pET$^{1-279}$IGFBP-2HIS, pET$^{1-132}$IGFBP-2 and pET$^{1-185}$IGFBP-2). Interestingly, the construction of IGFBP-2 PCR products for generation of these expression vectors was inhibited by secondary structure which was overcome by addition of 10 % DMSO.

Generation of C-Terminal Expression Vectors

Generation of the carboxyl-terminal expression vectors required the introduction of a unique restriction site and stop codon at the 3' end of the cDNA encoding the signal peptide. An *Apa* I restriction site was introduced by site directed mutagenesis as described in Section 2.4.2.3. The cDNA encoding the carboxyl-terminal amino acid residues $^{96-279}$IGFBP-2HIS, $^{137-279}$IGFBP-2HIS, $^{182-284}$IGFBP-2 were subsequently cloned downstream of the signal sequence in pGF8 (pGF8(96-279HIS), pGF8(137-279HIS) and pGF8(182-284)). $^{136-279}$IGFBP-2HIS was also cloned into the pET32a (+) expression vector (pET$^{136-279}$IGFBP-2HIS).

Expression, purification and characterisation of the truncated bIGFBP-2 proteins will be discussed in the following chapter.

CHAPTER 3

EXPRESSION, PURIFICATION AND CHARACTERISATION OF RECOMBINANT IGFBP-2 TRUNCATED PROTEINS

3.1 INTRODUCTION

In Chapter 2, mammalian and *E. coli* expression vectors encoding bIGFBP-2 and the truncated amino- and carboxyl-terminal fragments were generated. As discussed previously, these fragments were constructed based on IGFBP fragments previously reported in the literature. Interestingly, the size of the various IGFBP fragments isolated either from biological fluids or expressed recombinantly, differ significantly, both within IGFBP species and across family members. Furthermore, at the outset of this project, recombinant amino- and carboxyl-terminal fragments of IGFBP-2 did not exist. Expression of the various amino- and carboxyl-terminal IGFBP-2 fragments was therefore attempted for the first time in this study.

In this study, mammalian and *E. coli* expression systems were chosen for production of recombinant IGFBP-2 and IGFBP-2 truncated fragments. Mass spectroscopy and N-terminal sequencing was performed to determine the integrity of the protein expressed in these cells. Furthermore, the IGF binding properties of the recombinant proteins were investigated in preliminary IGF binding studies, Western ligand blot analysis and solution binding assays (for $^{1\text{-}185}$IGFBP-2). The results of the expressions and binding studies are discussed in the following sections.

3.2 MATERIALS

3.2.1 TISSUE CULTURE MATERIALS

Recombinant bIGFBP-2 was expressed in COS-1 (ATCC no: CRL 1650) monkey kidney cells grown and maintained in Dulbecco's modified Eagle's minimal medium (DMEM, from Gibco BRL, Glen Waverly, Victoria, Australia) and 10 % fetal calf serum (FCS; Flow Laboratories, North Ryde, NSW, Australia) or serum-free DMEM (from Gibco BRL, Glen Waverly, Victoria, Australia). Other tissue culture substrates including L-glutamine and trypsin were obtained from Gibco BRL, N-2-hydroxyethyl piperazine-N-2-ethane sulphonic acid (HEPES) was purchased from BDH Chemicals Australia Pty. Ltd. Kilsyth, Victoria, Australia; β-mercaptoethanol (β-ME) was purchased from Sigma Chemical Co. MO, USA, and insulin-transferrin sodium selenite media supplement (ITSS) was purchased from Boehringer Mannheim Australia, Sydney, NSW, Australia. Falcon plasticware used for tissue culture was supplied by Becton Dickinson Labware, Franklin Lakes, NJ, USA. For mammalian cell transfections, 0.4 cm gapped electroporation cuvettes and the Gene Pulser™ electroporation unit were purchased from Bio-Rad Pty. Ltd., North Ryde, NSW, Australia.

3.2.2 TISSUE CULTURE MEDIA AND BUFFERS

Mammalian tissue culture media, serum and PBS were prepared by Mrs J. McLean (Tissue Culture, Department of Biochemistry, Adelaide University, Australia) or by Francine Carrick. All solutions were made in water purified using the Milli-Q Ultra Pure Water System (Millipore Pty Ltd, North Ryde, NSW, Australia).

Dulbecco's Modified Eagles Medium (DMEM)
DMEM (net weight, 13.4 g pack), 40 mM $NaHCO_3$, 20 mM Hepes, 0.012 % (w/v) gentamycin, made up to 1 L in sterile H_2O, adjusted to pH 7.5 and filter sterilised (0.2 μm). Medium was freshly supplemented with sterile 1 mM L-glutamine, 0.01 mg/ml ITSS and 0.1 mM β-ME.

Serum Free DMEM
DMEM (net weight, 13.4 g pack) (with pyridoxine hydrochloride but without phenol red and sodium bicarbonate), 40 mM $NaHCO_3$, 20 mM Hepes, 0.012 % (w/v) gentamycin, made up to 1 L in sterile H_2O, adjusted to pH 7.5 and filter sterilised (0.2 μm). Medium was freshly supplemented with sterile 1 mM L-glutamine, 0.01 mg/ml ITSS and 0.1 mM β-ME.

Hepes Electroporation Buffer (HEBs)
0.1 M Hepes, 5 mM KCl, 1.2 mM $MgSO_4.7\ H_2O$ and 8 mM glucose
-Adjusted to pH 7.6 and filter sterilised (0.2 μm).

3.2.3 *E. COLI* PROTEIN EXPRESSION MEDIA AND BUFFERS

2YT
1.6 % (w/v) bacto®tryptone, 1 % (w/v) bacto® yeast extract, 0.5 % (w/v) NaCl
-Adjusted to pH 7.0 with NaOH

Fantastic Terrific Broth (FTB)
1.2 % (w/v) bacto®tryptone, 2.4 % (w/v) bacto®yeast extract, 0.4 % (v/v) glycerol
-After autoclaving, 10 % (v/v) sterile 17 mM KH_2PO_4, 72 mM K_2HPO_4 was added to the media.

Sonication Buffer
2.5 mM EDTA, 20 mM Tris-HCl
-Adjusted to pH 8.0

EkMax Buffer
50 mM Tris-HCl, 1 mM $CaCl_2$, 0.1 % Tween 20 (v/v)
-Adjusted to pH 8.0

3.2.4 MATERIALS FOR PROTEIN DETECTION AND PURIFICATION

All reagents were of analytical grade or higher. The following chemicals were obtained from Sigma Chemical Co., St Louis, MO, USA: activated charcoal, ammonium persulphate, 5-bromo-4-chloro-3-indolyl phosphate (BCIP), bovine serum albumin (BSA), bromophenol blue, Coomassie Brilliant Blue R250, imidazole, nickel sulphate, nitroblue tetrazolium (NBT),

polyoxethylene-sorbitan monolaurate (Tween 20), protamine sulphate, sodium dodecyl sulphate (SDS), N,N,N'N'-tetramethyl ethylene-diamine (TEMED) and Tris-HCl-(hydroxymethyl)aminomethane (Tris-HCl). Triton X-100 was obtained from Boehringer Mannheim Australia, Sydney, NSW, Australia. Acetic acid and HPLC grade methanol and acetonitrile were obtained from BDH Chemicals Australia Pty Ltd. Kilsyth, Victoria, Australia. Sequencing Grade trifluoroacetic acid (TFA) was obtained from Perkin Elmer, Applied Biosystems Division, Warrington, Great Britain. Acrylamide, Bis-acrylamide and the Mini-Protean II Gel system for casting and running protein gels were purchased from Bio-Rad Pty. Ltd., North Ryde, NSW, Australia. Nitrocellulose membranes (0.45 μm) were from Schleicher and Schuell, Dassel, Germany; while membranes for filtering were obtained from Millipore Corp., Bedford, MA, USA. Western transfer was performed using a Multiphor II Novablot electrophoretic transfer unit (Pharmacia, Uppsala, Sweden). Presiliconised tubes for protein storage and handling were obtained from Sorenson BioScience Inc., Salt Lake City, USA. Media was concentrated post culture using an Amicon Bioseparations 8400 stirred ultrafiltration cell purchased from Adelab Scientific, Norwood, SA, Australia, containing Pall Filtron disc membrane filter (type: Omega, 76 mm diameter with a 10 kDa nominal molecular weight cut off), purchased from Crown Scientific Pty Ltd., Beverly, SA, Australia. Affi-Gel®10 and Affi-Prep®10 matrix was obtained from Bio-Rad Pty. Ltd., North Ryde, NSW, Australia. Affinity and size exclusion chromatography were performed using the High Precision Pump P-500 system (Pharmacia Biotech, Uppsala, Sweden) with online Pharmacia UV-1 monitor set at 280 nm. Zymatrix nickel-iminodiacetate (Ni-IDA) affinity resin was purchased from Bioserve, Heidleberg West, Victoria, Australia. Nickel-nitrilotriacetate (Ni-NTA) conjugated to alkaline phosphatase was purchased from Qiagen Pty Ltd., Clifton Hill, Victoria, Australia. Enterokinase (EkMax) was obtained from Invitrogen, Carlsbad, CA, USA. HPLC was performed using two Waters 510 HPLC pumps, an online Waters 486 Tunable Absorbance Detector and Millennium Software from Waters, Sydney, NSW, Australia. The PE Brownlee™ Aquapore® C4 (100 x 10 mm) BU-300 column with 20 μm particles was purchased from Rainin

LC and Supplies, Mulgrave, Victoria, Australia. The Delta-Pak PrepLC (25 x 100 mm) column segments and guard packs were purchased from Waters, Sydney, NSW, Australia.

3.2.4.1 Protein Electrophoresis, Transfer and Ligand Blot Buffers

2 x Protein loading buffer
125 mM Tris-HCl, 4 % (w/v) SDS, 10 % (v/v) glycerol, 0.1 % Bromophenol Blue pH 6.8

Protein Gel Running Buffer
250 mM glycine, 25 mM Tris-HCl pH 8.3, 0.1 % (w/v) SDS

Western Ligand Buffer
100 mM Tris-HCl pH 7.5, 150 mM NaCl

Ligand Blot buffer 2
100 mM Tris-HCl pH 9.5, 100 mM NaCl, 5 mM $MgCl_2$

Gel Fixing Solution
50 % (v/v) ethanol, 10 % (v/v) acetic acid

Gel Destain Solution
10 % acetic acid

Protein Transfer Buffer
20 mM Tris-HCl pH 7.5, 150 mM glycine, 20 % (v/v) ethanol

Coomassie Blue
0.3 % (w/v) Coomassie Blue R-250, 10 % (v/v) acetic acid

Gel Drying Solution
5 % (v/v) glycerol, 30 % (v/v) ethanol

Substrate 1
2.5 mM luminol (3-aminophthalalhydrazide) (dissolved in DMSO), 0.4 mM p-coumaric acid (dissolved in DMSO), 100 mM Tris-HCl pH 8.5

Substrate 2
56 mM H_2O_2, 100 mM Tris-HCl pH 8.5

3.2.4.2 Chromatography Buffers

Superose®6 column buffer
100 mM sodium acetate, 20 % (v/v) ethanol, 0.05 % (w/v) SDS
-Adjusted to pH 7.0 and filter sterilised (0.45 μM)

IGF Affinity Column Buffer
50 mM sodium phosphate, 150 mM NaCl, 0.05 % (v/v) Tween-20

-Adjusted to pH 6.5 and filter sterilised (0.45 μM)

Resource-S Column Buffer A
50 mM ammonium acetate
-Adjusted to pH 6.0 and filter sterilised (0.45 μM)

Resource-S Column Buffer B
1 M ammonium acetate
-Adjusted to pH 7.5 and filter sterilised (0.45 μM)

3.2.4.3 HPLC Buffers

HPLC Buffer A
0.1 % (v/v) TFA
-Filtered (0.2 μm)

HPLC Buffer B
80 % acetonitrile, 0.088 % (v/v) TFA
-Filtered (0.2 μm)

3.2.4.4 Nickel Chromatography Buffers

$NiSO_4$ Charge Buffer
50 mM $NiSO_4$,
-Adjusted to pH 7.9 and filter sterilised (0.45 μM)

Binding Buffer
5 mM imidazole, 0.5 M NaCl, 20 mM Tris-HCl
-Adjusted to pH 7.9 and filter sterilised (0.45 μM)

Wash Buffer
10 mM imidazole, 0.5 M NaCl, 20 mM Tris-HCl
-Adjusted to pH 7.9 and filter sterilised (0.45 μM)

Elute Buffer
0.5 M imidazole, 0.5 M NaCl, 20 mM Tris-HCl
-Adjusted to pH 7.9 and filter sterilised (0.45 μM)

Strip Buffer
0.1 M EDTA, 0.5 M NaCl, 20 mM Tris-HCl
-Adjusted to pH 7.9 and filter sterilised (0.45 μm).

3.2.4.5 Charcoal Binding Assay Buffers

Charcoal Binding Buffer
0.2 M sodium phosphate, 150 mM NaCl, 0.25 % (w/v) BSA
-Made fresh prior to use and adjusted to pH 6.5

Activated Charcoal Solution
Charcoal binding buffer, 0.5 % (w/v) activated charcoal, 0.02 % (w/v) protamine sulphate
-Made fresh and stirred at 4 °C for at least 1 hour prior to use.

3.2.5 ANTIBODIES AND PROTEIN STANDARDS

Rabbit anti-serum raised against bovine IGFBP-2 was a kind gift from Dr B. Forbes (Adelaide University). Avidin alkaline phosphatase-conjugated goat anti-rabbit IgG was purchased from Sigma Chemical Co. St Louis, MO, USA. Horseradish peroxidase conjugated streptavidin was purchased from Amrad, Boronia, Vic, Australia. Rainbow™ [^{14}C] methylated protein molecular weight markers were obtained from Amersham Pharmacia, North Ryde, NSW, Australia. Biotinylated molecular weight markers were obtained from Bio-Rad Pty. Ltd., North Ryde, NSW, Australia. Mark 12 markers for Coomassie gels were obtained from NOVEX, Carlsbad, CA, USA. ^{125}I-IGF-I and ^{125}I-IGF-II were a kind gift from Dr Z. Upton or Dr S. Milner (CRC for Tissue Growth and Repair). Biotinylated IGF-I and biotinylated IGF-II were purchased from GroPep Ltd., Thebarton, SA, Australia.

3.3 METHODS

3.3.1 EXPRESSION OF bIGFBP-2 AND bIGFBP-2 TRUNCATIONS FROM MAMMALIAN COS-1 CELLS

3.3.1.1 FPLC Purification of DNA for Mammalian Cell Transfections

Prior to transfection into COS-1 cells, large-scale preparations of DNA (Section 2.3.2) were purified by Superose®-6 gel filtration (bed volume = 25 ml) (Amersham Pharmacia, North

Ryde, NSW, Australia) using fast performance liquid chromatography (FPLC). The column was equilibrated and the DNA sample eluted in Superose®-6 buffer at a flow rate of 1 ml/minute. DNA-containing fractions were precipitated at -20 °C in ice-cold RNase-free ethanol. The DNA concentration was quantitated by absorbance at 260 nm and the quality assessed by measuring absorbance in the range 210 nm to 300 nm using a Hewlett Packard 8451A DIODE Array Spectrophotometer.

3.3.1.2 Transfection of COS-1 Cells

Recombinant bIGFBP-2 was expressed in COS-1 (ATCC no:CRL 1650) simian kidney cells as previously described (Forbes *et al.*, 1998). COS-1 cells were thawed from stocks in liquid nitrogen and maintained in DMEM with 10 % FCS in 150 cm^2 flasks in an Infrared CO_2 Incubator (Forma Scientific), at 37 °C with 5 % CO_2. Cells were typically grown to 80-90 % confluency prior to seeding a fresh flask. Cells to be harvested for transfection were washed with PBS and treated with 0.1 % trypsin (w/v) in PBS at room temperature for 5 minutes. The detached cells were pelleted by centrifugation at 1000 x g for 5 minutes and washed twice in HEBs supplemented with 0.11 % glucose. A haemocytometer was used to estimate the number of unstained, viable cells in a known volume stained with 0.4 % (w/v) trypan blue. The COS-1 cells were subsequently resuspended in HEBs to a final density of 5 x 10^6 cells/500 µl. Transfections were performed in chilled (4 °C) cuvettes containing 50 µl FCS, 0.5 µg salmon sperm DNA, purified plasmid (10 µg) and 5 x 10^6 cells. Cells were subjected to a single electrical pulse (0.27 V, 250 µFD) using a Bio-Rad Gene Pulser followed by a recovery period of 10 minutes at room temperature. In small-scale experiments, the contents of one cuvette were placed in a 10 cm petri dish or 75 cm^2 flask with 10 mls pre-warmed DMEM and 10 % FCS. In larger experiments, electroporated cells from two cuvettes were combined to seed one 150 cm^2 flask overnight at 37 °C in DMEM and 10 % FCS. The cells were then washed twice with PBS and cultured in serum free DMEM for 24 hours at 37 °C in 5 % (v/v) CO_2 prior to

collection of the media. Media was collected each day for 5 days and stored in siliconised bottles at –20 °C. COS-1 cells were transfected with pGF8HIS, pGF8(1-93), pGF8(1-104), pGF8(1-132), pGF8(1-185), pGF8(96-279HIS), pGF8(96-284), pGF8(137-279HIS), pGF8(185-279HIS) and pGF8(185-284). In addition, pGF8 was transfected into COS-1 cells to confirm expression of correctly folded mature bIGFBP-2 and pXMT2 was used to determine background levels of sIGFBP-2 and sIGFBP-3.

3.3.1.3 Collection of Cell Lysates

Following collection of conditioned medium for 5 days, transfected COS-1 cells were harvested. Cells were detached from surfaces with 2 ml 0.1 % (w/v) trypsin/flask and centrifuged at 1000 x g for 5 minutes. The cells were washed with PBS and resuspended in a final volume of 200 µl PBS. Cell lysates (approximately 7.5 x 10^5 cells) were reduced in 2 x protein loading buffer with 5 % β-ME by heating to 100 °C for 5 minutes prior to loading on a 15 % polyacrylamide tricine gel.

3.3.2 EXPRESSION OF bIGFBP-2 AND TRUNCATIONS FROM *E. COLI* BL21 CELLS

The pET constructs (pET$^{1-279}$IGFBP-2HIS, pET$^{1-132}$IGFBP-2, pET$^{1-185}$IGFBP-2 and pET$^{136-279}$IGFBP-2HIS; described in Section 2.4.3) were transformed into *E. coli* BL21 cells for large-scale protein expression. Briefly, 2YT (2 L) containing carbencillin (100 µg/ml) was inoculated with an overnight culture (1:10), incubated at 37 °C with shaking and induced with 1 mM IPTG at an A_{600} of approximately 0.8. Protein was expressed for a minimum of 4 hours prior to pelleting the cells (5000 x g, 5 minutes, 4 °C). The cells were then resuspended to one tenth of the original volume in sonication buffer with lysozyme (100 µg/ml) and sonicated

(Sonifier Cell Disrupter B-30) for 3 x 30 seconds on ice. The soluble fraction was collected by centrifugation of the cell lysates (10000 x g, 10 minutes, 4°C) and filtered (1 μm).

3.3.3 IGF-AFFINITY CHROMATOGRAPHY

IGFBPs expressed from COS-1 cells were initially purified on an IGF-II affinity column (IGF-II, purchased from GroPep Ltd., Australia, was coupled to Affi-Prep-10 matrix; as recommended by the supplier Bio-Rad Pty. Ltd., North Ryde, NSW, Australia). Conditioned medium collected from transfected COS-1 cells was thawed at room temperature and filtered (0.45 μm), followed by addition of Tween-20 (0.05 %) to minimise non-specific protein interactions. The media was loaded onto the column using a peristaltic pump at a flow rate of 1 ml/minute then washed in IGF affinity column buffer with 0.01 % Tween 20, until a baseline absorbance at 280 nm was obtained. Specifically bound IGFBP was eluted in 0.5 M acetic acid and the fractions containing protein pooled for further purification on a Resource-S cation exchange column (1 ml column, Pharmacia, Stockholm, Sweden).

IGFBP-2 or truncated IGFBP-2s were separated from endogenously expressed sIGFBP-3 by Resource-S cation exchange. The column was washed with Resource-S column buffer B and equilibrated with 0.5 M acetic acid prior to loading the affinity-purified fractions at 1 ml/minute. The column was then equilibrated in Resource-S column buffer A and the IGFBPs eluted using a linear gradient of Resource-S column buffer B (0-100%) over 20 minutes at a flow rate of 1 ml/minute. Eluted protein was detected by absorbance at 280 nm and fractions were collected across the gradient.

The final purification step of COS-1 expressed IGFBP involved separating recombinant IGFBP-2 or truncated IGFBP-2s from the endogenous sIGFBP-2. This was achieved by rpHPLC on a C4 analytical column (Brownlee Aquapore BU300, 7 mm particle size, 300-Å pore size, 2.1 mm x 100 mm). The pooled Resource-S fractions were acidified with 0.1% TFA to pH 3.0 and loaded onto the rpHPLC column equilibrated with 75 % HPLC buffer A, 25 % HPLC buffer B at ambient temperature. The IGFBPs were eluted from the rpHPLC column in a

linear gradient of acetonitrile (20-50 %) over 30 minutes at a flow rate of 0.5 ml/minute. The eluted protein was detected by absorbance at 215 nm using a Flow Through Ultraviolet Detector (Waters, Model 490) and a Fluorescence Spectrometer (LS.4 Perkin Elmer, Norwalk CT, USA). Reverse phase HPLC utilised Waters Expert™ Chromatography software. The purified material was lyophilised and stored at -20 °C. The purity and quantity of each protein was determined by rpHPLC and confirmed by N-terminal sequencing.

Similarly, *E. coli* derived Trx^{1-279}IGFBP-2HIS was purified on a hydroxamated IGF-I affinity column (hydroxamated IGF-I (12 mg), a kind gift from GroPep Ltd., Australia, was coupled to Affi-Prep®10 matrix as recommended by the supplier Bio-Rad Pty. Ltd., North Ryde, NSW, Australia; final resin volume of 25 ml). The soluble sonicated protein preparation was filtered (1 μm) and diluted 1:2 with IGF affinity column buffer prior to loading onto the column at a flow rate of 1 ml/minute through a peristaltic pump. Upon completion of the loading, unbound protein was washed from the column with IGF affinity column buffer until a baseline absorbance at 280 nm was obtained. The remaining bound protein was eluted in 0.5 M acetic acid and the fractions containing protein pooled for further purification by rpHPLC.

3.3.4 NI-AFFINITY CHROMATOGRAPHY

The conditioned media of COS-1 cells transfected with pGF8(96-279HIS) or pGF8(137-279HIS) were concentrated approximately 4- to 6-fold by ultrafiltration at 4 °C with 250 kPa of pressure supplied by a nitrogen source. The concentrated sample was then loaded by gravity flow onto either a Ni-NTA or Ni-IDA column (resin volume was approximately 10 ml) charged with 4 column volumes of $NiSO_4$ charge buffer and equilibrated in 3 column volumes of binding buffer. Non-specifically bound protein was washed from the column with increasing imidazole concentrations; firstly 10 column volumes of binding buffer followed by 6 column volumes of wash buffer. Specifically bound HIS-tagged proteins were eluted in 6 column

volumes of elute buffer. The column was then stripped with 5 column volumes of strip buffer and stored at 4 °C. Eluted HIS-tagged proteins were further purified by rpHPLC.

Thioredoxin-tagged proteins expressed in *E. coli* cells were also purified by Ni-IDA affinity chromatography. The protocol was the same as that described for the purification of $^{137\text{-}279}$IGFBP-2HIS and $^{96\text{-}279}$IGFBP-2HIS, expressed in COS-1 cells, with a few notable exceptions. The bed volume of Ni-IDA resin was approximately 50 ml and no less than one tenth of the sample volume. The sonicated samples were filtered (1 μm) prior to batch binding overnight at 4 °C with rocking. Non-specific protein interactions were washed with increasing concentrations of imidazole and the HIS-tagged protein eluted in 0.5 M imidazole. The eluted protein was further purified by rpHPLC on a Delta-Pak PrepLC column. While initial large-scale preparations of Trx$^{1\text{-}279}$IGFBP-2HIS were purified by IGF-affinity chromatography, all subsequent large-scale expressions were purified by Ni-affinity chromatography.

3.3.5 ENTEROKINASE CLEAVAGE

The thioredoxin fusion-tag was removed from recombinantly expressed *E. coli* proteins by cleavage with enterokinase (EkMax 0.5 unit/mg protein) in EkMax buffer for 30 minutes at 37 °C. The resultant cleavage products were resolved by rpHPLC and lyophilised for storage at -20 °C.

3.3.6 GENERAL METHODS FOR PROTEIN EXPRESSION AND DETECTION

3.3.6.1 SDS Polyacrylamide Gel Electrophoresis

Conditioned media samples (500 μl) were concentrated using Centricon 10 microconcentrators (Amicon, Denvers, MA, USA) and the protein was separated by SDS polyacrylamide gel electrophoresis under non-reducing conditions (unless otherwise stated).

IGFBP-2 truncations were analysed either on 12.5 % polyacrylamide glycine gels using the system described by Laemmli (1970), or on 15 % polyacrylamide tricine gels as described by Schagger and von Jagow (1987). Protein samples were heated to 100 °C for 5 minutes in 2 x protein loading buffer prior to electrophoresis. The gels used for electrophoresis were 8 x 6 x 0.15 cm with an applied current of 30 mA per gel until adequate separation was achieved.

E. coli protein preparations were also analysed by polyacrylamide gel electrophoresis. Samples of induced and uninduced culture medium (1 ml) were pelleted and the cells resuspended in lysis buffer to a final concentration equivalent to 50 µl/OD unit and boiled for 10 minutes to reduce the cell membranes. The whole cell lysates (10 µl) were then loaded onto a 12.5 % polyacrylamide gel and electrophoresed at 30 mA per gel.

3.3.6.2 Coomassie Blue Staining of SDS Polyacrylamide Gels

Proteins, separated by SDS polyacrylamide gel electrophoresis, were either transferred to nitrocellulose filters or stained with Coomassie blue. Gels were fixed in gel fixing solution for 20 minutes, stained in a solution of Coomassie Blue for 60 minutes and then washed in gel destain solution, usually preheated to 42 °C, until the background staining was negligible.

3.3.6.3 Immunoblotting of Nitrocellulose Filters

Proteins separated by SDS polyacrylamide gel electrophoresis (Section 3.3.6.1) were transferred to nitrocellulose filters (0.45 µm) using a semi-dry Western transfer NOVA Blot Apparatus (Amersham Pharmacia, North Ryde, NSW, Australia) in transfer buffer for 90 minutes at 30 mA per gel. Nitrocellulose filters were blocked in Western ligand buffer with 1 % BSA and 1 % Tween 20 for 2 hours prior to the addition of polyclonal anti-bIGFBP-2 antiserum (1:5000) which was produced in this laboratory as previously described by Forbes *et*

al., 1990. Briefly, the antibody was allowed to bind for 6 hours with rocking at room temperature. After this incubation, filters were washed three times for 20 minutes each in Western ligand buffer with 0.1 % Tween 20. The secondary antibody, goat anti-rabbit IgG alkaline phosphatase-conjugate, was administered (1:10000) for 3 hours at room temperature followed by a single 20 minute wash in Western ligand buffer with 0.1 % Tween 20 and two 20 minute washes in ligand blot buffer 2. The substrates for the colour reaction, NBT (75 μg/ml) and BCIP (75 μg/ml), were added to 10 ml of the final wash buffer and incubated for several minutes in the dark as described by Bers and Garfin (1985). The reaction was stopped with 1 mM EDTA.

3.3.6.4 Western Ligand Blots

Western ligand blotting was essentially as described by Hossenlopp and co-workers (1986). Proteins transferred to nitrocellulose filters were washed with ligand buffer and 0.1 % Triton X-100 (v/v) for 10 minutes prior to blocking the filter for 2 hours in ligand buffer supplemented with 1 % BSA with 1 % Tween 20. The filters were then rocked overnight at 4 °C in 10 ml of the final blocking buffer with ^{125}I-IGF-II peptide (1 x 10^6 cpm) (prepared as previously described by Francis *et al.*, 1998). Unbound tracer was removed after this incubation period by three washes of 20 minutes at room temperature with ligand buffer and 0.1 % Tween 20. Following this, the filters were air-dried and exposed to a PhosphorImager screen for 24 hours (Molecular Dynamics, Sunnyvale, California, USA) and visualised using a Molecular Dynamics PhosphorImager and Image Quant software.

Alternatively, blots were probed with biotinylated IGF-I or monobiotinylated IGF-II (1 μg per 10 ml of Western ligand buffer). Following overnight incubation, the blots were washed three times for 20 minutes in Western ligand buffer and then incubated with horseradish peroxidase-conjugated streptavidin (diluted 1:100000 in Western ligand buffer) at room temperature for 30 minutes. The conjugate was removed by three 20 minutes washes with

Western ligand buffer. The blots were developed using equal quantities of Substrate 1 and Substrate 2 for 1 minute and subsequently exposed to X-ray film (Konica) and developed in an Auto-Rad developer.

3.3.6.5 Mass Spectroscopy and N-terminal Sequencing

Lyophilised protein samples (10-30 μg) were submitted for electrospray mass spectroscopy to the Australian Research Council EMS Unit, Adelaide, Australia. Yogi Hayasaka performed the analysis on a Perkin-Elmer SCI-EX API-300 triple quadruple mass spectrometer. N-terminal amino acid sequences were determined by Edman degradation using an Applied Biosystems 492 'Procise' protein sequencer (performed by Denise Miller and Francine Carrick, Department of Biochemistry, Adelaide University).

3.3.6.6 Solution binding assays

Charcoal binding assays were performed as described by Szabo and co-workers (1988). The assays were performed in 100 μl charcoal binding buffer using either full-length bIGFBP-2 or $^{1\text{-}185}$IGFBP-2 at various concentrations. The binding proteins were equilibrated for 3 hours with ^{125}I-IGF-II (10000 cpm/tube). The activated charcoal mix absorbed unbound ^{125}I-IGF-II for 30 minutes on ice. The ^{125}I-IGF-II:IGFBP complexes were separated from unbound ^{125}I-IGF-II by centrifugation at 13200 x g for 3 minutes. The percentage of bound ^{125}I-IGF-II was determined by counting radioactivity of the supernatant on a multichannel gamma counter (Bromma, LBK).

Percentage of ^{125}I-IGF bound was calculated as follows:

$$\% \text{ IGF bound} = \frac{\text{cpm-NSB}}{\text{total counts}} \times 100\ \%$$

(cpm: counts per minute; NSB: non-specific binding)

3.3.6.7 Biosensor Analyses

Preparation of biosensor chips and kinetic anaylses is described in detail the following chapter. Briefly, the association and dissociation rates of mammalian and *E. coli* derived proteins were compared in this study. Various concentrations of analyte (200, 100, 50, 25, 12.5 nM) in HBS running buffer, were injected for 5 minutes during the association phase (40 µl/minute). The dissociation phase, initiated by passage of HBS running buffer alone, was carried out over a period of 10 minutes. The biosensor surfaces were regenerated by a 60 second injection of 0.1 M HCl.

3.4 RESULTS

3.4.1 PROTEIN EXPRESSION

3.4.1.1 Expression of $^{1-132}$IGFBP-2, $^{1-185}$IGFBP-2, $^{96-284}$IGFBP-2, $^{96-279}$IGFBP-2HIS and $^{137-279}$IGFBP-2HIS from Mammalian COS-1 Cells

The truncated proteins $^{1-132}$IGFBP-2, $^{1-185}$IGFBP-2, $^{96-284}$IGFBP-2, $^{96-279}$IGFBP-2HIS and $^{137-279}$IGFBP-2HIS were successfully expressed from transfected COS-1 cells (Section 3.3.1.2) as indicated by immunoblotting of the conditioned medium (Figure 3.1). In addition, full-length bIGFBP-2 (30 kDa) and several presumed degradation products were detected in the conditioned medium of COS-1 cells transfected with pGF8. Basal levels of endogenous sIGFBP-2 and sIGFBP-3 were evident in the negative control and also observed in the conditioned medium of cells transfected with the truncated bIGFBP-2 constructs. The molecular masses of $^{1-132}$IGFBP-2, $^{1-185}$IGFBP-2, $^{96-284}$IGFBP-2, $^{96-279}$IGFBP-2HIS and $^{137-279}$IGFBP-2HIS were predicted to be 13604 Da, 19439 Da, 20960 Da, 21002 Da and 17039 Da respectively. The immunoreactive bands corresponding to these IGFBP-2 truncations did not migrate as expected from their predicted molecular masses as they all run above the 21 kDa trypsin inhibitor molecular weight marker. Interestingly, previously isolated bIGFBP-2

fragments have also behaved as apparently larger molecular mass proteins (Conover *et al.*, 1996; Baxter and Firth, 1996; Forbes *et al.*, 1998). As seen in Figure 3.1, $^{1-185}$IGFBP-2 migrates within the 12.5 % polyacrylamide glycine gel less distance than the larger $^{96-284}$IGFBP-2.

The ability of these truncated proteins to bind ^{125}I-IGF-II was assessed by Western ligand blotting (Figure 3.1). Full-length bIGFBP-2 and sIGFBP-2 (both migrate at approximately 30 kDa) bound ^{125}I-IGF-II as did a dimer of bIGFBP-2 at approximately 60kDa. A higher molecular weight band that runs consistently with endogenously expressed sIGFBP-3 (40-45kDa) also demonstrated ^{125}I-IGF-II binding capabilities. The recombinantly expressed N-terminal proteins, $^{1-132}$IGFBP-2 and $^{1-185}$IGFBP-2, bound ^{125}I-IGF-II by Western ligand blot (Figure 3.1). In contrast, the C-terminal proteins $^{96-284}$IGFBP-2, $^{96-279}$IGFBP-2HIS and $^{137-279}$IGFBP-2HIS, did not exhibit any detectable ^{125}IGF-II binding by Western ligand blot despite detecting high levels of secreted protein in the conditioned medium by immunoblotting.

3.4.1.2 Expression of $^{1-93}$IGFBP-2, $^{1-104}$IGFBP-2 and $^{182-284}$IGFBP-2 From Mammalian COS-1 Cells

In this study, expression of $^{1-93}$IGFBP-2, $^{1-104}$IGFBP-2 and $^{182-284}$IGFBP-2 was not detected in the conditioned media of COS-1 cells transfected with pGF8(1-93), pGF8(1-104) and pGF8(182-284). Although polyclonal antibodies against bIGFBP-2 identified both full-length bIGFBP-2 and endogenously expressed sIGFBP-2, the recombinantly expressed truncations were not detected on immunoblots at a position consistent with their predicted molecular masses (9680 Da, 10687 Da and 11799 Da respectively) (Figure 3.1). Lack of detectable expression is probably not due to failure of the polyclonal antibodies to recognise the recombinant peptides as cyanogen bromide fragments corresponding to the N- and C-terminal

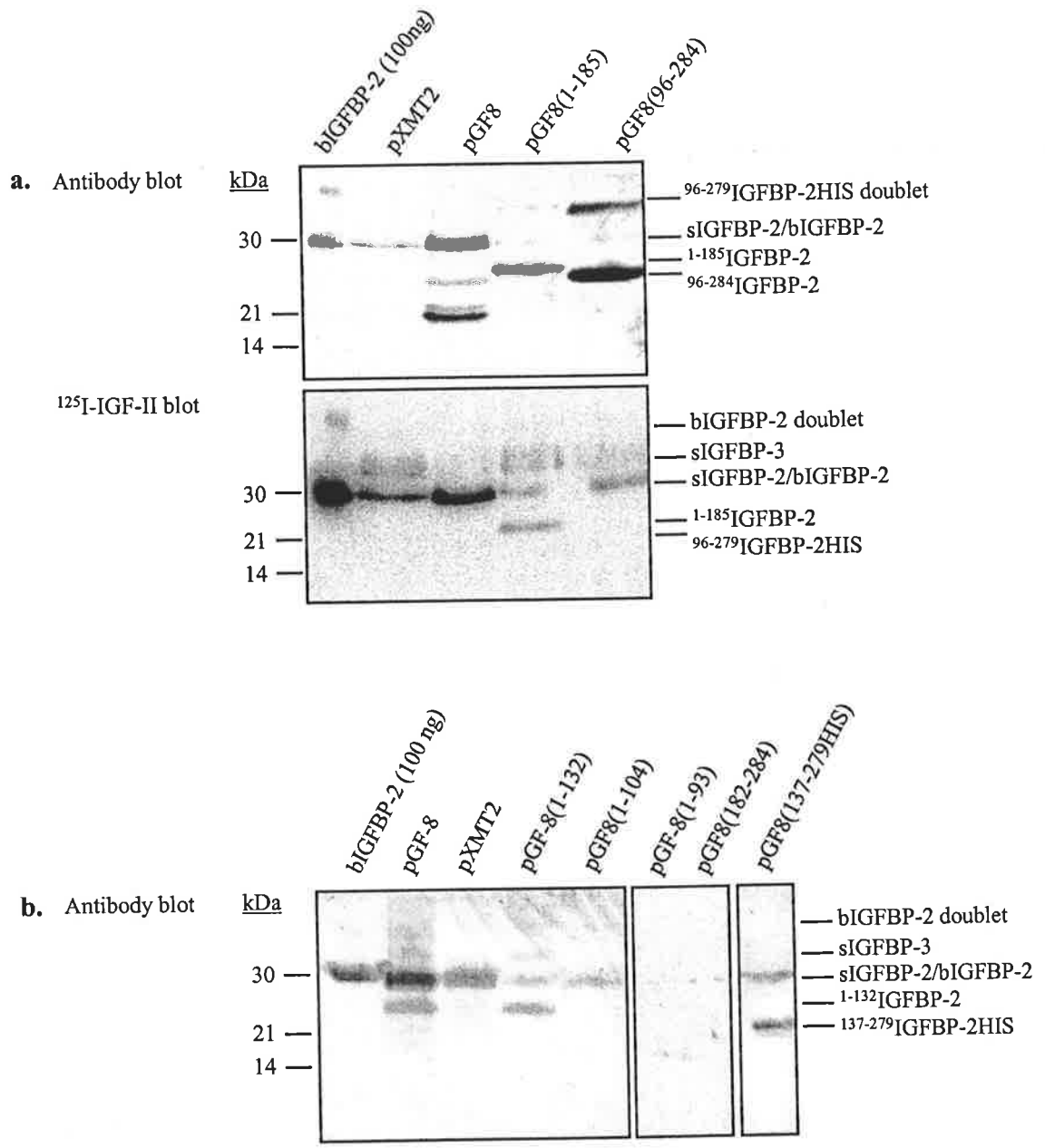

Figure 3.1 Antibody and ^{125}I-IGF-II Western blot analysis of recombinant bIGFBP-2 and truncated IGFBP-2s

Conditioned medium from the transfection of COS-1 cells with pGF8, pGF8*Apa*I, pGF8HIS, pGF8(1-93), pGF8(1-104), pGF8(1-132), pGF8(1-185), pGF8(96-279HIS), pGF8(96-284), pGF8(137-279HIS), pGF8(185-279HIS) and pGF8(185-284) were analysed for the expression of recombinant proteins. The equivalent of 500 µl of conditioned medium was separated by SDS-PAGE electrophoresis on a 12.5% glycine gels and either immunoblotted with polyclonal antibody against bIGFBP-2 (Section 3.3.6.3) or probed with ^{125}I-IGF-II (1 µg; Section 3.3.6.4). The vectors pGF8 and pXMT2 were transfected as controls. Purified bIGFBP-2 was loaded as a molecular weight standard and 14C Rainbow markers are indicated to the left of the gel. Endogenous expression of sIGFBP-2 in evident in the pXMT2 tracks and in all transfected conditioned media. Transfection of COS-1 cells with pGF-8 yielded wildtype bIGFBP-2 (~30 kDa) and several breakdown products.

domains of bIGFBP-2 isolated in this laboratory have been shown to be immunoreactive (Forbes *et al.*, 1998). Though unlikely, it is possible that the recombinantly expressed truncations may adopt an incorrect conformation that will not be recognised by the polyclonal antibodies raised against native bIGFBP-2. Furthermore, despite the detection of bIGFBP-2 with ^{125}I-IGF-II by Western ligand blotting, no ^{125}I-IGF-II binding fragments were detected in the conditioned media corresponding to fragments $^{1-93}$IGFBP-2, $^{1-104}$IGFBP-2 or $^{182-284}$IGFBP-2 (results not shown). These results suggest that $^{1-93}$IGFBP-2, $^{1-104}$IGFBP-2 and $^{182-284}$IGFBP-2 were not expressed at levels high enough for detection in conditioned medium. This could be due to rapid degradation of the secreted protein or alternatively due to the failure to synthesise or secrete the protein. Interestingly, a slightly larger amino-terminal protein encompassing amino acid residues 1-132 of IGFBP-2 was detected in the conditioned media of COS-1 transfected cells (Figure 3.1).

Failure to detect the recombinantly expressed fragments of IGFBP-2 may also be a consequence of their inability to be secreted into the conditioned media of transfected COS-1 cells, due to incorrect folding or incomplete processing. Preliminary investigations of pre-bIGFBP-2 truncations by the SignalP computer program (http://www.cbs.dtu.dk/services/SignalP/) however, predicted successful cleavage of the signal sequence allowing secretion of the protein from COS-1 cells. Although there are limitations to such programs, this would suggest that the inability to detect expression of $^{1-93}$IGFBP-2, $^{1-104}$IGFBP-2 and $^{182-284}$IGFBP-2 in conditioned medium is not likely to be due to a failure to secrete the protein. The successful secretion of $^{1-132}$IGFBP-2, $^{1-185}$IGFBP-2, $^{137-279}$IGFBP-2HIS, $^{96-279}$IGFBP-2HIS and $^{96-284}$IGFBP-2, as described in Section 3.4.1, further supported this. Indeed, the absence of immunoreactive bands at locations consistent with the predicted molecular masses upon analysis of whole cell lysates by SDS polyacrylamide gel electrophoresis indicated that the proteins were not retained within the cell lysates.

Difficulties associated with expression of $^{1-93}$IGFBP-2, $^{1-104}$IGFBP-2 and $^{182-284}$IGFBP-2 may be a consequence of transcription, translation or post-translational processes such as folding or degradation. Further investigations of $^{1-93}$IGFBP-2, $^{1-104}$IGFBP-2 and $^{182-284}$IGFBP-2

would include RNase protection assays or Northern analysis to determine the presence of mRNA transcripts in transfected COS-1 cells. In addition, while $^{1\text{-}93}$IGFBP-2, $^{1\text{-}104}$IGFBP-2 and $^{182\text{-}284}$IGFBP-2 have not been detected either in the cell lysates or conditioned medium, it is not known at this stage if this is due to failure to translate the message or due to degradation of the correctly translated and secreted protein. It appears that additional residues of both the amino- and carboxyl-terminal domains are required for the correct folding of the protein and are necessary for increased stability *in vivo*. Hence the residues of the linker peptide may contribute to maintaining the correct structural conformation of the amino- and carboxyl-terminal domains of bIGFBP-2.

3.4.1.3 Expression of Trx$^{1\text{-}279}$IGFBP-2HIS, Trx$^{1\text{-}132}$IGFBP-2, Trx$^{1\text{-}185}$IGFBP-2 and Trx$^{136\text{-}279}$IGFBP-2HIS from E. coli Cells

The expression of wildtype bIGFBP-2 and IGFBP-2 mutants and truncations in COS-1 cells has been a successful strategy in the laboratory to date. However, the quantity of recombinant protein that COS-1 cells are capable of producing is one of the limitations of this system (Table 3.1). It was essential for this study to establish an expression system and purification protocol capable of returning milligram quantities of IGFBP-2 and the truncated constructs. This is particularly important for the labelling of proteins with ^{15}N or ^{13}C for structural analysis by NMR. As described in Section 2.4.3, pET32a (+) vectors (pET$^{1\text{-}279}$IGFBP-2HIS, pET$^{1\text{-}132}$IGFBP-2, pET$^{1\text{-}185}$IGFBP-2 and pET$^{136\text{-}279}$IGFBP-2HIS) were generated for the expression of Trx$^{1\text{-}279}$IGFBP-2HIS, Trx$^{1\text{-}132}$IGFBP-2, Trx$^{1\text{-}185}$IGFBP-2 and Trx$^{136\text{-}279}$IGFBP-2HIS, respectively. The thioredoxin-tag could subsequently be cleaved with enterokinase to yield $^{1\text{-}279}$IGFBP-2HIS, $^{1\text{-}132}$IGFBP-2, $^{1\text{-}185}$IGFBP-2 and $^{136\text{-}279}$IGFBP-2HIS. Expression of the thioredoxin-tagged IGFBPs, optimisation of the purification and enterokinase cleavage reaction, and characterisation of the cleavage products will be discussed in the following sections.

TABLE 3.1 PROTEIN QUANTITIES PURIFIED BY IGF-AFFINITY AND NI-AFFINITY CHROMATOGRAPHY PROTOCOLS

Mammalian Expressed Protein	IGF-Affinity Chromatography	Ni-Chromatography Purification
bIGFBP-2	70 μg/L	-
$^{1-279}$IGFBP-2HIS	-	130 μg/100 ml
$^{1-93}$IGFBP-2	-	-
$^{1-104}$IGFBP-2	-	-
$^{1-132}$IGFBP-2	70 μg/700ml	-
$^{1-185}$IGFBP-2	68 μg/700ml	-
$^{96-279}$IGFBP-2HIS	-	139 μg/100 ml
$^{96-284}$IGFBP-2	64 μg/600 ml	-
$^{137-279}$IGFBP-2HIS	-	98 μg/100 ml
$^{185-284}$IGFBP-2	-	-

E. coli Expressed Protein	IGF-Affinity Chromatography	Ni-Chromatography Purification	After Cleavage
Trx$^{1-279}$IGFBP-2HIS	16.4 mg/L	~20 mg/ L	4.2 mg/20 mg
Trx$^{1-132}$IGFBP-2	-	~14 mg/L	2.2 mg/14 mg
Trx$^{1-185}$IGFBP-2HIS	-	~8 mg/L	102 μg/1 mg
Trx$^{136-279}$IGFBP-2HIS	-	~14 mg/L	190 μg/2 mg

The successful expression of Trx$^{1-279}$IGFBP-2HIS, Trx$^{1-132}$IGFBP-2, Trx$^{1-185}$IGFBP-2 and Trx$^{136-279}$IGFBP-2HIS in *E. coli* BL21 cells was detected by SDS-PAGE analysis and staining with Coomassie Blue-R250 as shown in Figure 3.2. The soluble protein fraction was collected by sonication with lysozyme (100 μg/ml) and centrifugation (10000 x g, 10 minutes, 4°C). Sonication was as efficient as, or better than, alternative methods for lysing cell membranes and releasing soluble periplasmic proteins. Indeed, purification of the soluble fraction collected from cell cultures that had been French pressed, resulted in multiple proteins being purified. Other techniques, including freeze-thawing, did not release the soluble protein sufficiently.

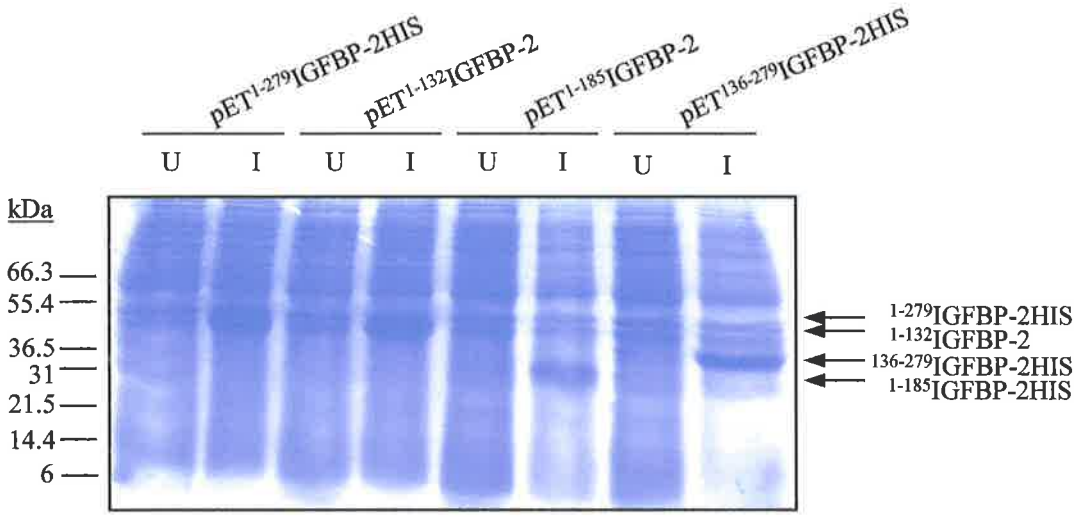

Figure 3.2 Coomassie stained gel of the *E. coli* expressed proteinsTrx$^{1-279}$IGFBP-2HIS, Trx$^{1-132}$IGFBP-2, Trx$^{1-185}$IGFBP-2 and Trx$^{136-279}$IGFBP-2HIS

Uninduced (U) and induced (I) cell culture samples from the *E. coli* expression of Trx$^{1-279}$IGFBP-2HIS, Trx$^{1-132}$IGFBP-2, Trx$^{1-185}$IGFBP-2, Trx$^{96-279}$IGFBP-2HIS and Trx$^{136-279}$IGFBP-2HIS (10 µl of 50 µl/ml/OD unit) were separated by electrophoresis on 12.5% polyacrylamide glycine gels under reducing conditions and stained with Coomassie Blue-R250 (as described in Section 3.3.6.2). Novex 12 molecular weight markers are indicated on the left.

3.4.2 PURIFICATION OF PROTEIN

3.4.2.1 IGF-Affinity Chormatography

Recombinant IGFBPs derived from mammalian COS-1 cells have been routinely purified in our laboratory using three enrichment steps: IGF-affinity chromatography, ion exchange chromatography and rpHPLC, as described by Forbes *et al.*, 1998. Furthermore, as an amino-terminal fragment of bIGFBP-2 (amino acid residues 1-222; Forbes *et al.*, 1998) was successfully purified by this protocol, truncated amino- and carboxyl-terminal IGFBP-2 proteins expressed in this study were processed similarly.

Briefly, COS-1 cell conditioned medium containing recombinantly expressed proteins was loaded onto the IGF-II affinity column at a flow rate of 1 ml/minute as described in Section 3.3.3. Unbound protein was washed from the column in IGF affinity buffer and upon obtaining a baseline, bound IGFBPs were eluted in 0.5 M acetic acid (as described in Section 3.3.3). Protein eluted from the IGF-II affinity column was further purified by cation exchange chromatography as described in Section 3.3.3. Simian IGFBP-2 and the recombinantly expressed bIGFBP-2 truncations were separated from sIGFBP-3 by a 20 ml ammonium acetate gradient of 0.05 M to 1 M over 20 minutes. The IGF affinity and Resource-S chromatography profiles are shown for the amino-terminal protein $^{1\text{-}185}$IGFBP-2 in Figure 3.3. Truncated $^{1\text{-}185}$IGFBP-2 eluted at approximately 0.34 M ammonium acetate. An additional peak eluted at approximately 0.72 M ammonium acetate and is likely to be sIGFBP-3, which routinely elutes at this salt concentration in COS-1 cell preparations of bIGFBP-2 (Forbes *et al.*, 1998). Unlike the protein peak obtained from the affinity purification of the amino-terminal proteins, the profile for $^{96\text{-}284}$IGFBP-2 contained multiple shoulders suggesting the presence of several proteins that were possibly degradation fragments possessing different affinities for the column (Figure 3.4). The final purification step involved separating endogenously expressed sIGFBP-2 from the recombinant IGFBP proteins by rpHPLC as described in Section 3.3.4. Protein was eluted by a 20-50 % gradient of acetonitrile over 30 minutes at 0.5 ml/minute.

a. IGF-Affinity Chromatogram of $^{1-185}$IGFBP-2

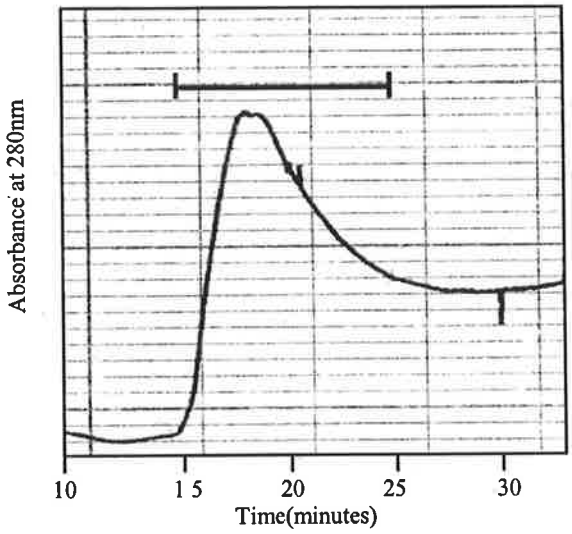

b. Ion Exchange Chromatogram of $^{1-185}$IGFBP-2

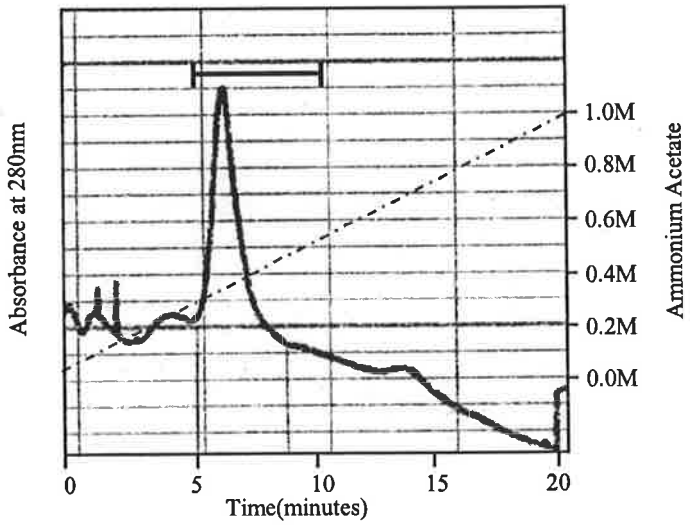

Figure 3.3 IGF-affinity and cation exchange chromatograms of the purification of $^{1-185}$IGFBP-2 from COS-1 cell conditioned medium

Conditioned medium collected from COS-1 cells transfected with pGF8(1-185) was loaded onto an IGF-II affinity column (Section 3.3.3). Specifically bound protein was eluted in 0.5 M acetic acid as indicated by the chromatogram presented. Proteins were eluted at 1 ml/minute and detected by absorbance at 280 nm. One minute fractions were collected between 10-25 minutes and pooled for further purification by cation exchange chromatography as described in Section 3.3.3. Proteins were bound to the column in 0.5 M acetic acid and eluted on a 0.05 M to 1 M gradient of ammonium acetate over 20 minutes. $^{1-185}$IGFBP-2 eluted at approximately 0.34 M ammonium acetate while the peak at 0.72 M represents endogenously expressed sIGFBP-3. Proteins were eluted at 1 ml/minute and detected by absorbance at 280 mm. One minute fractions between 5-9 minutes were pooled.

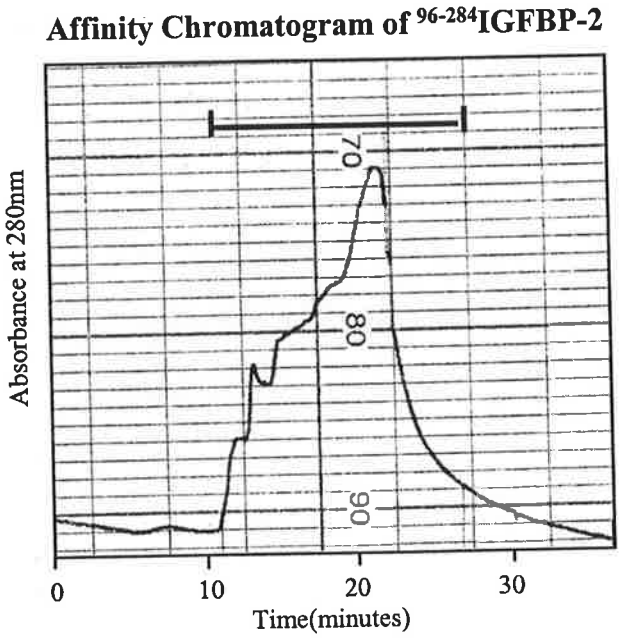

Figure 3.4 IGF-affinity chromatogram of the purification of $^{96-284}$IGFBP-2 from COS-1 cell conditioned medium

Conditioned medium collected from COS-1 cells transfected with pGF8(96-284) was loaded onto an IGF-II affinity column (Section 3.3.3). Specifically bound protein was eluted in 0.5 M acetic acid as indicated by the chromatogram presented. Proteins were eluted at 1 ml/minute and detected by absorbance at 280 nm. One minute fractions were collected between 12-27 minutes and pooled for further purification by cation exchange chromatography as described in Section 3.3.3. Multiple shoulders are evident in the elution profile indicating the presence of several different IGF-binding species.

Typically, 0.5-1 mg/L of wildtype bIGFBP-2 is obtained from COS-1 cell expressions. While the intensity of the immunoreactive bands of $^{1-132}$IGFBP-2, $^{1-185}$IGFBP-2 and $^{96-284}$IGFBP-2 against the bIGFBP-2 standard suggested at least 0.7 mg of protein existed in 700 ml of conditioned medium (Figure 3.1), approximately 70 μg of $^{1-132}$IGFBP-2, 68 μg of $^{1-185}$IGFBP-2 and 64 μg of $^{96-284}$IGFBP-2 were successfully purified as determined by integration of the area under the HPLC peak. Recovery from the conditioned media was poor (less than 10 %) and a large amount of protein was lost during the affinity chromatography step due to the inability of the truncated IGFBPs to bind IGF strongly. Therefore the purification protocol designed for native bIGFBP-2 was not optimal for purification of recombinant bIGFBP-2 mutants which exhibit significantly reduced affinity for the IGF peptides. This is particularly true for $^{96-284}$IGFBP-2, which failed to bind ^{125}I-IGF-II in a Western ligand blot. Furthermore, immunoblotting of $^{96-284}$IGFBP-2 indicated degradation products suggesting the truncated protein was unstable during storage (results not shown). Degradation may contribute to its inability to bind to the IGF-affinity column thus explaining the lower yields.

3.4.2.2 Ni-Affinity Chromatography

IGF-affinity chromatography was not a successful strategy for the purification of truncated IGFBP-2 fragments in this study. Therefore, an alternative method of purification that did not rely upon the high affinity interaction with IGF ligands was introduced. Previously, Forbes and co-workers (1998) reported that the C-terminal 48 amino acid residues of bIGFBP-2 could be removed without influencing its IGF binding affinity. Hence, incorporation of a hexahistidine-tag at the C-terminus of bIGFBP-2 should not alter its ability to bind IGF-I or IGF-II, while providing an invaluable tool for purification of the recombinant proteins. Purification of HIS-tagged IGFBP-2 proteins is discussed in the following section.

As described in Section 2.4.2.2, the cDNA encoding a hexahistidine-tag was incorporated into the C-terminal vectors for the expression of $^{96-279}$IGFBP-2HIS and

$^{137-279}$IGFBP-2HIS. The sixth last residue of bIGFBP-2 is a histidine, hence in this study the five C-terminal residues were mutated to histidine to generate a 6-histidine-tag for enhanced purification (Figure 2.10). An alternative approach would be to incorporate an additional six histidine residues after the C-terminal residue Gln284. Histidine-tagged proteins were purified from COS-1 cell conditioned media using Ni-NTA or Ni-IDA chromatography followed by rpHPLC (Section 3.3.4). The conditioned media was concentrated using an ultrafiltration unit with a 10 kDa molecular weight cut-off filter prior to filtering (0.45 μm) and then loaded onto the Ni-affinity column charged with nickel sulfate. Non-specific proteins were eluted with increasing concentrations of imidazole and HIS-tagged proteins were eluted in 0.5 M imidazole. A sample of the wash and the elution fractions for the purification of $^{96-279}$IGFBP-2HIS were dot blotted and probed with anti-bIGFBP-2 antibody (Figure 3.5). The binding buffer and wash buffer samples were immunoreactive corresponding to the removal of endogenously expressed sIGFBP-2 as well as possibly some recombinant bIGFBP-2. Elution fractions 3-5 were immunoreactive and contained the majority of the recombinantly expressed HIS-tagged fragment. These fractions were loaded onto the rpHPLC column and eluted with a 20-50 % acetonitrile gradient. While the $^{96-279}$IGFBP-2HIS protein was the predominant component of the HPLC chromatogram, several other peaks were also present which did not correspond to $^{96-279}$IGFBP-2HIS (Figure 3.5). It is apparent that several COS-1 proteins were co-purified by Ni-chromatography, however purification of the soluble fraction of *E. coli* cultures yielded only the recombinantly expressed HIS-tagged protein. It is also evident that the carboxyl-terminal fragments are susceptible to proteolysis; hence proteolysed fragments, which retain the C-terminal HIS-tag, will be co-purified with either $^{96-279}$IGFBP-2HIS or $^{137-279}$IGFBP-2HIS preparations. This purification approach returned greater quantities of protein than were obtained by IGF-affinity chromatography (Table 3.1).

Although evidence suggests that removal of the final six amino acid residues of IGFBP-2 would not influence IGF binding (Forbes *et al.*, 1998), incorporation of the HIS-tag on bIGFBP-2 was investigated. The cDNA encoding a hexahistidine-tag was therefore incorporated into the pGF8 vector for expression of $^{1-279}$IGFBP-2HIS (as described in Section

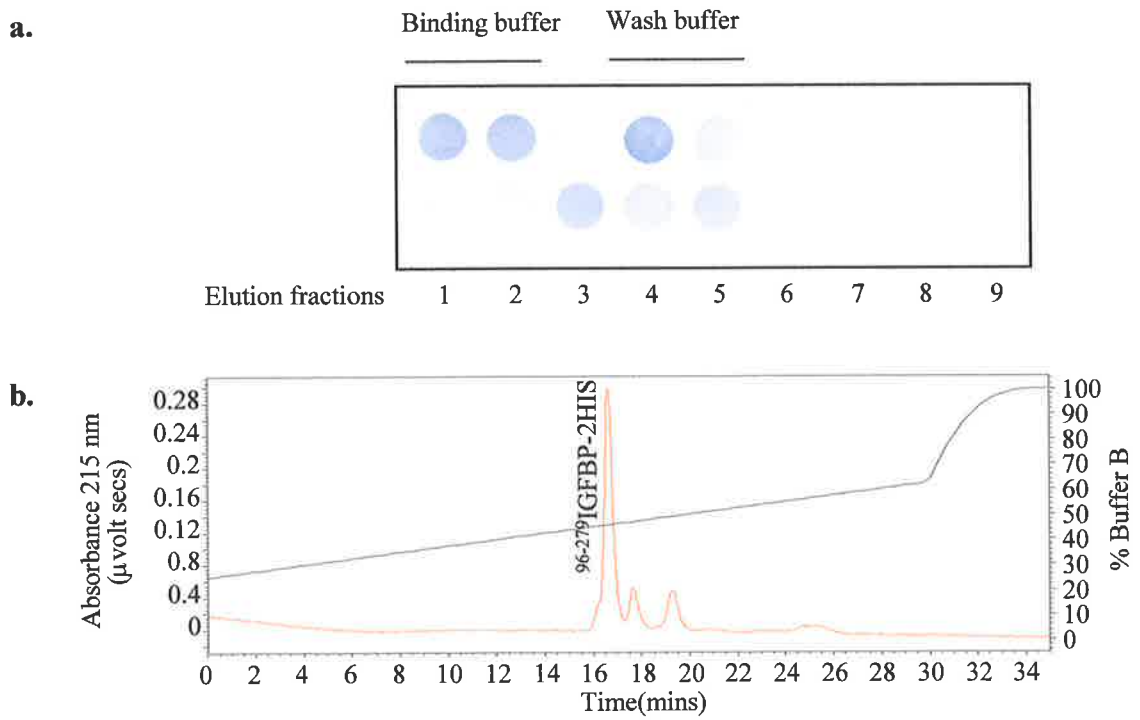

Figure 3.5 Purification of $^{96-279}$IGFBP-2HIS by Ni-affinity chromatography and rpHPLC
Conditioned medium from COS-1 cells transfected with pGF8(96-279HIS) was concentrated approximately 4- to 6-fold by ultrafiltration (as described in Section 3.3.4). The concentrated sample was then loaded onto a $NiSO_4$ charged Ni-NTA column by gravity flow, and non HIS-tagged proteins removed by washing with binding buffer and wash buffer. HIS-tagged proteins were then eluted with 0.5 M imidazole in elute buffer and all fractions were dot blotted onto a nitrocellulose filter and probed with an anti-IGFBP-2 antibody (a). Elution fractions 3-5 were further purified by rpHPLC (b). The peak corresponding to $^{96-279}$IGFBP-2HIS has been labelled accordingly.

2.4.2.4). The yields obtained from the Ni-affinity purification of $^{1-279}$IGFBP-2HIS were again higher than those obtained from the standard IGF-affinity chromatography protocol (130 μg/100 ml compared with 70 μg/L obtained from IGF chromatography; Table 3.1). Purified $^{1-279}$IGFBP-2HIS and COS-1 derived bIGFBP-2, elute at identical concentrations of acetonitrile (Figure 3.6), migrate consistently in SDS-PAGE gels and bind IGF in Western ligand blots. The IGF binding integrity of $^{1-279}$IGFBP-2HIS therefore was not compromised by addition of the hexahistidine-tag, which was further emphasized in the BIAcore analysis of $^{1-279}$IGFBP-2HIS and bIGFBP-2 as described later in Section 3.4.3.3.

The thioredoxin-fused proteins were purified by Ni-chromatography and rpHPLC (Delta-Pak PrepLC column). Interestingly, purification of Trx$^{1-279}$IGFBP-2HIS was performed by both IGF-affinity chromatography and Ni-chromatography and although a hydroxamated-IGF-I column was made with a capacity greater than the quantity of protein to be purified, a large quantity of protein remained in the flow through (Figure 3.7). This may be an indication of the proportion of Trx$^{1-279}$IGFBP-2HIS that is active, correctly folded and functional. Alternatively, it may indicate the limitation of this method for purifying large quantities of IGFBP as similar flow-through problems were observed during purification of COS-1 preparations. Significantly larger quantities of protein were purified by Ni-chromatography, especially when batch bound overnight, compared to IGF-affinity chromatography (Table 3.1). All subsequent purifications of *E. coli* proteins were performed by Ni-chromatography.

3.4.2.3 Enterokinase Digestion of Thioredoxin IGFBPs

The amino-terminal thioredoxin-fusion protein was removed from the *E. coli* expressed proteins by cleavage with enterokinase and the resultant products separated by rpHPLC (Figure 3.8). The enterokinase cleavage site is sequence specific (DDDDK) and does not exist in

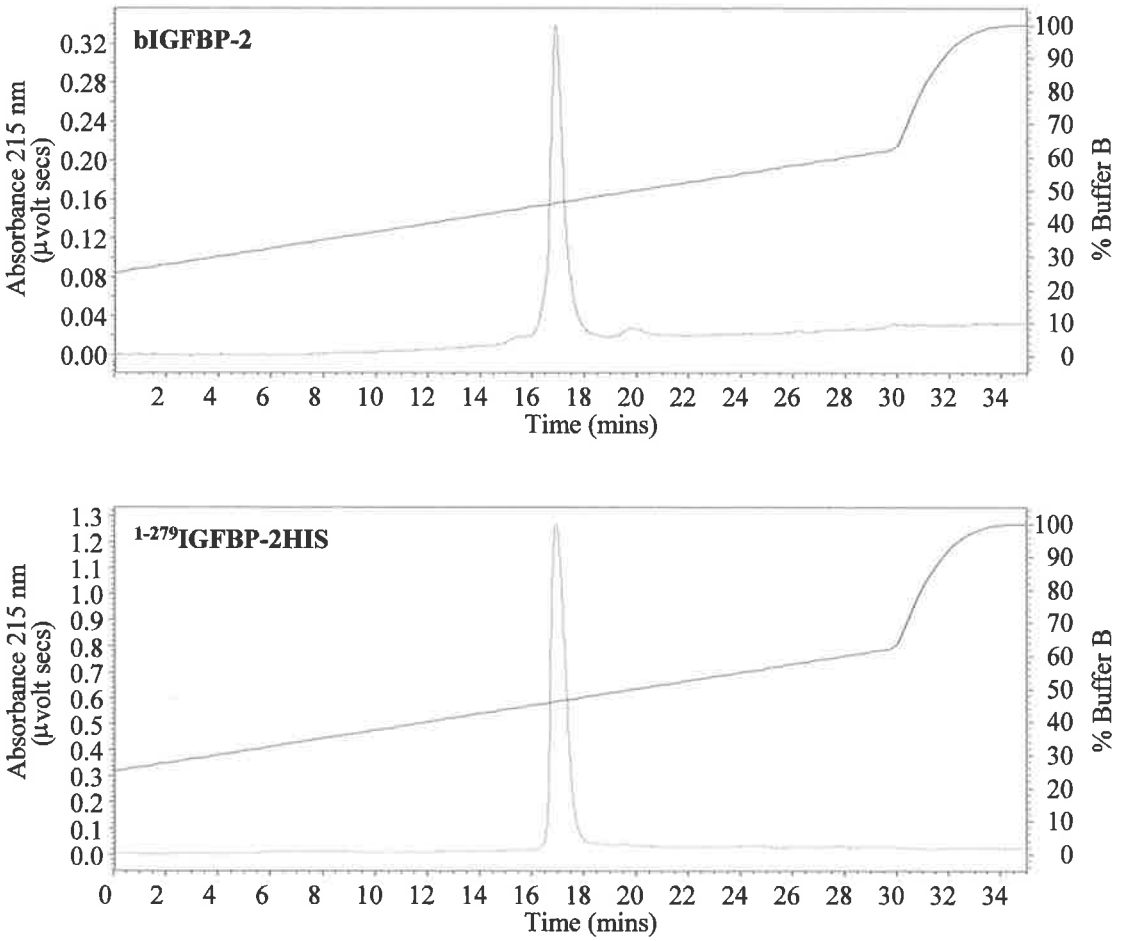

Figure 3.6 Purification of COS-1 derived bIGFBP-2 and $^{1-279}$IGFBP-2HIS by rpHPLC
Analysis of purified bIGFBP-2 and $^{1-279}$IGFBP-2HIS expressed in mammalian COS-1 cells by rpHPLC on a C4 analytical column. The retention time was assessed on a 20-50% acetonitrile gradient over 30 minutes at room temperature.

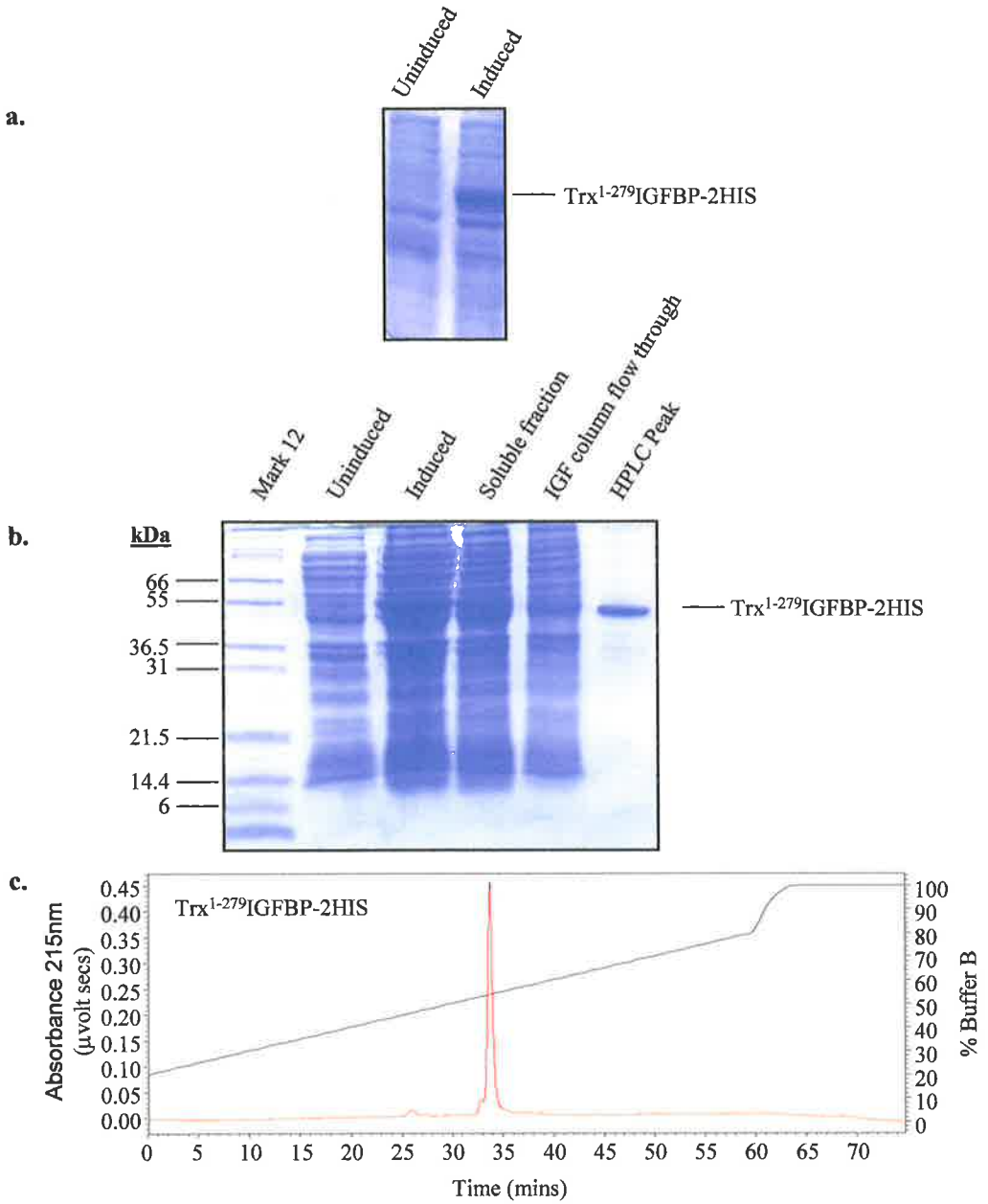

Figure 3.7 Analysis of the IGF-affinity purification of Trx$^{1-279}$IGFBP-2HIS

a) Sonicated samples (1 ml) of uninduced and induced cultures expressing Trx$^{1-279}$IGFBP-2HIS in *E. coli* BL21 cells (described in Section 3.4.1.3) were pelleted and the cells resuspended in lysis buffer to a final concentration equivalent to 50 µl/OD unit and boiled for 10 minutes to reduce the cell membranes.

b) Equivalent volumes of the whole cell lysates, soluble fraction, IGF-affinity column flow-through and rpHPLC peak (10 µl) were then loaded onto a 12.5 % polyacrylamide gel and electrophoresed at 30 mA per gel prior to staining with Coomassie blue.

c) rpHPLC chromatogram of Trx$^{1-279}$IGFBP-2HIS eluted on a 20-80 % acetoniltrile gradient over 60 minutes. The peak corresponding to Trx$^{1-279}$IGFBP-2HIS is labelled accordingly.

bIGFBP-2. However, preparations of enterokinase vary in purity and specificity. Interestingly, a 99 % pure sample of enterokinase obtained from Sigma completely digested IGFBP-2. Enterokinase (EkMax) purchased from Invitrogen was significantly more specific than the enterokinase provided by Sigma. However, digestion with various concentrations of EkMax for 60 minutes (as recommended by the supplier) showed that 0.01 units/20 μg of Trx^{1-279}IGFBP-2HIS completely degraded the protein (Figure 3.8a). Furthermore, digestion with 0.001 units/20 μg only cleaved a portion of the available Trx^{1-279}IGFBP-2HIS. A time trial with 0.005 units of EkMax suggested this was the case even after 6 hours of incubation at 37 °C (Figures 3.8b and 3.9). This may be indicative of the proportion of folded protein with an accessible DDDDK cleavage sequence. Preincubation of Trx^{1-279}IGFBP-2HIS with IGF inhibited the cleavage altogether, suggesting that the N-terminal region of IGFBP-2 is obscured in the presence of IGF, either by direct interaction, or indirect conformational change induced by the interaction (Figure 3.8c).

Enterokinase cleavage (0.5 units/mg protein, Invitrogen EkMax) successfully yielded $^{1-279}$IGFBP-2HIS, $^{1-132}$IGFBP-2, $^{1-185}$IGFBP-2 and $^{136-279}$IGFBP-2HIS proteins (Figure 3.10). A typical cleavage profile for Trx^{1-279}IGFBP-2HIS is shown in Figure 3.11 while the HPLC chromatograms for the truncated IGFBP-2 fragments are shown in Figure 3.12. Although the thioredoxin-tag was successfully removed from the fusion protein to yield the desired recombinant proteins, the cleavage reaction was the limiting step of the purification strategy. The desired enterokinase product was at least 50 % of the starting material (66 % for $^{1-279}$IGFBP-2HIS), however, only 20 % (w/w) was recovered after cleavage. Optimisation of the cleavage reaction would be desirable for the routine production of IGFBPs in this *E. coli* expression system.

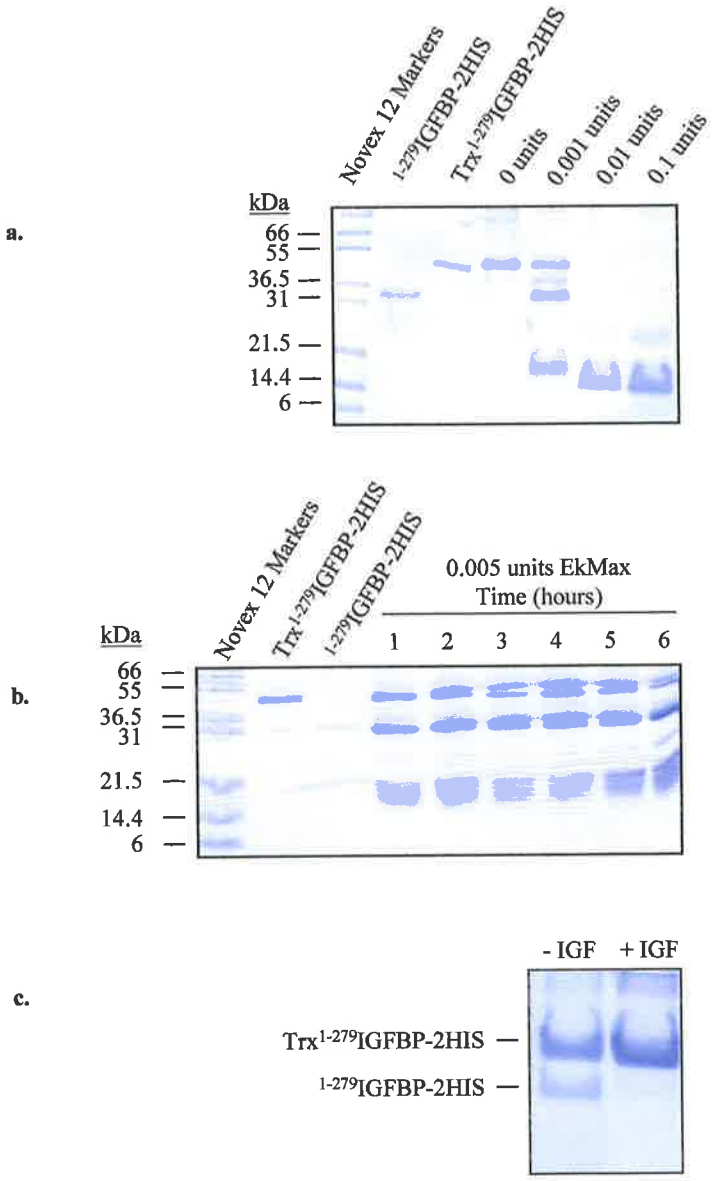

Figure 3.8 Optimisation of the Enterokinase cleavage of Trx$^{1-279}$IGFBP-2HIS

a) Trx$^{1-279}$IGFBP-2 (20 µg) was cleaved with 0, 0.001, 0.01 and 0.1 units EkMax for 60 minutes at 37 °C prior to separation on a 12.5 % glycine gel and staining with Coomassie Blue-R250.

b) Cleavage of Trx$^{1-279}$IGFBP-2HIS for 6 hours at 37 °C with 0.005 units of enterokinase was assessed by SDS-PAGE analysis on a 12.5 % glycine gel stained with Coomassie Blue-R250.

c) Cleavage of Trx$^{1-279}$IGFBP-2HIS in the presence and absence of IGF-I was performed for 60 minutes at 37 °C with 0.005 units of enterokinase. The removal of the thioredoxin-tag was inhibited by the presence of IGF ligand.

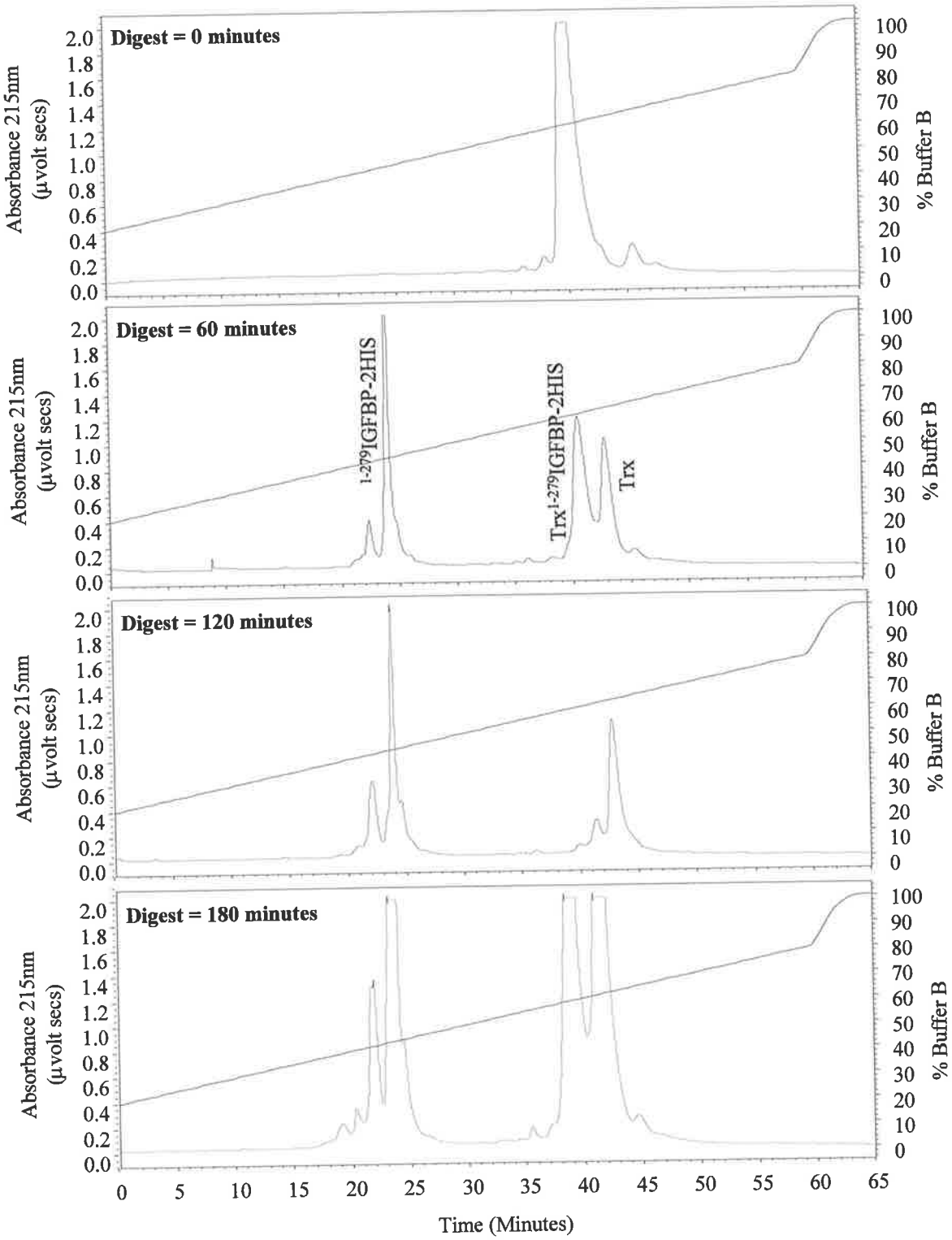

Figure 3.9 Reverse phase HPLC of the Enterokinase cleavage of Trx$^{1-279}$IGFBP-2HIS
Analysis of the enterokinase cleavage reaction at times 0, 60, 120 and 180 minutes by rpHPLC on a C4 analytical column. The retention time was assessed on a 20-80 % buffer B gradient over 60 minutes at room temperature. The peak corresponding to Trx$^{1-279}$IGFBP-2HIS and the cleavage products $^{1-279}$IGFBP-2HIS and Trx have been labelled accordingly.

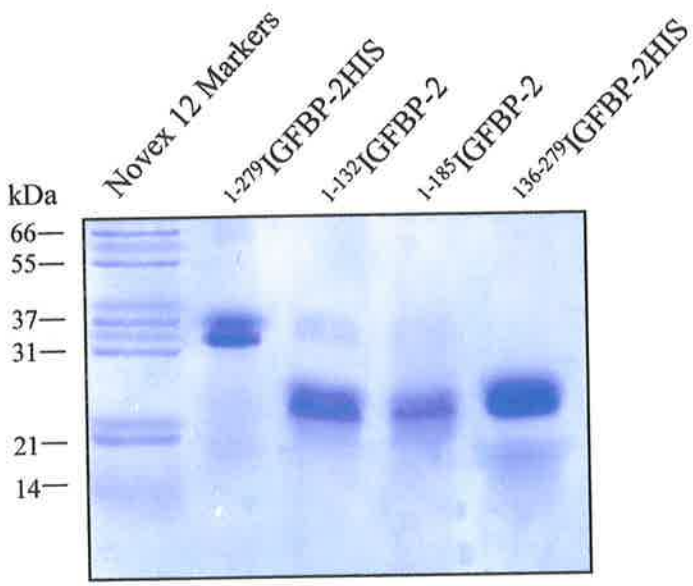

Figure 3.10 SDS PAGE analysis of bIGFBP-2HIS and truncated mutants
$^{1-279}$IGFBP-2HIS, $^{1-132}$IGFBP-2, $^{1-185}$IGFBP-2, $^{96-279}$IGFBP-2HIS and $^{136-279}$IGFBP-2HIS (1 μg) were separated by electrophoresis on 12.5 % polyacrylamide glycine gels under non-reducing conditions and stained with Coomassie Blue-R250. Molecular weight markers were loaded in the first lane as indicated and the corresponding molecular weights are indicated to the left of the figure.

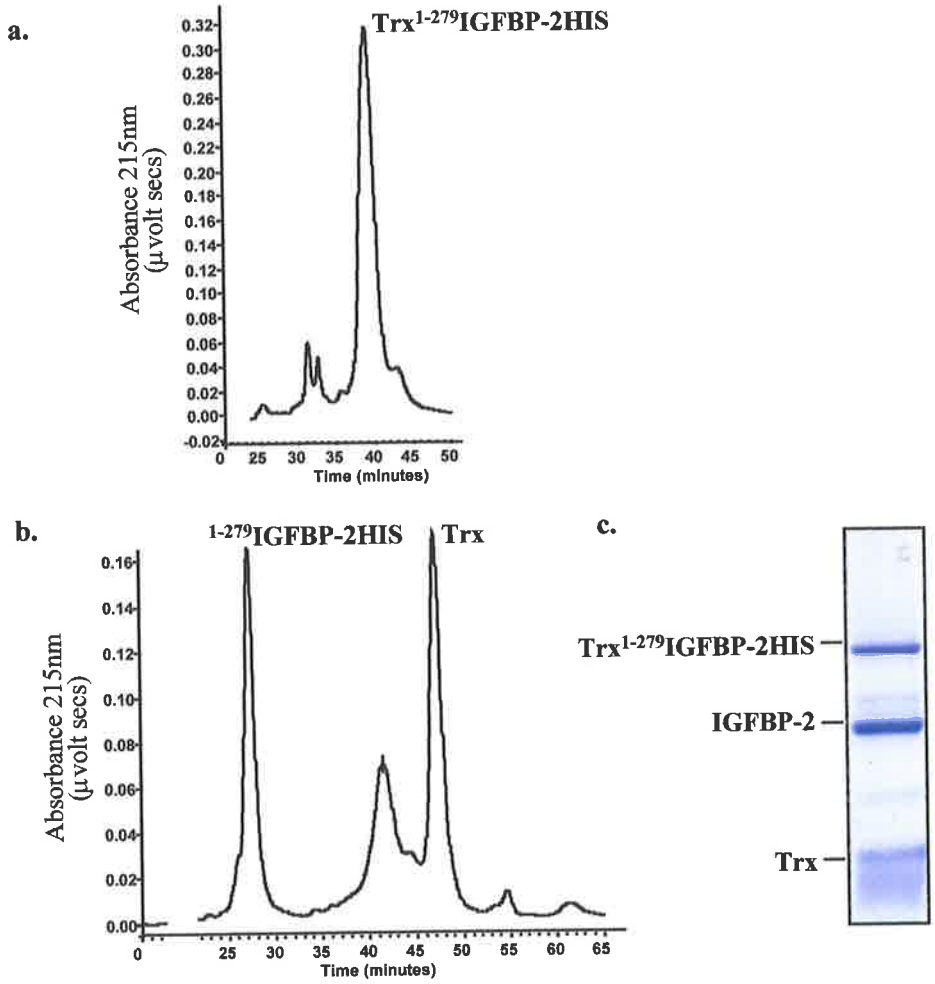

Figure 3.11 Purification of $^{1-279}$IGFBP-2HIS
Trx$^{1-279}$IGFBP-2HIS (20 µg) was purified by rpHPLC (a.) then digested with 0.01 units of enterokinase at 37 °C for 30 minutes. The cleavage products were then separated by rpHPLC (b: 20-80 % Buffer B over 60 minutes) and analysed by SDS-PAGE on a 12.5 % glycine gel stained with Coomassie Blue-R250 (c.). Approximately 20 % of the starting material (w/w) was recovered as $^{1-279}$IGFBP-2HIS

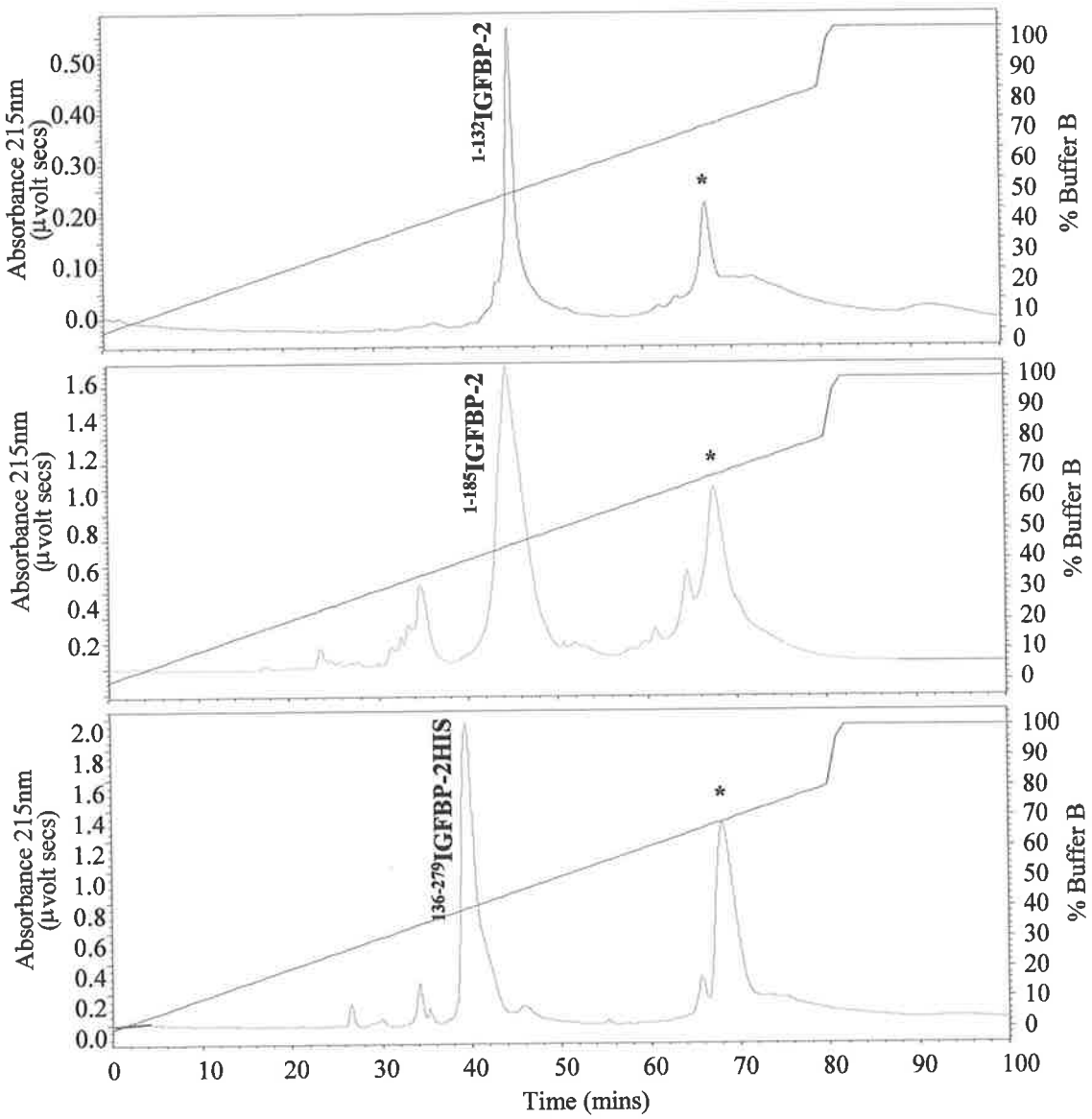

Figure 3.12 Reverse phase HPLC purification of the Enterokinase digested TrxIGFBP-2 truncations

Analysis of the enterokinase cleavage reaction for $^{1-132}$IGFBP-2, $^{1-185}$IGFBP-2 and $^{136-279}$IGFBP-2HIS by rpHPLC on a C4 analytical column. The retention time was assessed on a 20-80 % buffer B gradient over 80 minutes at room temperature. The peaks corresponding to the cleavage products have been labelled accordingly. Peaks corresponding to thioredoxin are indicated (*).

3.4.3 PRELIMINARY BINDING ASSAYS AND PROTEIN INTEGRITY

3.4.3.1 Mass Spectroscopy and N-Terminal Sequencing

N-terminal sequencing of the COS-1 derived material confirmed the correct amino-termini for $^{1-132}$IGFBP-2 (EVLFR-), $^{1-185}$IGFBP-2 (EVLFR-), $^{96-279}$IGFBP-2HIS (AEYSA-) and $^{137-279}$IGFBP-2HIS (GAGRK-). An alternatively processed form of the COS-1 protein preparations with the N-terminal sequence GARAE-, was co-purified. This sequence arises presumably due to alternative post-translational processing of the pre-peptide and is usually observed in preparations of full-length bIGFBP-2 and other bIGFBP-2 mutants (Forbes *et al.*, 1998). Electrospray mass spectroscopy was consistent with the N-terminal sequencing data for COS-1 derived material, identifying both native and GARAE- forms for $^{1-185}$IGFBP-2 (19439 and 19784 Da) and $^{96-279}$IGFBP-2HIS (21002 and 21355 Da) preparations. As a consequence of the cloning strategy, material derived from *E. coli* expression incorporated an additional three N-terminal amino acid residues (AMA) which were reflected in the molecular masses: $^{1-279}$IGFBP-2HIS (31177 Da), $^{1-132}$IGFBP-2 (13866 Da) and $^{136-279}$IGFBP-2HIS (17374 Da).

3.4.3.2 Solution Binding Assays

A solution-based assay was performed to quantitate the affinity of $^{1-185}$IGFBP-2 for both ^{125}I-IGF-I and ^{125}I-IGF-II compared with wildtype bIGFBP-2 (Figure 3.13). Titration of ^{125}I-IGF-I and ^{125}I-IGF-II with increasing amounts of binding protein indicated that $^{1-185}$IGFBP-2 exhibited a significantly reduced ability to bind IGF peptides compared with native bIGFBP-2. Native bIGFBP-2 reaches a maximal binding of approximately 42 % total counts and the curve is sigmoidal in shape. The curve resulting from the interaction of $^{1-185}$IGFBP-2 with ^{125}I-IGF-II is similar in shape to that of full-length bIGFBP-2 but the curve is shifted to the right. This suggests that a higher concentration of $^{1-185}$IGFBP-2 is required for maximal binding of ^{125}I-

bIGFBP-2 and $^{1-185}$IGFBP-2 Binding to ^{125}I-IGF-I

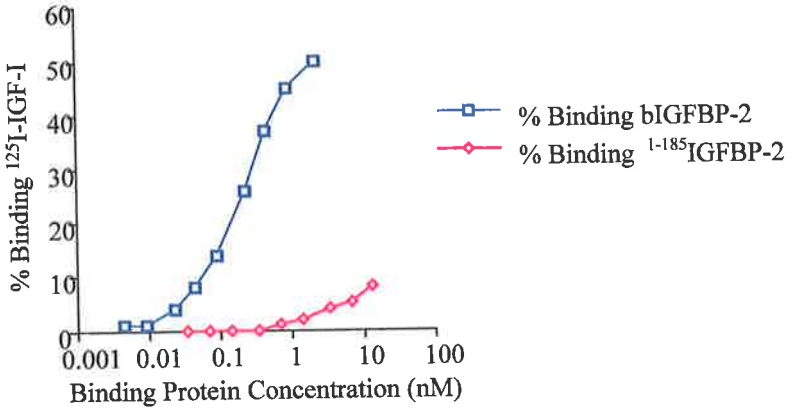

bIGFBP-2 and $^{1-185}$IGFBP -2 Binding to ^{125}I-IGF-II

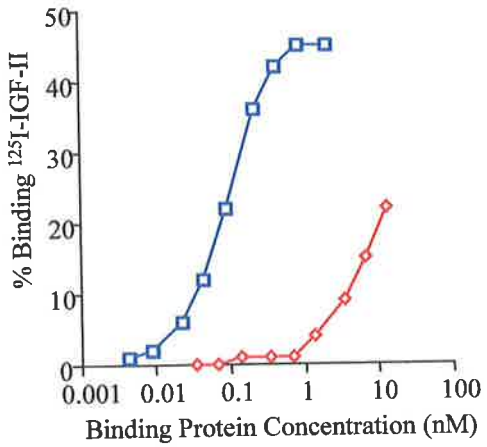

Figure 3.13 Analysis of the $^{1-185}$IGFBP-2 binding properties by solution binding assays
The ability of $^{1-185}$IGFBP-2 to bind both IGF-I and IGF-II in solution binding assays was compared to bIGFBP-2 as described in Section 3.4.3.4. Binding was expressed as a percentage of total counts bound to the IGFBPs (^{125}I-IGF), against a log scale of increasing IGFBP concentrations.

IGF-II. Comparison of the approximate half maximal binding values for both bIGFBP-2 and $^{1-185}$IGFBP-2 suggests the truncated construct has a 79-fold reduction in ^{125}I-IGF-II binding affinity (Figure 3.13). Maximum binding of $^{1-185}$IGFBP-2 was not observed even at concentrations as high as 200 nM in solution binding assays. This is consistent with the results obtained from the Western ligand blot which showed low levels of ^{125}I-IGF-II binding to $^{1-185}$IGFBP-2 relative to the level of expression as detected by immunoblots (Figure 3.1). At the maximum concentration of $^{1-185}$IGFBP-2 used in this assay (200 nM), maximal binding was not achieved. This assay does not determine whether $^{1-185}$IGFBP-2 reaches the same maximal binding as bIGFBP-2. Further experiments, using the BIAcore (Section 4.4.1), will determine the association and dissociation rates of the interaction in real time. Such experiments will also determine how strong or fast the interaction is and how many molecules are involved. In summary, it can only be estimated from the results of the solution-binding assay that $^{1-185}$IGFBP-2 has an approximate 79-fold lower relative binding affinity for ^{125}I-IGF-II than does full length bIGFBP-2. Solution assays indicate a reduced ability to bind ^{125}I-IGF-I compared with ^{125}I-IGF-II.

3.4.3.3 Comparison of the Binding Kinetics of bIGFBP-2 and $^{1-279}$IGFBP-2HIS with IGF-I and IGF-II

It was important to establish that incorporation of the hexahistidine-tag at the C-terminus of IGFBP-2 did not alter the binding kinetics of the interaction with IGF. Forbes and co-workers (1998) previously established that removal of the C-terminal residues 237-284 of bIGFBP-2 did not significantly alter the IGF binding affinity of the protein. However, incorporation of a HIS-tag may interfere with the ligand binding site or the conformation of the protein. Mammalian derived bIGFBP-2 and $^{1-279}$IGFBP-2HIS were compared by BIAcore analysis (Section 3.3.6.7). The dissociation constants for IGF-I and IGF-II were similar (Figure 3.14 and Table 3.2). Hence, histidine substitution of the last five amino acid

residues of bIGFBP-2 (Thr280His, Gln281His, Arg282His, Met283His and Gln284His) did not greatly alter the affinity of bIGFBP-2 for IGF-I or IGF-II. Incorporation of a histidine-tag for enhanced purification of the carboxyl-terminal fragments was therefore anticipated not to adversely influence the IGF binding interaction.

TABLE 3.2 COMPARISON OF THE KINETICS OF THE INTERACTION BETWEEN bIGFBP-2 AND $^{1-279}$IGFBP-2HIS WITH IGF-I AND IGF-II USING THE 1:1 LANGMUIR BINDING MODEL

IGF-I	k_a ($x10^5$)	relative k_a	k_d ($x10^{-4}$)	relative k_d	K_D ($x10^{-9}$)	relative k_D	χ^2
bIGFBP-2	0.45	1.0	1.29	1.0	2.89	1.0	0.46
$^{1-279}$IGFBP-2HIS	1.1	2.4	3.0	2.3	2.2	0.76	0.39
IGF-II							
bIGFBP-2	0.28	1.0	1.19	1.0	4.27	1.0	0.38
$^{1-279}$IGFBP-2HIS	0.9	3.2	2	1.6	2.7	0.63	0.12

The 1:1 Langmuir binding model was used to fit kinetic data shown in Figure 3.14 for the interaction between bIGFBP-2 and $^{1-279}$IGFBP-2HIS across both IGF-I and IGF-II biosensor surfaces. χ^2 values for sensorgram curve fits were equal to or less than 0.5. Association rates (k_a), dissociation rates (k_d), and dissociation constants ($K_D=k_d/k_a$) are given. Dissociation constants relative to bIGFBP-2 are presented (K_D bIGFBP-2 /$^{1-279}$IGFBP-2HIS).

3.4.3.4 Comparison of Mammalian and E. coli Expressed IGFBPs

The mammalian COS-1 cell expression system is well established in the laboratory and has been used routinely to express wildtype, truncated and point mutated bIGFBP-2s. The pET32a (+) expression vectors and *E. coli* BL21 cell expression of bIGFBPs were used for the first time in this study. A comparison of the IGF binding properties of *E. coli* and mammalian derived $^{1-279}$IGFBP-2HIS and $^{136-279}$IGFBP-2HIS using BIAcore analysis revealed that protein from both sources behaved essentially identically (Figure 3.15).

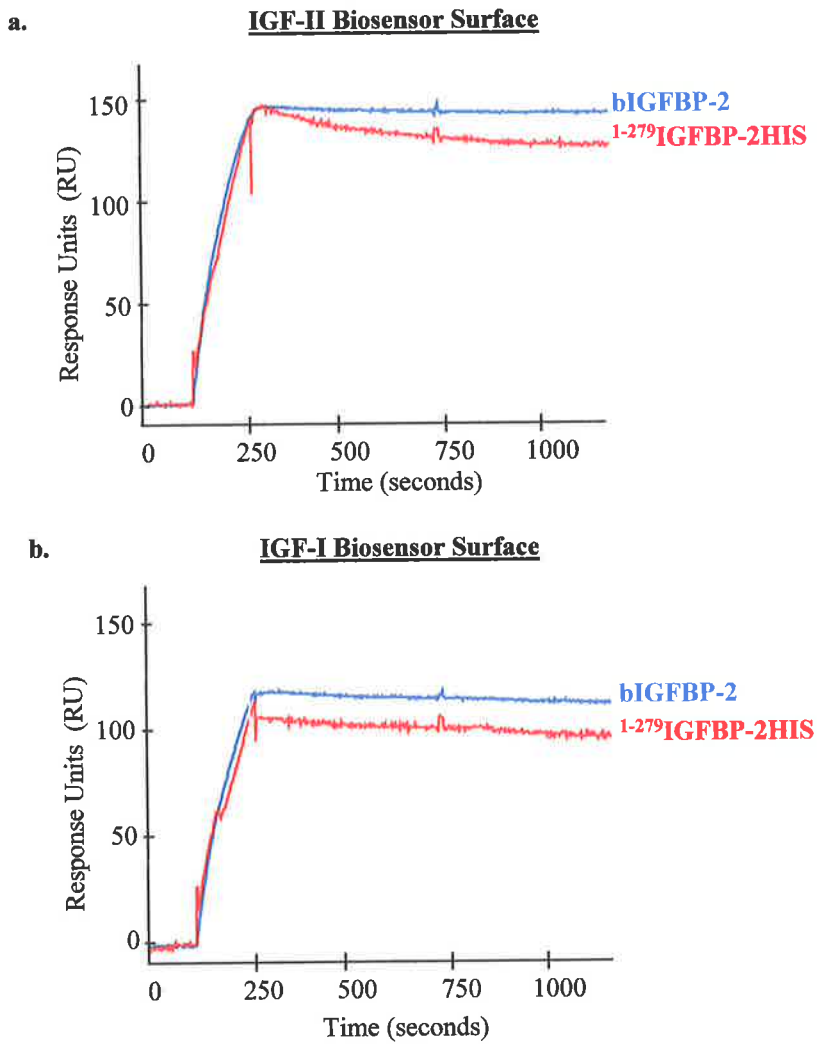

Figure 3.14 Comparison of the IGF Binding Properties of bIGFBP-2 and $^{1-279}$IGFBP-2HIS Biosensorgrams are presented for the interaction between bIGFBP-2 and $^{1-279}$IGFBP-2HIS with a) IGF-II and b) IGF-I biosensor surfaces. Biosensor experiments were performed at a flow rate of 40 µl/minute in HBS running buffer as described in Section 3.3.6.7. A single concentration curve (100 nM) has been presented across both IGF-I and IGF-II biosensor surfaces.

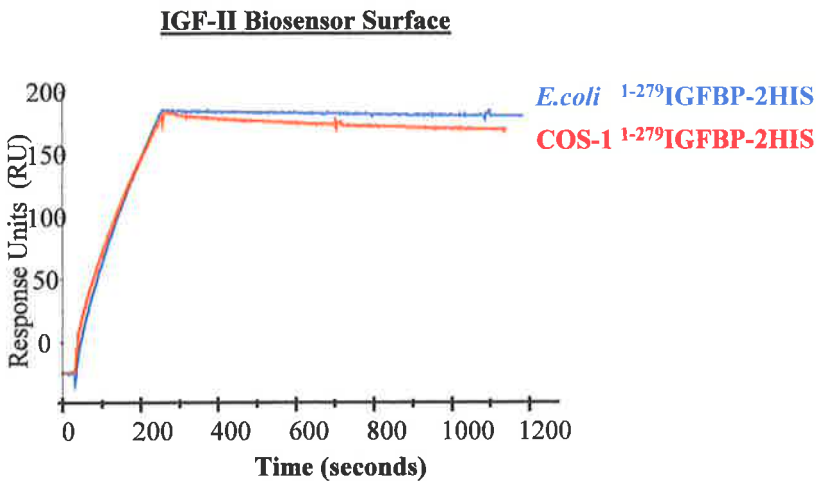

Figure 3.15 Comparison of the IGF binding properties of *E. coli* and mammalian derived proteins

The IGF binding properties of mammalian COS-1 and *E. coli* cell expressed $^{1-279}$IGFBP-2HIS were compared in BIAcore experiments. Biosensorgrams are presented for the interaction with IGF-II biosensor surfaces performed at a flow rate of 40 µl/minute in HBS running buffer as described in Section 3.3.6.7. A single concentration curve (100 nM) has been presented.

3.4.3.5 Integrity of the IGFBP-2 Truncations

The mammalian COS-1 cells express endogenous sIGFBP-2 and sIGFBP-3 and hence contain the machinery necessary for the correct synthesis and packaging of IGFBPs. However, when expressing truncated forms of the native protein it is important to establish that they have been correctly expressed and folded. This is especially true for the carboxyl-terminal proteins, which have been recombinantly engineered to incorporate the signal sequence in a non-native environment. Both amino- and carboxyl-terminal fragments are recognised by polyclonal antibodies directed against native bIGFBP-2 (Figure 3.1). In addition, the amino- and carboxyl-terminal fragments also retain the ability to bind IGF (as discussed in detail in the following chapter) and hence, are folded such that a functional IGF binding site forms.

Furthermore, the change in intrinsic fluorescence of Trp^{243} of bIGFBP-2 was the same for both $^{1\text{-}279}$IGFBP-2HIS and $^{136\text{-}279}$IGFBP-2HIS upon IGF binding, indicating a similar change in environment of Trp^{243} in both full length and truncated bIGFBP-2 (Figure 3.16; Dr Briony Forbes, Adelaide University; unpublished). The sole IGFBP-2 tryptophan is located in the C-terminus of the protein; hence investigation of the change in fluorescence upon IGF ligand binding was limited to the carboxyl-terminal proteins. Site-directed mutagenesis to incorporate single tryptophan residues elsewhere in the intact IGFBP molecule is currently under investigation (Dr Briony Forbes, Adelaide University). The amino-terminal fragments will therefore also be targeted for changes in intrinsic fluorescence activity upon ligand binding.

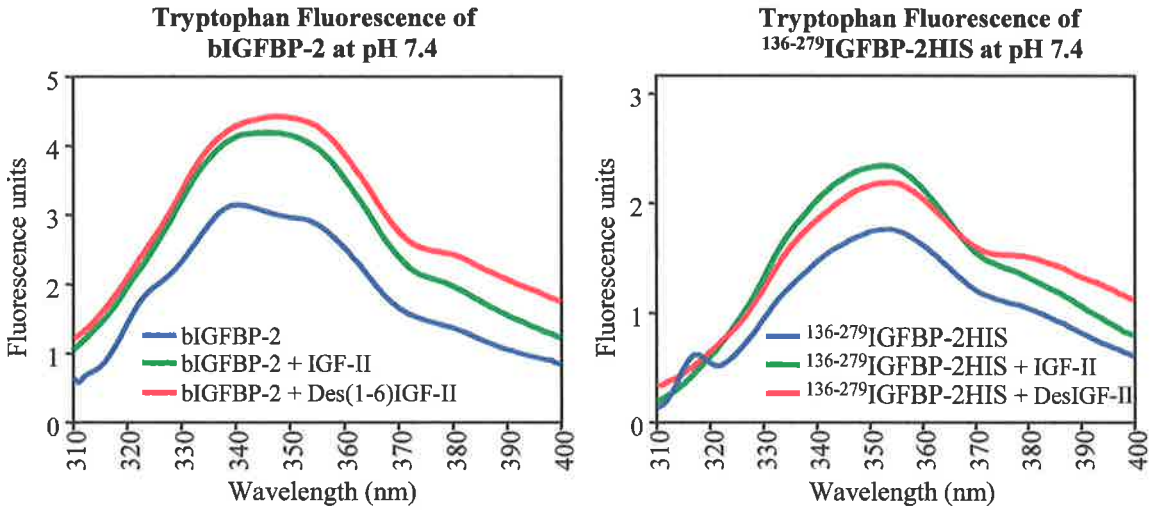

Figure 3.16 Tryptophan fluorescence spectroscopy of bIGFBP-2 and $^{136-279}$IGFBP-2HIS
Tryptophan fluorescence of $^{136-279}$IGFBP-2HIS (2.5 μM) complexed to IGF-II or des(1-6)IGF-II (1:2 molar ratio)was measured between 300 and 400 nm upon excitation at 295 nm with an Aminco Bowman Series 2 Luminescence spectrometer and performed by Dr B. Forbes (Adelaide University). There was a decrease in overall fluorescence intensity and a shift of 10 nm in maximum emission to a longer wavelength for $^{136-279}$IGFBP-2HIS complexed to IGF-II compared with bIGFBP-2. Despite these differences, IGF-II and Des(1-6)IGF-II induced similar changes in fluorescence intensity of Trp243 in both $^{136-279}$IGFBP-2HIS and bIGFBP-2

3.5 DISCUSSION

The aim of this study was to express the amino- and carboxyl-terminal domains of bIGFBP-2 as independent proteins and assess their potential to bind IGF peptides. Characterisation of these truncated proteins will contribute to defining the ligand-binding site on IGFBPs. At the time this project was initiated, no complete structural model for any member of the IGFBP family had been reported due to their mass being too large for NMR and their failure to form suitable crystals for x-ray diffraction analysis. However, recently, a solution structure of a fragment of mini-IGFBP-5 has been reported (Kalus *et al.*, 1998). It is likely therefore, that the structure of the whole bIGFBP-2 molecule can be derived from the amino- and carboxyl-terminal fragments particularly as the two domains have been shown not to be linked by disulphide bonds (Forbes *et al.*, 1998).

Both the amino-terminal domain alone (amino acid residues 1-93, 1-104) and carboxyl-terminal domain alone (amino acid residues 182-284) were targeted for recombinant expression and IGF binding analysis. In addition, these individual domains were combined with the linker domain to investigate the role of this region in IGF binding (amino acid residues: 1-132, 1-185, 96-284 and 136-284). Interestingly, it appears that the central region is indeed important for the integrity of the protein upon secretion from the cell. Furthermore, the amino-terminal fragments bind ^{125}I-IGF-II on Western ligand blots. The binding affinity of $^{1-185}$IGFBP-2 for IGF-II was 79-fold lower compared with bIGFBP-2 in solution binding assays and exhibited an even weaker affinity for IGF-I. The carboxyl-terminal fragments ($^{96-279}$IGFBP-2HIS, $^{96-284}$IGFBP-2 and $^{137-279}$IGFBP-2HIS) did not appear to bind IGF by Western ligand blot.

3.5.1 EXPRESSION OF $^{1-93}$IGFBP-2, $^{1-104}$IGFBP-2 AND $^{182-284}$IGFBP-2

Expression of the short forms of the amino-terminal domain (residues 1-93 and 1-104) and carboxyl-terminal domain (residues 182-284) of bIGFBP-2 was not successful in the present investigation. Interestingly, truncated forms of other IGFBPs, of similar size to those in this study, have been expressed previously in Chinese hamster ovary (CHO) cells. The N-terminal 88 amino acid residues of IGFBP-3 did not bind ^{125}I-IGF-I by Western ligand blot (Baxter and Firth, 1996) but did exhibit a weak association by affinity cross-linking in another independent study (Sommer *et al.*, 1991). Successful expression of the 88 N-terminal amino acid residues of IGFBP-3 possibly reflects differences in structure compared with bIGFBP-2.

$^{1-93}$IGFBP-2, $^{1-104}$IGFBP-2 and $^{182-284}$IGFBP-2 may not have been successfully expressed due to a number of reasons; an absence of mRNA transcripts, failure to secrete the protein from COS-1 cells or due to post-translational processes such as incorrect folding or degradation. It would be interesting to determine which stage of the expression of $^{1-93}$IGFBP-2, $^{1-104}$IGFBP-2 and $^{182-284}$IGFBP-2 is inhibited. The first step would be to assess the mRNA levels in COS-1 cell lysates to identify the presence of the transcript.

Alternatively, the linker peptide may be involved in maintaining the integrity of the amino- and carboxyl-terminal domains of bIGFBP-2. This is supported by the successful expression of $^{1-279}$IGFBP-2HIS, $^{1-132}$IGFBP-2, $^{1-185}$IGFBP-2, $^{96-279}$IGFBP-2HIS, $^{96-284}$IGFBP-2 and $^{137-279}$IGFBP-2HIS in the present investigation. While the linker region has not been highly conserved throughout evolution, it has not been deleted and is presumably required for connecting the domains of IGFBPs. Previously, IGFBP-3 mutants with a deletion of the linker peptide (Δ89-184: Baxter and Firth, 1996; and Δ92-184 and Δ92-223: Sommer *et al.*, 1991) have been expressed successfully in CHO cells. Sommer and co-workers (1991) showed that these peptides bound IGFs poorly in affinity cross-linking experiments.

Expression of the individual domains of bIGFBP-2 remains an important objective. In this study, the smallest fragments of IGFBP-2 generated were $^{1-132}$IGFBP-2 and

$^{136-279}$IGFBP-2HIS, which divides the protein into two nearly equal halves. Additional studies may involve increasing the number of amino acid residues of the small fragments ($^{1-104}$IGFBP-2 and $^{182-284}$IGFBP-2), to generate correctly folded, stable amino- and carboxyl-terminal domains of bIGFBP-2. Purification strategies for these fragments will need to be optimised, as they will presumably have altered IGF binding affinities. Incorporation of a histidine-tag enhanced purification of the carboxyl-terminal fragments without influencing the IGF binding interaction and hence could be used for the purification of shorter fragments, which will potentially exhibit reduced IGF binding affinity.

3.5.2 EXPRESSION OF $^{1-132}$IGFBP-2, $^{1-185}$IGFBP-2, $^{96-279}$IGFBP-2HIS, $^{96-284}$IGFBP-2, $^{136-279}$IGFBP-2HIS, $^{137-279}$IGFBP-2HIS AND $^{1-279}$IGFBP-2HIS

In this study, full-length bIGFBP-2 and amino- and carboxyl-terminal fragments of bIGFBP-2 were successfully expressed and purified from both mammalian COS-1 and *E. coli* BL21 cells. Recombinant fragments of IGFBP-2 had not been reported prior to the onset of this project and indeed, amino- and carboxyl-terminal fragments of any IGFBP had not been isolated concomitantly in the one study for the analysis of their combined IGF binding properties. Here, bovine IGFBP-2, $^{1-279}$IGFBP-2HIS, $^{1-132}$IGFBP-2, $^{1-185}$IGFBP-2, $^{96-279}$IGFBP-2HIS, $^{96-284}$IGFBP-2 and $^{137-279}$IGFBP-2HIS were successfully expressed and purified from mammalian COS-1 cells (Figure 3.1). An *E. coli* expression system was also established in this study as described in Section 2.4.3, and successfully yielded $^{1-279}$IGFBP-2HIS, $^{1-132}$IGFBP-2, $^{1-185}$IGFBP-2, and $^{136-279}$IGFBP-2HIS upon removal of the thioredoxin fusion partner (Figure 3.11 and 3.12). Interestingly, the recombinant IGFBPs expressed either in COS-1 or *E. coli* cells, migrated by SDS-PAGE electrophoresis as apparently larger molecular masses than their predicted sizes. Furthermore, only the amino-terminal IGFBP fragments exhibited ^{125}I-IGF-II binding affinity by Western ligand blot and $^{1-185}$IGFBP-2 had a 79-fold reduced affinity compared with bIGFBP-2 for ^{125}I-IGF-II in solution

binding assays. The carboxyl-terminal fragments did not bind ^{125}I-IGF-II by Western ligand blot.

Naturally occurring fragments of IGFBPs with reduced IGF binding affinities have been previously reported in the literature. Huhtala and co-workers (1986) were first to identify a 21kDa N-terminal proteolytic fragment of IGFBP-1 that did not bind IGF-I or IGF-II by Western ligand blotting. Similarly, a 23kDa N-terminal fragment of IGFBP-5, isolated from cultured fibroblasts, was shown to bind IGF-I and IGF-II in solution although very poorly and only when present at a high concentration (Andress and Birnbaum, 1990). Recently, a seventh IGFBP, IGFBP-7, has been identified. This is homologous only to the N-terminal domain of the IGFBP family and has a 5-25 fold lower affinity for the IGF peptides than IGFBP-3. In the current investigation, the N-terminal domain and linker peptide of bIGFBP-2 has been shown to have a 79-fold reduction in relative IGF-II binding and therefore loss of the C-terminal domain of bIGFBP-2 has a greater impact on IGF binding compared with IGFBP-7.

In studies elsewhere, recombinantly expressed N-terminal fragments of IGFBPs have exhibited dramatically reduced IGF binding capabilities. Brinkman and co-workers (1991a) found that deletion of 60 N-terminal amino acid residues of IGFBP-1 completely abolished IGF-I binding, while single point mutations within the N-terminal domain had no effect on IGF binding. This suggests that the N-terminal domain contains part of the IGF binding domain, a result that is supported by the current investigation. N-terminal fragments of IGFBP-3 containing amino acid residues 1-88 and 1-184 did not bind ^{125}I-IGF-I by Western ligand blot (Baxter and Firth, 1996) but similar mutants (1-88 and 1-161) did exhibit weak association by affinity cross-linking (Sommer *et al.*, 1991). In the present investigation, expression of amino acid residues 1-93 of bIGFBP-2 was not successful, while the long N-terminal fragment of bIGFBP-2 (amino acid residues 1-185) bound ^{125}I-IGF-II by Western ligand blot and by solution binding assays, albeit with a 79-fold reduction in affinity.

Attempts to define the IGF binding site of bIGFBP-2 in this laboratory has provided evidence to suggest that the N-terminal domain contains one of the IGF binding determinants. Chemical modification studies showed that Tyr60 in the N-terminal domain of bIGFBP-2 was

protected from iodination when complexed with IGF (Hobba *et al.*, 1996; Hobba *et al.*, 1998). IGF binding was also inhibited when Tyr60 was iodinated. Furthermore, Forbes and co-workers (1998) successfully deleted 14, 36 and 48 C-terminal amino acid residues of bIGFBP-2 without disrupting the capacity to bind IGF-I and IGF-II. Deletion of a further 15 amino acids residues from the C-terminal domain of bIGFBP-2 significantly altered the binding preference for IGF-II (to become approximately equal to IGF-I) while also reducing its IGF affinity by approximately 130-fold. It is plausible then to suggest that one IGF binding site of bIGFBP-2 is localised to the N-terminal domain and another in the C-terminal domain as is further supported by the results presented in this thesis.

A naturally occurring 21kDa fragment of IGFBP-2 has been isolated from a rat liver cell line (Wang *et al.*, 1989). This fragment was found to correspond to amino acid residues 148-270 of native IGFBP-2 and was reported to have a 5- to 25-fold lower affinity for IGF-I in solution binding assays. Most recently, Ho and Baxter (1997) reported the isolation of a 14kDa C-terminal fragment of IGFBP-2 from milk. This fragment, extending from Gly^{169} presumably to the end of hIGFBP-2 (amino acid residue 289), retained the ability to bind IGF-I and IGF-II in solution binding assays. Although results presented in the current thesis show that $^{96\text{-}284}$IGFBP-2 (amino acids 99-284) does not bind ^{125}I-IGF-II on a Western ligand blot, $^{96\text{-}284}$IGFBP-2 may however demonstrate ^{125}I-IGF-II interactions in solution.

Lalou and co-workers (1996) isolated a 16kDa fragment of IGFBP-3 that had no detectable affinity for IGF peptides in solution assays. Interestingly, this fragment was shown to be a potent inhibitor of IGF actions *in vivo*, presumably retaining its ability to interact with the putative membrane receptor for IGFBP-3. Despite the apparent inability to bind IGF-II, it is plausible that the C-terminal domain of IGFBP-2 contributes significantly to modulating IGF activity. This domain may be involved in maintaining the correct conformation of the N-terminus for maximum binding of IGF-II. This is consistent with the present results that suggest the N-terminal (1-185) domain has a 79-fold reduced affinity for IGF-II when expressed alone.

3.5.3 HOW DO THE PURIFICATION PROTOCOLS COMPARE?

Purification of IGFBPs with low affinity for IGFs has been shown in this, and other studies, to be technically difficult. $^{1-132}$IGFBP-2, $^{1-185}$IGFBP-2 and $^{96-284}$IGFBP-2 were successfully expressed and secreted into the conditioned medium of mammalian COS-1 cells, but a large proportion remained in the flow-through of the IGF affinity column load during purification. The low IGF binding affinity of the recombinant fragments significantly inhibited the yields of purified proteins and indeed, although $^{96-284}$IGFBP-2 was detected with antibody in Western analysis, it did not bind ^{125}I-IGF-II by Western ligand blotting. In addition, instability of the IGFBP fragments during purification and storage may have contributed to reducing protein yields.

Optimisation of the purification of $^{96-284}$IGFBP-2 involved incorporation of a histidine-tag, which significantly increased recovery of protein from conditioned media (~98 μg/100 ml). Potentially, a similar tag could be incorporated for expression of the amino-terminal fragments, as the standard purification protocol yielded only small quantities of protein (~70 μg/700 ml conditioned medium). Amino-terminal fragments incorporating a histidine-tag at their C-terminus would have to be studied for any adverse structural or IGF binding effects. Alternative purification procedures may also involve isolating low affinity recombinant fragments from conditioned medium using an antibody-affinity column rather than the IGF-affinity column, as all fragments are recognised by the polyclonal anti-IGFBP-2 antibody used routinely in the laboratory.

Additional N-terminal sequences were present after purification of both mammalian and *E. coli* expressed proteins. An alternative N-terminal form of bIGFBP-2 was co-purified from transfected COS-1 cell conditioned media. GARA-IGFBP-2 arises from alternative cleavage of the signal peptide and has been shown by charcoal binding assays to have the same relative binding affinity for the IGF peptides as bIGFBP-2. GARA-forms of each of the recombinant proteins were identified. Likewise, an additional three N-terminal amino acid residues (AMA-)

were incorporated into each of the *E. coli* expressed proteins upon cleavage with enterokinase. This was a consequence of the cloning strategy. Although BIAcore analysis of *E. coli* $^{1-279}$IGFBP-2 with COS-1 $^{1-279}$IGFBP-2HIS indicated these proteins were essentially the same, the cDNA encoding these residues could potentially be removed.

3.5.4 HOW DO MAMMALIAN AND *E. COLI* EXPRESSED PROTEINS COMPARE?

Protein was successfully expressed and purified from both COS-1 and *E. coli* cells in this study. Furthermore, BIAcore analysis suggests proteins from either source behave identically. Although the COS-1 cells have been used routinely in the laboratory to express both wildtype bIGFBP-2 and truncated mutants, the protein yields were very low. This study has involved expressing protein in *E. coli* BL21 cells using the pET32a (+) expression vector. Consequently, protein yields in standard *E. coli* expressions were 10-fold greater than those obtained from COS-1 cell expressions. Large-scale optimised expressions were capable of yielding 40-60 mg/L. Furthermore, protein yields of Trx$^{1-279}$IGFBP-2HIS were greater when purified by Ni-affinity chromatography than by IGF-affinity chromatography (Table 3.1). The limitation of the *E. coli* expression system established in this study was the enterokinase cleavage reaction, which returned only approximately 20% (w/w) of the starting material. The total quantity of protein recovered after the cleavage reaction still far exceeded that obtained from the COS-1 cell conditioned media. However, the enterokinase recognition sequence could be replaced with that of a protease that exhibits greater specificity and hence results in a higher protein return.

3.5.5 CONCLUDING REMARKS

This chapter described the successful expression and purification of IGFBP-2 fragments encompassing the amino- and carboxyl-terminal domains with varying lengths of the linker

region. The following fragments were expressed in mammalian COS-1 cells: bIGFBP-2, $^{1-279}$IGFBP-2HIS, $^{1-132}$IGFBP-2, $^{1-185}$IGFBP-2, $^{96-279}$IGFBP-2HIS, $^{96-284}$IGFBP-2 and $^{137-279}$IGFBP-2HIS (Figure 2.1). An *E. coli* expression system was established for the large-scale production of IGFBP-2 and the truncated fragments. This system was used successfully in combination with Ni-affinity purification and enterokinase cleavage to generate the following proteins: $^{1-279}$IGFBP-2HIS, $^{1-132}$IGFBP-2, $^{1-185}$IGFBP-2, and $^{136-279}$IGFBP-2HIS. Truncated mutant IGFBPs $^{1-93}$IGFBP-2, $^{1-104}$IGFBP-2 and $^{182-284}$IGFBP-2 could not be expressed in this study. Purification of low affinity carboxyl-terminal fragments was enhanced by the incorporation of a hexahistidine-tag, which was shown in BIAcore analyses not to influence the IGF binding properties of the IGFBPs. Analyses of the IGF binding properties of the amino- and carboxyl-terminal fragments by Western ligand blot suggest only the N-terminal fragments bind ^{125}I-IGF-II. The IGF binding properties of these fragments as determined by BIAcore analysis, will be discussed in the following chapter.

CHAPTER 4

BIACORE ANALYSIS OF AMINO- AND CARBOXYL-TERMINAL bIGFBP-2 FRAGMENTS

4.1 INTRODUCTION

The successful expression of amino- and carboxyl-terminal domain fragments of IGFBP-2 was described in Chapter 3. In addition to attempting to define the IGF binding site on bIGFBP-2, the possibility of reconstituting the high-affinity complex with IGF using the truncated IGFBP fragments was investigated. Furthermore, in the absence of a tertiary structure for the IGFBPs either in the presence or absence of IGF ligand, orientating the two molecules in complex with each other would contribute significantly toward understanding and perhaps manipulating the interaction. Therefore, the IGF binding properties of these fragments were carefully investigated by BIAcore analysis.

Fragments of IGFBPs that bind IGFs have been reported in the literature and have helped in broadly defining the binding site. However, many studies have not exhaustively characterised these isolated peptides and therefore only provide limited information. Many investigations of the IGF binding site on IGFBPs to date have been inhibited by a lack of structural information (for example, no disulfide map until recently) and by the anomalous electrophoretic behaviour of IGFBPs. In many cases the IGF binding properties of naturally occurring and recombinantly expressed IGFBP fragments have been assessed solely by Western ligand blot (Powell *et al.,* 1989; Baxter and Firth, 1996). Western ligand blotting with ^{125}I-IGF proved advantageous over affinity crosslinking techniques in the detection of nanogram quantities of membrane immobilised IGFBPs and identification of basic binding units of the IGFBPs (Hossenlopp *et al.*, 1986). However, this method has proven to be of limited value in detecting binding for mutants with lowered affinity for IGFs (Ocrant *et al.,* 1992) and underestimates the total IGFBP content, especially when IGF is present in the preparation (Bicsak *et al.*, 1990). There are also limitations to estimating the molecular weight of IGFBPs and IGFBP fragments by SDS-PAGE analysis as known molecular weight IGFBPs have not migrated in a manner consistent with their molecular weight size markers on polyacrylamide gels (Baxter and Firth, 1996). The information derived from studies that have identified proteolytic fragments of IGFBPs on the basis of SDS-PAGE electrophoresis, identification of

molecular weights and occasionally N-terminal sequencing provides limited information about the IGF binding site on IGFBPs (Zapf *et al.,* 1990; Binoux *et al.,* 1991; McCusker *et al.,* 1991; Schmid *et al.,* 1991; Sommer *et al.,* 1991; Suikkari and Baxter, 1991; Andress and Birnbaum, 1992; Conover *et al.,* 1995). Indeed, these fragments remain largely undefined and the specific residues that contribute to the IGF binding interactions cannot be determined.

Recently, detection of IGF binding of IGFBPs and IGFBP fragments by Western ligand blot has been assisted by using mono- and di-biotinylated IGFs (Shalamanova *et al.*, 2000). Biotinylated IGFs bind IGFBP-2 with high affinity, are stable and eliminate handling of radiation. Instead of autoradiographic evaluation of ^{125}I-IGF probed membranes, detection of biotinylated IGFs is achieved by streptavidin-coupled HRP and enhanced chemiluminescence (ECL). Despite the obvious advantages to this technique, limitations have been reported as IGFBP-4 was not detected by biotinylated IGF-II in Madin Darby canine kidney cells (MDCK) (Shalamanova *et al.*, 2000). Although probing membrane-immobilised preparations of IGFBPs with either ^{125}I- or biotinylated-IGF provides rapid identification of IGFBPs and IGFBP fragments, this technique is not definitive and in many cases may fail to identify small quantities of protein, IGFBPs with weak or no IGF binding properties and possibly some species of IGFBPs. Alternative methods for the detection of IGF binding must complement initial Western ligand blot techniques.

Several studies have used biosensor technology to investigate the interaction between IGF and IGF mutants, and the IGFBPs including mutants and truncated fragments (Dubaquie and Lowman, 1999; Heding *et al.,* 1996; Hobba *et al.*, 1998; Jansson *et al.*, 1998; Kalus *et al.*, 1998; Marinaro *et al.,* 1999; Standker *et al.*, 2000; Wong *et al.*, 1999). This technology enables the real time investigation of protein-protein interactions in an automated system (Canziani *et al.*, 1999; Nice *et al.*, 1999) and unlike standard solution binding assays, does not require large quantities of protein nor radiolabelled ligand. Briefly, the BIAcore monitors the change in surface plasmon resonance upon binding of a molecule in solution (the 'analyte') to a second molecule covalently attached to the biosensor surface (the 'ligand') (Figure 4.1). The change in resonance units (RU) on the surface of a gold chip is a measure of the association of the two

molecules. The dissociation phase of the interaction is then determined by passage of analyte-free solution over the ligand.

In this study, the binding of IGF by bIGFBP-2, $^{1-279}$IGFBP-2HIS, $^{1-132}$IGFBP-2, $^{1-185}$IGFBP-2 and $^{136-279}$IGFBP-2HIS was investigated using biosensor technology. Three experiments were performed to investigate the IGF binding site on bIGFBP-2. Initially the kinetics of the interaction between IGF and IGFBP-2 fragments were assessed in straightforward kinetic experiments. Secondly, the possibility of reconstituting the high affinity interaction was investigated using a variety of approaches including pre-incubation and sequential injection of amino- and carboxyl-terminal fragments across biosensor surfaces. The final series of experiments utilised IGF analogues to define the orientation of the molecule in the binding complex. The results of these experiments will be discussed in the following sections.

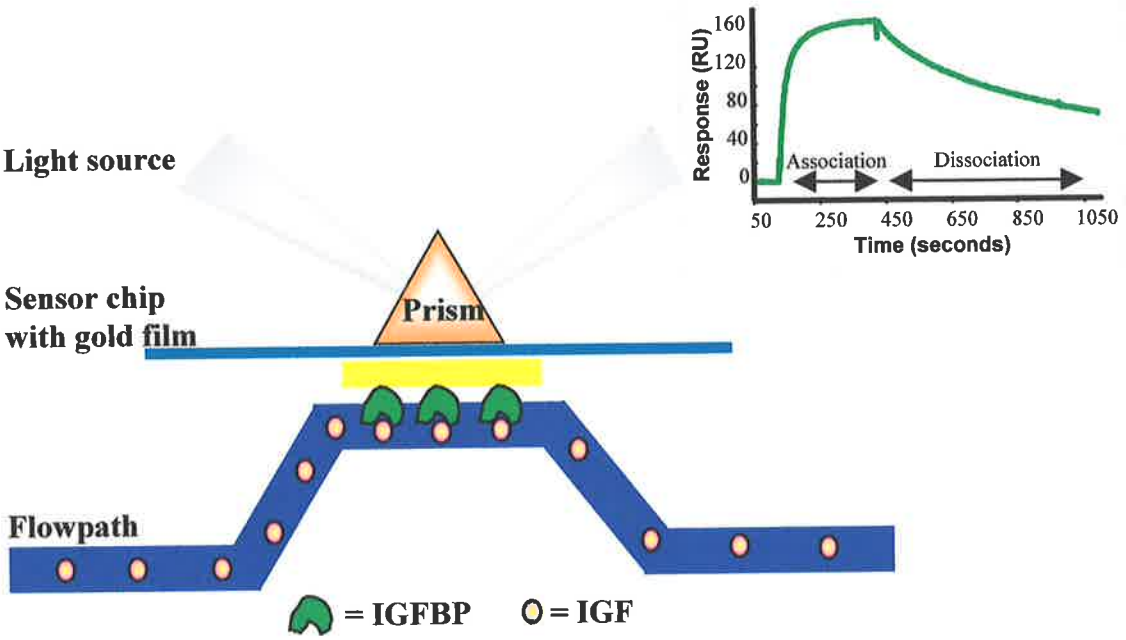

Figure 4.1 BIAcore analysis of the interaction between IGF and IGFBP-2
BIAcore experiments involve passage of an analyte in solution (IGF) across a biosensor surface which has a ligand (IGFBP-2) covalently immobilised. The subsequent change in surface mass upon binding of the analyte to the ligand is detected by diffraction of a light source. The change in the angle of light diffraction is recorded in resonance units (RU) over time and presented as a chromatogram with association and dissociation phases defined.

4.2 MATERIALS

The BIAcore™-2000 instrumentation, CM5 sensor chips, surfactant P20 and amine coupling reagents, N-ethyl-N'-[(dimethylamino)propy)]carbodi-imide (EDC), N-hydroxysuccin-imide (NHS) and ethanolamine were purchased from AMRAD Biotech, Melbourne Australia. N-2-Hydroxyethylpiperazine-N-2-ethanesulphonic acid (HEPES) was obtained from BDH Laboratory Supplies (Poole, England).

4.2.1 SOLUTIONS FOR BIACORE

Hepes Buffered Saline (HBS)

10 mM Hepes, 150 mM NaCl, 3.4 mM EDTA, 0.05 % (v/v) surfactant P20

-Prepared fresh from a 10 x concentration of stock solution

-Adjusted to pH 7.4 and filter sterilised (0.2 μm)

4.3 METHODS

4.3.1 BIOSENSOR SURFACE PREPARATION

Two types of CM5 biosensor chips were generated in this study. The first chip had immobilised IGF-I, IGF-II and insulin while the second chip was coupled with $^{1-279}$IGFBP-2HIS, $^{1-132}$IGFBP-2 and $^{136-279}$IGFBP-2HIS. A reference surface, to which no ligand was bound, was included on both chips to assess the differences in refractive index due to changes in buffers and to monitor the non-specific binding of analyte to the carboxylmethylated dextran matrix. Ligands were covalently immobilised to the CM5 gold surfaces by amine coupling as previously described (Buck *et al.,* 1989). Briefly, the peptides to be immobilised (12.5 μg/ml in 50 mM sodium acetate pH 4.6) were injected onto the activated CM5 surface at 5

μl/minute in HBS running buffer. The surfaces were then deactivated by passage of 1 M ethanolamine. Biosensor surfaces were coupled to final resonance values of approximately 200 response units (RU) for IGF/insulin chips and 600 RU for IGFBP-2 chips. The maximal binding capacity of the binding surfaces prepared this way was typically shown to be approximately 80 % of maximal theoretical binding (Melinda Lucic, PhD. Thesis, Adelaide University, 2000).

4.3.2 ACQUISITION OF KINETIC BINDING DATA

BIAcore experiments provided insight into the association and dissociation kinetics between IGF ligands and the amino- and carboxyl-terminal fragments of IGFBP-2. Briefly, various concentrations of analyte (200, 100, 50, 25, 12.5 nM) in HBS running buffer, were injected (40 μl/minute) for 5 minutes during the association phase. The dissociation phase, initiated by passage of HBS running buffer alone, was carried out over a period of 10 minutes. The biosensor surfaces were regenerated by a 60 second injection of 0.1 M HCl. Melinda Lucic, (Adelaide University, 2000) performed experiments to determine the optimal flow rate for BIAcore analyses so as to minimise mass transport limitation effects. A flow rate of 40 μl/minute was considered acceptable for the binding analyses of IGF and IGFBPs. Samples were injected in duplicate in random order in at least two separate experiments. Furthermore, to ensure that the coupling reaction was not responsible for the different IGF binding activities of the IGFBPs, kinetic analyses were performed in both orientations of protein immobilised to the CM5 gold chip: i.e. the CM5 chips were derivatised with either bIGFBP-2/truncated bIGFBP-2 or IGF, with the analyte therefore being IGF or bIGFBP-2/truncated bIGFBP-2, respectively.

Insight into the interaction between IGF and IGFBP can also be derived from studies using IGF analogues that possess different IGFBP binding affinities. In this study, passage of various concentrations of R_3IGF-I, des(1-3)IGF-I, R_6IGF-II and des(1-6)IGF-II (200, 200, 50, 25 and 12.5 nM) across biosensor surfaces coupled with $^{1-279}$IGFBP-2HIS, $^{1-132}$IGFBP-2 and

$^{136-279}$IGFBP-2HIS, contributed to our understanding of the orientation of the two molecules in complex with each other. Experiments were performed as for wildtype IGF-I and IGF-II ligands.

The possibility of reconstituting the high affinity interaction between native IGFBP-2 and IGF using the amino- and carboxyl-terminal fragments was investigated by two approaches in this study. In the first experiment, $^{1-132}$IGFBP-2 (200 nM) and $^{136-279}$IGFBP-2HIS (200 nM) were pre-incubated in HBS running buffer prior to injection across IGF biosensor surfaces for 5 minutes. The dissociation phase was determined by passage of HBS running buffer alone for 10 minutes. Secondly, the function of the amino- and carboxyl-terminal domains of bIGFBP-2 was investigated by sequential injection of IGF-II (200 nM) followed after 300 seconds by $^{1-132}$IGFBP-2 (200 nM) or $^{136-279}$IGFBP-2HIS (200 nM) across $^{1-279}$IGFBP-2HIS, $^{1-132}$IGFBP-2 and $^{136-279}$IGFBP-2HIS biosensor surfaces at 40 μl/minute. Dissociation of the complexes was achieved by passage of HBS running buffer for 10 minutes. Furthermore, the IGFBP truncations were injected across the IGFBP biosensor surfaces alone to ensure they did not associate non-specifically to each other.

4.3.3 EVALUATION OF KINETIC BINDING DATA

Kinetic data for the interaction between IGFs and IGFBPs was derived by fitting the experimental association and dissociation curves simultaneously using the BIAevaluation Software 3.0. All binding curves were corrected for background and bulk refractive index contribution by subtraction of the reference flow cells. Models were fitted both globally (simultaneously across the entire concentration series) across the data sets (Roden and Myszka, 1996) and for each of the individual concentrations. Models used were a) the 1:1 Langmuir binding interaction describing 1:1 binding between analyte (A) and ligand (B) ($A+B \leftrightarrow AB$), and b) the two-state reaction (conformational change) model, based on a 1:1 binding of analyte to an immobilised ligand followed by a conformational change ($A+B \leftrightarrow AB \leftrightarrow AB^*$) (see Appendix 1).

Bourner and co-workers (1992) previously established the 1:1 stoichiometry for the interaction between IGFs and IGFBPs. The two binding models were assessed for goodness of fit both visually and by their low χ^2 values, which provide a standard statistical measure of the goodness of fit.

Binding kinetics derived for the IGF:IGFBP interaction were similar using either the 1:1 Langmuir binding model or the two-state reaction (conformational change) model (Table 4.1). Interestingly, the two state reaction (conformational change) model was a better fit than the 1:1 Langmuir binding model when comparing 50 nM concentrations of IGF over IGFBP biosensor surfaces (also described by Melinda Lucic, PhD. Thesis, Adelaide University, 2000) (Figure 4.2). Heding and co-workers (1996) previously determined rate constants of IGF and IGFBP using 50 nM concentration curves. Fitting the kinetic data to the two state conformational change model involved fixing the value for Rmax (i.e the maximal binding capacity of the sensor chip surface) after visual assessment, fixing the refractive index value to zero and locally fitting all other parameters (as previously described by Melinda Lucic, PhD Thesis, Adelaide University, 2000) (Appendix 1).

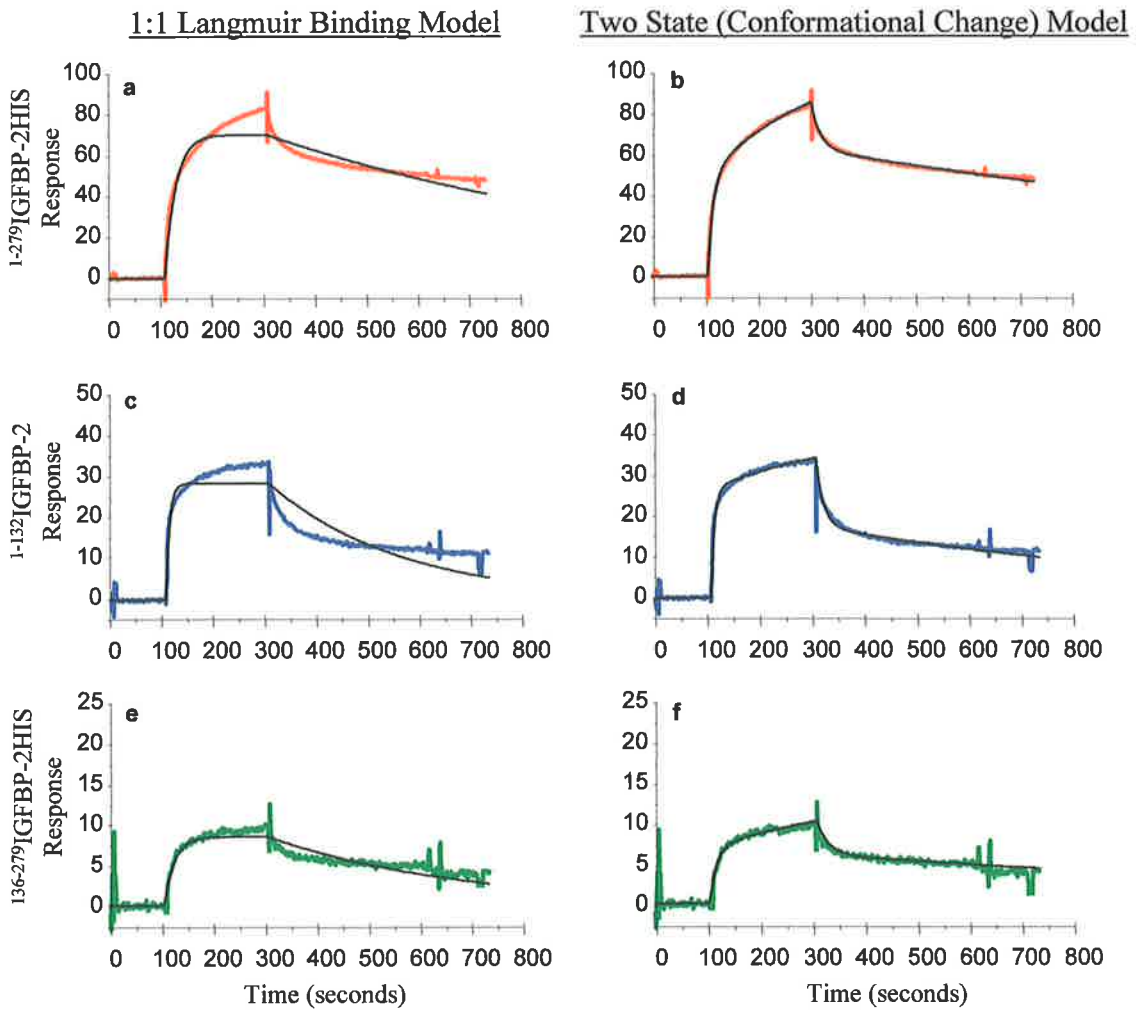

Figure 4.2 Comparison of the goodness of fit for the 1:1 Langmuir and two state (conformational change) reaction binding models
Models were fitted to concentration curves obtained using 50 nM IGF-II over $^{1\text{-}279}$IGFBP-2HIS (a, b), $^{1\text{-}132}$IGFBP-2 (c, d) and $^{136\text{-}279}$IGFBP-2HIS (e, f) biosensor surfaces respectively. The black lines represent the results of fitting the binding data to the kinetic models: 1:1 Langmuir binding model and the two state (conformational change) reaction binding model.

4.4 RESULTS

The BIAcore provided insight into the kinetics of the association and dissociation phases of wildtype and mutant bIGFBP-2 with immobilised IGF-I, IGF-II and insulin biosensor surfaces. The BIAcore was used to investigate three real time interactions of the bIGFBP-2 mutants with IGF peptides. Initially, the affinities of the amino- and carboxyl-terminal mutants for IGF ligand were assessed in a straightforward kinetic study of the free peptides across biosensor surfaces. Secondly, reconstitution of the IGFBP affinity for IGF was attempted by forming the IGFBP complex by preincubation of the amino- and carboxyl-terminal mutants prior to injection across the biosensor surfaces or by sequential injection of IGF-II followed by $^{1-132}$IGFBP-2 or $^{136-279}$IGFBP-2HIS across the IGFBP biosensor surfaces. Finally, the orientation of the molecules in the high affinity complex was investigated using IGF analogues. The BIAcore analyses of the IGF:IGFBP interaction will be discussed in the following sections.

4.4.1 DO THE AMINO- AND CARBOXYL-TERMINAL DOMAIN FRAGMENTS BIND IGF-I AND IGF-II?

The kinetic analysis in this study was performed with two orientations of the IGFBP; in one experiment, the IGFBP was the analyte and in another experiment IGFBP was the immobilised ligand (as described in Section 4.3.2). Kinetic data was shown to be identical in both experiments, providing evidence that the coupling reaction was not responsible for the observed IGF binding differences exhibited by the IGFBP fragments. Bovine IGFBP-2, $^{1-279}$IGFBP-2HIS, $^{1-132}$IGFBP-2, $^{1-185}$IGFBP-2, $^{96-279}$IGFBP-2HIS and $^{136-279}$IGFBP-2HIS bound IGF-I and IGF-II in both orientations of immobilised ligand (Figure 4.3 and Figure 4.4), but did not bind either insulin or Protein G, indicating that interactions with IGF were specific. Previously some IGFBP fragments have been shown to bind insulin at high protein concentrations (Heding *et al.*, 1996).

The association and dissociation kinetics of the interaction between IGF and the IGFBP fragments were initially assessed by fitting the data globally to a 1:1 Langmuir binding model.

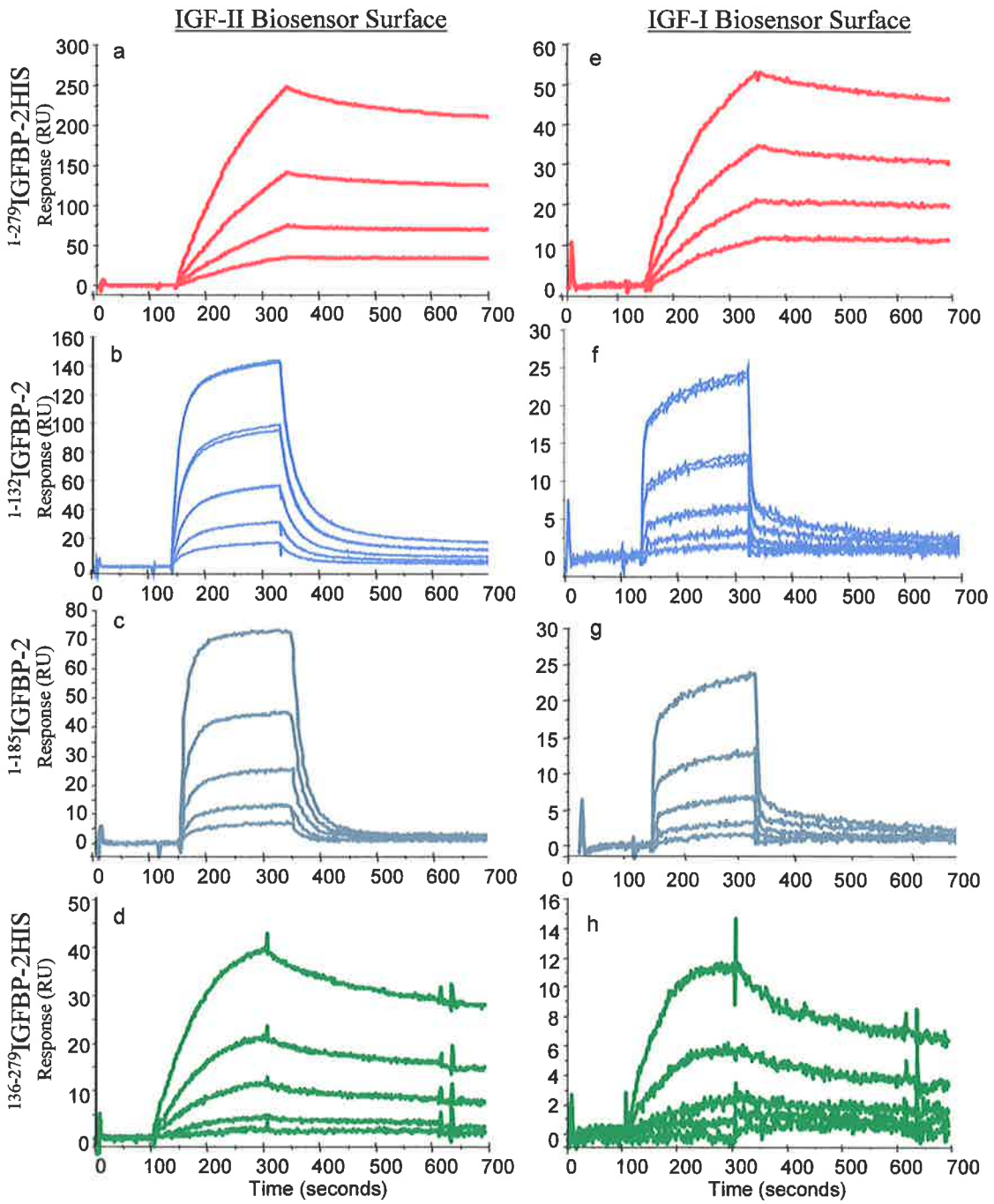

Figure 4.3 BIAcore analysis of $^{1-279}$IGFBP-2HIS and truncated fragments over IGF biosensor surfaces

Biosensorgrams are presented for the interaction of bIGFBP-2 mutants, $^{1-279}$IGFBP-2HIS (a, e), $^{1-132}$IGFBP-2 (b, f), $^{1-185}$IGFBP-2 (c, g) and $^{136-279}$IGFBP-2HIS (d, h) with IGF-II and IGF-I biosensor surfaces respectively. A concentration range (200, 100, 50, 25 and 12.5 nM; 200 nM was not analysed for $^{1-279}$IGFBP-2HIS) was analysed across IGF-I and IGF-II biosensor surfaces at a flow rate of 40 µl/minute in HBS running buffer.

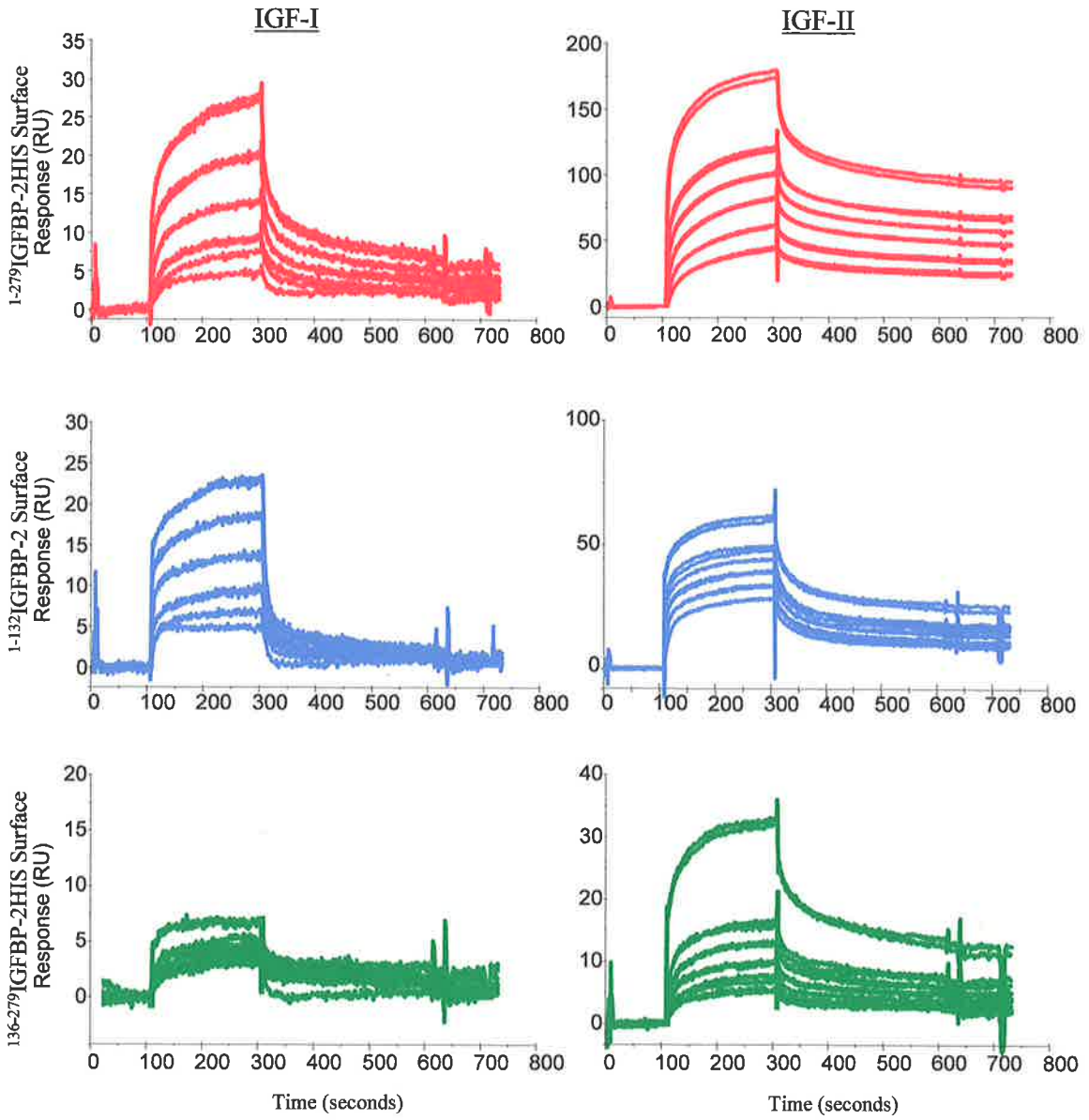

Figure 4.4 BIAcore analysis of IGF-I and IGF-II ligands over IGFBP biosensor surfaces Biosensorgrams are presented for the interaction of IGF-I and IGF-II with $^{1\text{-}279}$IGFBP-2HIS (a, d), $^{1\text{-}132}$IGFBP-2 (b, e) and $^{136\text{-}279}$IGFBP-2HIS (c, f) biosensor surfaces respectively. A concentration range (200, 100, 50, 25 and 12.5 nM) was analysed across the IGFBP biosensor surfaces at a flow rate of 40µl/minute in HBS running buffer.

$^{1-279}$IGFBP-2HIS exhibited a fast association rate with both IGF-I (k_a=1.14 x 10^5 Ms^{-1}) and IGF-II (k_a=0.87 x 10^5 Ms^{-1}) biosensor surfaces. The resultant complexes between $^{1-279}$IGFBP-2HIS and the IGF peptides were stable as illustrated by slow dissociation rates (k_d IGF-I: 0.25 x 10^{-3} $s^{-1}$and IGF-II: 0.23 x 10^{-3} s^{-1}) (Figure 4.3a and 4.3e). Kinetic analysis of the biosensorgram curves suggests $^{1-279}$IGFBP-2HIS exhibits a 1.2-fold preference for IGF-I (K_D=2.2 nM) over IGF-II surfaces (K_D=2.7 nM) (Table 4.1). Similar kinetic parameters were derived from both the global fitting of data (Figure 4.2) to the two state reaction (conformational change) model and by using a single concentration curve (50 nM) with either model.

TABLE 4.1 KINETIC ANALYSIS OF bIGFBP-2 MUTANTS INTERACTIONS WITH IGF BIOSENSOR SURFACES USING THE 1:1 LANGMUIR BINDING MODEL

IGF-I	k_a (x$10^5$1/Ms)	Relative k_a	k_d (x10^{-3} 1/s)	Relative k_d	K_D (x10^{-9} M)	Relative K_D	Relative to IGF-II
$^{1-279}$IGFBP-2HIS	1.14	1	0.25	1	2.22	1	0.83
bIGFBP-2	1.48	1.3	0.24	0.96	1.63	0.73	0.51
$^{1-132}$IGFBP-2	6.36	5.58	23.1	92.4	36.3	16.4	0.7
$^{1-185}$IGFBP-2	7.94	6.96	6.2	24.8	78.1	35.2	0.62
$^{136-279}$IGFBP-2HIS	0.65	0.57	1.55	6.2	23.8	10.7	1.77

IGF-II	k_a (x$10^5$1/Ms)	Relative k_a	k_d (x10^{-3} 1/s)	Relative k_d	K_D (x10^{-9} M)	Relative K_D
$^{1-279}$IGFBP-2HIS	0.87	1	0.23	1	2.7	1
bIGFBP-2	0.81	0.93	0.26	1.13	3.2	1.2
$^{1-132}$IGFBP-2	2.89	3.32	15	65.2	51.8	19.5
$^{1-185}$IGFBP-2	1.35	1.55	16.8	73	125	47
$^{136-279}$IGFBP-2HIS	0.68	0.78	1.1	4.9	16.3	6.1

The 1:1 Langmuir binding model was used to fit kinetic data shown in Figure 4.2 for the interaction between $^{1-279}$IGFBP-2HIS, bIGFBP-2, $^{1-132}$IGFBP-2, $^{1-185}$IGFBP-2 and $^{136-279}$IGFBP-2HIS across both IGF-I and IGF-II biosensor surfaces. χ^2 values for sensorgram curve fits were equal to or less than 6.4. Association rates (k_a), dissociation rates (k_d), and dissociation constants (K_D=k_d/k_a) are given. Dissociation constants relative to $^{1-279}$IGFBP-2HIS and the IGF-I dissociation constants relative to IGF-II are also presented (K_D IGF-I / K_D IGF-II).

The interactions of the amino-terminal mutants $^{1-132}$IGFBP-2 and $^{1-185}$IGFBP-2 with IGF-II and IGF-I biosensor surfaces are shown in Figure 4.3 (b,f and c,g respectively). The

kinetic analysis shows faster association rates and significantly increased dissociation rates compared with $^{1-279}$IGFBP-2HIS (Table 4.1). $^{1-185}$IGFBP-2 exhibited association rates with IGF-I (k_a=7.94 x 10^5 Ms^{-1}) and IGF-II (k_a=1.35 x 10^5 Ms^{-1}) that were 7- and 1.6-fold respectively more rapid than $^{1-279}$IGFBP-2HIS (IGF-I: k_a=1.14 x 10^5 Ms^{-1}; IGF-II: k_a=0.87 x 10^5 Ms^{-1}) (Table 4.1). Similarly, $^{1-132}$IGFBP-2 associated with IGF-I (k_a=6.36 x 10^5 Ms^{-1}) and IGF-II (k_a=2.89 x 10^5 Ms^{-1}) biosensor surfaces 5.6- and 3.3-fold more rapidly than $^{1-279}$IGFBP-2HIS. Both the amino-terminal fragments associated more rapidly with IGF-I than IGF-II. The dissociation rates of $^{1-132}$IGFBP-2 and $^{1-185}$IGFBP-2 from both IGF-I and IGF-II surfaces were also increased compared with $^{1-279}$IGFBP-2HIS ($^{1-132}$IGFBP-2: 92- and 65-fold and $^{1-185}$IGFBP-2: 24.8- and 73-fold respectively for IGF-I and IGF-II) (Table 4.1). The BIAcore data for $^{1-185}$IGFBP-2 was in agreement with the reduced IGF binding affinities determined by solution-binding assays (Section 3.4.3.2). Furthermore, the amino-terminal fragments mimic the preference of $^{1-279}$IGFBP-2HIS for IGF-I ligand over IGF-II (Table 4.1).

$^{136-279}$IGFBP-2HIS exhibited a slower association with both IGF-I (k_a=6.5 x 10^4 Ms^{-1}) and IGF-II (k_a=6.8 x 10^4 Ms^{-1}) biosensor surfaces compared with $^{1-279}$IGFBP-2HIS (0.57- and 0.78-fold respectively) and these rates were essentially identical (Table 4.1). The dissociation rate of $^{136-279}$IGFBP-2HIS from IGF was much slower than exhibited by the amino-terminal fragment, however more rapid than the wildtype protein (6.2- and 4.9-fold from IGF-I and IGF-II surfaces respectively) (Table 4.1). Interestingly, unlike the amino-terminal fragment $^{1-132}$IGFBP-2 that exhibited a slight preference for IGF-I (K_D=36.3 nM) over IGF-II (K_D=51.8 nM), $^{136-279}$IGFBP-2HIS had a 1.5-fold preference for IGF-II (K_D=16.3 nM) over IGF-I (K_D=23.8 nM) attributable to its dissociation component (Table 4.1). The carboxyl-terminal fragment $^{96-279}$IGFBP-2HIS bound both IGF-I and IGF-II biosensor surfaces so poorly that association and dissociation kinetics could not be quantitated. Similarly, Galanis and co-workers (2001) were unable to derive apparent kinetic constants for a carboxyl-terminal fragment of IGFBP-3 (amino acid residues 165-264).

4.4.2 CAN THE AMINO- AND CARBOXYL-TERMINAL DOMAIN FRAGMENTS RECONSTITUTE THE HIGH AFFINITY IGF:IGFBP INTERACTION?

Reconstitution of the wildtype binding interaction between bIGFBP-2 and IGF ligands was investigated by two mechanisms. Initially, the amino- and carboxyl-terminal fragments of bIGFBP-2 were preincubated in HBS running buffer prior to injection across IGF biosensor surfaces. Secondly, IGF-II and the truncated IGFBP fragments were sequentially injected across the three IGFBP biosensor surfaces [viz: $^{1\text{-}279}$IGFBP-2HIS, $^{1\text{-}132}$IGFBP-2 and $^{136\text{-}279}$IGFBP-2HIS]. The $^{1\text{-}185}$IGFBP-2 and $^{96\text{-}279}$IGFBP-HIS fragments could not be used concurrently in the same BIAcore experiment due to non-specific interactions with each other; presumably through the common hydrophobic central region (amino acid residues 96-185). Interestingly, the carboxyl-terminal fragment $^{96\text{-}279}$IGFBP-2HIS bound not only the amino-terminal biosensor surface but also to itself on the biosensor surface. This was not observed for $^{1\text{-}132}$IGFBP-2, $^{1\text{-}185}$IGFBP-2 or $^{136\text{-}279}$IGFBP-2HIS. Preincubation of $^{1\text{-}132}$IGFBP-2 and $^{136\text{-}279}$IGFBP-2HIS failed to reconstitute the high affinity binding interaction of bIGFBP-2 with IGF (Figure 4.5). This would suggest the requirement for the two halves of the molecule to be linked to each other to produce the high affinity complex.

The amino- and carboxyl-terminal halves of bIGFBP-2 were also injected over $^{1\text{-}279}$IGFBP-2HIS, $^{1\text{-}132}$IGFBP-2 and $^{136\text{-}279}$IGFBP-2HIS biosensor surfaces that already had IGF-II prebound. Briefly, IGF was injected over bIGFBP-2 mutant biosensor surfaces followed immediately by injection of bIGFBP-2 mutants or HBS buffer. The change in RU of IGF-II-complexed $^{1\text{-}279}$IGFBP-2HIS biosensor surfaces was identical whether HBS, $^{1\text{-}132}$IGFBP-2 or $^{136\text{-}279}$IGFBP-2HIS was present in the dissociation phase (Figure 4.6a). This strongly suggests that the dissociation of IGF-II was not affected by passage of either the amino- or carboxyl-terminal fragments.

When $^{136\text{-}279}$IGFBP-2HIS was passed over the IGF-II complexed $^{1\text{-}132}$IGFBP-2 biosensor surface, a slower dissociation rate was observed compared with HBS or buffer containing $^{1\text{-}132}$IGFBP-2 (Figure 4.6b). This effect could be attributed to a combination of $^{136\text{-}279}$IGFBP-2HIS binding to the IGF-II-complexed $^{1\text{-}132}$IGFBP-2 biosensor surface and

competition by the higher affinity $^{136-279}$IGFBP-2HIS for IGF-II. Similarly, the increased response upon addition of $^{1-132}$IGFBP-2 across the IGF-II-complexed $^{136-279}$IGFBP-2HIS biosensor surface suggests $^{1-132}$IGFBP-2 binds to the complex (Figure 4.6c).

4.4.3 HOW ARE THE IGF-IGFBP MOLECULES ORIENTATED IN THE HIGH AFFINITY COMPLEX?

Kinetic analyses derived using the two state (conformational change) model for passage of 50 nM concentrations of IGF-II, des(1-6)IGF-II and R_6IGF-II over immobilised $^{1-279}$IGFBP-2HIS, $^{1-132}$IGFBP-2 and $^{136-279}$IGFBP-2HIS biosensor surfaces are presented here (Table 4.2). Due to the significantly poorer response of the IGF-I analogues and IGF-II analogues over $^{136-279}$IGFBP-2HIS biosensor surfaces, kinetic parameters could not be accurately derived, however biosensorgrams have been presented for qualitative comparisons (Figure 4.7).

Native IGF-I and IGF-II biosensorgrams have been presented showing binding to each of the immobilised bIGFBP-2 analogue biosensor surfaces (Figure 4.7). R_3IGF-I and R_6IGF-II bind $^{1-279}$IGFBP-2HIS, $^{1-132}$IGFBP-2 and $^{136-279}$IGFBP-2HIS with higher affinity than do the corresponding truncated analogues, consistent with previously reported solution binding assays (King *et al.*, 1992; Francis *et al.*, 1993). Relative to native IGF-II, R_6IGF-II exhibits 3.4- and 4.0-fold decreased equilibrium affinities for $^{1-279}$IGFBP-2HIS and $^{1-132}$IGFBP-2 biosensor surfaces respectively (Table 4.2). In contrast, R_3IGF-I and R_6IGF-II bind $^{136-279}$IGFBP-2HIS biosensor surfaces as well as do their respective native IGF (Figure 4.7c and f). These results suggest the glutamate residue is specifically involved in binding the amino-terminal domain of bIGFBP-2. In contrast, des(1-3)IGF-I and des(1-6)IGF-II exhibited reduced binding to $^{1-279}$IGFBP-2HIS, $^{1-132}$IGFBP-2 and $^{136-279}$IGFBP-2HIS biosensor surfaces. The amino-terminal tripeptide of IGF-I and hexapeptide of IGF-II, therefore, influenced binding to both the amino- and carboxyl-terminal domains of bIGFBP-2.

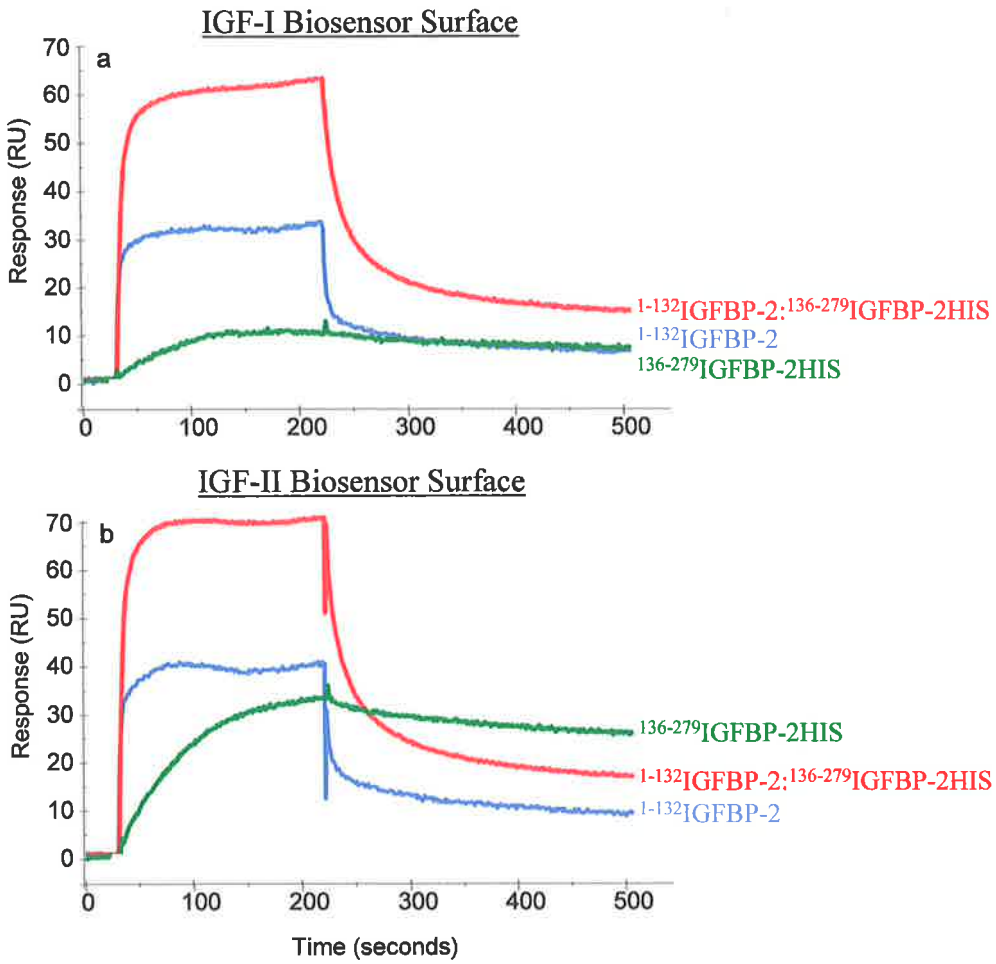

Figure 4.5 BIAcore analysis of preincubated $^{1-132}$IGFBP-2 and $^{136-279}$IGFBP-2HIS analogues over IGF biosensor surfaces
$^{1-132}$IGFBP-2 (–), $^{136-279}$IGFBP-2HIS (–) and preincubated $^{1-132}$IGFBP-2:$^{136-279}$IGFBP-2HIS (1:1)(–) (200 nM) were injected across IGF-I (a) and IGF-II (b) biosensor surfaces at a flow rate of 40 µl/minutes in HBS running buffer.

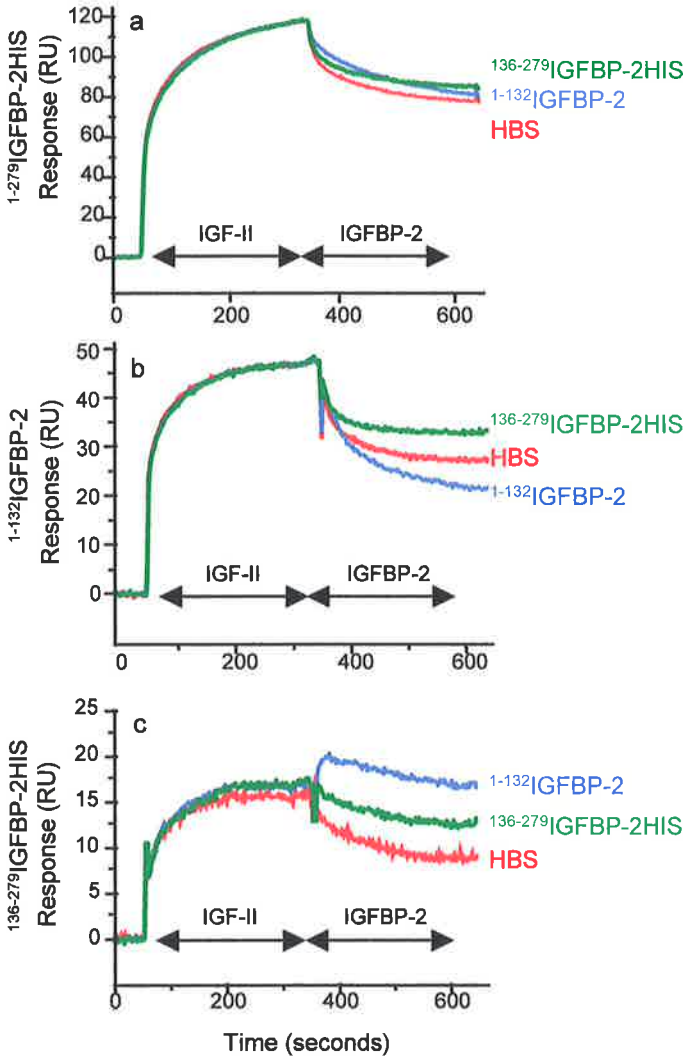

Figure 4.6 BIAcore analysis of the sequential injection of IGF and bIGFBP-2 mutants across $^{1-279}$IGFBP-2HIS, $^{1-132}$IGFBP-2 and $^{136-279}$IGFBP-2HIS biosensor surfaces
IGF-II (200 nM) was injected across bIGFBP-2 biosensor surfaces for 300 seconds, followed immediately by either passage of HBS running buffer (–), $^{1-132}$IGFBP-2 (–) or $^{136-279}$IGFBP-2HIS (–) (200 nM) at a flow rate of 40 µl/minute.

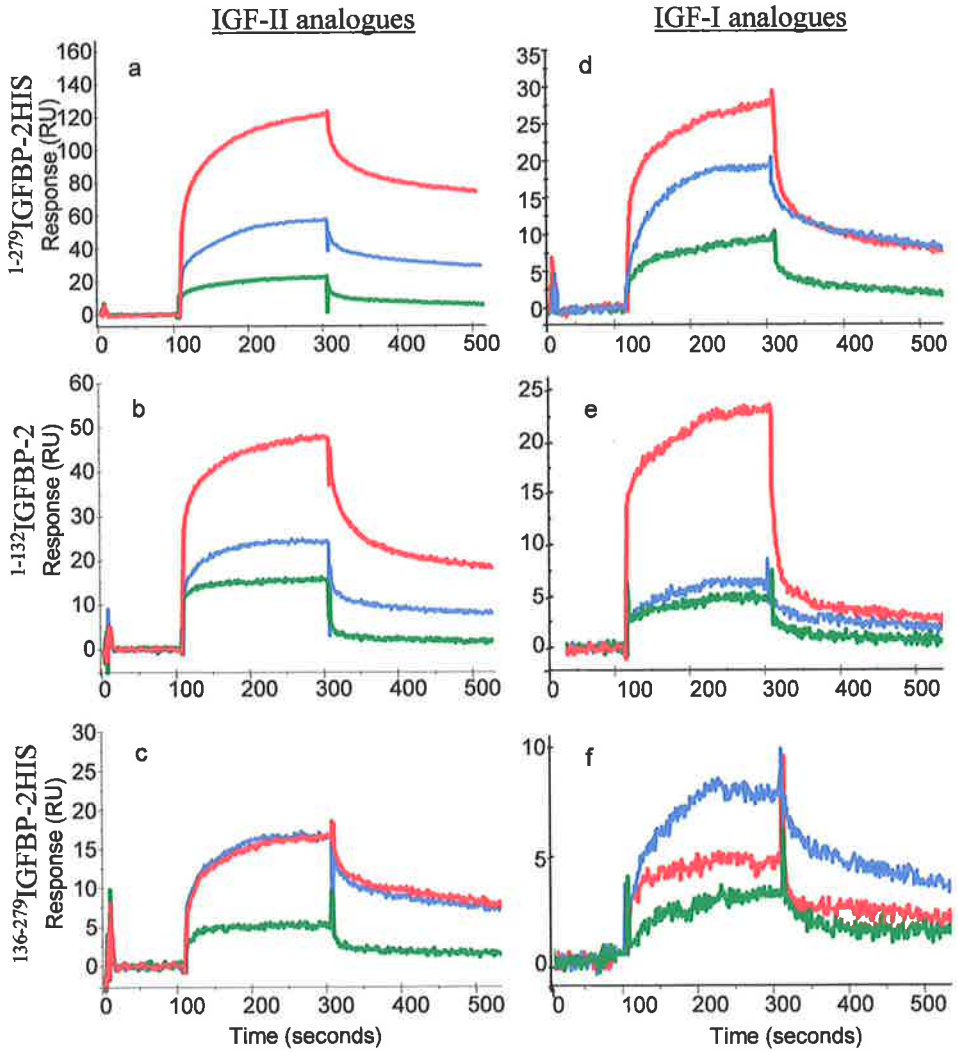

Figure 4.7 BIAcore analysis of IGF mutant analogues across bIGFBP-2 biosensor surfaces Representative biosensorgrams of IGF-II (—), des(1-6)IGF-II (—) and R_6IGF-II (—) (50 nM) across $^{1-279}$IGFBP-2HIS (a), $^{1-132}$IGFBP-2 (b) and $^{136-279}$IGFBP-2HIS (c) biosensor surfaces are shown. Similarly IGF-I (—), des(1-3)IGF-I (—) and R_3IGF-I (—) (50 nM) across $^{1-279}$IGFBP-2HIS (d), $^{1-132}$IGFBP-2 (e) and $^{136-279}$IGFBP-2HIS (f) biosensor surfaces are presented also. Binding curves were obtained at a flow rate of 40 µl/minute in HBS running buffer. Traces are representative of duplicate analyses.

TABLE 4.2 KINETIC ANALYSIS OF IGF-II ANALOGUES ACROSS WILDTYPE AND MUTANT bIGFBP-2 BIOSENSOR SURFACES USING THE TWO STATE CONFORMATIONAL CHANGE MODEL

	k_{a1} ($x10^5$ 1/Ms)	k_{a2} ($x10^{-3}$ 1/Ms)	k_{d1} ($x10^{-2}$ 1/s)	k_{d2} ($x10^{-4}$ 1/s)	K_D ($x10^{-9}$ M)	Relative K_D
$^{1-279}$IGFBP-2HIS Biosensor Surface						
IGF-II	7.9	8.6	4.8	8.3	5.8	1
R_6IGF-II	7.8	6.3	9.5	10.2	19.8	3.4
des(1-6)IGF-II	5.1	4.8	12.3	20.4	101	17.4
$^{1-132}$IGFBP-2 Biosensor Surface						
IGF-II	16	4.4	6.5	14.2	13.3	1
R_6IGF-II	7.9	3.5	14.4	10.1	53	4.0
des(1-6)IGF-II	8.4	1.8	40	37.4	1000	75.2

Kinetic parameters were based on a two state conformational change binding model using 50 nM biosensor curves of IGF-II analogues over $^{1-279}$IGFBP-2HIS, $^{1-132}$IGFBP-2 and $^{136-279}$IGFBP-2HIS biosensor surfaces. χ^2 values for sensorgram curve (Figure 4.7) fits were equal to or less than 0.8 except R_6IGF-II over $^{136-279}$IGFBP-2HIS (χ^2=3.5). Dissociation constants were derived using both association (k_a) and dissociation (k_d) rates ($K_D = (k_{d1}/k_{a1})(k_{d2}/k_{a2})$).

4.5 DISCUSSION

This study clearly demonstrates that both the amino- and carboxyl-terminal domains of bIGFBP-2 bind IGF-I and IGF-II. The amino-terminal fragments $^{1-132}$IGFBP-2 and $^{1-185}$IGFBP-2 exhibit rapid association but lack the components essential for maintaining a stable complex. In contrast, $^{136-279}$IGFBP-2HIS binds IGFs less rapidly than either amino-terminal fragments or $^{1-279}$IGFBP-2HIS, but retains the ligand in a more stable complex than $^{1-132}$IGFBP-2. These findings suggest that both the highly conserved amino- and carboxyl-terminal domains of bIGFBP-2 are required for sequestering IGF ligands. Indeed, they appear to act in a coordinated fashion in the high affinity interaction. Furthermore, we have shown that the amino-terminal residues of IGF are critical binding determinants for both $^{1-132}$IGFBP-2 and $^{136-279}$IGFBP-2HIS, while the glutamate at position 3 and 6 of IGF-I and IGF-II, respectively, is important for the interaction with the amino-terminal domain of bIGFBP-2. The recent

co-crystallization of IGF-I with mini-IGFBP-5 showed direct contact between Glu3 of IGF-I and Tyr50 and His71 of mini-IGFBP-5 (Żesławski *et al.*, 2001).

The present investigation shows in real time the high affinity association of the amino-terminal fragments $^{1-132}$IGFBP-2 and $^{1-185}$IGFBP-2 with IGF-I (k_a=6.36 x 10^5 Ms^{-1} and k_a=7.94 x 10^5 Ms^{-1}) and IGF-II (k_a=2.89 x 10^5 Ms^{-1} and k_a=1.35 x 10^5 Ms^{-1}). The amino-terminal domains of IGFBPs 1-6 (usually incorporating all twelve cysteine residues) have been reported to bind IGF (Andress *et al.*, 1993; Chernausek *et al.*, 1995; Hashimoto *et al.*, 1997; Durnham *et al.*, 1995; Conover *et al.*, 1995; Zapf *et al.*, 1998; Spencer and Chan, 1995). Interestingly, the central linker region appears to contribute to the structural integrity and hence IGF binding potential of these amino-terminal fragments. Hashimoto and co-workers highlighted the importance of inclusion of the linker region since a fragment of rat IGFBP-3 (amino acid residues 1-93) retained only 4.2% IGF binding while addition of linker peptide residues (94-186) increased IGF binding to 12% of native rat IGFBP-3 (Hasimoto *et al.*, 1997). An even greater effect was seen in this study. In fact, expression of $^{1-94}$IGFBP-2, $^{1-104}$IGFBP-2 and $^{182-284}$IGFBP-2 was not successful in the present investigation due presumably to increased susceptibility to proteolysis resulting from a lack of structural integrity.

The present study has confirmed the ability of the carboxyl-terminal half of bIGFBP-2 (amino acid residues 136-279) to bind IGF-I (K_D=23.8 nM) and IGF-II (K_D=16.3 nM). Previously, there was some debate about the ability of the carboxyl-terminal domain to bind IGF. While C-terminal fragments of hIGFBP-4 (Qin *et al.*, 1998) and hIGFBP-5 (Kalus *et al.*, 1998) had no demonstrable IGF binding, similar fragments including a naturally occurring truncation of hIGFBP-2 (amino acid residues 169-289), retained partial IGF binding (Wang *et al.*, 1988; Sommer *et al.*, 1991; Spencer and Chan, 1995). Furthermore, C-terminal deletion studies of bIGFBP-2 clearly indicated the importance of the carboxyl-terminal domain in IGF binding (Forbes *et al.*, 1998). Removal of 14, 36 and 48 amino acid residues from the C-terminus appeared to have no effect on IGF binding but removal of a further 14 amino acid residues dramatically reduced IGF binding. Other studies have shown that removal of most or

all of the C-terminal domains of IGFBP-3 (Sommer *et al.,* 1991; Firth *et al.,* 1998), IGFBP-4 (Qin *et al.*, 1998) or IGFBP-5 (Andress *et al.*, 1993) reduces IGF binding significantly.

It is clear that the amino- and carboxyl-terminal domains are required to work together to form the high affinity complex. However, whether the amino- or carboxyl-terminal domain of IGFBP is the major binding site is a matter of interpretation. The present investigation clearly shows the amino-terminal domain is required for rapid association with IGF, and the carboxyl-terminal domain for its ability to maintain IGF in a complexed form. Recently, Galanis and co-workers reported that the recombinant expression of IGFBP-3 fragments encompassing amino- and carboxyl-terminal residues (1-88 and 165-264) bind IGF-I and IGF-II with reduced affinity (Galanis *et al.*, 2001). Consistent with the current findings, the amino-terminal fragment (N-88) dissociated 50- and 75-fold faster from IGF-I and IGF-II biosensor surfaces compared with the carboxyl-terminal fragment (C-165). In addition, Kalus and co-workers purified two amino-terminal fragments of hIGFBP-5 (amino acid residues 1-94 and 40-92) that exhibited similar affinity for IGF, both with 200-fold reduced affinity compared to wildtype (Kalus *et al.*, 1998). Imai and co-workers confirmed the importance of corresponding amino-terminal residues in IGFBP-3 (Imai *et al.*, 2000) and Qin and co-workers for IGFBP-4 (Qin *et al.*, 1998). Furthermore, as amino acid residues 1-39 of hIGFBP-5 did not contribute to stabilising the complex, it was concluded that additional components required for IGF-IGFBP-5 complex stability would be derived from the C-terminal residues of IGFBPs (Kalus *et al.*, 1998). It is feasible therefore, that the IGF binding sites located in the amino- and carboxyl-terminal domains of IGFBPs, combine with each other to create one high affinity-binding site. Indeed, Lys222-Asn236 of bIGFBP-2 may be located in close enough proximity to the N-terminal domain to allow both domains to interact with IGF (Forbes *et al.*, 1998). Site directed mutagenesis of Gly203 and Gln209 in the equivalent region of rIGFBP-5, resulted in an 8- and 6-fold reduction in IGF-I binding affinity (Bramani *et al.*, 1999). Therefore it is essential that both domains to be linked covalently for the high affinity interaction to occur.

The amino terminal residues of IGF are known to be essential for interaction with IGFBPs as IGF analogues, des(1-3)IGF-I and des(1-6)IGF-II, have significantly reduced

binding affinity (Bagley *et al.*, 1989; Francis *et al.*, 1993; Sara *et al.,* 1986). Ho and Baxter orientated the IGF molecule in complex with hIGFBP-2 using the analogue des(1-6)IGF-II (Ho and Baxter, 1997). Des(1-6)IGF-II was found to displace tracer from intact hIGFBP-2 with 10 % the activity of native ligand, however was totally inactive in displacing IGF-II tracer from a C-terminal fragment (amino acid residues 169-289). These results suggest the amino-terminus of IGF-II interacts with the carboxyl-terminal domain of hIGFBP-2. Photoaffinity labelling experiments by Horney and co-workers further supported this conclusion (Horney *et al.*, 2001). However, the present study showed that not only did the amino-hexapeptide of IGF-II influence binding to the carboxyl-terminal half of bIGFBP-2, but also to the amino-terminal half. This indicates the existence of binding sites for the hexapeptide of IGF within both the amino- and carboxyl-terminal domains of IGFBP-2. A summary of these findings is represented schematically in Figure 4.8. Furthermore, Glu6 of IGF-II appeared to specifically affect IGF binding only to $^{1\text{-}132}$IGFBP-2 and did not alter binding to $^{136\text{-}279}$IGFBP-2HIS. It will be interesting to determine the ability of $^{1\text{-}132}$IGFBP-2 and $^{136\text{-}279}$IGFBP-2HIS to bind other IGF analogues known to influence interaction with IGFBPs (viz: IGF-I: Glu3, Thr4, Gln15, Phe16 (Bayne *et al.,* 1988); Thr4, Glu9, Phe16 (Magee *et al.*, 1999); Phe49, Arg50, Ser51 (Cascieri *et al.*, 1989) and IGF-II: Phe26, Phe48, Arg49, Ser50 (Bach *et al.*, 1993)). The specific residues of IGF-I and IGF-II involved in binding to either the amino- or carboxyl-terminal domains was investigated by nuclear magnetic resonance (NMR), as described in Chapter 7.

Based on the present findings, a model for the modulation of IGF activity by IGFBPs is presented in Figure 4.8. Classical high affinity IGF binding only occurs when both the amino- and carboxyl-terminal domains of IGFBPs are linked together, as is evident also from partial proteolysis studies (reviewed by Conover, 1998). Two binding sites exist, one in the amino-terminal domain that has a fast association component, and one in the carboxyl-terminal domain that is essential for the stability of the complex. These sites must be combined to form one high-affinity binding site. Glu3 of IGF-I and Glu6 of IGF-II interact directly with the N-terminal domain of IGFBP-2 while the amino-terminal tripeptide of IGF-I and hexapeptide of IGF-II are critical for binding to both the amino- and carboxyl-terminal fragments of IGFBP-2.

While the objective of this study was to elucidate the IGF binding site on IGFBP-2, it will also be interesting to investigate the modulation of IGF activity by IGFBP fragments in biological assays.

The present experiments further emphasise the requirement for the two halves of the IGFBP to exist concomitantly in order to establish a high affinity-binding complex with IGF, but it is not clear yet by which means the two domains come together to form the high affinity binding interaction. The IGF binding site of IGFBPs obviously requires further investigation. Determining the residues involved in the IGF-IGFBP interaction will ultimately allow researchers to develop a comprehensive insight into the molecular dynamics of the binding interaction making it possible to produce mutant binding proteins for therapeutic applications. Not until we can derive a 3D structure of the complex, by NMR or X-ray crystallography, will we truly understand this interaction.

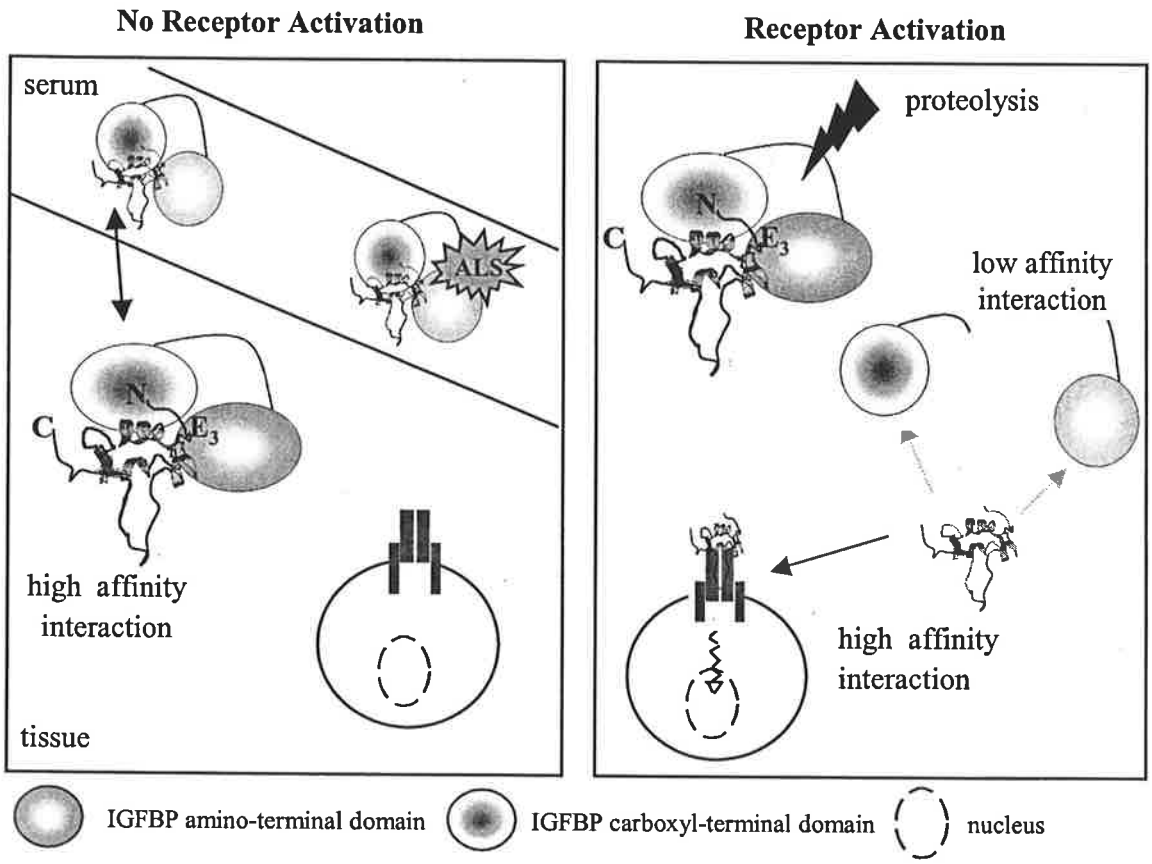

Figure 4.8 Model of the orientation of the molecules in the IGF·IGFBP-2 complex
This model is based on the data presented. The amino-termini of IGF-I and IGF-II interact with both the highly conserved amino- and carboxyl-terminal domains of bIGFBP-2. The N-terminal glutamate of IGF interacts specifically with the amino-terminal domain of bIGFBP-2, shown here for IGF-I. This is a high affinity complex preventing interaction with the type-1 IGF receptor. Proteolysis of the IGFBPs yields amino- and carboxyl-terminal fragments, similar to those produced recombinantly in this study, which exhibit reduced IGF binding affinities compared to the native protein.

CHAPTER 5

PREPARATION OF PROTEIN FOR STRUCTURAL STUDIES

5.1 INTRODUCTION

Despite the numerous studies targeting the IGF·IGFBP binding interaction, there remains a distinct lack of information regarding the specific residues of both IGFs and IGFBPs involved in the interaction. Although many studies have been directed toward elucidating the interacting residues, they would benefit greatly from a more detailed knowledge of the structure of the IGFBPs. Indeed, in the absence of a tertiary structure, understanding the mechanism of the binding interaction becomes very difficult. Knowledge of the IGFBP structure could also provide a basis to predict other amino acid residues that may be accessible for interacting with the IGFs. Furthermore, structural knowledge of a protein may enable interpretation of the effects that particular amino acid substitutions elicit.

Until recently, structure determination studies of the IGFBPs had not been reported in the literature. Disulfide bond determination, deuterium exchange studies and NMR analysis of the IGF·IGFBP interaction indicates that there in increasing interest in elucidating the structure of IGFBPs (Ehring, 1999; Forbes *et al.*, 1998; Jansson *et al.,* 1998; Neumann and Bach, 1999). Indeed, an NMR structure has been determined for an amino-terminal IGF binding fragment of IGFBP-5 (amino acid residues 40 to 92, Kalus *et al.*, 1998) and recently a crystal structure of this IGFBP-5 fragment in complex with IGF-I has been published (Żesławski *et al.*, 2001). However, the structure of the entire IGFBP molecule remains to be elucidated and hence forms one of the objectives of this study.

There are several approaches for structure determination, including X-ray crystallography and NMR, which provide different and complementary information regarding protein structure. One common requirement for all structure studies however is large quantities of purified protein. In addition, NMR structure determination of large protein molecules can benefit from labelling with ^{15}N and/or ^{13}C and by exchange of the labile protons with deuterium. This chapter describes the large-scale production of both IGFs and IGFBP-2 for structure studies. IGF-I and IGF-II were labelled and/or deuterated for NMR analysis. Large-

scale preparations of $^{1-279}$IGFBP-2HIS and thioredoxin-fused IGFBP-2 fragments were generated for both crystallisation and NMR analysis. Furthermore, the binding properties of the *E. coli* Trx-IGFBPs were analysed and the formation of IGF·IGFBP complexes assessed under a variety of pH conditions.

5.2 MATERIALS

5.2.1 MATERIALS FOR PROTEIN EXPRESSION, PURIFICATION AND CHARACTERIZATION

Materials for bacteria culture and fermentation media were as described in Sections 2.2 and 3.2.2. $^{15}NH_4Cl$, ^{13}C-glucose and $^{2}H_2O$ were purchased from NovaChem, Victoria, Australia. Hydroxylamine was obtained from Sigma Chemical Co., MO, USA, while the H64A subtilisin was a kind gift from Gro*Pep* Ltd., Thebarton, SA, Australia. Dithiothreitol (DTT), 2-hydroxyethyl disulfide (oxidizing βME), urea, LiOH and tricine were purchased from Sigma Chemical Co., MO, USA. Citric acid for BIAcore analyses was purchased from Ajax Chemicals Ltd., Sydney, Australia. All other chemicals were of analytical reagent grade.

5.2.2 BACTERIAL STRAINS

E. coli JM101:	supE thi-1 Δ(lac-proAB)(F'traD36proABlacI^{q}ZΔM15
E. coli BL21:	*E. coli* B F$^-$dcm ompT hsdS ($r_B^-m_B^-$) gal (DE3)

5.2.3 VECTORS FOR PROTEIN EXPRESSION

pETIGFBP-2HIS	Carrick *et al.*, 2001	Figure 2.10 (Section 2.4.4.1)
pGH(1-11)-VN-IGF-I	King *et al.*, 1992	Figure 5.1
pGH(1-11)-VNFAHY-IGF-II	Francis *et al.*, 1993	Figure 5.1
pGH(1-11)-VNPAPH-IGF-II	Lien *et al.*, 2001	Figure 5.1

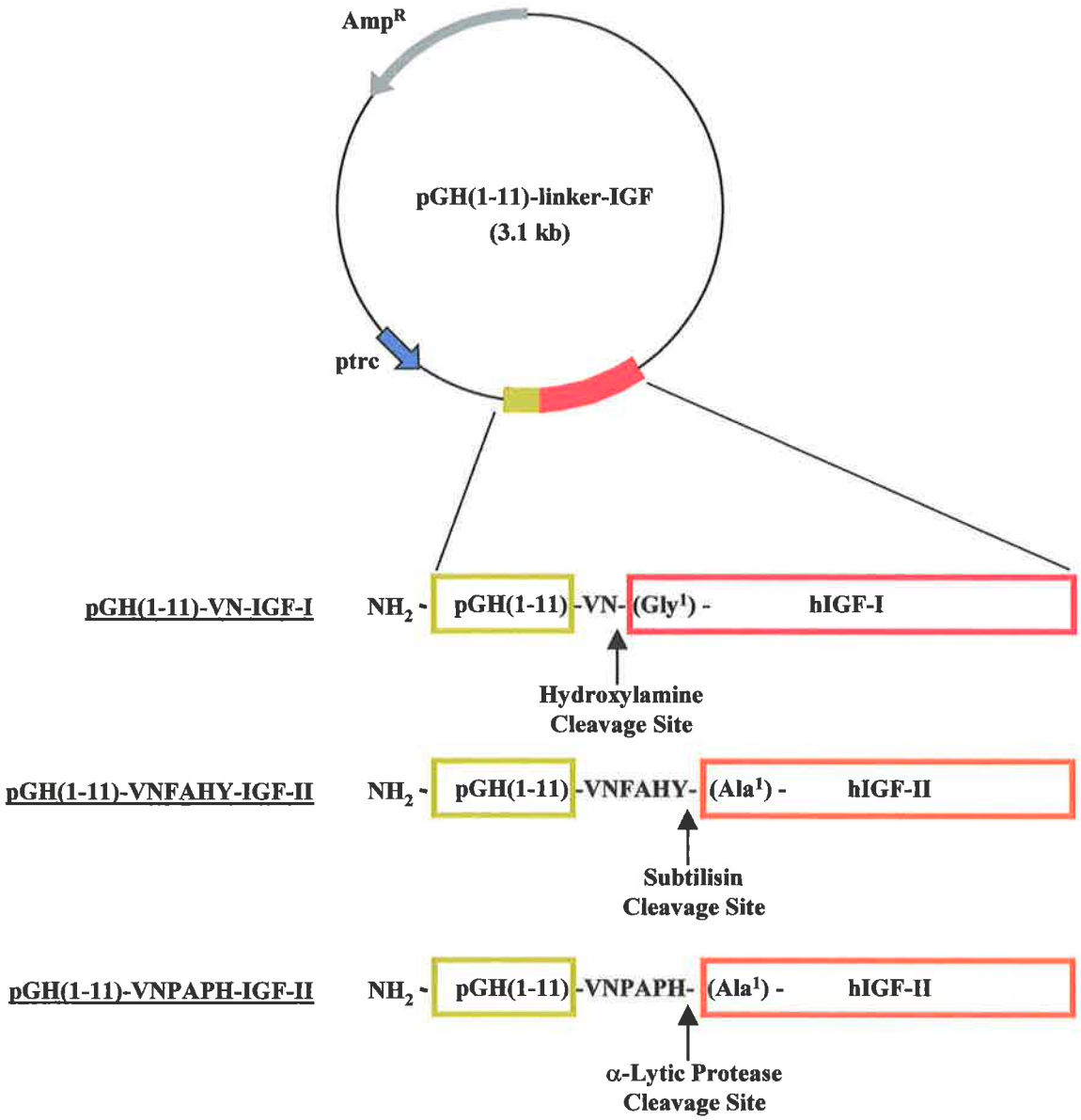

Figure 5.1 IGF expression vectors and fusion proteins
The cDNA encoding either IGF-I or IGF-II was cloned downstream of cDNA encoding the first 11 amino acid residues of human growth hormone to produce the *E. coli* expression vectors: pGH(1-11)-VN-IGF-I, pGH(1-11)-VNFAHY-IGF-II, pGH(1-11)-VNPAPH-IGF-II. cDNA encoding a Asn-Gly hydroxylamine cleavage site connects the fusion protein to the IGF-I and facilitates cleavage of the native ligand. Two linker peptides have been inserted into the IGF-II expression vector, one to facilitate cleavage with subtillisin (-VNFAHY-) and the other with an α-lytic protease (-VNPAPH-). The vector contains a *trc* promoter (p*trc*), an optimized ribosome binding site, a transcription termination sequence and an ampicillin resistance gene (Amp) (King *et al.*, 1992).

5.2.4 FERMENTATION MEDIUM

NH_4Cl	1.61 g
K_2SO_4	1.21 g
KH_2PO_4	1.59 g
Na_2HPO_4	2.6 g
For 1L:	Dissolve in 800 ml water and autoclave in 1L Schott bottle.

Glucose	25 g
$MgSO_4.7H_2O$	0.56 g

Dissolve in 200 ml water and filter sterilise.

Trace Elements: 100 ml (500 x) Stock:

	g/100 ml
$FeSO_4.7H_2O$	1.9 g
$MnSO_4.H_2O$	0.255 g
$ZnSO_4.7H_2O$	0.43 g
$CuSO_4.5H_2O$	0.0375 g
Na_3citrate	4.4 g
HCl (conc)	2 ml

To 800ml medium add glucose/$MgSO_4$ solution (200 ml), trace elements (2 ml/L), thiamine (0.04 g/L) and Ampicillin (50 μg/ml) under sterile conditions.

5.2.5 BUFFERS FOR PROTEIN PURIFICATION

Homogenisation Buffer
10 mM KH_2PO_4, 30 mM NaCl, 0.5 mM $ZnCl_2$ pH 7.8

Desalt Buffer
8 M urea, 0.1 M Tris, 40 mM glycine, 0.5 mM $ZnCl_2$, 1.6 mM DTT
pH 9.1, filtered (1 μm)

10 x Refold Buffer
1 M Tris, 66.67 mM EDTA
pH 9.1, filtered (1 μm)

FFS Buffer A
8 M urea, 50 mM NaAcetate
pH 4.8 (glacial acetic acid)

FFS Buffer B
8 M urea, 50 mM NaAcetate, 1 M NaCl
pH 4.8 (glacial acetic acid)

FFQ Buffer A
20 mM Tris
pH 9.0 (glacial acetic acid)

FFQ Buffer B
20 mM Tris, 200 mM NaCl
pH 9.0 (glacial acetic acid)

5.2.6 MATERIALS FOR GEL FILTRATION

The Smart®System, including the μSeparation unit, the μPrecision Pump and the μPeak Monitor, and the Superdex 200 column were purchased from Amrad Pharmacia Biotech (Uppsala, Sweden). Proteins for high molecular weight standards (thyroglobulin, ferritin, human IgG, transferrin, ovalbumin, myoglobin and vitamin B12) were obtained from Sigma Chemical Co. MO, USA and Pharmacia Biotech, Uppsala, Sweden .

5.2.7 GEL FILTRATION BUFFERS

Gel Filtration Buffer
50 mM sodium phosphate
150 mM NaCl
-Adjusted to pH 6.4, filter sterilised (1 μm)

5.2.8 McILVAINE'S CITRIC ACID PHOSPHATE BUFFER (Diem *et al.*, 1962)

Buffer A
0.1 M citric acid
Filtered (0.45 μm)

Buffer B
0.2 M Na_2HPO_4
Filtered (0.45 μm)

Citric Acid Buffer pH 3.4
71.5 ml buffer A, 28.5 ml buffer B

Citric Acid Buffer pH 4.4
55.9 ml buffer A, 44.1 ml buffer B

Citric Acid Buffer pH 5.4
44.25 ml buffer A, 55.75 ml buffer B

Citric Acid Buffer pH 6.4
30.75 ml buffer A, 69.25 ml buffer B

Citric Acid Buffer pH 7.4
9.15 ml buffer A, 90.85 ml buffer B

5.3 METHODS

5.3.1 FERMENTATION OF IGF-I AND IGF-II

Recombinant human IGF was expressed and purified from *E. coli* cells as previously described (King *et al* 1992, Francis *et al.,* 1993). Both IGF-I and IGF-II were produced intracellularly in *E. coli* as fusions with porcine growth hormone amino acid residues 1-11 (pGH(1-11), Francis *et al.,* 1993). The pGH(1-11)VN-IGF-I vector was used for the expression of IGF-I constructs and encodes a hydroxylamine cleavage site. In this study, two vectors with differing linker peptides were used for the expression of IGF-II ligands. The pGF(1-11)VNFAHY-IGF-II expression vector encoded for a H64A subtilisin cleavage site, while an alternate form of the expression vector, pGF(1-11)VNPAPH-IGF-II (Lien *et al.*, 2001), required cleavage of the fusion protein product with an α-lytic protease. Fermentations of the JM101 transformants were performed in a bioreactor (Applikon Bioreactor, Schiedam, Holland) as described by King and co-workers (1992). Fermentations of ^{15}N IGF-I, $^{15}N/^{2}H$ IGF-I and $^{15}N/^{2}H$ IGF-II were performed by Mrs C. Senn (Bresatec Ltd., Thebarton, South Australia). Briefly, *E. coli* strain JM101 was transformed with each of the IGF expression vectors and maintained in the presence of 100 μg/ml ampicillin. A single transformant was then used to inoculate 20 ml of minimal fermentation media containing ampicillin and incubated overnight at 37 °C with shaking. The overnight culture was subcultured into fresh minimal media (250 μl into 125 ml) and grown overnight for inoculation of the fermenter (100 ml). The fermenter culture was maintained in minimal media (pH 7.0) and grown at 37 °C, 55 % pO_2 until the optical density (A_{600}) was 5-7. The culture was induced with IPTG (250 μM), supplemented with an additional 1.6 g/L $^{15}NH_4Cl$ and grown for a further six hours before storage at 4 °C. Growth was controlled at 37 °C and pH 7.0 by automatic injection of either

concentrated ammonia or NaOH. Inoculums contained $^{15}NH_4Cl$ as the sole nitrogen source (King *et al.,* 1992) and 50 % $^{2}H_2O$ for deuterated proteins.

Fermentation of $^{13}C/^{15}N/^{2}H$ IGF-I was performed by Francine Carrick and Ms Kerrie McNeil (Department of Molecular BioSciences, Adelaide University). The fermentation was performed in four 2 L conical flasks, each containing 500 ml minimal media with 1 % ^{13}C-glucose, $^{15}NH_4Cl$ and $^{2}H_2O$ (as described in Section 5.2.4). Each flask was inoculated with 5 ml of an overnight culture of JM101 cells transformed with pGH(1-11)-VN-IGF-I, and grown with vigorous shaking to an A_{600} of approximately 1 prior to induction with IPTG (250 μM). The media was also supplemented with an additional 1.6 g $^{15}NH_4Cl$/L upon induction and the cultures grown for a further 5 hours at 37 °C. Cells were then pelleted at 7000 x g and stored at -20 °C.

Homogenisation and inclusion body (IB) isolation were performed generally as described by King *et al.,* (1992). For fermentations performed at BresaGen, cells were disrupted by 4 passes through a homogeniser at 9000 psi and IBs pelleted by centrifugation at 9000 x g for 10 minutes at 4 °C. In contrast, the $^{13}C/^{15}N/^{2}H$ IGF-I culture pellets were resuspended in H_2O (50 ml) and the cells homogenised by a single pass through the French Press (1000 psi). Collected IBs were washed twice in homogenisation buffer and centrifuged at 6000 x g for 10 minutes then 10000 x g for 10 minutes at 4 °C. The wet weight of the IBs was determined. A sample of each of the IBs was reduced in desalt buffer containing 40 mM DTT and electrophoresed on a 12.5 % tricine gel and stained with Coomassie Blue-R250. Isolated IBs were stored at -80°C.

5.3.2 PURIFICATION OF IGF-I AND IGF-II LIGANDS

The purification procedure used for generating IGF-I and IGF-II was based on the methods described by King *et al.*, 1992; Francis *et al.*, 1992; and Upton *et al.*, 1992; and were

performed together with Ms Kerrie McNeil and Dr Briony Forbes (Department of Molecular BioSciences, Adelaide University, South Australia, Australia).

5.3.2.1 Purification of Labelled IGF-I

IBs were solubilized in desalt buffer (30 ml) with 20 mM DTT for 20 minutes at room temperature in a final concentration of 10 ml/g IBs. Refolding of Long IGF-I was performed in a final concentration of 2 M urea, 0.1 M Tris, 10 mM glycine, 5 mM EDTA, pH 9.1, by diluting the protein sample in 1 x refold buffer and water. The final protein concentration was 0.125 mg/ml. Oxidising βME was added to the sample of refold stirring slowly for 90 minutes at room temperature. The reaction was monitored by rpHPLC on a C4 analytical column (Brownlee Aquapore BU300, 7 mm particle size, 300-Å pore size, 2.1 x 100 mm) on a 20-50 % acetonitrile gradient over 30 minutes in the presence of 0.1 % TFA at a flow rate of 0.5 ml/minute. Protein was detected by absorbance at 215 nm. The reaction was stopped by acidification with HCl to pH 2.5. The refolded protein was then purified by fast flow S (FFS) cation-exchange chromatography (Pharmacia-LKB Pty Ltd, North Ryde, NSW, Australia: bed volume 50 ml). The column had been sanitised with one column volume NaOH (0.5 M) and H_2O prior to equilibrating in 0.5 M acetic acid. The refold solution was filtered (1 μm) and loaded onto the column at a flow rate of 10 ml/minute, then washed with FFS buffer A until baseline was obtained. IGF-I was eluted on a 0-1 M NaCl gradient using FFS buffers A and B (Section 5.2.5) over 20 minutes at a flow rate of 5 ml/minute. The IGF-I peak was collected in a single fraction. In this and subsequent steps, IGF-I fusion peptides were followed by analytical rpHPLC as described above.

The IGF moiety was released from the fusion partner by hydroxylamine cleavage. The [Met1-pGH(1-11)-Val-Asn-IGF-I] fusion protein was cleaved by diluting protein to 0.2 mg/ml in 2 M urea, 1 M hydroxylamine, 0.1 M Tris pH 8.65 (LiOH). The cleavage reaction was sparged with N_2 and incubated at 37 °C with stirring for 17 hours (or until cleavage was

complete as determined by rpHPLC) and terminated by acidification to pH 2.5 with HCl while stirring on ice. The cleaved IGF-I was separated from the growth hormone leader protein and uncleaved proteins by rpHPLC (C4 Prep Pak column: 24-50 % acetonitrile over 210 minutes in the presence of 0.1 % TFA at 5 ml/minute). Fast Flow Q (FFQ) cation exchange chromatography was then performed to remove contaminating growth hormone leader protein from IGF-I. The column was sanitised and equilibrated in FFQ buffer A prior to use. The rpHPLC protein sample was diluted in FFQ buffer A adjusted to pH 9.0 and loaded directly on to the FFQ column at a flow rate of 5 ml/minute. IGF-I was then eluted on a 30 minute gradient of 0-100 % FFQ buffer B (Section 5.2.5) at a flow rate of 5 ml/minute. The final desalt was performed by rpHPLC (Delta Pak PrepLC column). The FFQ protein sample was acidified to approximately pH 3 and loaded onto the rpHPLC column at a flow rate of 5 ml/minute using a Waters pump. The protein was eluted in 20-50 % acetonitrile over 124 minutes in the presence of 0.1 % TFA at a flow rate of 5 ml/minute. Fractions containing biologically active IGF were pooled, lyophilised and quantified. The quantity and purity of IGF-I produced were assessed by rpHPLC monitored by absorbance at 215 nm. IGF-I obtained from Gro*Pep* Ltd. was used as a standard. N-terminal amino acid analysis of the first five residues confirmed the identity and purity (>87%) of the recombinant proteins.

5.3.2.2 Purification of Labelled IGF-II

The IBs were solubilized as described previously for IGF-I (Section 5.3.2.1) and filtered through a 1 μm Gradipore filter. As IGF-II preparations were readily susceptible to degradation by proteolysis, they were desalted on an XK-50 Sephadex G-25 column (2 L; GroPep, Thebarton, South Australia, Australia) to remove proteases from the sample. The column had been sanitised with 500 ml of 0.5 M NaOH followed by three washes with water prior to overnight equilibration with 2 L of desalt buffer at 2 ml/minute. The dissolved IB sample was then loaded onto the XK-50 column at 2 ml/minute and desalted overnight at 2

ml/minute in desalt buffer (Section 5.2.5). Fusion protein was detected at 280 nm and fractions containing Long-IGF-II were identified by rpHPLC. The fractions corresponding to Long-IGF-II were then diluted 1:1 with 1 x refold buffer to obtain the refold conditions of 2 M Urea/ 0. 1 M Tris/10 mM glycine/5 mM EDTA pH 9.1. The final protein concentration was 0.15 mg/ml. The refold reaction was performed as previously described for IGF-I.

Following refolding, FFS chromatography was performed as described for IGF-I (Section 5.3.2.1). Fractions corresponding to Long-IGF-II were pooled and cleaved with H64A subtilisin (approximately 1 mg/ 30 mg Long-IGF-II) in 3 M urea, 20 mM Tris, 5 mM $CaCl_2$, 200 mM NaCl, pH 8.5 and 37 °C at a final protein concentration of 0.2 mg/ml for approximately 24 hours (Francis *et al.,* 1993). Alternatively, α-lytic protease was used to remove the fusion partner from Long-IGF-II containing the PAPH- linker (Lien *et al.*, 2001). This cleavage reaction was performed in 3 M urea, 0.1 M Tris pH 8 at 37 °C for 180 minutes at an enzyme:protein ratio of 1:500. The cleavage reactions were monitored by rpHPLC and stopped by acidification with HCl to pH 2.5. IGF-II was separated from the growth hormone leader protein and uncleaved protein by rpHPLC (C4 Prep Pak column) on a 20-50 % acetonitrile gradient over 124 minutes in the presence of 0.1 % TFA at a flow rate of 5 ml/minute. Unfortunately, the PAPH- leader protein coeluted with the native IGF-II ligand by rpHPLC resulting in higher leader peptide contamination compared to those achieved from preparations of pGH(1-11)-VNFAHY-IGF-II. The fractions corresponding to correctly folded IGF-II were pooled, lyophilised and quantified as described for IGF-I. N-terminal sequencing determined the purity of the sample.

5.3.3 GLUCOSE TRIALS FOR ^{13}C IGF-I FERMENTATIONS

Minimal glucose requirements for the expression of IGF-I were determined prior to labelling with ^{13}C-glucose. JM101 cells transformed with pGH(1-11)VN-IGF-I were grown in minimal media (Section 5.2.4) with varying concentration of glucose (2.5 %, 2.0 %, 1 %, 0.5

%, 0.25 % and 0.15 % (w/v)) for 7 ½ hours at 37 °C with shaking. The optical density was recorded every hour until the A_{600} was approximately 0.6 and every half hour thereafter.

5.3.4 LARGE SCALE EXPRESSION OF TRX^{1-279}IGFBP-2HIS, TRX^{1-132}IGFBP-2 AND $TRX^{136-279}$IGFBP-2HIS

The large-scale expression of Trx^{1-279}IGFBP-2HIS, Trx^{1-132}IGFBP-2 and $Trx^{136-279}$IGFBP-2HIS was essentially as described in Section 3.3.2. Briefly, the pET constructs were transformed into *E. coli* BL21 cells immediately prior to large-scale expression. Two litre cultures were grown in 2YT broth containing carbenicillin (100 μg/ml) at 37 °C with shaking and induced with 1 mM IPTG at A_{600} of approximately 0.6. Protein was expressed for a minimum of 4 hours prior to pelleting the cells (5000 x g, 5 minutes, 4 °C). The cells were then resuspended to one tenth of the original volume in binding buffer (Section 3.3.2), lysed (lysozyme; 100 μg/ml) and sonicated 3 x 30 seconds on ice. The cells were pelleted and the soluble fraction was filtered (1 μm). For large-scale preparations of *E. coli* proteins, the soluble protein fraction in binding buffer was incubated with $NiSO_4$-charged Ni-IDA resin overnight with rocking at 4 °C (Section 3.3.5). The resin was then washed with binding buffer and wash buffer to remove non-specific interacting proteins, and the specifically bound protein was eluted with elute buffer. The eluate was then desalted by rpHPLC on a C4 Prep Pak column. Fractions across the protein peak were analysed on a C4 analytical column prior to pooling Trx^{1-279}IGFBP-2HIS fractions and lyophilization. The thioredoxin-fused IGFBPs were generally left intact for structure determination studies, however cleavage with enterokinase and subsequent separation by rpHPLC was sometimes performed (as described in Section 3.3.6). All protein samples were lyophilised and stored at 4 °C.

5.3.5 BIACORE ANALYSIS

Generation of biosensor chips and BIAcore analyses were generally as described in Section 4.3.1 and in Carrick *et al.*, (2001). Two BIAcore experiments were performed. The first experiment simply involved comparing the binding kinetics of bIGFBP-2 and Trx^{1-279}IGFBP-2HIS across IGF biosensor surfaces. Briefly, various concentrations of bIGFBP-2 or Trx^{1-279}IGFBP-2HIS (200, 100, 50, 25 and 12.5 nM) were injected across IGF-I and IGF-II biosensor surfaces for 5 minutes at 40 µl/minute in HBS running buffer. Kinetic analysis was performed using the 1:1 Langmuir binding model as described in Section 4.3.3. The second BIAcore experiment investigated the effect of pH on the binding affinity of bIGFBP-2 for IGF immobilised to a biosensor surface. In this experiment, bIGFBP-2 (100 nM) was injected across biosensor surfaces for 5 minutes at 40 µl/minute. Biosensorgrams were recorded in citric acid buffer at pH 3.4, 4.4, 5.4, 6.4 and 7.4. The dissociation phase, initiated by passage of citric acid buffer alone, was carried out over a period of 10 minutes. The biosensor surfaces were regenerated by a 60 second injection of 0.1 M HCl. Samples were injected in duplicate in random order in at least two separate experiments.

5.3.6 GEL FILTRATION

Gel filtration experiments were performed on a Superdex 200 column and SMART® System from Amrad Pharmacia Biotech (Section 5.2.6). Bovine IGFBP-2 and Trx^{1-279}IGFBP-2HIS were loaded onto the column at a concentration of 7.5 mg/ml in gel filtration buffer at a flow rate of 40 µl/minute. The elution profile was compared to the high molecular weight standards mix of thyroglobulin (669 kDa), ferritin (440 kDa), human IgG (160 kDa), transferrin (81 kDa), ovalbumin (43 kDa), myoglobin (17.6 kDa) and vitamin B12 (1.4 kDa). Absorbance was detected at 215 nm.

5.4 RESULTS AND DISCUSSION

5.4.1 IGF FERMENTATIONS AND PURIFICATION

IGF-I and IGF-II have been routinely expressed and purified in our laboratory and by Gro*Pep* Ltd., (Thebarton, SA, Australia), generally as described previously by King *et al.*, 1992; Francis *et al.*, 1992; and Upton *et al.*, 1992. The IGFs were expressed in *E. coli* JM101 cells as N-terminal fusion peptides with an [Met^1]-pGH(1-11) extension via a Val-Asn dipeptide linker for IGF-I and a Val-Asn-Phe-Ala-His-Tyr linker for IGF-II. A hydroxylamine cleavage site exists between the Asn and Gly^1 of IGF-I while the fusion peptide is removed from the mature IGF-II ligand by cleavage with subtilisin between Tyr and Ala^1 of IGF-II.

Optimal growth in the fermentations was achieved as described in Section 5.3.1. Dr Gary Shooter previously determined the limiting $^{15}NH_4Cl$ concentrations (PhD Thesis, 2001) and established that addition of 1.6 g/L $^{15}NH_4Cl$ at induction benefited cell growth and protein expression. Similarly, the maximum deuterium content permissive in minimal media without compromising high cell growth was investigated in this study. JM101 cells transformed with pGH(1-11)VN-IGF-I or pGH(1-11)VNFAHY-IGF-II were grown in various concentrations of deuterium oxide (0 %, 50 %, 70 %, 80 % and 90%) for 4 hours after an A_{600} of 0.6 was achieved. Growth in 50 % deuterium oxide was less inhibited than growth in 70 %, 80 % or 90% ^2H_2O (Table 5.1). Therefore, fermentations requiring deuterium labelling of proteins were performed in 50 % ^2H_2O.

The fusion proteins were expressed as IBs with fermentation yields of 2.6 g and 3.5 g wet weight per 2 L for ^{15}N IGF-I and $^{15}N/^2H$ IGF-I, respectively, and 12 g wet weight per 2 litres for $^{15}N/^2H$ IGF-II. Approximately one tenth of the wet weight was fusion protein. Tricine gels showed the IBs contained protein at the correct molecular weight (Figure 5.2). Following refolding and purification, all IGF peptides gave rise to a single peak by rpHPLC analysis with retention times similar to native IGF-I or IGF-II (Figure 5.3). In the present study, the fermentations and purification of ^{15}N IGF-I, $^{15}N/^2H$ IGF-I and $^{15}N/^2H$ IGF-II successfully

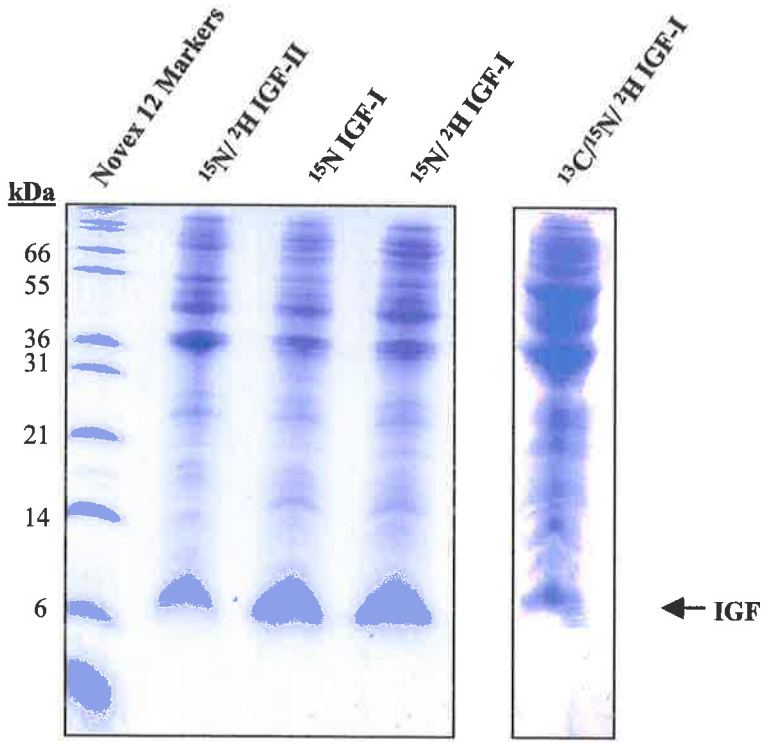

Figure 5.2 Coomassie stained tricine gel of labelled IGF ferments
Inclusion bodies from the large-scale ferment of IGF-I and IGF-II were weighed and resuspended in desalt buffer with 40 mM DTT to a final concentration of 10 µl/mg (as described in Section 5.3.1). The samples were then incubated at room temperature for 30 minutes to allow reduction of the disulfide bonds. A sample (10 µl) was then electrophoresed on a 12.5 % tricine gel and stained with Coomassie blue.

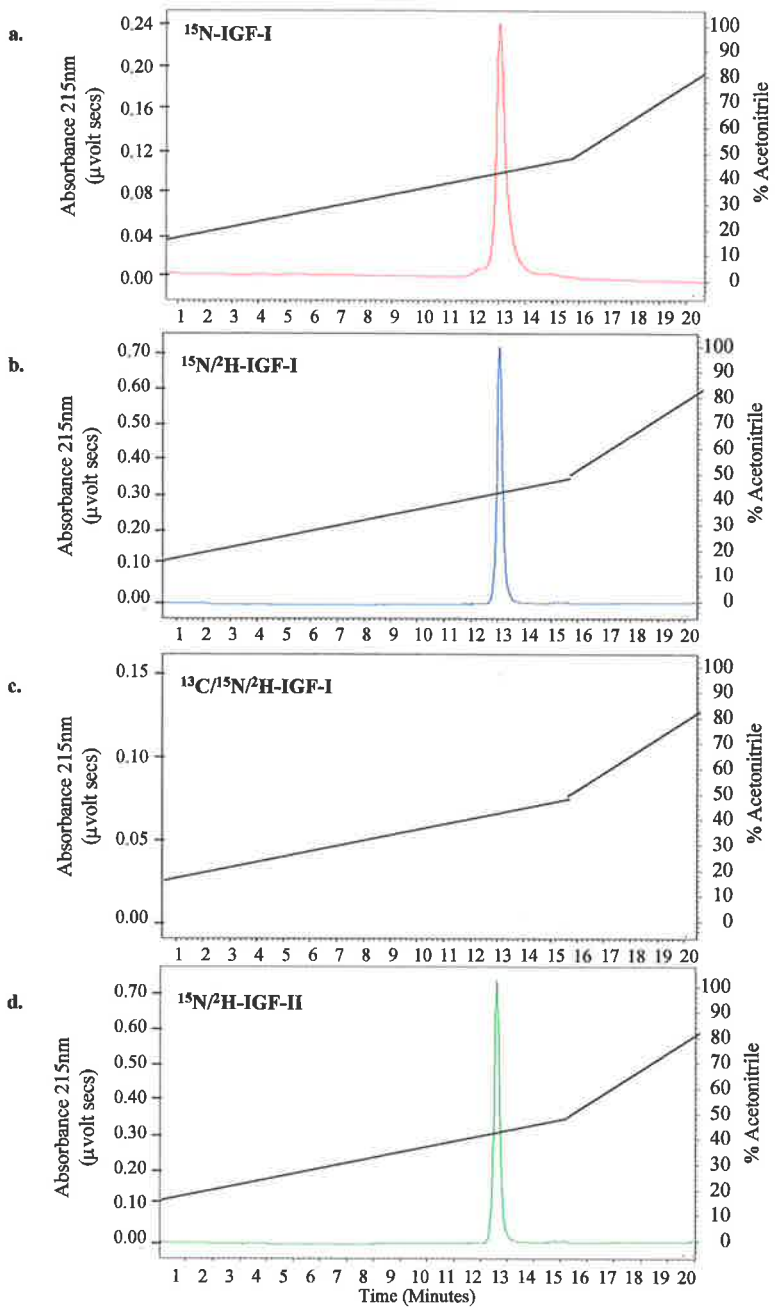

Figure 5.3 HPLC chromatograms of the purified labelled IGF-I and IGF-II ligands
The purified labeled IGF ligands were analysed by rpHPLC on a 20-50 % acetronitrile gradient over 15 minutes as described in Section 5.3.2. Chromatograms are presented for (a) ^{15}N-IGF-I, (b) ^{15}N/^{2}H-IGF-I, (c) ^{13}C/^{15}N/^{2}H-IGF-I and (d) ^{15}N/^{2}H IGF-II.

TABLE 5.1 OPTICAL DENSITY OF CELL CULTURES GROWN IN DEUTERIUM OXIDE

pGH(1-11)VN-IGF-I	70 % ^2H_2O	80 % ^2H_2O	90 % ^2H_2O	99 % ^2H_2O
Induction	0.87	0.83	0.72	0.018
Post Induction (4 hours)	1.079	1.1	0.77	-

pGH(1-11)VNFAHY-IGF-II	0 % ^2H_2O	50 % ^2H_2O	70 % ^2H_2O
Induction	0.574	0.661	0.674
Post Induction (4 hours)	0.815	0.806	0.539

The optical density at 600 nm (A_{600}) of transformed JM101 cell cultures grown in 0 %, 50 %, 70% and 90 % ^2H_2O were recorded at induction and at 4 hours post induction.

yielded between 8.2 mg and 12 mg of protein as summarised in Table 5.2. N-terminal amino acid analysis of the first five residues confirmed the N-terminal sequence for IGF-I (G-P-E-T-L-) and IGF-II (A-Y-R-P-S-) and determined the purity (>87 %) of each of the recombinant proteins: ^{15}N IGF-I (87 % + 7 % leader), $^{15}N/^2H$ IGF-I (93 %), and $^{15}N/^2H$ IGF-II (90 %). These results are summarised in Table 5.2. Leader contamination was more significant for IGF-I preparations, which was not unexpected as IGF-I and the leader peptide elute similarly by rpHPLC. In addition, cleavage of Long-IGF-II with H64A subtilisin was more successful than cleavage with α-lytic protease combined with the present purification protocol. Electrospray mass spectrometry was not conducted in the present study due to the random incorporation of deuterium into the IGF preparations.

5.4.2 FERMENTATION OF $^{13}C/^{15}N/^2H$ IGF-I

Heteronuclear 2D experiments require isotopically labelled proteins to detect a correlation between two different nuclei. As discussed in Chapter 7, the chemical shift assignments of IGF-I, particularly in complex with Trx^{1-279}IGFBP-2HIS, were ambiguous based on those reported in the literature, hence experiments requiring ligand labelled with ^{15}N, ^{13}C and deuterium were performed. Fermentation of $^{13}C/^{15}N/^2H$ IGF-I and subsequent homogenisation of the IBs was as described in Section 5.3.1. ^{13}C-glucose is an expensive

isotope and using 2.5 % ^{13}C-glucose (25 g/L), ordinarily present in minimal media, was not economically feasible. Therefore, the minimal glucose concentration required for normal growth was determined prior to the ferment (as described in Section 5.3.3). The expression of IGF-I in *E. coli* JM101 cells was assessed with various concentrations of glucose (2.5 %, 2.0 %, 1.0 %, 0.5 %, 0.25 % and 0.15 %) (Figure 5.4). Although 0.15 % glucose has been shown to be sufficient for the expression of *E. coli* biotin carboxyl carrier protein from BL21 cells (Roberts *et al.*, 1999), cultures containing less than 0.5 % glucose did not reach the same A_{600} as cultures grown in media containing 2.5 % glucose in this study. Interestingly, 0.5 % glucose maintained growth and IGF production as well as the standard concentration of 2.5 % glucose (Figure 5.4). All ^{13}C-labelled fermentations of *E. coli* JM101 cells were therefore performed with 0.5 % glucose. The fermentation yield for ^{13}C/^{15}N/^{2}H IGF-I was 0.57 g/2 L wet weight. Refolding, cleavage and purification of ^{13}C/^{15}N/^{2}H IGF-I were as described in Section 5.3.2. yielding 1.62 mg of protein as summarised in Table 5.2. N-terminal sequence analysis gave the expected N-terminal sequence for IGF-I (G-P-E-T-L-).

TABLE 5.2 SUMMARY OF THE IGF-I AND IGF-II FERMENTATIONS AND PURIFICATION

	A_{600}	Inclusion Body weight	Sequence	Purity	Quantity (rpHPLC)
^{15}N IGF-I	7.7-9.5	2.6 g	G-P-E-T-L	87 %	8.3 mg
^{15}N/^{2}H IGF-I	6.3-8.4	3.5 g	G-P-E-T-L	93 %	8.2 mg
^{13}C/^{15}N/^{2}H IGF-I	2.4	0.57 g	G-P-E-T-L	90 %	1.62 mg
^{15}N IGF-II	12.2-16.1	3 g	A-Y-R-P-S	>96 %	11.5 mg
^{15}N/^{2}H IGF-II	12.6-16.3	12 g	A-Y-R-P-S	90 %	18.4 mg

Fermentations (2 L) were performed as described in Section 5.3.1. The final A_{600} of the ferments and the inclusion body weight were recorded. IGF-I and IGF-II peptides were purified as described in Section 5.3.2 and the purity of the final preparation analysed by N-terminal sequencing. The final quantity of protein was determined by rpHPLC analysis.

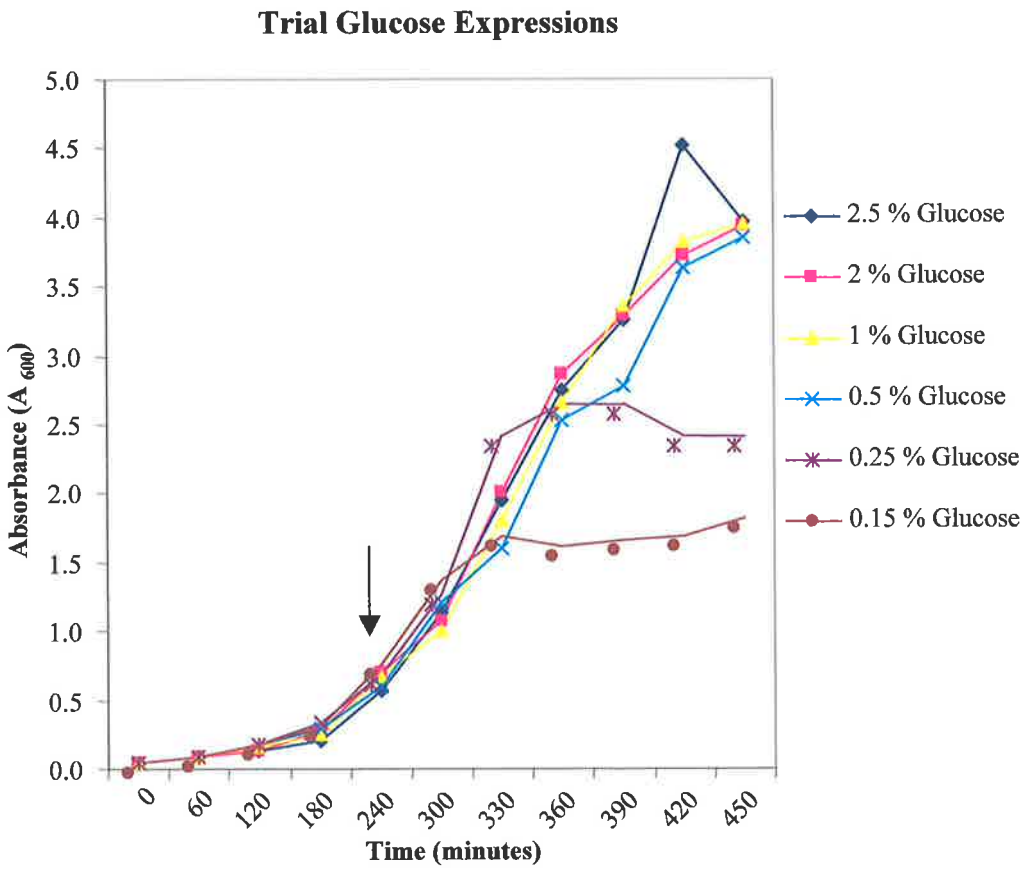

Figure 5.4 IGF-I expressions with various glucose concentrations
Minimal glucose requirements for the expression of IGF-I were determined prior to labelling with ^{13}C-glucose. *E. coli* JM101 cells transformed with pGH(1-11)VN-IGF-I were grown in minimal media for 7 ½ hours at 37 °C with shaking with varying concentration of glucose (2.5 %, 2.0 %, 1 %, 0.5 %, 0.25 % and 0.15 % (w/v)) (as described in Section 5.3.3). The optical density was recorded every hour until the A_{600} was approximately 0.6 (indicated by the arrow) and every half hour thereafter.

5.4.3 LARGE-SCALE EXPRESSION OF TRX$^{1-279}$IGFBP-2HIS, TRX$^{1-132}$IGFBP-2 AND TRX$^{136-279}$IGFBP-2HIS

The *E. coli* expression of Trx$^{1-279}$IGFBP-2HIS, Trx$^{1-132}$IGFBP-2 and Trx$^{136-279}$IGFBP-2HIS was performed essentially as described in Section 3.3.2. Generally a 2 L expression of *E. coli* cells transformed with pET$^{1-279}$IGFBP-2HIS expressed 10-20 mg/L of fusion protein while fermentation of Trx$^{1-132}$IGFBP-2 or Trx$^{136-279}$IGFBP-2HIS produced approximately 20-30 mg/L of protein. The higher levels of protein obtained for Trx$^{1-132}$IGFBP-2 and Trx$^{136-279}$IGFBP-2HIS may be a consequence of the method of purification. The soluble Trx$^{1-132}$IGFBP-2 and Trx$^{136-279}$IGFBP-2HIS fractions were incubated with the charged Ni-IDA resin overnight at 4°C prior to washing and eluting. In contrast, Trx$^{1-279}$IGFBP-2HIS was purified either by IGF-affinity chromatography or by Ni-affinity chromatography with gravity flow loading.

5.4.4 COMPARISON OF THE IGF BINDING ACTIVITY OF TRX$^{1-279}$IGFBP-2HIS AND bIGFBP-2 BY BIACORE ANALYSIS

This chapter has described the large-scale production of IGF and IGFBP for structural studies. As discussed in Section 3.4.2.1 and Section 5.4.3, removal of the thioredoxin fusion protein is the limiting step in the purification of *E. coli* expressed $^{1-279}$IGFBP-2HIS. Indeed, the substantial loss of protein during cleavage is not ideal particularly when the protein is labelled with expensive isotopes for NMR analysis. Interestingly, Trx$^{1-279}$IGFBP-2HIS and bIGFBP-2 interact similarly with IGF-I and IGF-II immobilised to biosensor surfaces (Figure 5.5) and the binding kinetics derived using a 1:1 Langmuir binding model were essentially the same (Table 5.3). These results suggest that Trx$^{1-279}$IGFBP-2HIS can be used in structure determination studies and is particularly suitable for NMR studies of IGF chemical shift perturbations in the free and complexed forms. Trx$^{1-132}$IGFBP-2, Trx$^{1-185}$IGFBP-2 and Trx$^{136-279}$IGFBP-HIS also bind IGF-I and IGF-II biosensor surfaces with affinities comparable to their thioredoxin-free counterparts (Figure 5.6 compared with Figure 4.3).

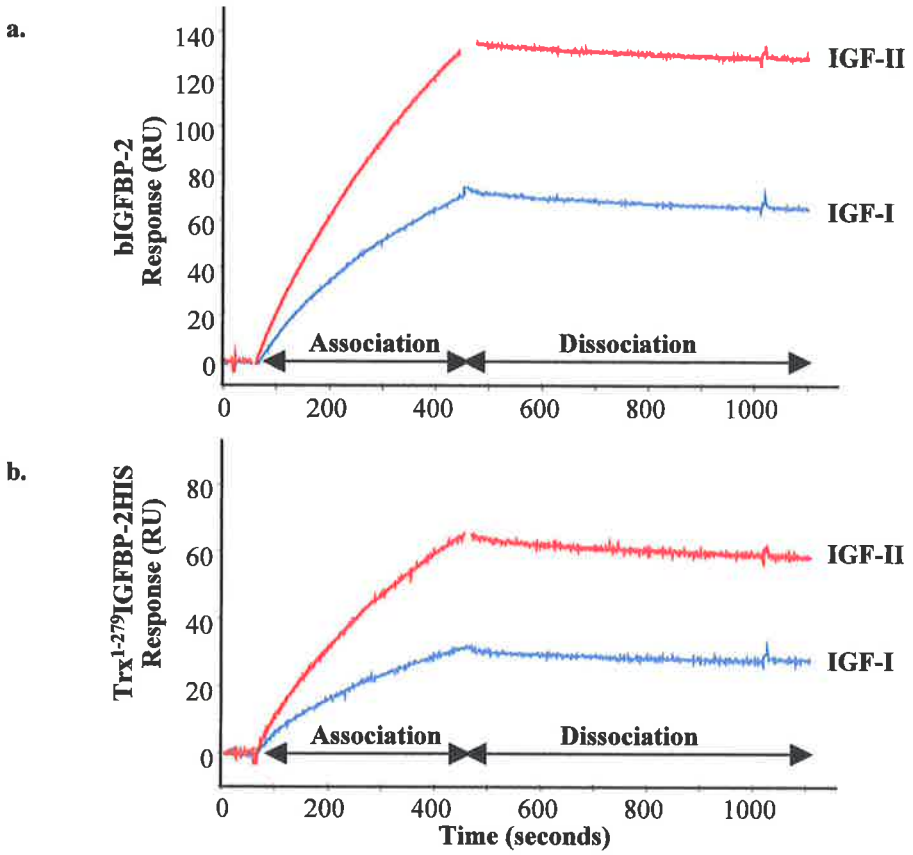

Figure 5.5 BIAcore comparison of bIGFBP-2 and TrxIGFBP-2HIS over IGF biosensor surfaces

Biosensorgrams are presented for the interaction of a) bIGFBP-2 and b) TrxIGFBP-2HIS (100 nM) over IGF-I and IGF-II biosensor surfaces. Biosensor experiments were conducted at a flow rate of 40 µl/minute in HBS running buffer as described in Section 5.3.5.

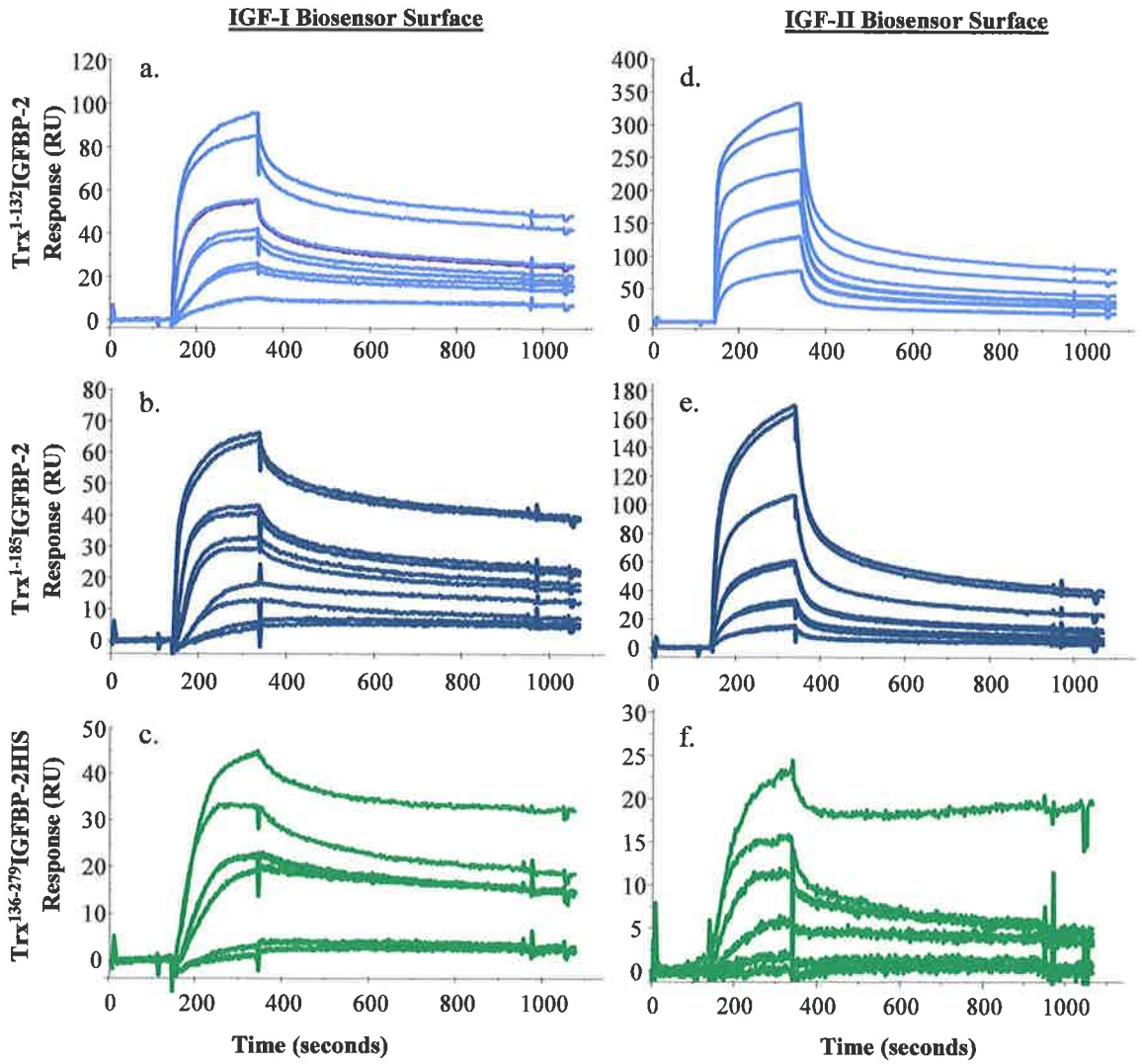

Figure 5.6 BIAcore analysis of Trx^{1-132}IGFBP-2, Trx^{1-185}IGFBP-2 and $Trx^{136-279}$IGFBP-2HIS over IGF biosensor surfaces

Biosensorgrams are presented for the interaction of Trx^{1-132}IGFBP-2 (a, d), Trx^{1-185}IGFBP-2 (b, e) and $Trx^{136-279}$IGFBP-2HIS (c, f) with IGF-I and IGF-II biosensor surfaces respectively. A concentration range (200, 100, 50, 25 and 12.5 nM) was analysed across IGF-I and IGF-II biosensor surfaces at a flow rate of 40 µl/minute in HBS running buffer.

TABLE 5.3 COMPARISON OF THE KINETICS OF THE INTERACTION BETWEEN bIGFBP-2 AND TRX$^{1-279}$IGFBP-2HIS WITH IGF-I AND IGF-II USING THE 1:1 LANGMUIR BINDING MODEL

IGF-I	k_a ($x10^4$)	relative k_a	k_d ($x10^{-4}$)	relative k_d	K_D ($x10^{-9}$)	relative k_D	χ^2
bIGFBP-2	4.47	1.00	1.29	1.00	2.89	1.00	0.46
Trx$^{1-279}$IGFBP-2HIS	3.27	0.73	1.42	1.10	4.35	1.51	0.40
IGF-II							
bIGFBP-2	2.78	1.00	1.19	1.00	4.27	1.00	0.38
Trx$^{1-279}$IGFBP-2HIS	2.48	0.89	0.64	0.54	2.60	0.61	0.33

The 1:1 Langmuir binding model was used to fit kinetic data shown in Figure 5.5 for the interaction between bIGFBP-2 and Trx$^{1-279}$IGFBP-2HIS across both IGF-I and IGF-II biosensor surfaces. χ^2 values for sensorgram curve fits were equal to or less than 0.46. Association rates (k_a), dissociation rates (k_d), and dissociation constants (K_D=k_d/k_a) are given. Dissociation constants relative to bIGFBP-2 for IGF-I and IGF-II biosensor surfaces are also presented (K_D bIGFBP-2 / Trx$^{1-279}$IGFBP-2HIS). The association and dissociation rates are also given relative to bIGFBP-2 for IGF-I and IGF-II biosensor surfaces.

5.4.5 INVESTIGATION OF THE EFFECT OF PH ON THE IGF·IGFBP INTERACTION BY BIACORE ANALYSIS

NMR spectra are generally recorded at low pH to improve solubility and reduce aggregation. Low pH however disrupts the IGF·IGFBP complex so an optimal pH for recording NMR spectra of the IGF·IGFBP complex needed to be established. BIAcore analysis was performed to provide insight into the effect of pH on the interaction between bIGFBP-2 and IGF ligand. Kinetic analyses were performed with IGF-I and IGF-II immobilised to the CM5 gold chip as described in Section 5.3.5. Bovine IGFBP-2 analyte in citric acid running buffer (pH 3.4, 4.4, 5.4, 6.4 or 7.4) was passed over the IGF biosensor surfaces that had been equilibrated at the same pH. The association and dissociation phases of the interaction were recorded as previously described in Section 5.3.5. The IGF binding interaction with bIGFBP-2 appears very similar at pH 7.4, 6.4 and 5.4 (Figure 5.7). The dissociation of IGFBP-2 from IGF is slightly faster at pH 4.4 and significantly faster at pH 3.4. Although biosensor experiments indicate significant binding at pH 3.4, chemical shift perturbations observed at the low pHs may not be representative of the interaction at physiological pH. Consequently, in this study, NMR

studies investigating the changes in IGF chemical shifts upon binding of IGFBP-2 were conducted at approximately pH 5.

The atypical biosensor curves particularly noticeable across the IGF-I biosensor surface at the lower pHs (Figure 5.7), were not likely to be due to a matrix effect (personal communication Mr Rick Filonzi/Dr Robert Karlsson BIACORE) but most probably attributable either to a) aggregation of the analyte; or b) change in conformation of the bound ligand. Interestingly, Melinda Lucic proposed that possible dimerisation of the IGF analyte was responsible for the less than perfect fits obtained when fitting data globally to the two-state reaction (conformational change) model (PhD Thesis, Adelaide University, 2000). Self-association of IGF has been observed in NMR studies where high concentrations of proteins were used for structure determination (Cooke *et al.*, 1991, Terasawa *et al.*, 1994; Torres *et al.*, 1995) and indeed gel filtration experiments (Section 5.4.6) indicate that aggregation of bIGFBP-2 is significant at millimolar concentrations and pH 7.4. Although high concentrations of IGF were not used in this study, it is possible that the accumulation of IGF at the biosensor surface may produce high local concentrations enabling IGF to dimerise. Insulin itself dimerises under physiological conditions (Jeffery *et al.*, 1976, Helmerhorst and Stokes, 1987).

IGFBPs are believed to undergo a conformational change upon binding of IGF-I and IGF-II. A conformational change in the bound ligand may account for the uncharacteristic biosensor curves observed at low pH. Indeed, amino acid sequences required for glycosaminoglycan binding by IGFBP-2 are exposed upon binding of IGF, which is believed to be due to a conformational change in the IGFBP (Arai *et al.*, 1996b). Similarly, proteolysis of IGFBP-4 by pregnancy-associated plasma protein-A (PAPP-A) is IGF dependent and may be the consequence of a conformational change in IGFBP-4 upon IGF binding (Lawrence *et al.*, 1999).

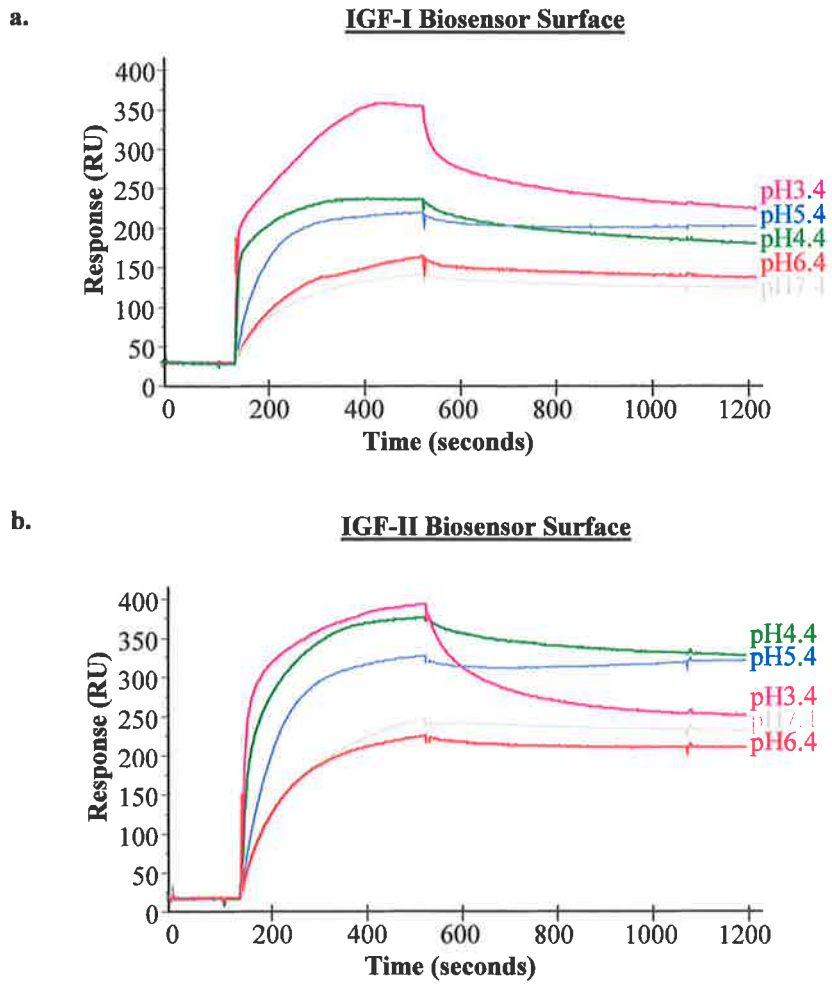

Figure 5.7 BIAcore analysis of the effect of pH on the IGF-IGFBP interaction
Biosensorgrams are presented for the interaction of bIGFBP-2 (100 nM) with a) IGF-I and b) IGF-II biosensor surfaces in citric acid running buffer at pH 3.4, 4.4, 5.4, 6.4 and 7.4. Biosensorgrams were recorded at a flow rate of 40 µl/minute as described in Section 5.3.5.

5.4.6 GEL FILTRATION EXPERIMENTS

Aggregation of proteins poses a particular problem for structure determination studies. The aggregation of a globular protein hinders the formation of crystals and adversely influences diffraction of the X-rays. Similarly, aggregation in NMR samples contributes to line broadening and subsequent reduction in the quality of the NMR spectrum. Therefore, the quaternary states of bIGFBP-2 and Trx^{1-279}IGFBP-2HIS were analysed at millimolar concentrations by gel filtration (Section 5.3.6 and 5.4.6). Bovine IGFBP-2 aggregates at high protein concentrations and neutral pH (Figure 5.8). Indeed, dimers, tetramers and octamers of bIGFBP-2 were identified by gel filtration. Aggregation of bIGFBP-2 however is also evident at lower protein concentrations as dimers are routinely observed on nitrocellulose filters after SDS-PAGE analysis under denaturing conditions (Figure 3.1). In contrast, Trx^{1-279}IGFBP-2HIS remained monomeric under identical gel filtration conditions. Thus it would appear that the thioredoxin fusion contributes both to the solubility of proteins during the expression in *E. coli* cells, and limits aggregation of the purified protein. Trx^{1-279}IGFBP-2HIS therefore is ideal for structure determination studies. Furthermore, inclusion of the thioredoxin-tag may contribute to the analysis by providing a reference point for orientation of the molecule.

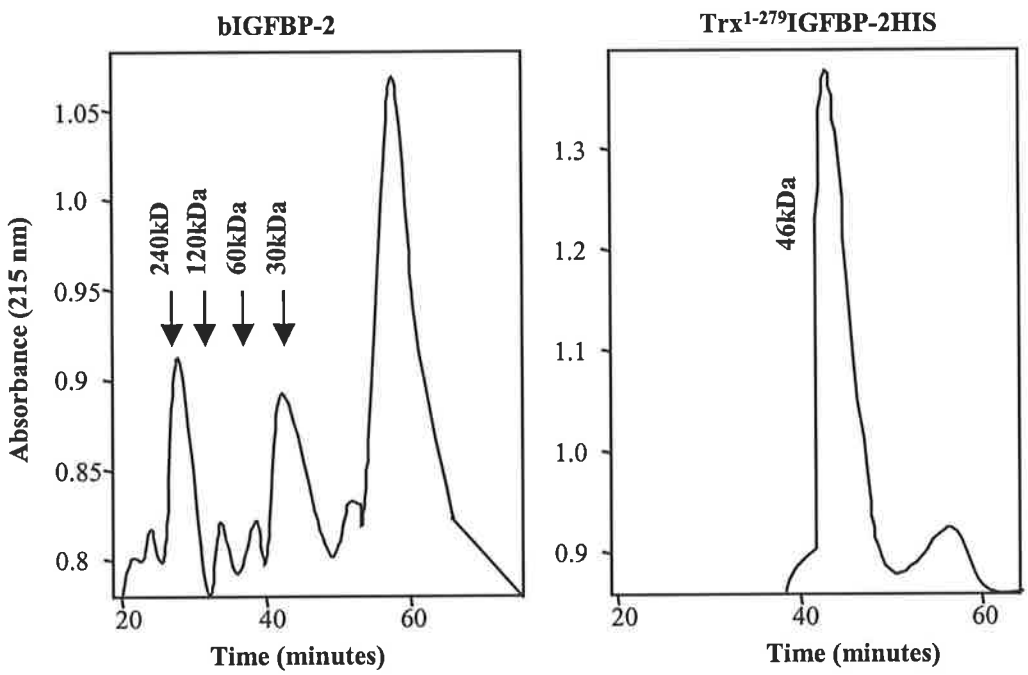

Figure 5.8 Gel filtration of bIGFBP-2 and Trx$^{1-279}$IGFBP-2HIS
Gel filtration experiments were performed using the SMART system as described in Section 5.3.6. Bovine IGFBP-2 and TrxIGFBP-2HIS were loaded onto a Superdex 200 column at a concentration of 7.5 mg/ml in phosphate buffer at a flow rate of 40 µl/minute. The elution profile was compared to the high molecular weight standards mix of thyroglobulin (669 kDa), ferritin (440 kDa), human IgG (160 kDa), transferrin (81 kDa), ovalbumin (43 kDa), myoglobin (17.6 kDa) and vitamin B12 (1.4 kDa). Absorbance was detected at 215 nm.

5.5 SUMMARY

The fermentation and purification of ^{15}N IGF-I, $^{15}N/^{2}H$ IGF-I, $^{13}C/^{15}N/^{2}H$ IGF-I, ^{15}N IGF-I, ^{15}N IGF-II and $^{15}N/^{2}H$ IGF-II has yielded various amounts of protein as summarised in Table 5.2. Although growth of *E. coli* in media containing 70 % $^{2}H_2O$ was reduced, growth in 50 % $^{2}H_2O$ did not affect cell growth. The minimal glucose required for JM101 cells expressing either IGF-I or IGF-II was 0.5 %, however protein yields were considerably lower than fermentations performed in media containing either $^{15}NHCl_4$ or $^{2}H_2O$. The labelled IGF ligands were used in NMR studies to investigate the conformational changes induced upon binding of bIGFBP-2 and the amino- or carboxyl-terminal fragments as described in Chapter 7.

Large-scale expression of Trx^{1-279}IGFBP-2HIS, Trx^{1-132}IGFBP-2 and $Trx^{136-279}$IGFBP-2HIS yielded at least 10 mg/L of purified protein. Indeed, greater quantities of protein were achieved upon optimisation of the purification strategy. Batch binding the soluble, sonicated fraction overnight with $NiSO_4$-charged resin was the most successful purification protocol and returned at least 20 mg/L of protein. As described previously however, enterokinase cleavage of the fusion protein returned only approximately 20 % (w/w) of the starting material. Interestingly, Trx^{1-279}IGFBP-2HIS was shown to possess similar IGF binding properties to wildtype IGFBP-2, and indeed, the thioredoxin fused amino- and carboxyl-terminal IGFBP-2 fragments (Trx^{1-132}IGFBP-2, Trx^{1-185}IGFBP-2 and $Trx^{136-279}$IGFBP-2HIS) also bound IGF-I and IGF-II similarly to their Trx-free counterparts. Hence the fusion proteins were used in structure determination studies without prior cleavage of the thioredoxin-tag. Based on the results presented in this chapter there may be many advantages for using Trx^{1-279}IGFBP-2HIS as opposed to native bIGFBP-2. Indeed, incorporation of the thioredoxin fusion proved advantageous for the solubility of the protein (as discussed in Section 5.4.6), which is favourable for crystal growth.

Sufficient protein was expressed for structure determination studies of bIGFBP-2 by X-ray crystallography, NMR and electron microscopy. These studies will be discussed in the

following chapter. In addition, isotope-labelling of IGF-I and IGF-II permitted investigation of the specific IGF residues involved in binding full-length IGFBP-2 or amino- and carboxyl-terminal fragments of IGFBP-2. The heteronuclear NMR spectroscopy studies of IGF-I and IGF-II will be discussed in Chapter 7.

CHAPTER 6

IGFBP-2 STRUCTURE DETERMINATION X-RAY CRYSTALLOGRAPHY, NMR AND ATOMIC FORCE MICROSCOPY

6.1 INTRODUCTION

It is often desirable to modulate the function or activity of a molecule in a biological system and indeed, the ability to moderate the interaction between two molecules has provided the basis for generation of many therapeutic agents. Random mutagenesis or systematic screening of a molecule is often an impracticable approach to determine the specific nucleic acids or amino acid residues involved in an interaction. A basic knowledge of the structure of a molecule or complex however significantly contributes toward defining binding epitopes. X-ray crystallography and NMR are both powerful structure determination techniques that have resolved many nucleic acid and protein structures. These techniques provide different and complementary information regarding protein structure. Electron microscopy is another approach often used to determine the quaternary structure of large proteins and protein aggregates, usually with low resolution.

Typically, NMR has been used to complement X-ray crystallography studies. X-ray crystallography requires well-ordered crystals that diffract X-rays strongly but these are often difficult and very slow to grow. In contrast, NMR does not require crystals and structures are determined in solution. Indeed, the conditions used to determine tertiary structures by NMR can be varied to allow for comparison of native or denatured states and for investigation of intermolecular interactions with other solute molecules. NMR however has molecular weight limitations and generally structures can only be determined for proteins of less than 30 kDa. Furthermore, line broadening, resulting from aggregation or an increase in viscosity (which is not uncommon in concentrated samples), inhibits structure determination. Size limitations of NMR technology however can be extended by replacement of labile protons with deuterium to reduce the number of resonance lines observed and by use of TROSY-based techniques (discussed in the following chapter).

In this study, structure determination of bIGFBP-2 was investigated by X-ray crystallography, NMR spectroscopy and electron microscopy and these will be discussed separately. This chapter is the culmination of work with various collaborators whom I sincerely

acknowledge. The X-ray crystallography work was done in collaboration with Dr Peter Colman (Walter and Eliza Hall Institute (WEHI), Parkville, Victoria, Australia) and Ms Patricia Pilling (CSIRO Division of Health and Nutrition, Parkville, Victoria, Australia) (both formerly of the Biomolecular Research Institute (BRI), Parkville, Victoria, Australia). Professor Ray Norton performed all of the NMR spectral analyses and provided expertise for these studies (BRI and WEHI, Parkville, Victoria, Australia). Mr John Terlet and Dr Marilyn Henderson kindly provided access to The Centre For Electron Microscopy And Microstructure Analysis (CEMMSA) at Adelaide University, South Australia.

6.2 X-RAY CRYSTALLOGRAPHY STUDIES

At the outset of this thesis, there were no reported crystals of either IGFs or IGFBPs in the literature. Recently, crystal structures of IGF-I complexed to mini-IGFBP-5 (Żesławski *et al.*, 2001) and in complex with a detergent, deoxy big CHAPS (Vajdos *et al.*, 2001) have been published. Crystals for any of the full-length IGFBPs, either alone or in complex with IGF ligands, continue to elude researchers. This is believed to be due to the largely flexible nature of the IGFBPs (preliminary NMR data for IGFBP-2 and -6, Professor R. Norton, *unpublished*), which is not conducive to formation of quality crystals capable of diffracting X-ray beams. Indeed, the formation of large holes between individual protein molecules with irregular surfaces and shapes inhibits the growth of well-ordered crystals. Often the holes can occupy more than half of the volume of the crystal and are filled with disordered solvent molecules. Generally, the tighter the molecules pack, the better the diffraction pattern (Branden and Tooze, 1991).

In addition to being difficult to achieve, crystal formation can be slow and may require several months' growth. Formation of crystals is dependent on a number of different parameters including pH, temperature, protein concentration, the nature of the solvent and precipitant as well as the presence of added ions or ligands to the protein solution. Proteins for crystallization also need to be greater than 97 % pure and homogenous (Branden and Tooze, 1991).

Briefly, crystals form when the molecules are precipitated very slowly from super-saturated solutions. The method used in this study is the hanging drop method of crystallization, in which a drop of protein solution is brought very gradually to supersaturation by loss of water from the droplet to the larger reservoir that contains salt or precipitant solution. Equilibrium between the drop and the well is slowly reached through vapour diffusion and the salt concentration in the drop is increased by loss of water to the reservoir. If all conditions are right, including pH and temperature, protein crystals will form in the drop.

6.2.1 MATERIALS

$^{1-279}$IGFBP-2HIS and Trx$^{1-279}$IGFBP-2HIS for crystallography studies were expressed in *E.coli* cells and purified as described in Section 5.3.4. Media grade IGF-II was purchased from GroPep Ltd., Thebarton, South Australia, Australia. CSIRO Division of Health Science and Nutrition (Parkville, Victoria, Australia) kindly supplied all other materials and equipment. Glass coverslips were siliconised using Sigmacote (Sigma Chemical Co., MO, USA). Falcon, 24-well plates were obtained from Becton Dickinson Labware, Franklin Lakes, NJ, USA. All reagents used were of analytical grade or higher.

6.2.2 METHODS

6.2.2.1 Hanging Drop Method of Crystallization

Solubility screens were performed to determine the optimal salt, alcohol and precipitant concentrations for $^{1-279}$IGFBP-2HIS and Trx$^{1-279}$IGFBP-2HIS. Crystal screens were performed for $^{1-279}$IGFBP-2HIS, Trx$^{1-279}$IGFBP-2HIS and Trx$^{1-279}$IGFBP-2HIS in complex with IGF-II. Complexes were formed at a 1:1 molar ratio of IGF-II: Trx$^{1-279}$IGFBP-2HIS in 50 mM phosphate buffer, pH 7. Samples were resuspended to a final concentration of 10 mg/ml in a buffer below saturation. The protein solution (1 μl) was then placed onto the middle of a siliconised coverslip together with 1 μl of the well solution and sealed with Vaseline dropside down over a single well in a 24-well plate. Each well was filled with 1 ml of the precipitant solution that was at a concentration above saturation. Well solutions contained various salt, alcohol and precipitant combinations as detailed in Table 6.1. Plates were stored at 20 °C in a vibration free room and examined periodically through a microscope for crystal formations. Alternatively, some crystal screens were incubated at 30 °C.

TABLE 6.1 SCREENS FOR THE ANALYSIS OF OPTIMAL CONDITIONS FOR CRYSTAL GROWTH

Screen #1	Screen #2	Screen #3	Screen #4	Screen #5
1M CaCl 50mM Ac 4.6 15% MPD	2M NaCl - 10% PEG6K	4mM CoCl 40mM MES 6.5 0.72M $(NH_4)_2SO_4$	0.1M Tris 8.5 3.5M Hexanediol	0.1M Tris 8.5 1.75M Hexanediol
- - 0.4M NaKTart	0.01M TMAB 0.5M NaCl 0.1M $MgCl_2$	60mM $(NH_4)_2SO_4$ 30mM MES 6.5 9% PEGMME5K	0.1M Tris 8.5 4M Hexanediol	0.1M Tris 8.5 2M Hexanediol
- - 0.4M$(NH_4)_2PO_4$	- - 25% Ethy Glycol	6mM $ZnSO_4$ 60mM MES 6.5 15%PEGMME550	0.1M Tris 8.5 4.5M Hexanediol	0.1M Tris 8.5 2.25M Hexansdiol
- 33mM Tris 8.5 0.66M$(NH_4)_2SO_4$	- - 35% Dioxane	- - 0.8M NaCit 6.5	0.1M Tris 8.5 50% ethyl. Glycol	0.1M Tris 8.5 2.5M Hexanediol
0.1M NaCit 50mM Hepes 7.5 15% MPD	0.8M $(NH_4)_2SO_4$ - 2% Propanol	0.5M $(NH_4)_2SO_4$ 0.1M Hepes 7.5 30% MPD	0.1M Tris 8.5 60% ethyl. Glycol	0.1M Tris 8.5 2.75M Hexanediol
40mM MgCl 20mM Tris 8.5 6% PEG4K	- - 1M Imidazole	50mM Hepes 7.5 5% PEG6K 2.5% MPD	0.1M Tris 8.5 70% ethyl glycol	0.1M Tris 8.5 3M Hexanediol
- 70mM Caco 6.5 0.98M NaAc	- 5% PEG1K 5% PEG8K	- 70mM Hepes 7.5 14% Jeff M-600	0.1M Tris 8.5 3.5M Hexanediol 0.1M $MgCl_2$	0.1M Tris 8.5 1.75M Hexanediol 50mM $MgCl_2$
0.1M NaCit 50mM Caco 6.5 15% Propanol	1.05M NaCl - 7% Ethanol	50mM NaCl 50mM Hepes 7.5 0.8M $(NH_4)_2SO_4$	0.1M Tris 8.5 4M Hexanediol 0.1M $MgCl_2$	0.1M Tris 8.5 2M Hexanediol 50mM $MgCl_2$
66mM NH_4Ac 33mM Citrate 10% PEG4K	- 0.1M Ac 4.6 2M NaCl	- 0.1M Hepes 7.5 2M NH_4Form	0.1M Tris 8.5 4.5M Hexanediol 0.1M $MgCl_2$	0.1M Tris 8.5 2.25M Hexanediol 50mM $MgCl_2$
66mM NH_4Ac 33mM Ac 4.6 10% PEG4K	0.1M NaCl 50mM Ac 4.6 15% MPD	0.05M $CdSO_4$ 0.1M Hepes 7.5 1M NaAc	0.1M Tris 8.5 50% ethyl glycol 0.1M $MgCl_2$	0.1M Tris 8.5 2.5M Hexanediol 50mM $MgCl_2$
- 0.1M Citrate 1M $(NH_4)_2PO_4$	0.01M CoCl 0.1M Ac 4.6 1M Hexanediol	- 40mM Hepes 7.5 28% MPD	0.1M Tris 8.5 60% ethyl glycol 0.1M $MgCl_2$	0.1M Tris 8.5 2.75M Hexanediol 50mM $MgCl_2$
0.1M MgCl 50mM Hepes 7.5 15% Propanol	50mM CaCl 50mM Ac 4.6 15% PEG 400	- 50mM Hepes 7.5 2.15M NaCl	0.1M Tris 8.5 70% ethyl glycol 0.1M $MgCl_2$	0.1M Tris 8.5 3M Hexanediol 50mM $MgCl_2$
0.1M NaCit 50mM Tris 8.5 15% PEG400	0.1M $(NH_4)_2SO_4$ 50mM Ac 4.6 15% PEGMME2K	50mM Hepes 7.5 5% PEG8K 4% Ethy Glycol	0.1M Tris 8.5 3.5M Hexanediol 0.2M $MgCl_2$	0.1M Tris 8.5 35% glycerol
0.1M CaCl 50mM Hepes 7.5 14% PEG400	80mM NaK Tart 40mM Citrate 0.8M $(NH_4)_2SO_4$	- 30mM Hepes 7.5 6% PEG10K	0.1M Tris 8.5 4M Hexanediol 0.2M $MgCl_2$	0.1M Tris 8.5 45% glycerol
66mM$(NH_4)_2SO_4$ 33mM Caco 6.5 10% PEG8K	0.35M $(NH_4)_2SO_4$ 70mM Citrate 5.6 0.7M $LiSO_4$	60mM MgCl 30mM Tris 8.5 1.02M Hexanediol	0.1M Tris 8.5 70% glycerol 0.2M $MgCl_2$	0.1M Tris 8.5 55% glycerol
- 60mM Hepes 7.5 0.9M $LiSO_4$	0.5M NaCl 0.1M Citrate 5.6 4% Polyethylene	- 60mM Tris 8.5 15% Tert-But	0.1M Tris 8.5 50% ethyl glycol 0.2M $MgCl_2$	0.1M Tris 8.5 35% glycerol 50mM $MgCl_2$

TABLE 6.1 SCREENS FOR THE ANALYSIS OF OPTIMAL CONDITIONS FOR CRYSTAL GROWTH (cont)

Screen #1	Screen #2	Screen #3	Screen #4	Screen #5
40mM $LiSO_4$ 20mM Tris 8.5 6% PEG4K	- 50mM Citrate 5.6 17.5% tert-but	0.01M NiCl 0.1M Tris 8.5 1M $L1SO_4$	0.1M Tris 8.5 60% ethyl glycol 0.2M $MgCl_2$	0.1M Tris 8.5 45% glycerol 50mM $MgCl_2$
66mM MgAc 33mM Caco 6.5 6.6% PEG8K	0.01M $FeCl_2$ 0.1M Citrate 5.6 10% Jeff M-600	0.9M $(NH_4)_2SO_4$ 60Mm Tris 8.5 7.2% Glycerol	0.1M Tris 8.5 70% ethyl glycol 0.2M $MgCl_2$	0.1M Tris 8.5 55% glycerol 50mM $MgCl_2$
0.1M NH_4Ac 50mM Tris 8.5 15% Propanol	7mM $MnCl_2$ 70mM Citrate 5.6 1.75M Hexanediol	60mM $(NH_4)_2PO_4$ 30mM Tris 8.5 15% MPD	0.1M Tris 8.5 3.5M Hexanediol 0.3M $MgCl_2$	0.1M Tris 8.5 30% ethyl glycol
80mM$(NH_4)_2SO_4$ 40mM Ac 4.6 10% PEG4K	- 60mM MES 6.5 0.96M $MgSO_4$	- 0.1M Tris 8.5 20% Ethanol	0.1M Tris 8.5 4M Hexanediol 0.3M $MgCl_2$	0.1M Tris 8.5 40% ethyl glycol
0.1M MgAc 50mM Caco 6.5 15% MPD	0.2M $NaKPO_4$ 0.1M MES 6.5 2M NaCl	3mM NiCl 30mM Tris 8.5 6% PEGMME2K	0.1M Tris 8.5 68% glycerol 0.3M $MgCl_2$	0.1M Tris 8.5 50% ethyl glycol
40mM NaAc 20mM Tris 8.5 6% PEG4K	- 50mM MES 6.5 6% PEG 20K	50mM NaCl 50mM Bicine 9.0 15% PEGMME550	0.1M Tris 8.5 50% ethyl glycol 0.3M $MgCl_2$	0.1M Tris 8.5 30% ethyl glycol 50mM $MgCl_2$
0.1M MgCl 50mM Hepes 7.5 15% PEG400	0.8M $(NH_4)_2SO_4$ 50mM MES 6.5 5% Dioxane	- 50mM Bicine 9.0 1M $MgCl_2$	0.1M Tris 8.5 60% ethyl glycol 0.3M $MgCl_2$	0.1M Tris 8.5 40% ethyl glycol 50mM $MgCl_2$
0.1M $CaCl_2$ 50mM Ac 4.6 10% Propanol	0.025M CsCl 50mM MES 6.5 15% Jeff M-600	1% dioxane 50mM Bicine 9.0 5% PEG 20K	0.1M Tris 8.5 68% ethyl glycol 0.3M $MgCl_2$	0.1M Tris 8.5 50% ethyl glycol 50mM $MgCl_2$

Various salt, alcohol and precipitant combinations and concentrations were analysed in an attempt to generate IGFBP crystals. Crystals were obtained for $^{1-279}$IGFBP-2HIS under the conditions highlighted in red. Abbreviations are listed in the appropriate section at the beginning of this thesis.

6.2.3 RESULTS AND DISCUSSION

Crystallization of $^{1-279}$IGFBP-2HIS, Trx$^{1-279}$IGFBP-2HIS and the complex of IGF-II and Trx$^{1-279}$IGFBP-2HIS was attempted in this study. Initially the limits of salt, PEG and alcohol concentrations were established to avoid $^{1-279}$IGFBP-2HIS and Trx$^{1-279}$IGFBP-2HIS precipitation. IGFBP-2 solutions were shown to precipitate in concentrations of 1 M salt, 15 % alcohol and 5 % PEG (pH >7) or 10 % PEG (pH<7). Hence, buffer conditions that exceeded these concentrations were omitted from crystal screens. Traces of crystals were often evident in well solutions containing hexanediol, so variations of hexanediol and salt concentrations were screened to optimise conditions for crystal growth (eg. screen #5, Table 6.1). Small crystals of $^{1-279}$IGFBP-2HIS were obtained at pH 8.5 in the presence of hexanediol (Figure 6.1). These

crystals took about four months to grow at room temperature and were approximately 10 μm in length, which is too small for X-ray diffraction analyses. Further attempts are underway to repeat crystal growth under the same conditions and with variations of the hexanediol and salt precipitant. The current crystals of $^{1-279}$IGFBP-2HIS have been stored at the CSIRO Division of Health Sciences and Nutrition, Parkville, Victoria, Australia.

When all crystal screens have been exhausted, the $^{1-279}$IGFBP-2HIS crystals could be used to seed growth of larger crystals that could subsequently be used for X-ray diffraction analyses. Diffraction quality crystals sized >100 microns are necessary to obtain X-ray data. Recent advances in instrumentation however, are permitting crystallographers to investigate macromolecular samples of either very small crystals, or crystals with very large unit cells (reviewed by Hendrickson, 1991). While 3 Å resolution is adequate for determining a protein's backbone and discerning the general shape of its side chains, higher resolution is required to more precisely obtain the positions of individual side chains for modelling of binding mimetics. Molecular replacement methods using the known structure of mini-IGFBP-5 could also assist in structure determination (Varghese *et al.,* 1994). Therefore, with the correct technology and instrumentation, X-ray diffraction analysis could be performed using the $^{1-279}$IGFBP-2HIS crystals.

The thiorexdoxin fusion partner contributed to the solubility of the protein enabling large-scale production in *E.coli* cells. Furthermore, as discussed in Section 3.4, Trx$^{1-279}$IGFBP-2HIS, unlike the native protein, remained monomeric at millimolar concentrations, which is advantageous for crystal formation. Interestingly, crystals of Trx$^{1-279}$IGFBP-2HIS either alone or in complex with IGF-I were not observed in this study. Thioredoxin itself readily crystallizes and the structure of the oxidised protein has been reported by X-ray crystallography (Holmgren *et al.*, 1975; Katti *et al.*, 1990). The reduced form of the protein has also been determined by NMR (Dyson *et al.*, 1990). The overall conformation is similar in both studies although significant local conformational differences were observed that can be attributed to intermolecular contacts in the crystal. It has so far proved possible to crystallize thioredoxin only in the presence of Cu^{2+} ions that cross link two molecules by

Figure 6.1 Crystals of bIGFBP-2
Crystal screens were set up with Ms Patricia Pilling at the Biomolecular Research Institute (BRI) Parkville Victoria Australia. Small crystals (10 μm) were obtained under the precipitant conditions 0.1 M Tris pH 8.5, 1.75 M 1,6 hexanediol, 50 mM $MgCl_2$. These crystals took approximately 4 months to grow at room temperature.

coordination at Ser1, Asp2 and Asp10. This requirement for Cu^{2+} precludes crystallization of the reduced protein containing a dithiol pair at the active site.

The requirement of Cu^{2+} ions for crystallization of thioredoxin is further explained by NMR experiments. In solution, thioredoxin residues 1-3 are clearly disordered (Dyson *et al.*, 1990; Stone *et al.*, 1993). In the crystal structure however, this region is stabilised by copper binding forming an ordered β-strand structure in the crystal through a cross-link to a neighbouring molecule (Katti *et al.*, 1990). Indeed, both crystal packing and binding of the Cu^{2+} ions required for crystallization caused significant local perturbations in both backbone and side chain structure (Clore and Gronenborn, 1993). Therefore, thioredoxin fused IGFBPs expressed in this study, may crystallize in the presence of copper ions. This possibility is currently being investigated.

Recently, IGF-I has been crystallized in complex with mini-IGFBP-5 thus providing a spatial understanding of the interacting molecules (Żesławski *et al.*, 2001)(Figure 1.5). Interestingly, the fold of mini-IGFBP-5 was conserved in complex with IGF-I. Two regions of mini-IGFBP-5 remain poorly defined including the five C-terminal residues and the solvent exposed loop (Pro62-Pro69), which was rigidified in the presence of ligand. Crystallization of mini-IGFBP-5 was successful with 10 % Jeffamine M-600, 0.1 M sodium citrate, 0.01 M ferric chloride pH 5.6. Crystals of IGF-II complexed to Trx^{1-279}IGFBP-2HIS were not observed in the present study using similar well solutions containing Jeffamine M-600 (Table 6.2). The large linker domain of full-length IGFBPs may be responsible for preventing compact packing and crystal formation of native IGFBPs to date. Certainly, it would be interesting to attempt crystallization of a truncated form of IGFBP missing the central domain. Ultimately, crystal structures of the full-length IGFBPs in complex with the IGF ligands will enable a complete understanding of the molecular interaction.

IGF-I has also recently been shown to crystallize in the presence of the detergent deoxy big CHAPs (Vajdos *et al.*, 2001). The resulting 1.8 Å resolution structure defined the disordered regions of the C-region, which exhibited a type II β-turn similar to the solution

structure of IGF-II (Torres *et al.*, 1995). The structure of IGF-I in this detergent complex is similar to that in complex with mini-IGFBP-5 and is not dissimilar to the structure of the free ligand determined in solution by NMR (Cooke *et al.*, 1991; Sato *et al.*, 1992).

6.3 NMR SPECTROSCOPY ANALYSIS

NMR and X-ray crystallography are important tools in the determination of tertiary structure of proteins and nucleic acids. NMR is complementary to X-ray crystallography analysis and few structural differences have been reported between solution and crystal forms of proteins (Wűthrich, 1995; Engh *et al.*, 1993). NMR however has the advantage that structure determination is carried out in a biological context (in solution, albeit of relatively high concentration), thus allowing protein dynamics to be investigated. For proteins that fail to crystallize, including the IGFBPs, NMR analysis is a valuable approach. Furthermore, NMR contributes significantly to the field of structure determination when proteins fail to form good crystals that yield high-resolution structures.

NMR spectroscopy is a powerful structure determination technique that has determined the structures of more than 1000 proteins and nucleic acids. To date, NMR contributes only approximately 17 % of structures currently deposited in the Protein Data Bank (PDB) (Berman *et al.*, 2000) as NMR spectroscopy has been limited to smaller molecular weight proteins. Indeed, few NMR derived structures exist for molecular weights above 25 kDa. NMR structural studies require good sensitivity and spectral resolution for quality spectra, however these basic requirements are harder to achieve with increasing molecular weights. Low sensitivity and line broadening, due to rapid transverse spin relaxation, and extensive signal overlap, due to the high complexity of the spectra, are limiting factors in high molecular weight samples. Due to the increased difficulties and costs associated with structure determination of large molecular weight proteins, NMR has largely been used only to complement X-ray crystallography studies of these molecules.

To date, the tertiary structures of full-length IGFBPs have not been determined by either NMR or X-ray crystallography. Until recent advances in technology, the IGFBPs (>30 kDa) were considered too large for NMR spectroscopy and discrete modules of the native protein were targeted for structure determination studies. The first report of an IGFBP structure was for an amino-terminal IGF-binding fragment of hIGFBP-5 (mini-IGFBP-5). This binding fragment

consisted of a compact arrangement of three short antiparallel β-strands (residues 46-47, 59-61, 78-82; Kalus *et al.*, 1998) (Figure 1.9) and provided a basis for the determination of the structure of the remaining IGFBPs. Indeed, the high degree of sequence homology and the conserved pattern of cysteine residues throughout IGFBPs 1-5 suggest a common structure across these high-affinity IGFBPs. In this study, NMR structure determination of bIGFBP-2 was investigated.

6.3.1 MATERIALS

Acetic acid-(d_4) was purchased form Sigma Chemical Co. MO, USA. Trx^{1-279}IGFBP-2HIS for NMR spectral analysis was expressed and purified as described in Section 5.3.4. NMR spectra were recorded on a DRX-600 spectrometer. Spectra were processed and analysed on Silicon Graphics workstations using XWINNMR (version 1.3, Bruker). Collection of NMR spectral data was performed by Professor Ray Norton (BRI, Parkville, Victoria, Australia).

6.3.1.1 NMR BUFFERS

Phosphate Buffer
50 mM sodium phosphate, 5 % ^2H_2O
-Adjusted to pH 5.0

6.3.2 METHODS

6.3.2.1 NMR *Spectroscopy*

Samples for NMR were prepared by dissolving $^{1-279}$IGFBP-2HIS or Trx^{1-279}IGFBP-2HIS (0.5 mM) in 550 µl phosphate buffer (Section 6.3.1.1) to a final concentration of 0.5 mM at pH 5.65, 4.5 and 1.7. One-dimensional ^{1}H NMR spectra were

recorded on a Bruker DRX-600 spectrometer with a probe temperature of 37 °C although some spectra were also collected at 10 °C and 25 °C. Typically, 512 scans were acquired using 2 K data points. Sweep widths were 7122.5 Hz for all samples. Spectra were processed and analysed on Silicon Graphics workstations using XWINNMR (version 1.3, Bruker).

6.3.3 RESULTS AND DISCUSSION

$^{1-279}$IGFBP-2HIS and Trx$^{1-279}$IGFBP-2HIS in aqueous solution were analysed by ^{1}H NMR spectroscopy as described in Section 6.3.2. Gel filtration studies (Section 5.4.6) indicated that Trx$^{1-279}$IGFBP-2HIS remains monomeric during studies at acidic pH and is stable upon storage. In contrast to the thioredoxin-fused protein, $^{1-279}$IGFBP-2 exhibits a lower threshold for precipitation and subsequently aggregation. Spectra recorded at pH 5.65 in 50 mM phosphate buffer were quite sharp and there were several small peaks resolved from the main spectral bands, indicating the presence of both flexible and more structured regions (Figure 6.2 and 6.3). Several peaks were shifted upfield and downfield from the normal chemical shift range expected for a random coil protein.

The spectra acquired in this study indicate the potential to derive a tertiary structure of IGFBP-2 by NMR spectral analysis. However, the spectra are complex, due to there being signals from 284 amino acid residues for full-length IGFBP-2 alone. Although the presence of the thioredoxin-tag is advantageous for structure determination studies, particularly for the solubility of the protein at NMR concentrations (as discussed in Section 5.4.6), the subsequent increase in molecular weight (>46 kDa) is presently beyond NMR spectral resolution. The interpretation of the data would rely heavily on analogy with reported chemical shift data for mini-IGFBP-5 and additional interpretation could be achieved by producing single site mutations within IGFBP-2.

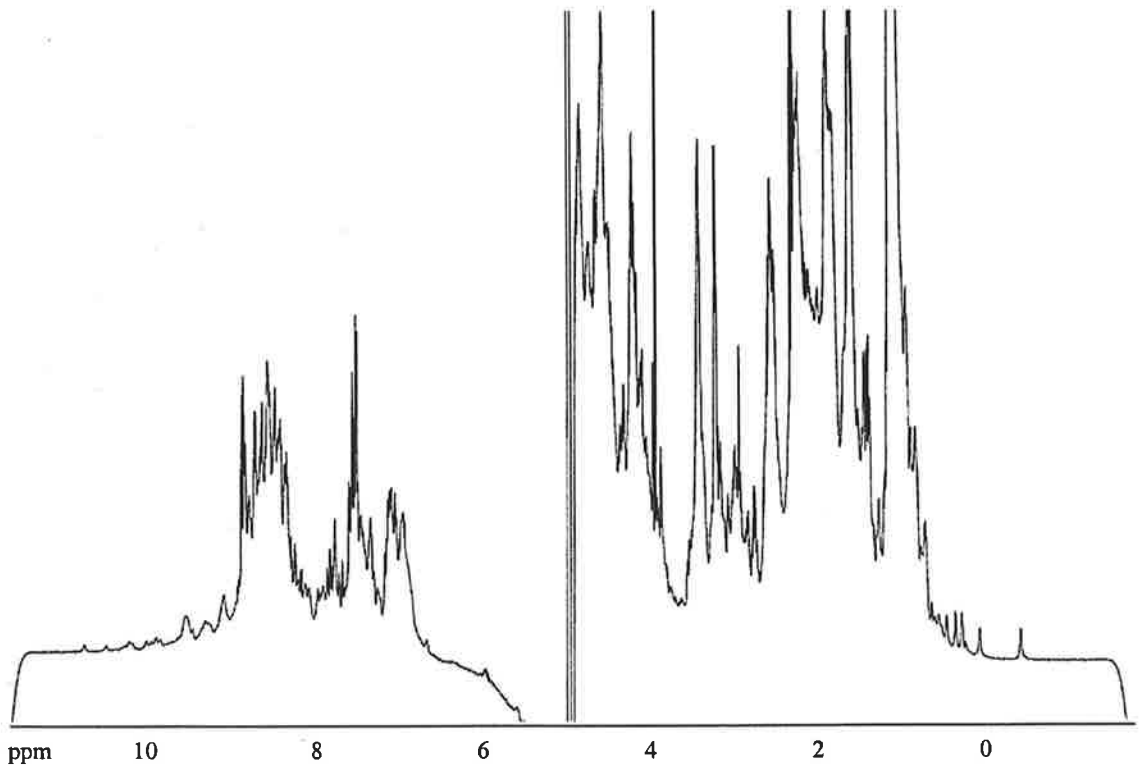

Figure 6.2 ^{1}H NMR spectrum of Trx$^{1-279}$IGFBP-2HIS
^{1}H NMR spectra of Trx$^{1-279}$IGFBP-2HIS (0.5 mM in 50 mM phosphate buffer) were recorded at 600 MHz, pH 4.3 and with a probe temperature of 37 °C. Spectra were processed and analysed on Silicon Graphics workstations using XWINNMR (version 1.3, Bruker).

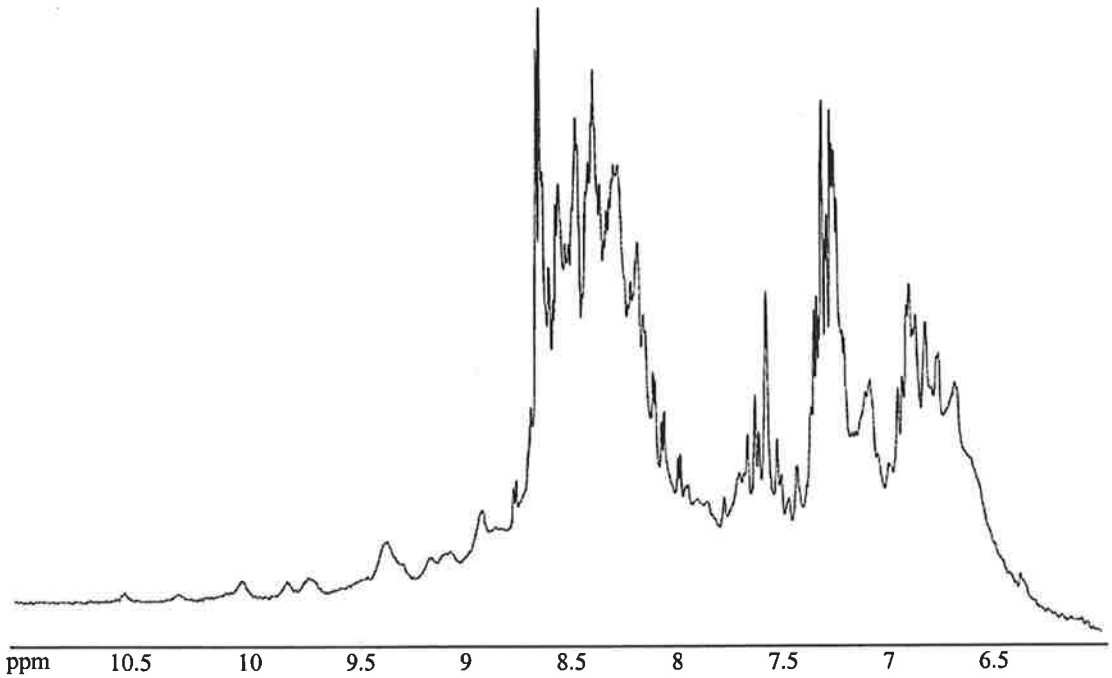

Figure 6.3 ^{1}H NMR spectrum of Trx$^{1-279}$IGFBP-2HIS
^{1}H NMR spectra of Trx$^{1-279}$IGFBP-2HIS (0.5 mM in 50 mM phosphate buffer) were recorded at 600 MHz, pH 4.3 and with a probe temperature of 37 °C. Spectra were processed and analysed on Silicon Graphics workstations using XWINNMR (version 1.3, Bruker).

As mentioned previously, structural information has been derived for many large protein molecules by analysis of discrete folding domains of the full-length protein. Indeed, the structure of an amino-terminal IGF-binding fragment of IGFBP-5 was determined by NMR spectroscopy (Kalus *et al.*, 1998). There is a high degree of sequence homology in the corresponding region of IGFBP-2 and IGFBP-6 (Figure 6.4) and it is likely that structures in this region will be similar to the well-defined region of IGFBP-5. Preliminary spectra of the N-terminal domain of hIGFBP-6 by Professor R. Norton in collaboration with Associate Professor L. Bach (*unpublished*) indicate that it contains little ordered secondary structure and several flexible regions. In contrast, the C-domain shows greater spectral dispersion and appears to be structured. Indeed, discrete amino- and carboxyl-terminal fragments of IGFBP-2 were generated in this study, which are well within the molecular weight limitations for NMR resolution. Structure determination studies by NMR will be performed on these fragments. Furthermore, the molecular weights of the thioredoxin-fused amino- and carboxyl-terminal fragments of IGFBP-2 remain less than 30 kDa.

Comparsion of the structures of the amino- and carboxyl-terminal domains of IGFBP-2, IGFBP-5 and IGFBP-6 will provide important information regarding differences between the IGFBPs. Structural differences between IGFBP-2 and IGFBP-6 may provide important information regarding IGF specificity, as these molecules (particularly IGFBP-6) exhibit IGF-II preferences. Interestingly, the disulfide pairs within the N-terminal domain of IGFBP-6 differ from those of IGFBP-2 and IGFBP-5. NMR could therefore be used to compare the structural and dynamic consequences of these variations.

```
IGFBP-2  50 ARLEGEACGVYTPRCGQGLRCYPHPGSELPLQALVMGEGTC 90
IGFBP-5  40 ALAEGQSCGVYTERCAQGLRCLPRQDEEKPLHALLHGRGVC 80
IGFBP-6  40 LRREGQECGVYTPNCAPGLQCHPPKDDEAPLRALLLGRGRC 80
```

Figure 6.4 Sequence alignment of amino-terminal binding fragments of IGFBP-2, IGFBP-5 and IGFBP-6
A sequence alignment of the amino-terminal binding fragment of IGFBP-2, IGFBP-5 and IGFBP-6. Residues are numbered according to the human sequences. Residues in yellow are conserved across each IGFBP. Residues boxed in green formed contacts with IGF-I in the crystal structure (Żesławski *et al.*, 2001).

6.4 ELECTRON MICROSCOPY ANALYSIS

Electron microscopy is an important technique capable of providing three-dimensional images of cells or molecules. Atomic force microscopy (AFM) is the most powerful of microscopy techniques for the analysis of biological samples (reviewed in Lal and John, 1994; Hoh and Hansma, 1992). AFM differs from scanning electron microscopy in that it can image living cells and molecules in a fluid environment, often with greater resolution. This has obvious advantages for biological samples and permits imaging in fluids including physiological buffers. AFM has also been used to manipulate membranes and molecules and is capable of measuring a variety of local and biophysiological surface properties, including physical topography. Indeed, many proteins have been imaged with AFM including immunoglobulins, fibrins, phosphorylase and actin (Drake *et al.*, 1989, Edstrom *et al.*, 1990, Weisenhorn *et al.*, 1990, Smith and Radford, 2000). In an earlier study, transmission electron microscopy was used to define the tetrameric arrangement of pyruvate carboxylase monomers and the localisation of the biotin prosthetic group (Mayer *et al.*, 1980; Johansson *et al.*, 1993; Rohde *et al.*, 1986).

Scanning probe microscopes (including AFM) operate by passing a very sharp tip attached to a soft cantilever, which acts as a spring, over the surface of a molecule. Deflections in the tip that correspond to surface topography are recorded as surface images. In this study, AFM was used to investigate the surface topography of IGFBP-2. In particular we were interested to see if the conformation of the IGFBP-2 altered significantly in the presence of IGF ligand. These studies were designed to complement the NMR analysis of the chemical shift perturbations of IGF-I and IGF-II upon binding IGFBP-2 (discussed in the following Chapters).

6.4.1 MATERIALS

Mr John Terlet and Dr Marilyn Henderson (CEMMSA, Adelaide University, South Australia, Australia) kindly permitted access to the Scanning Probe Microscope (SPM) and software (TopoMetrix, Santa Clara, California, USA) and provided expertise in the technology.

6.4.2 METHODS

6.4.2.1 Sample Preparation for Atomic Force Microscopy (AFM)

A 6.6 μM stock of IGF·IGFBP-2 was diluted 1:100 in H_2O. The sample for AFM was prepared by placing a 10 μl droplet of IGF·IGFBP-2 on a 2 x 2 mm piece of mica, and after resting for 3 minutes, excess moisture was removed by wicking with the edge of a piece of filter paper. The mica was then transferred to the TopMetrix Environmental Cell and scanned.

6.4.3 RESULTS AND DISCUSSION

AFM provides great insight into the tertiary fold of protein molecules especially in fluid environments. The resolution of biological specimens by AFM however is relatively poor (1-50 nm), comparable to scanning electron microscopy but significantly higher quality than images obtained from light microscopes. This was true also for analysis of IGFBP-2. The resolution of the protein molecules was too poor to define conformational epitopes or to distinguish differences between free and IGF-bound IGFBPs. Although AFM permits scanning in fluid solutions, hydration layers and thermal molecular motion are believed to contribute to poor resolution. Image resolution however can be improved by reducing the mobility of a molecule, for example by being embedded in a membrane. Indeed, features as small as 10 nm have been described on the surface of whole cells, however they have not been identified with certainty. Other limitations of this technique are the potential of the tip forces to cause deformation of the

sample or for the tip to significantly broaden tall features of a surface and subsequently record untrue images.

Although AFM has successfully defined the surface topography and molecular arrangement of many protein molecules, structural information could not be gained for IGFBP-2, either in the presence and absence of IGF. An alternative approach to defining the conformational states of bIGFBP-2 and the kinetics of protein folding and association could involve small angle X-ray scattering (SAXS) experiments. Using this approach, information regarding the overall size and shape, gyration radius and association state of bIGFBP-2 could be generated in a time-resolved fashion.

6.5 CONCLUDING REMARKS

The structure of the full-length IGFBP continues to elude all researchers to date. In this study, attempts to elucidate the structure of IGFBP-2 by NMR analysis were inhibited by size restraints. Amino- and carboxyl-terminal fragments, however, may help to overcome these shortcomings. Crystals were obtained for bIGFBP-2, which continue to be cultivated to diffractable quality. Despite the potential for electron microscopy to provide invaluable insight into the overall conformation of IGFBP-2, NMR or X-ray crystallization studies will offer the greatest information for the structure of IGFBP-2 and the IGF·IGFBP complex.

CHAPTER 7

IDENTIFICATION OF SPECIFIC IGF-I AND IGF-II RESIDUES INVOLVED IN BINDING bIGFBP-2 BY HETERONUCLEAR NMR SPECTROSCOPY

7.1 INTRODUCTION

Given the diverse biological effects of IGFs and the central role of IGFBPs in the regulation of IGF activity, the molecular interactions between the IGFs and IGFBPs are of particular interest. High-resolution NMR structures of both IGF-I and IGF-II have been published (Cooke *et al.*, 1991; Sato *et al.*, 1992; Terasawa *et al.*, 1994; Torres *et al.*, 1995), which have enabled detailed correlation of IGF structure-function relationships to be made. However, at the outset of this thesis, the tertiary structures of the IGFBPs and of the complex with IGFs were unknown. Furthermore, the IGF·IGFBP binding interfaces and the specific amino acid residues involved in the interaction were largely undefined. As such, binding site studies were limited to mutagenesis and chemical modification approaches. Therefore a priority in IGF research was the determination of the structure of IGFBPs and a thorough investigation of the residues involved in the interaction between IGFs and IGFBPs.

7.1.1 IGFBP BINDING SITE ON IGFS

Various techniques have been used to investigate the IGF residues involved in binding IGFBPs, and these include residue or domain swapping with the homologous insulin molecule and amino acid deletions or mutations. Analogue studies have shown the importance of the B- and A-domains of the IGFs in binding to the IGFBPs (Figure 7.1a). Homologue domain swapping of the B-domain of IGF-I for the corresponding insulin B-domain confers the ability on insulin to interact with IGFBP (De Vroede *et al.*, 1985). Conversely, replacement of the IGF-I B-domain with the insulin B-domain reduces serum IGFBP binding (Bayne *et al.*, 1988). Furthermore, Glu3 of IGF-I was shown by site directed mutagenesis studies and deletion analyses to contribute to the IGFBP interaction (Bagley *et al.*, 1989). The corresponding residue in IGF-II, Glu6, is also required for IGFBP binding (Francis *et al.*, 1993).

a. Mutagenesis Studies

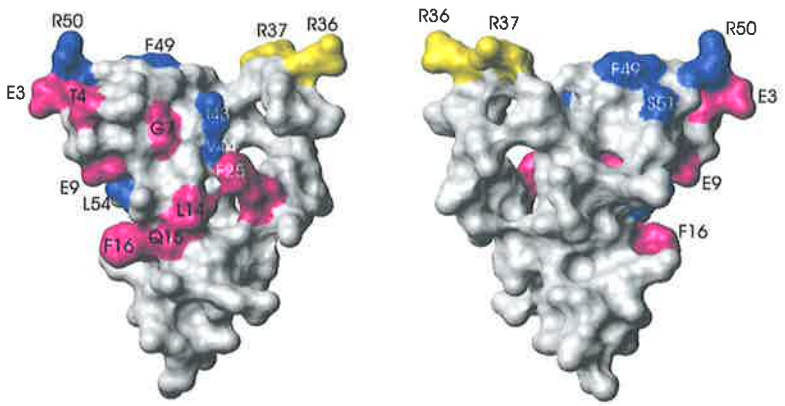

b. NMR with IGFBP-1 - Jansson *et al.*, 1998

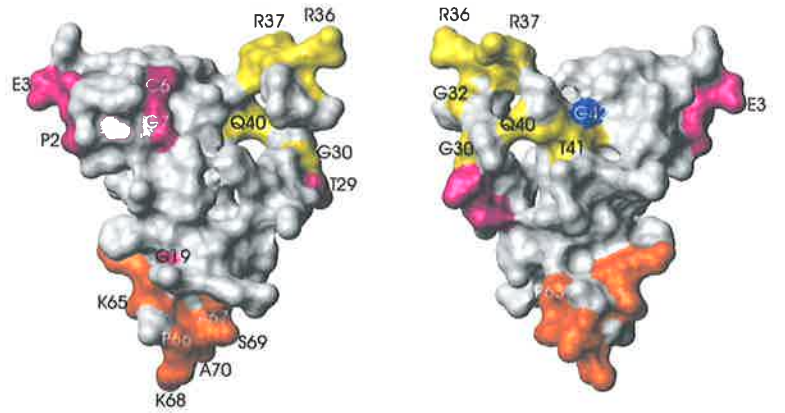

c. Crystal Structure - Zesławski *et al.*, 2001

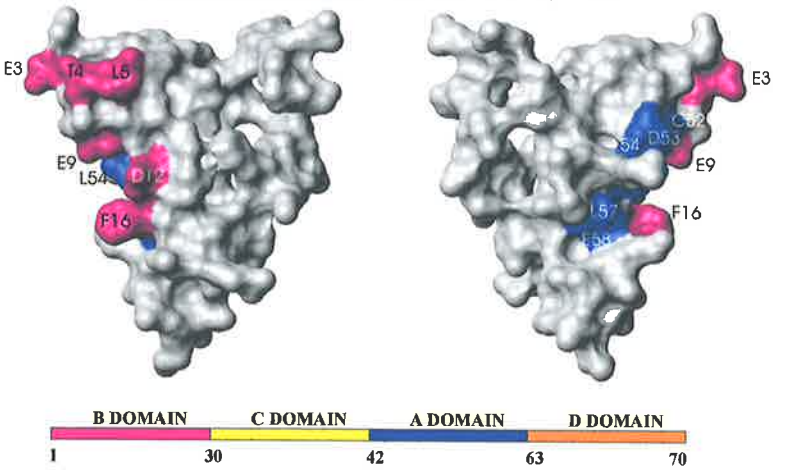

Figure 7.1 Surface representation of IGF-I with residues involved in binding IGFBPs highlighted

The residues of IGF-I identified to be important for binding IGFBPs by mutagenesis (a. as discussed in Section 1.5) and by heteronuclear NMR experiments (b. Jansson *et al.*, 1998) are highlighted with respect to their domains (pink: B-domain; yellow: C-domain; blue: A-domain and orange: D-domain. The residues which were within 5 Å of mini-IGFBP-5 in the crystal structure are also highlighted (c. Zesławski *et al.*, 2001). IGF-I has been presented in two orientations with rotation of 180° about the vertical axis. This figure was generated in MOLMOL (Koradi *et al.*, 1996).

IGF-I B-domain residues Gln15 and Phe16 are also involved in IGFBP binding. When these residues were mutated in combination with residues Glu3 and Thr4 to the corresponding insulin residues, binding to serum IGFBP was decreased by up to 600-fold (Bayne *et al.*, 1988). Furthermore, sequential alanine mutagenesis across the entire IGF-I molecule identified B-domain residues Gly7, Leu10 and Phe25 as important for the IGFBP-I interaction (Dubaquie and Lowman, 1999). Mutagenesis of residue Phe26 in IGF-II to either Ser or Leu also affected binding to IGFBPs (Bach *et al.*, 1993) as well as the type-I IGF and insulin receptors (Sakano *et al.*, 1991).

A-domain residues, Phe49, Arg50, and Ser51 of IGF-I (Clemmons *et al.*, 1992; Oh *et al.*, 1993) and Phe48, Arg49 and Ser50 of IGF-II (Bach *et al.*, 1993) are also important for IGFBP interactions. Interestingly, alanine substitution of IGF-I A-domain residues Ile43, Val44 or Leu54 reduced binding to IGFBP-1 up to 4-fold, but had a negligible effect on IGFBP-3 binding (Dubaquie and Lowman, 1999). Indeed, different IGF analogues affect binding to each IGFBP family member to varying degrees (Clemmons *et al.*, 1992; Bach *et al.*, 1993; Magee *et al.*, 1999) and this observation appears to be true also for these A-domain residues.

NMR structures of IGF-I (Cooke *et al.*, 1991; Sato *et al.*, 1992) and IGF-II (Terasawa *et al.*, 1994; Torres *et al.*, 1995) have enabled spatial interpretation of the mutagenesis data. For example, the glutamates at position 3 and 6 in IGF-I and IGF-II respectively, are solvent exposed and not directly involved in the maintenance of IGF protein structure, thus allowing for the interpretation that they are directly involved in binding IGFs (Cook *et al.*, 1991; Torres *et al.*, 1995). Indeed, the recent co-crystallization of IGF-I and mini-IGFBP-5 (Żesławski *et al.*, 2001) confirms specific interaction between Glu3 of IGF-I and Tyr50 and His71 of mini-IGFBP-5 (Figure 7.1c). NMR has also been used to directly investigate residues on IGF-I that are perturbed upon binding of IGFBP-1 (Jansson *et al.*, 1998). Perturbed residues include Pro2, Glu3, Cys6, Gly7, Gly19, Pro28-Gly30, Gly32, Arg36, Arg37, Gln40-Gly42, Pro63, Lys65, Pro66 and Lys68-Ala70 (Jansson *et al.*, 1998) (Figure 7.1b). Furthermore, alanine substitution of each arginine residue in the protein showed that the analogues R36A, R37A IGF-I and R50A IGF-I were impaired in their ability to interact with IGFBP-1 (Jansson *et al.*, 1998).

Clearly, both B- and A-domain residues of IGFs are important for interaction with the IGFBPs. Several studies have shown however, that mutations to the IGF molecules exhibit varying affinity for each of the IGFBPs (Clemmons *et al.*, 1992; Bach *et al.*, 1993; Magee *et al.*, 1999). Therefore the objective of this chapter was to determine the specific residues of both IGF-I and IGF-II involved in binding IGFBP-2.

7.1.2 NMR AS A TOOL FOR DEFINING BINDING INTERFACES

NMR is a useful technique to determine structural differences between wildtype and mutant proteins and can also provide detailed information regarding conformational changes that accompany ligand binding (Craik and Wilce, 1997). NMR uses the magnetic spin properties of atomic nuclei to identify atoms that are close together in space (Howard, 1998). ^{1}H, ^{15}N, ^{13}C and ^{31}P nuclei orientated partially by a magnetic field absorb radiation at characteristic frequencies that manifest as NMR peaks (Howard, 1998). The frequencies at which a nucleus resonates is dependent on the local environment of the atom of interest and is generally expressed as a chemical shift in parts per million (ppm) relative to a reference signal (Roberts, 1993).

Chemical shifts observed in NMR spectra can be used to monitor changes in the environment of the nuclei that occur upon complex formation (Craik and Wilce, 1997). These studies require that one of the components of the complex be selectively observed from the bulk of the protein resonances, thereby simplifying the analysis of the spectra and allowing the structural information to be obtained readily (Fesik, 1989; 1991). This can be achieved through isotope labelling of one of the protein components with ^{15}N and/or ^{13}C, which can be selectively observed by isotope-edited two-dimensional (2D) (Fesik *et al.*, 1988; Wider *et al.*, 1990) or heteronuclear three-dimensional (3D) NMR techniques (Fesik and Zuiderweg, 1988)(discussed in Section 7.1.3).

Changes in the local environment of amino acid residues as they interact with the ligand are observed as chemical shift perturbations in both the nitrogen and the proton dimensions of

Heteronuclear Single Quantum Coherence (HSQC) or Transverse Relaxation Optimised Spectroscopy (TROSY) spectra. Amino acid residues that exhibit chemical shift perturbations may be directly involved in the binding interface or they may map to regions of the protein that undergo a conformational change upon complex formation (Foster *et al.*, 1998). Consequently, the extent of the binding interface may be overestimated (Ramos *et al.*, 2000). However, mapping the observed chemical shift changes to the structure of the protein allows interpretation of the involvement of specific amino acid residues and of the structure-function relationship of the interacting molecules.

As mentioned above, NMR has previously been used to identify residues of IGF-I involved in binding IGFBP-1 (Jansson *et al.*, 1998). As discussed in section 7.1.1, IGF analogues exhibit variability upon binding each of the IGFBPs and indeed, the IGFBPs themselves display preferential binding for either IGF-I or IGF-II. It was therefore important to determine if a common binding site exists for each of the IGFBPs or if specific residues are responsible for the interaction. Residues of both IGF-I and IGF-II that were perturbed in the presence of IGFBP-2 were investigated in this chapter. Furthermore, amino- and carboxyl-fragments of IGFBP-2 permitted localisation of IGF binding sites for the highly conserved domains of IGFBPs.

7.1.3 NMR SPECTROSCOPY

High molecular weight proteins generally exhibit poor resolution in NMR spectroscopic studies. Resolution depends inversely on resonance line widths and these widths depend in turn on effective molecular weight. Although the present studies are targeted at observing signals from the IGF ligand, the effective molecular mass of the Trx^{1-279}IGFBP-2HIS·IGF complex (~ 53 kDa) is approaching the upper limit of current solution-state NMR methods. In recent years, size limitations have been extended by isotope enrichment ($^{13}C/^{15}N$ and ^{2}H) (Gardner and Kay, 1998) and extension of spectra to three and four dimensions. Most recently TROSY techniques

in combination with high magnetic fields have been used for high molecular weight protein samples (Riek *et al.*, 2000).

In a one-dimensional (1D) ^{1}H experiment, the spectral overlap of proton resonances is such that structure determination of even a small protein is not possible (Howard, 1998). Resolution is improved significantly in 2D homonuclear (same nuclei) or heteronuclear (different nuclei eg. ^{1}H-^{15}N) NMR experiments. Heteronuclear 2D experiments require labeled proteins to detect a correlation between two different nuclei. In ^{1}H-^{15}N HSQC experiments the resulting spectrum consists of cross peaks (one for each residue except proline and additional cross peaks for side chain resonances), which correlate the ^{1}H chemical shifts of an amide proton with the ^{15}N chemical shift of its directly-bonded nitrogen. Heteronuclear 2D methods usually suffice for proteins of molecular weight of up to 12 kDa (eg. oxidised and reduced forms of thioredoxin (108 amino acids; Dyson *et al.*, 1989)). However, uniform ^{15}N- and ^{13}C-labeling and multidimensional heteronuclear NMR methods are used to assign resonances of proteins with molecular weight greater than around 12 kDa (Clore and Gronenborn, 1991a).

Conventional NMR spectra of large molecules in solution typically display broad lines that result in poor resolution and sensitivity (Wider and Wüthrich, 1999). In addition, extensive signal overlap due to the high complexity of the spectra, limits analyses of proteins to those less than 30-40 kDa. Considerable effort therefore has gone into extending the size limit for analysis of larger molecules. The TROSY technique suppresses transverse nuclear spin relaxation (Pervushin *et al.,* 1997), which is the direct cause of the deterioration of the NMR spectra of large molecular structures, thus extending the size limitations beyond 40 kDa. Typically in 2D experiments, the multiplet components are decoupled into a single, centrally located cross peak with the intention to simplify the spectrum and improve sensitivity. However for large proteins the differential line broadening of the individual multiplet components is very pronounced and results in deterioration of the average signal. In TROSY experiments, only the narrowest, most slowly relaxing cross peak of each multiplet is retained resulting in improved spectral resolution and improved effective sensitivity. For proteins with molecular weights above 20 kDa, TROSY experiments achieve a superior ratio of peak height

to noise compared with conventional 2D experiments. Indeed, Riek and co-workers (1999) reported an improvement in spectral resolution and sensitivity in ^{15}N-^{1}H TROSY correlation spectra compared to conventional spectra of 7,8-dihydroneopterin aldolase (DHNA) - a molecule containing eight subunits of 121 amino acid residues and with a total molecular mass of 110 kDa. Sensitivity was improved further by a combination of TROSY and cross-correlated relaxation-enhanced polarization transfer (CRINEPT) techniques (Riek *et al.*, 2000).

Therefore, the chemical shift perturbations of IGF-I and IGF-II upon complex formation with Trx^{1-279}IGFBP-2HIS were investigated by a series of TROSY spectra. These studies were aimed at defining the residues of IGF involved in binding IGFBP-2 and to compare the binding sites of both IGF-I and IGF-II. Furthermore, these studies also aimed to identify the specific residues of IGF involved in binding the highly conserved amino- and carboxyl-terminal domains of IGFBP-2.

7.2 MATERIALS

Acetic acid-(d_4) was purchased from Sigma Chemical Co. MO, USA. Labelled IGF-I and IGF-II were expressed and purified as described in Section 5.3.3. Trx^{1-279}IGFBP-2HIS, Trx^{1-132}IGFBP-2 and $Trx^{136-279}$IGFBP-2HIS for NMR spectral analysis were expressed and purified as described in Section 5.3.4. Shigemi NMR tubes were purchased from Shigemi, Inc. Pennsylvania, USA, all other NMR tubes were purchased from Wilmad Glass Company, New Jersey, USA.

7.2.1 NMR BUFFERS

NaAc(d_4) Buffer
10 mM acetic acid (d_4), 5 % ^2H_2O
-Adjusted to pH 5.0

Citrate Buffer
5 mM citrate, sodium phosphate, 5 % ^2H_2O
-Adjusted to pH 5.0

7.3 METHODS

7.3.1 SAMPLE PREPARATION

Samples for complex analysis were prepared by dissolving lyophilized IGF-I or IGF-II in 550 µl NaAc(d_4) buffer to a final concentration of 0.5 mM prior to addition of lyophilised Trx^{1-279}IGFBP-2HIS, Trx^{1-132}IGFBP-2 or $Trx^{136-279}$IGFBP-2HIS (0.5 mM). The samples of both free and complexed IGF-I were adjusted to approximately pH 5 prior to recording of NMR spectra.

7.3.2 NMR SPECTROSCOPY

NMR spectra of labelled IGF-I and IGF-II were recorded both as the free ligand and in complex with Trx^{1-279}IGFBP-2HIS, Trx^{1-132}IGFBP-2 or $Trx^{136-279}$IGFBP-2HIS on either Bruker AMX-500 or DRX-600 spectrometers with a probe temperature of 37 °C. Spectra were also recorded at 27 °C and 45 °C as indicated. Typically, 70-90 t_1 increments were acquired, with a final matrix size of 2048 and 256 complex points in the ^{1}H and ^{15}N dimensions respectively. The number of scans collected was 512 with recycle times of 1.8 seconds and 1.4 seconds for 1D and 2D spectra, respectively. Presaturation or pulsed-field gradients were used to suppress unwanted coherences and the water resonance (Sklenar *et al.,* 1993). Sweep widths were 5813.95 Hz and 7122.5 Hz for 500 MHz and 600 MHz experiments, respectively. Spectra were processed and analysed on Silicon Graphics workstations using XWINNMR (version 1.3, Bruker) and assigned with the XEASY graphics program (Bartels *et al.,* 1995). Professor R. Norton acquired all NMR spectra, which included: 2D ^{1}H-^{15}N HSQC, 2D ^{1}H-^{15}N TROSY, 2D ^{15}N-filtered ^{1}H-^{1}H NOESY with a 150 ms NOESY mixing period and a 3D HNCA (see Figure 7.6). Sweep widths for the 3D HNCA spectra were 3156.6 Hz, 1824 Hz and 4980.1 Hz in the ^{1}H, ^{15}N and ^{13}C dimensions respectively. Typically 70-90 t_1 increments were acquired with 48 scans per increment. Spectra were referenced to an intrinsic peak at 0.15 ppm in the ^{1}H dimension and indirectly using the experimentally determined frequency ratio for ^{15}N (0.101329118) and ^{13}C (0.251449519 (T-300K) x 1.04 x 10 e^{-9}) (Wishart *et al.*, 1995).

7.3.3 CHEMICAL SHIFT ASSIGNMENTS

Chemical shift assignments of free IGF-I were made based on sequential alignment of strips from a 3D HNCA spectrum. The derived chemical shift list was then transferred to both HSQC spectra of ^{15}N-IGF-I acquired at 37 °C, pH 4.9 for comparison with the literature assignments and TROSY spectra of ^{2}H/^{15}N-IGF-I acquired at 37 °C, pH 4.8 for comparison with chemical shift assignments of IGF-I in complex with Trx^{1-279}IGFBP-2HIS. Assignment of the

resonances of complexed IGF-I ligand were similarly made from the HNCA and transferred to the TROSY spectrum acquired at 37 °C, pH 4.8. Chemical shift assignments for IGF-II were based on those reported by Torres *et al.*, 1995. Chemical shift assignments reported in this study were compared with values in the literature and in the databases: BioMagResBank (BMRB: www.bmrb.wisc.edu) and Protein Data Bank (PDB: www.rcsb.org/pdb).

7.4 RESULTS

IGF molecules are difficult to study structurally because of regions of high mobility, conformational averaging and aggregation at millimolar concentrations. Because of these problems, the most serious of which is aggregation, IGF-I and IGF-II yield poor quality NMR spectra at pH values above 3.0. Sato and co-workers reported an improvement in IGF-I spectral quality upon addition of 10 % acetic acid (Sato *et al.*, 1992) and 20 % acetic acid (Sato *et al.*, 1993), although the same was not true for IGF-II spectra (Torres *et al.*, 1995). Attempts to crystallize IGF have only recently been successful and only as stabilized complexes (Żesławski *et al.*, 2001; Vajdos *et al.*, 2001).

The first step in defining the IGFBP binding site on IGF-I and IGF-II was to record a series of 2D ^{1}H-^{15}N NMR spectra (described in Section 7.3.2). This study involved analysis of both ^{15}N- and $^{2}H/^{15}N$-labelled IGF-I and IGF-II. NMR spectra of IGF-I and IGF-II complexed to Trx^{1-279}IGFBP-2HIS were then acquired at pH 5 (or close to) to ensure near wildtype binding kinetics at physiological temperature (determined by BIAcore analysis as described in Section 5.4.5). Furthermore, equimolar concentrations of IGF ligand to IGFBP (around 0.5 mM) ensured that 99.98 % of IGF was bound in solution (assuming K_D 10 nM (Section 4.4.1) based on Equation 7.1).

Equation 7.1

$$K_D\ (nM) = \frac{(ConcA - ConcAB)(ConcB - ConcAB)}{ConcAB}$$

Where: A + B ↔AB equilibrium

7.4.1 COMPARISON OF DEUTERATED AND PROTONATED SAMPLES

Deuteration of proteins has been used in a number of structural studies to improve spectral sensitivity and resolution and is particularly useful for resonance assignment of high molecular weight proteins (reviewed by Goto and Kay, 2000; Gardner and Kay, 1998). Incorporation of ^{2}H to various levels eliminates many of the relaxation pathways that would otherwise be present in fully protonated samples and is particularly beneficial for TROSY experiments (Salzmann *et al.*, 1998).

In this study, IGF-I and IGF-II were labelled with ^{15}N- and $^{2}H/^{15}N$- (50 % $^{2}H_2O$ in growth media as described in Section 5.3.1). The quality of HSQC spectra for the deuterated IGF-I sample was significantly improved compared to the fully protonated sample (Figure 7.2a and 7.2b). The broad peaks evident in the spectrum of ^{15}N-IGF-I (Figure 7.2 box A) are sharpened significantly upon deuteration of the ligand and indeed, several additional peaks can be observed (Figure 7.2 boxes B and C). Generally, for a monomeric protein of 7 kDa, deuteration would be of limited benefit to spectral resolution. In this study however, the effective molecular mass of the sample was increased by aggregation of IGF-I and IGF-II and consequently, line widths are broadened and spectral resolution reduced. Complex formation with Trx^{1-279}IGFBP-2HIS would further compromise spectral resolution; hence TROSY experiments were performed with deuterated ligand as discussed in the following section.

7.4.2 COMPARISON OF HSQC VS TROSY SPECTRA

TROSY experiments are important for resonance assignment and structure determination of high molecular weight proteins and have greatly extended the size limitations of NMR spectroscopy. In this study, the TROSY spectrum of ^{15}N-IGF-I was much improved over the HSQC spectrum of the equivalent sample recorded at 600 MHz, pH 4.8 and 30 °C,

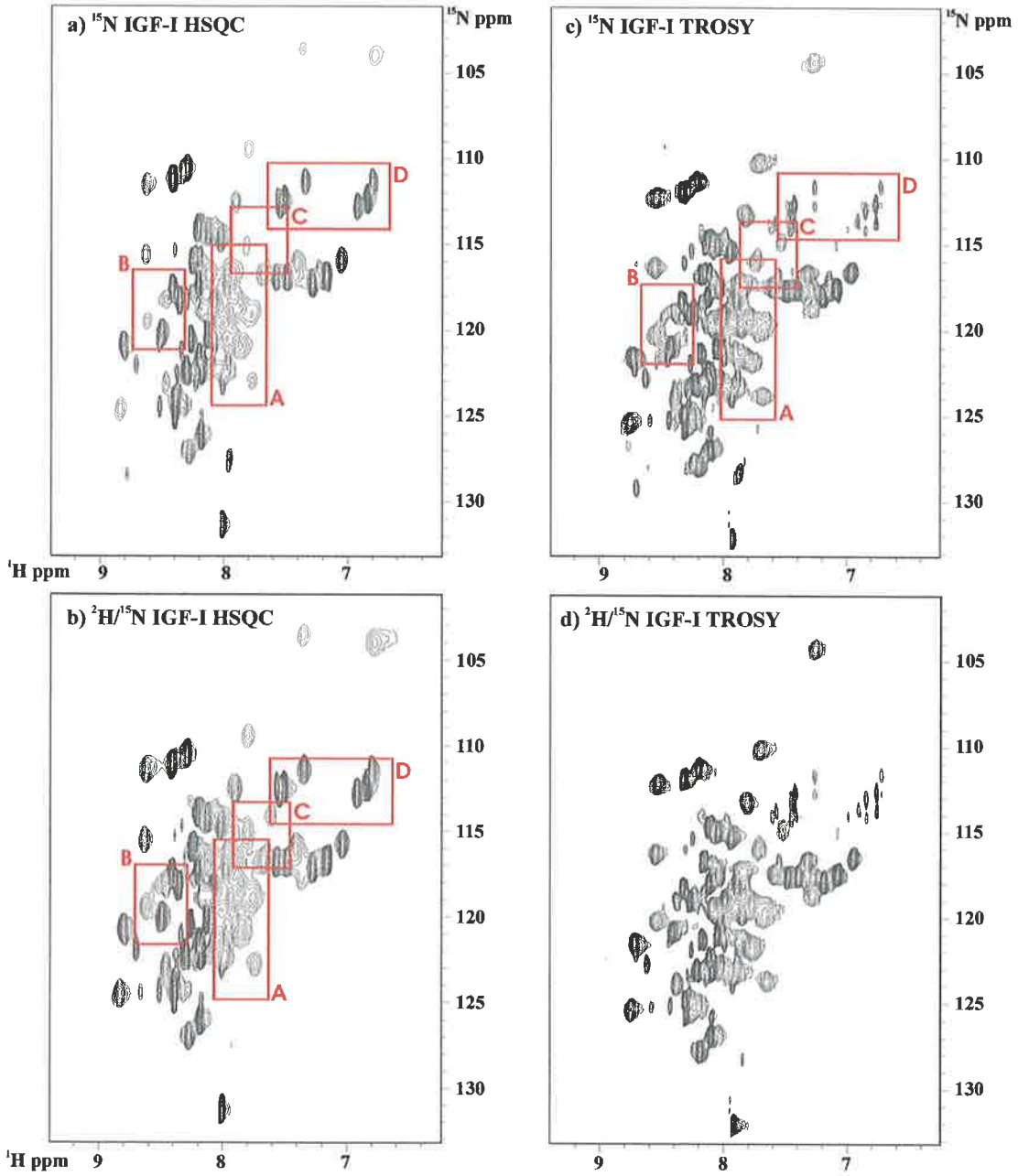

Figure 7.2 HSQC and TROSY spectral quality improved with deuterated ^{15}N IGF-I
Spectra of ^{15}N IGF-I (a and c) and ^{2}H/^{15}N IGF-I (b and d) were acquired on a Bruker DRX-600 spectrometer at 30 °C, pH 4.9. HSQC spectra (a and b) and TROSY spectra (c and d) were recorded for comparison of spectral quality. Box A depicts broad regions of the ^{15}N IGF-I HSQC spectrum (a) which were improved in the TROSY spectrum (c) and boxes B and C indicate regions where additional peaks were observed due to improved spectral quality. Box D indicate side chain resonances. This figure was prepared in XEASY (Bartels *et al.*, 1995).

(Figure 7.2a and 7.2c). As discussed above in Section 7.4.1, IGF molecules are within the size limitations of NMR spectroscopy, but aggregation compromises spectral resolution as the ligand behaves as a larger molecular weight protein. Therefore, TROSY based experiments are beneficial for the study of IGF-I and IGF-II. Indeed, the resolution of the peaks defined in box A of Figure 7.2 is greater in the TROSY spectrum of ^{15}N-IGF-I than in the HSQC spectra of either protonated or deuterated ligand. Furthermore, the side-chain resonances of IGF-I are weaker in the TROSY spectra than in the HSQC spectra of the equivalent samples (Figure 7.2 box D). The TROSY spectrum of ^{2}H/^{15}N-IGF-I was only slightly improved over the protonated sample.

TROSY spectra were required following addition of Trx$^{1-279}$IGFBP-2HIS. The effective increase in molecular weight of the sample resulted in slow tumbling of the molecule, which contributed to line broadening and increased viscosity. Limited information could be derived from HSQC spectra of the complex as many of the resonances were no longer evident (results not shown). TROSY spectra of deuterated ^{15}N-IGF-I and ^{15}N-IGF-II complexed to Trx$^{1-279}$IGFBP-2HIS however, were successfully recorded at 600 MHz and the expected number of resonances was observed for each ligand (Figure 7.3 and Figure 7.20).

7.4.3 IDENTIFICATION OF IGF-I CHEMICAL SHIFT PERTURBATIONS UPON INTERACTION WITH TRX$^{1-279}$IGFBP-2HIS

7.4.3.1 IGF-I Chemical Shift Assignments

Two-dimensional HSQC and TROSY spectra were acquired for free ^{15}N- and ^{2}H/^{15}N-IGF-I at 37 °C pH 4.9 and pH 5, respectively. The spectra acquired in this study are of high quality, but characteristic of the IGF molecules, the spectra were not well dispersed and significant overlap of resonances made chemical shift assignments difficult (Figure 7.3). Furthermore, both sharp, well-resolved peaks (e.g. Q15, G32 and A70) and broader, poorly defined peaks (e.g. F16, V44 and R55) were observed (see Figure 7.3).

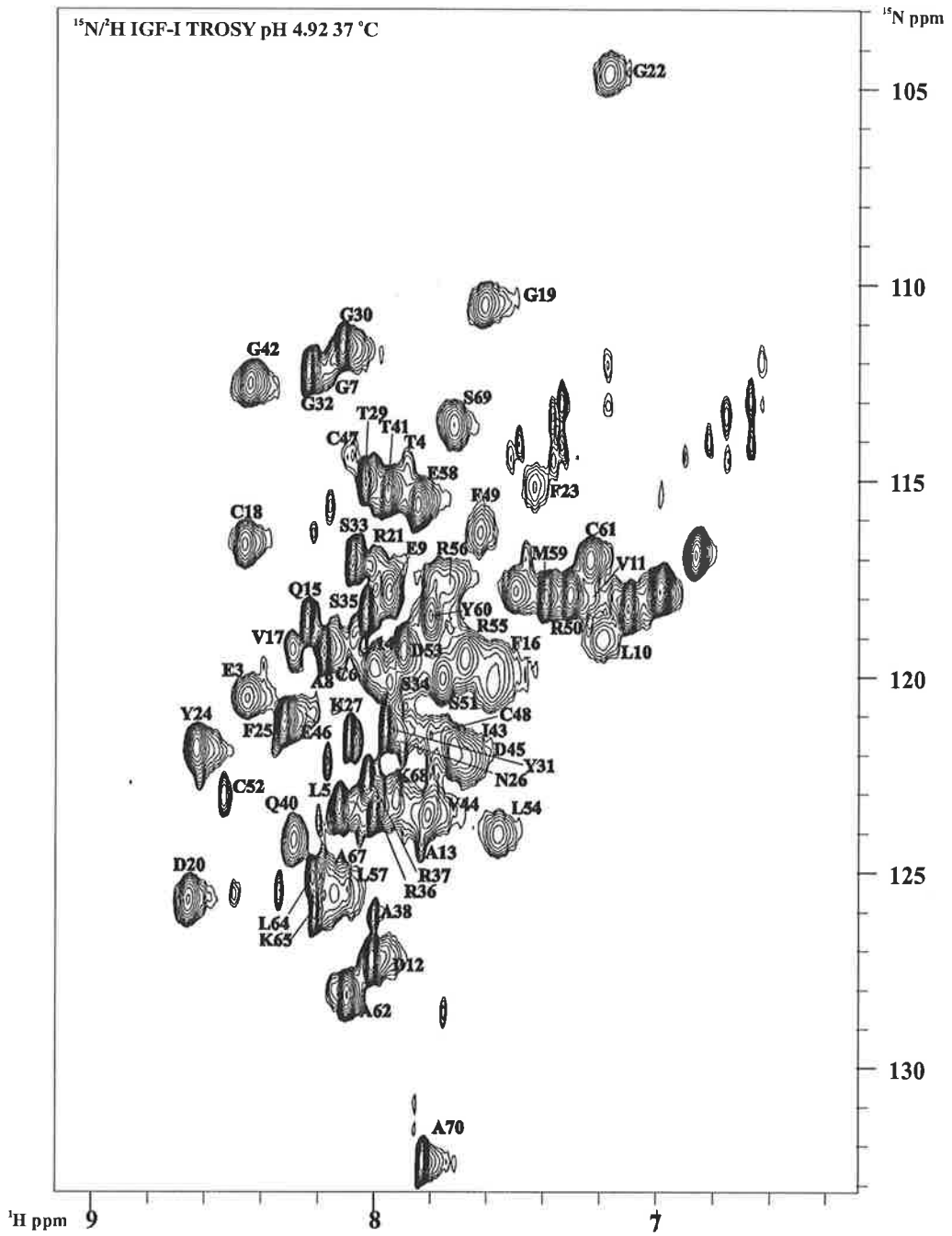

Figure 7.3 TROSY spectrum of $^{2}H/^{15}N$ IGF-I with chemical shift assignments
Contour plot of a fully assigned 600 MHz 2D ^{1}H-^{15}N TROSY spectrum. Spectra were recorded on a 0.5 mM solution of partially deuterated ^{15}N-IGF-I in acetate buffer + 5 % D_2O at 37 °C, pH 4.9. All residues are shown except Gly1 and the proline residues 2, 28, 39, 63 and 66. Additional unlabelled peaks are either side chain resonances or arise from contamination by the leader sequence. This figure was prepared in XEASY (Bartels *et al.*, 1995).

There are significant differences among chemical shift values reported in the literature for IGF-I (Cooke *et al.*, 1991 (PDB 2GF1); Sato *et al.*, 1992 (PDB 1BQT)); Long-[Arg-3]-IGF-I (Laajoki *et al.*, 1997 (BMRB 4494) and Long-[Leu-60]-IGF-I (Laajoki *et al.*, 1999 (BMRB 4278)). Variations between chemical shift values reported by Cooke and co-workers (1991) and Sato and co-workers (1992) are small and probably due to the different temperatures at which the spectra were acquired (50 °C pH 2.9 and 40 °C pH 3, respectively)(Figure 7.4). The greatest variation in chemical shift values between Cooke *et* al., (1991) and Sato *et al.*, (1992) is 0.11 ppm for Asp20.

The proton chemical shifts published by Laajoki and co-workers (1997) for Long-[R-3]-IGF-I vary significantly from the earlier studies of native IGF-I (Cooke *et al.*, 1991; Sato *et* al., 1992), more so than would be expected for variation in temperature (30 °C) and pH (pH 4.1)(Figure 7.4). This was despite the fact that the 13 amino acid N-terminal extension and mutation of Glu3Arg was reported to have little effect on the secondary structure of the IGF-I domain (Laajoki *et al.*, 1997). Significant chemical shift differences relative to those reported by Sato *et al.*, (1992) include:

Cys6	-0.29 ppm	Asp20	-0.22 ppm	Cys48	0.55 ppm
Gly7	0.75 ppm	Tyr24	-0.28 ppm	Cys52	0.86 ppm
Ala8	-0.58 ppm	Phe25	-0.37 ppm	Leu54	0.76 ppm
Leu10	-0.52 ppm	Lys27	-0.38 ppm	Leu57	-0.50 ppm
Gln15	-0.27 ppm	Ser35	-0.29 ppm	Glu58	-0.20 ppm
Phe16	-0.20 ppm	Gly42	-0.26 ppm	Leu64	-0.18 ppm
Val17	-0.25 ppm	Val44	-0.27 ppm	Lys65	-0.21 ppm
Cys18	-0.18 ppm	Glu46	-0.36 ppm		

The chemical shift values for Long-[Arg-3]-IGF-I (BMRB 4494) also differ significantly from those submitted to the BMRB for Long-[Leu-60]-IGF-I (Laajoki *et al.,* 1999) (Figure 7.5). Variations from native ligand therefore are not likely to be attributed solely to the thirteen amino acid N-terminal extension peptide.

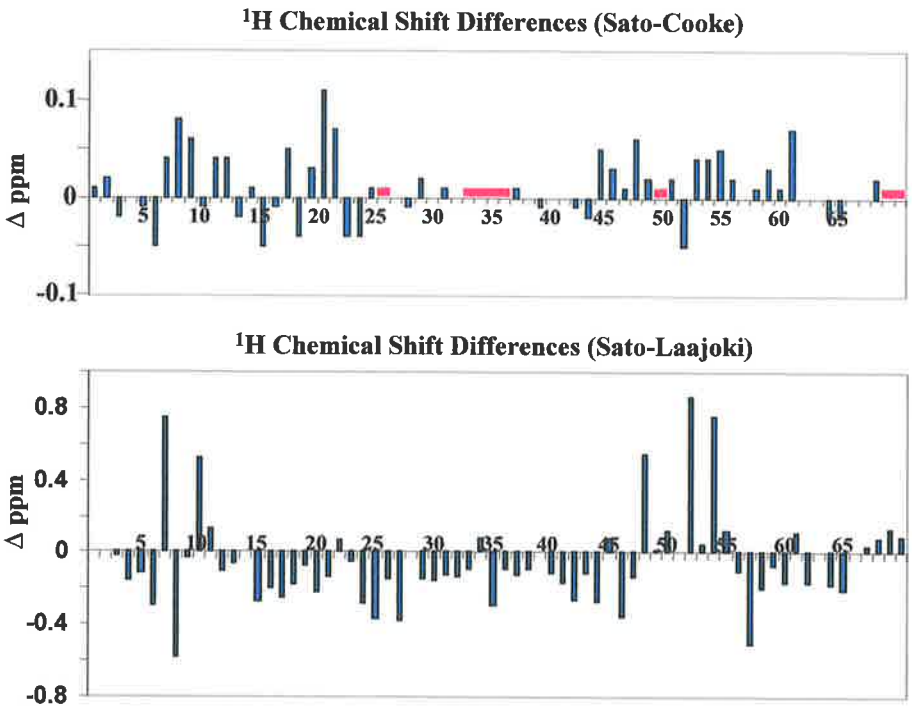

Figure 7.4 Differences in published proton chemical shift assignments for IGF-I
Variations in ^{1}H chemical shift assignments by Cooke *et al.*, 1991, Sato *et al.*, 1992 and Laajoki *et al.*, 1997. Graphs are presented relative to chemical shift values reported by Sato *et al.,* 1992. The red lines indicate residues not reported by Cooke and co-workers (1991).

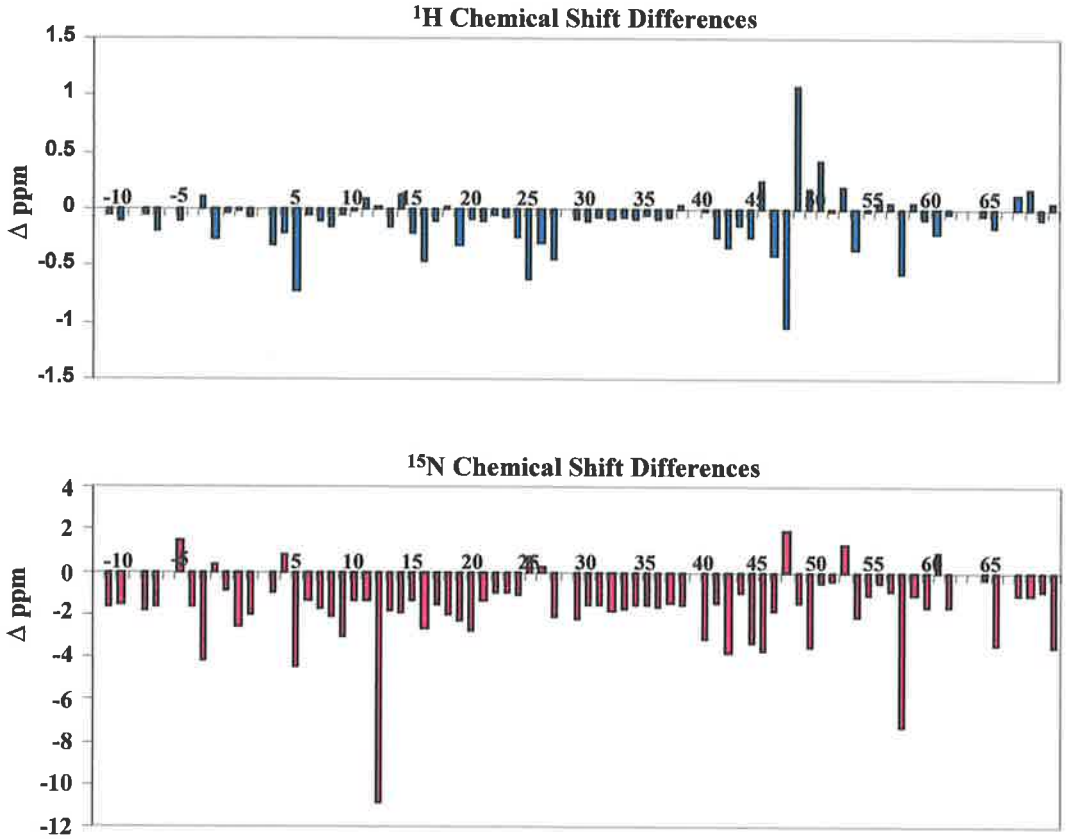

Figure 7.5 Differences in published proton chemical shift assignments for IGF-I
Variations in ^{1}H and ^{15}N chemical shift assignments for Long-[R-3]-IGF-I (Laajoki *et al.*, 1997) and Long-[L-60]-IGF-I (Laajoki *et al.*, 1999) are displayed as bar graphs relative to chemical shift values reported for Long-[R-3]-IGF-I. Published chemical shift assignments for Long-[R-3]-IGF-I and Long-[L-60]-IGF-I were obtained from the BioMagResBank database with accession numbers 4494 and 4278, respectively.

The ambiguities in reported chemical shift values were resolved in this study by analysis of a 3D HNCA experiment (acquired at 37 °C pH 4.86). The significant resonance overlap in both the amide nitrogen and proton dimensions of our HSQC and TROSY spectra (Figure 7.2) could not be adequately resolved by ^{15}N-edited Nuclear Overhauser Effect Spectroscopy (NOESY) experiments. These experiments define NOE interactions between the NH protons along the F_2 axis and the C_αH protons along the F_1 dimension. Although this experiment has the potential to resolve a large number of cross peaks, many of the cross peaks have identical chemical shifts in one or the other dimension and hence could not be resolved in this study. Three-dimensional experiments however, allow sequential assignment based solely on through-bond connectivities via heteronuclear couplings (Ikura *et al.*, 1990). The types of connectivities observed in a 3D HNCA experiment (Figure 7.6) are entirely predictable and provide an independent method for linking the resonances of one residue with those of the adjacent residue, thus eliminating ambiguities in the sequential assignment. In this study, the 3D HNCA was ordered into columns (referred to as strips) based on ^{15}N- chemical shifts such that ideally one amino acid was represented per strip. The strip was selected based on the nitrogen frequency and the amide proton chemical shift, however some amino acids with very close ^{15}N chemical shifts reside in the same strip due to poor resolution in the nitrogen dimension (e.g Phe23 and Asp45). Sequential amino acid residues were determined by the presence of strong cross peaks present in the 3D spectra.

Therefore chemical shift assignments for IGF-I were made by aligning cross peaks from the 3D HNCA experiment (Figure 7.7) and transferring the assignments to cross peaks in a TROSY spectrum of IGF-I recorded at 37 °C, pH 4.8 (as described in Section 7.3.2)(Figure 7.3). Chemical shift resonances were unambiguously assigned for all IGF-I residues except for the amino terminal glycine residue and the proline residues Pro2, Pro28, Pro39, Pro63 and Pro66, which do not give rise to chemical shift resonances in 2D ^{1}H-^{15}N spectra (Table 7.1).

The secondary structure of IGF-I, based on the chemical shift assignments made in this study, is consistent with published structures. The C_α chemical shifts from the HNCA

Correlation of Nuclei in 3D HNCA Experiments

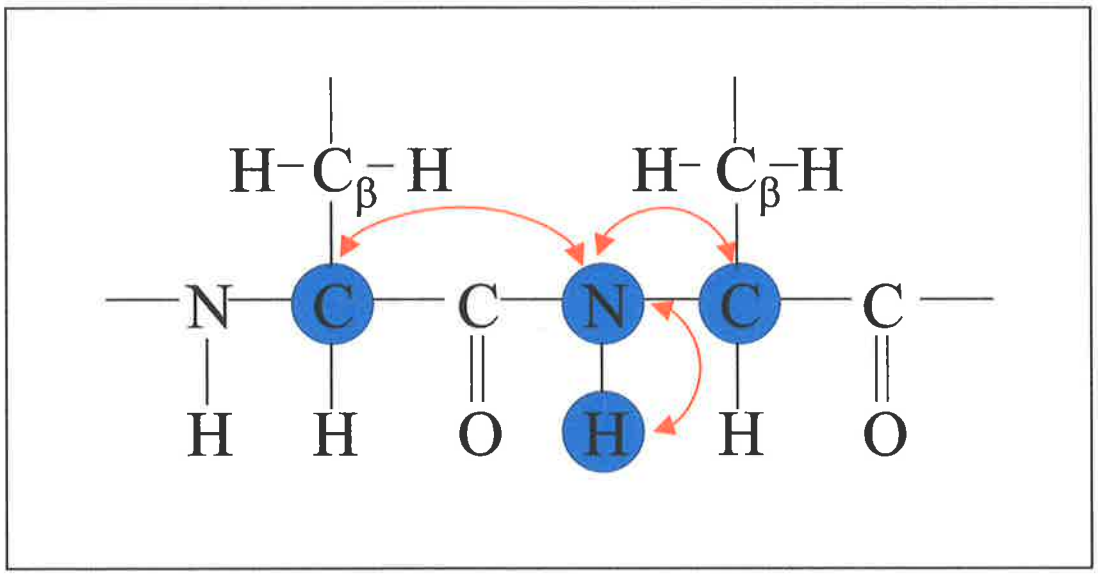

Figure 7.6 Correlation of nuclei in 3D HNCA experiments
A schematic representation of the nuclei that are correlated in the 3D HNCA experiment. Nuclei for which the chemical shift is measured is the 3D experiment are marked in blue circles. Magnetisation transfer in these experiments is marked by the curved red lines and the direction of the transfer is marked by arrows.

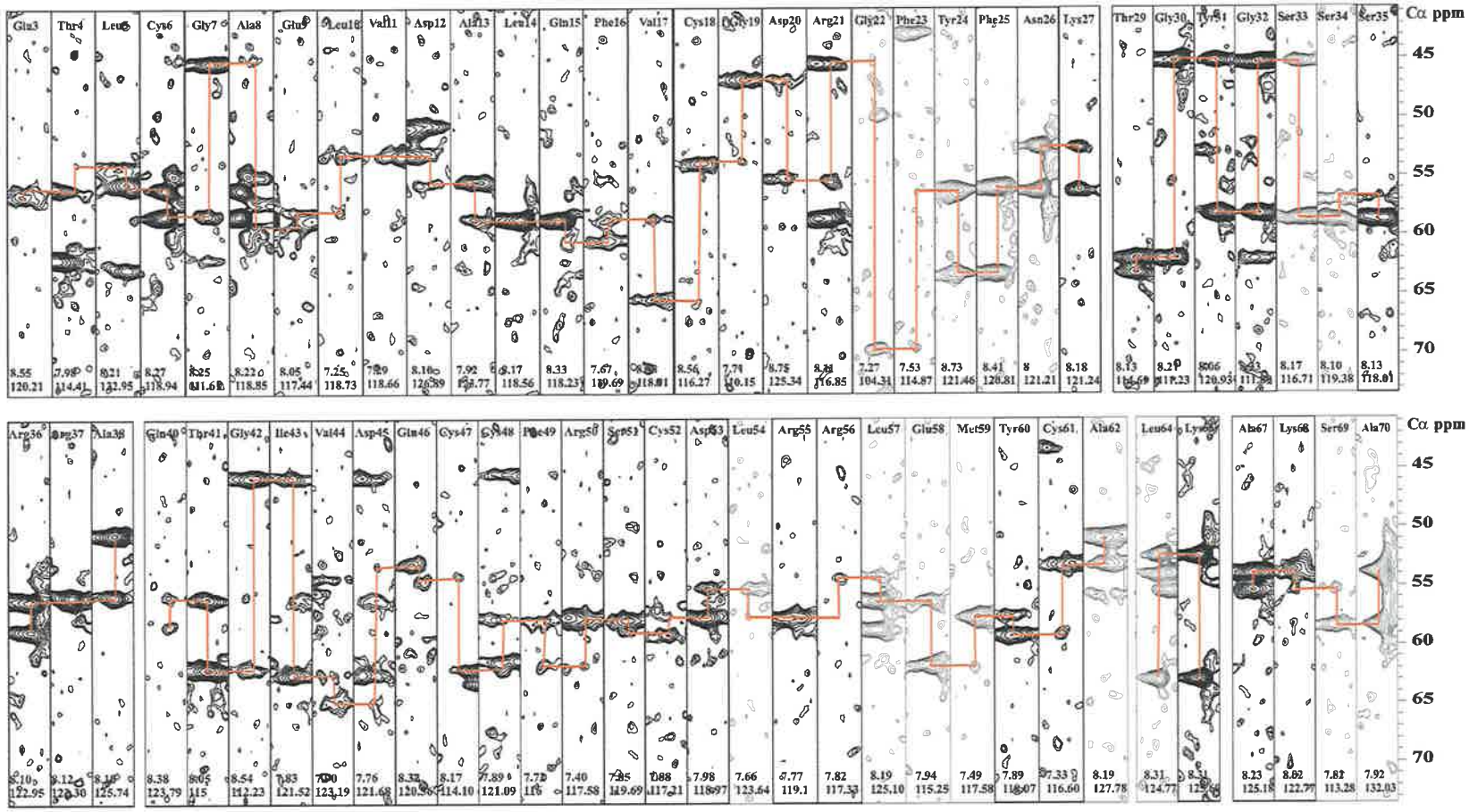

Figure 7.7 Strip plot of $^{2}H^{/15}N^{/13}C$-IGF-I 3D-HNCA experiment

Strip plot of $^{2}H^{/15}N^{/13}C$IGF-I. Three-dimensional HNCA data was acquired on a Bruker DRX-600 spectrometer at 37°C and pH 4.82. Data was analysed using XEASY (Bartels *et al.*, 1995). Strips are shown with cross peaks indicated by connecting red lines. Amino acid residues presented in each strip are indicated at the top of the strip. The ^{1}H and ^{15}N chemical shift values (ppm) are indicated at the bottom of the strips.

TABLE 7.1 CHEMICAL SHIFT ASSIGNMENTS FOR IGF-I

		Free IGF-I		Complexed IGF-I	
Residue	**Residue Name**	**^{1}H**	**^{15}N**	**^{1}H**	**^{15}N**
1	Gly				
2	Pro				
3	Glu	8.55	120.2		
4	Thr	7.98	114.4		
5	Leu	8.21	123.0	8.33	122.6
6	Cys	8.27	118.9	8.37	118.2
7	Gly	8.25	111.6	8.43	110.2
8	Ala	8.22	118.9	8.34	117.9
9	Glu	8.05	117.4		
10	Leu	7.25	118.7		
11	Val	7.29	118.7		
12	Asp	8.11	126.9	8.29	126.8
13	Ala	7.92	123.8		
14	Leu	8.17	118.6	8.25	117.0
15	Gln	8.33	118.2	8.43	117.2
16	Phe	7.67	119.7		
17	Val	8.38	118.9		
18	Cys	8.56	116.3		
19	Gly	7.71	110.2		
20	Asp	8.75	125.3		
21	Arg	8.11	116.8	8.25	115.6
22	Gly	7.27	104.3		
23	Phe	7.53	114.9		
24	Tyr	8.73	121.5		
25	Phe	8.41	120.8	8.52	119.8
26	Asn	8.00	121.2	8.28	120.2
27	Lys	8.18	121.2	8.35	120.7
28	Pro				
29	Thr	8.13	114.7	8.22	113.3
30	Gly	8.21	111.3	8.32	110.5
31	Tyr	8.06	120.9	8.16	119.5
32	Gly	8.33	111.9	8.44	110.9
33	Ser	8.17	116.7	8.28	116.3
34	Ser	8.10	119.4	8.27	117.9
35	Ser	8.13	118.0	8.27	117.7
36	Arg	8.10	123.0	8.22	122.1
37	Arg	8.12	122.3	8.22	120.9
38	Ala	8.10	125.7	8.21	125.6
39	Pro				
40	Gln	8.38	123.8	8.49	122.6
41	Thr	8.05	115.0	8.14	113.7
42	Gly	8.54	112.2	8.57	111.3
43	Ile	7.81	121.5	7.95	120.8
44	Val	7.90	123.2		
45	Asp	7.76	121.7		
46	Glu	8.32	120.6	8.43	119.1
47	Cys	8.17	114.1	8.27	113.9

* Assigned from a 3D HNCA experiment using $^{2}H/^{15}N/^{13}C$-IGF-I (37 °C, pH 4.8). Chemical shifts correspond to cross peaks in the TROSY spectra acquired at 37 °C, pH 4.9 (Figure 7.3).

TABLE 7.1 CHEMICAL SHIFT ASSIGNMENTS FOR IGF-I (cont)

		Free IGF-I		Complexed IGF-I	
Residue	**Residue Name**	**^{1}H**	**^{15}N**	**^{1}H**	**^{15}N**
48	Cys	7.89	121.1	8.00	120.2
49	Phe	7.72	116.0		
50	Arg	7.40	117.6		
51	Ser	7.85	119.7		
52	Cys	7.88	117.2		
53	Asp	7.98	119.0		
54	Leu	7.66	123.6		
55	Arg	7.77	119.1		
56	Arg	7.82	117.3		
57	Leu	8.19	125.1	8.21	122.6
58	Glu	7.94	115.2		
59	Met	7.49	117.6		
60	Tyr	7.89	118.1		
61	Cys	7.33	116.6		
62	Ala	8.19	127.8		
63	Pro				
64	Leu	8.31	124.8	8.40	124.0
65	Lys	8.31	125.6	8.40	124.7
66	Pro				
67	Ala	8.23	125.2	8.38	123.5
68	Lys	8.02	122.8	8.09	121.6
69	Ser	7.82	113.3		
70	Ala	7.92	132.0	8.04	131.3

* Assigned from a 3D HNCA experiment using ^{2}H/^{15}N/^{13}C-IGF-I (37 °C, pH 4.8). Chemical shifts correspond to cross peaks in the TROSY spectra acquired at 37 °C, pH 4.9 (Figure 7.3).

experiment were plotted as an indication of predicted secondary structure (Wishart *et al.,* 1992). As shown in Figure 7.8, the chemical shift index (CSI) plot is indicative of α-helices in positions consistent with published IGF-I structures. Indeed, the lack of dispersion of nitrogen chemical shifts in the 2D spectra is further indicative of the helical structure of IGF.

In contrast to the 26 amino acid assignments made for the free ligand at 30 °C by Jansson and co-workers (1998), all of the possible 64 amino acid resonances were identified in the present study. Jansson and co-workers assigned 84 % of HN, N, $^{13}C_{\alpha}$ and $^{13}C_{\beta}$ chemical shifts at 50 °C and pH 3.4 in free IGF-I, but the spectral quality for the complex was improved by lowering the temperature to 30 °C, which permitted only partial assignment of the free ligand (viz: Pro2-Gly3, Gly7, Gly19, Pro28-Thr41, Ser51, Met59, Pro63-Ala70). Unfortunately, the chemical shift assignments of Jansson and co-workers (1998) are not available either through the literature or database deposition.

The chemical shift assignments made in this study were largely consistent with the corresponding residues reported in the literature. The HNCA-connectivities determined in this study unambiguously defined chemical shifts for residues where discrepancies existed in the literature. The proton assignments varied consistently from those reported by Sato *et al.*, (1992) by approximately 0.2 ppm (Figure 7.9). The largest chemical shift differences were observed for Tyr24 (0.35 ppm), Phe25 (0.30 ppm), Glu46 (0.44 ppm), Cys52 (–1.0 ppm) and Leu54 (-0.69 ppm). The proton chemical shifts assigned in this study also varied from Laajoki and co-workers (1997) for Gly7 (0.51 ppm), Ala8 (-0.76 ppm), Leu10 (0.37 ppm), Val17 (-0.32 ppm), Lys27 (-0.25 ppm), Ser35 (-0.25 ppm), Cys48 (0.53 ppm) and Lys68 (-0.20 ppm). In the nitrogen dimension, variations were observed for amino acid residues Ala8 (-11.5 ppm), Leu10 (-3.0 ppm), Arg21 (-2.9 ppm), Lys27 (-2.7 ppm), Gln 40 (2.3 ppm), Cys48 (3.9 ppm), Arg50 (-2.3 ppm), and Ser51 (6.4 ppm). Other chemical shifts varied by less than 0.16 ppm in the proton dimension and by less than 2 ppm in the nitrogen dimension (Figure 7.9). Other deviations in chemical shift assignments may be due to pH and temperature variations between experiments. Interestingly, some chemical shift values varied insignificantly in either

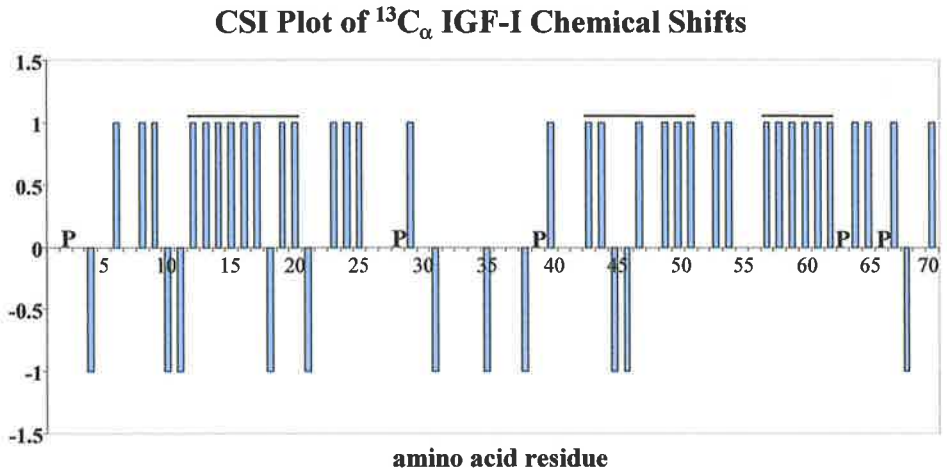

Figure 7.8 $^{13}C_{\alpha}$ chemical shift index plot for IGF-I chemical shift assignments
A chemical shift index (CSI) plot (Wishart *et al.,* 1992) was generated based on the $^{13}C_{\alpha}$ chemical shifts reported in this study. Chemical shifts were assigned based on analysis of a 3D HNCA spectrum acquired at 37 °C and pH 4.9. P indicates proline residues for which no assignments were made. As indicated by horizontal lines in the plot α-helices are predicted between amino acid residues 12-19, 43-51 and 57-62, which is consistent with the structure for IGF-I (α-helices 8-18, 42-48 and 54-61) (Cooke *et al.*, 1991; Sato *et al.*, 1992).

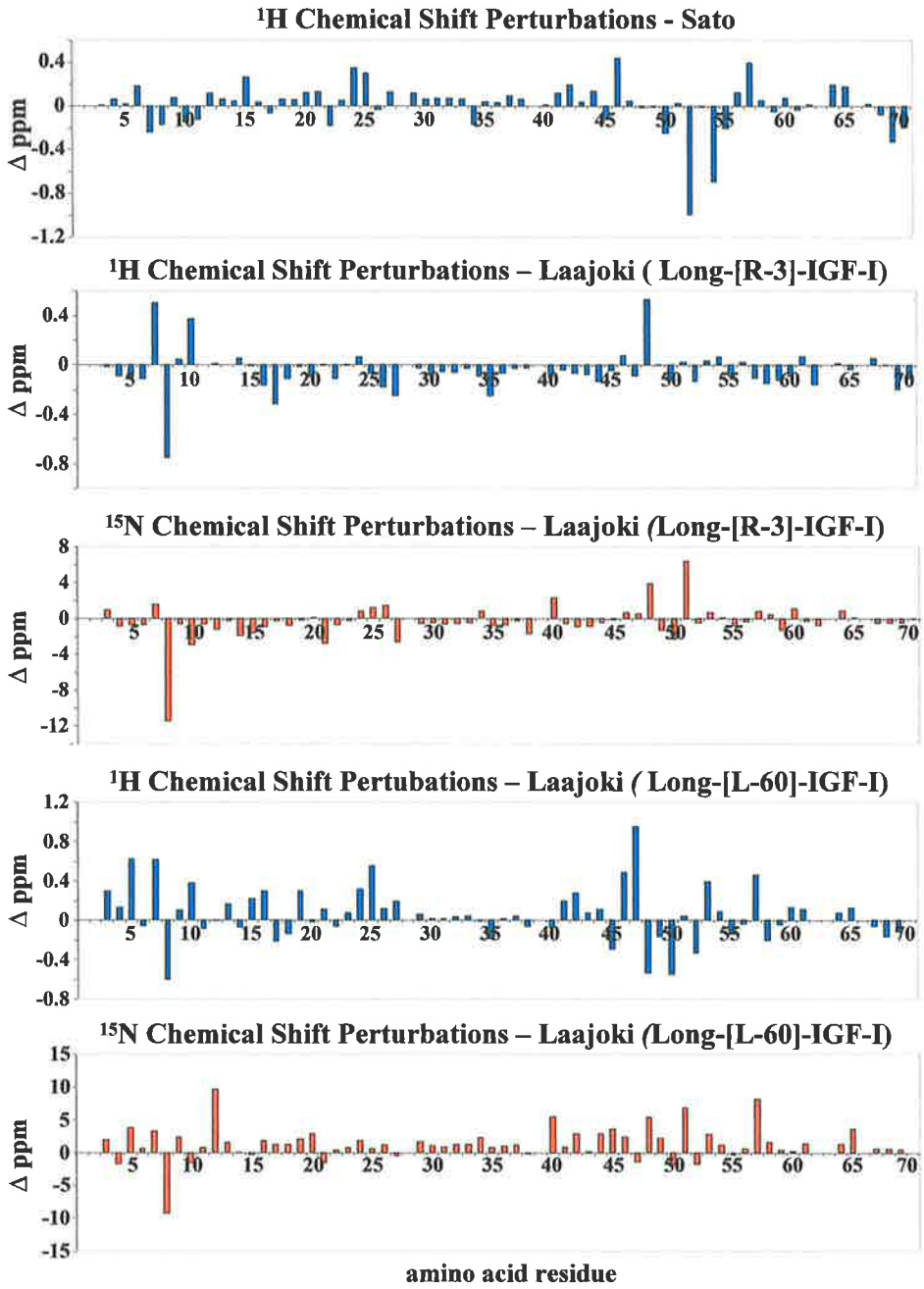

Figure 7.9 Comparison of chemical shift assignments of IGF-I with values in the literature The chemical shift assignments made for IGF-I in this study are compared to previously published chemical shift data by Sato *et al.,* 1992; Laajoki *et al.,* 1997 (Long-[R-3]-IGF-I) and Laajoki *et al.,* 1999 (Long-[L-60]-IGF-I). Graphs are plotted as the difference between chemical shift values derived in this study and values reported in the literature.

dimension from Laajoki's reported chemical shift values, including Gly19, Asp20, Arg54, Cys61, Lys65 and Ala70. Additional unassigned peaks in the spectra are most likely attributable to the minor leader contamination (< 7 %) in IGF-I preparations (discussed in Section 5.4.1).

One of the major anomalies between chemical shift assignments made in this study and those reported in the literature was the chemical shift assignments for Ala8 and Leu10 published by Laajoki *et al.*, 1997 (ΔHN: –0.76, Δ^{15}N: –11.45 and ΔHN: 0.37, Δ^{15}N: -2.97, respectively). The chemical shifts assigned to Ala8 and Leu10 by Laajoki and co-workers also differed from both Cooke *et al.* (1991) and Sato *et al.* (1992) by 0.5 ppm in the proton dimension (Figure 7.4). To interpret the anomalies in chemical shift assignments observed in the literature (particularly for Ala8 and Leu10), NMR spectra of IGF-I were acquired at various temperatures and pH values (pH 5 37 °C, 45 °C; pH 4.1 37 °C, 30 °C; pH 3.0 37 °C, 45 °C) (Figure 7.10). Interestingly, resonances corresponding to values reported by Laajoki *et al.* (1997) were not observed under any of the pH or temperature conditions investigated in this study. Furthermore, neither Cooke *et al.*, (1991) nor Sato *et al.*, (1992) reported resonances at corresponding chemical shift values.

It is possible that the chemical shift differences observed between the present study and those reported by Laajoki and co-workers (1997) are due to differences between the two molecules, in particular in a localised region at Ala8 and Leu10. Although the present study is largely in agreement with the chemical shift assignments made by Laajoki *et al.* (1997), analysis of 3D HNCA spectra of the free ligand support ^{1}H chemical shifts for Ala8 and Leu10 reported by both Cooke *et al.*, (1991) and Sato *et al.*, (1992) (ΔHN: -0.18 and -0.15, respectively). Although line widths of the resonance peak of Ala8 and Leu10 were extremely broad in this and other studies (Sato *et al.*, 1992), connectivities clearly exist (Figure 7.7).

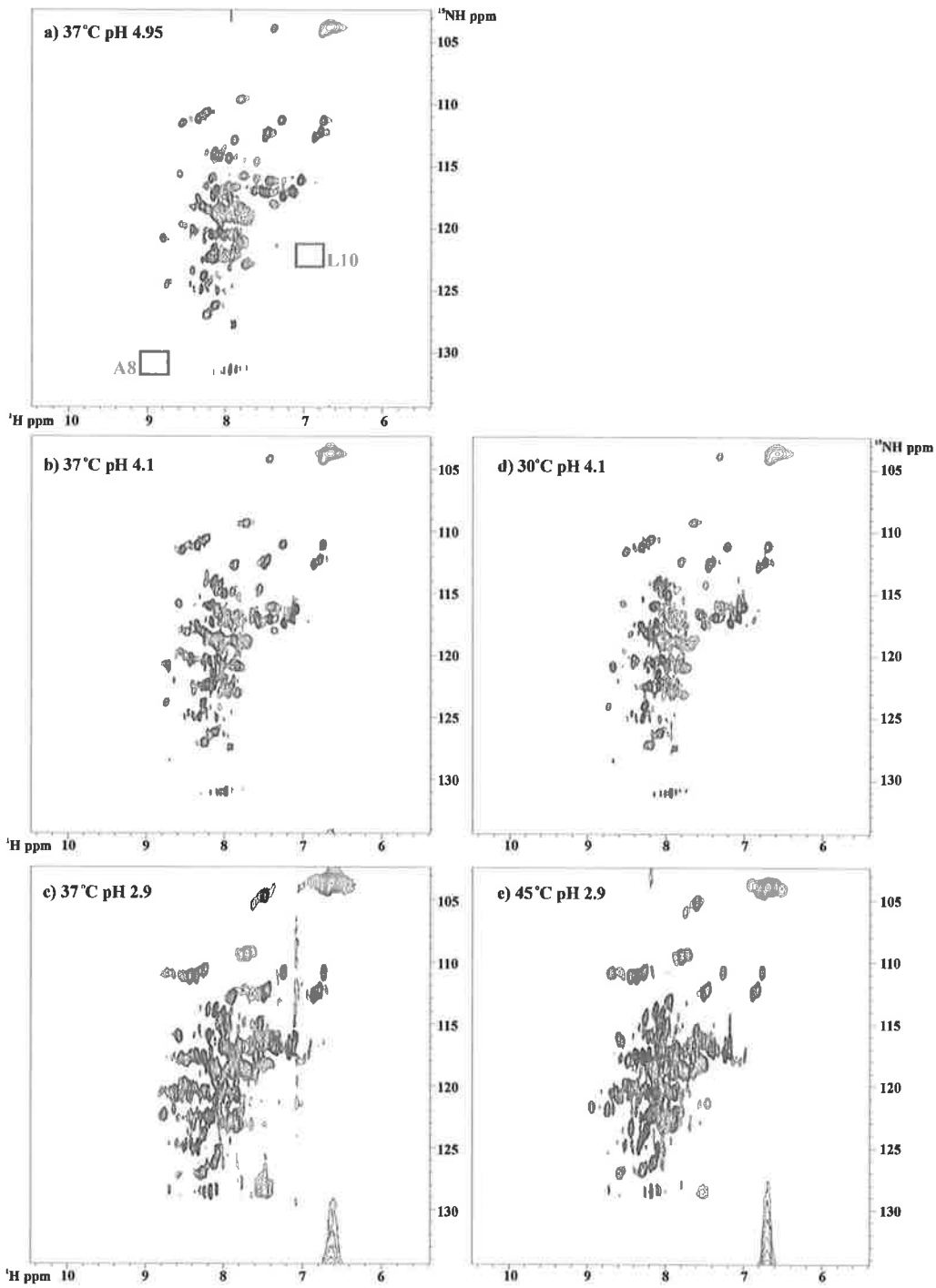

Figure 7.10 Temperature and pH titration of ^{15}N IGF-I
The spectral quality of ^{15}N IGF-I was compared in various HSQC experiments recorded at a) 37°C, pH 5.0, b) 37 °C, pH 4.1, c) 37 °C, pH 2.9, d) 30 °C, pH 4.1 and e) 45 °C, pH 2.9. Boxes represent chemical shifts of Ala8 (HN: 8.98 ^{15}N: 130.3) and Leu10 (HN: 6.88, ^{15}N: 121.7) reported by Laajoki *et al.*, 1997. Spectra were acquired at 500 MHz and processed in XWINNMR (Bruker) and plotted in XEASY (Bartels *et al.*, 1995).

7.4.3.2 Chemical Shift Assignments of IGF-I Complexed to Trx$^{1-279}$IGFBP-2HIS

TROSY spectra of IGF-I bound to Trx$^{1-279}$IGFBP-2HIS varied significantly from the free spectra and chemical shift assignments could not be readily transferred from one spectrum to the other (Figure 7.11). Therefore, the perturbation of IGF-I resonances upon binding of Trx$^{1-279}$IGFBP-2HIS was investigated by varying the pH of the sample to titrate between free and bound forms. NMR spectra were acquired at 600 MHz, 37 °C and various pH values (5.1, 3.8, 3.5 and 2.8) (Figure 7.12). There was slow exchange between free and bound forms of IGF-I resulting in two resonances for each state - that is bound and unbound forms. In comparison, fast exchange results in a single resonance peak that reflects the weighted average of the chemical shifts of the two individual states (Lian and Roberts, 1993). In this study, IGF-I remained in complex with Trx$^{1-279}$IGFBP-2HIS at pH 3.5 and perturbed resonances did not titrate between free and bound positions. At pH 2.8, the spectrum resembled that of the free ligand (Figure 7.12).

Partial chemical shift assignments of IGF-I in complex with Trx$^{1-279}$IGFBP-2HIS were derived from a 3D HNCA experiment with deuterated ^{13}C- and ^{15}N-labelled ligand. These experiments were performed in a Shigemi tube. This tube allowed the use of smaller sample volumes that effectively increased the concentration within the NMR coil. Upon collapsing the C_α dimension of the HNCA spectrum to resemble a 2D ^{1}H-^{15}N spectrum (e.g Figure 7.3), only the sharp resonances were visible (Figure 7.13). Therefore only partial chemical shift assignments could be made for IGF-I in complex with Trx$^{1-279}$IGFBP-2HIS (Figure 7.14). Furthermore, the observable resonances for the complexed IGF-I were not significantly perturbed from the free state. Resonances that were already broad in TROSY spectra were not distinguishable in the HNCA experiment. Consequently, assignments were made only for Leu5-Ala8, Asp12, Leu14-Gln15, Arg21, Phe25-Lys27, Thr29-Ala38, Gln40-Ile43, Glu46-Cys48, Leu57, Leu64-Lys65, Ala67-Lys68 and Ala70 (Table 7.1). These residues were not significantly perturbed compared with chemical shift assignments of the free ligand (as shown

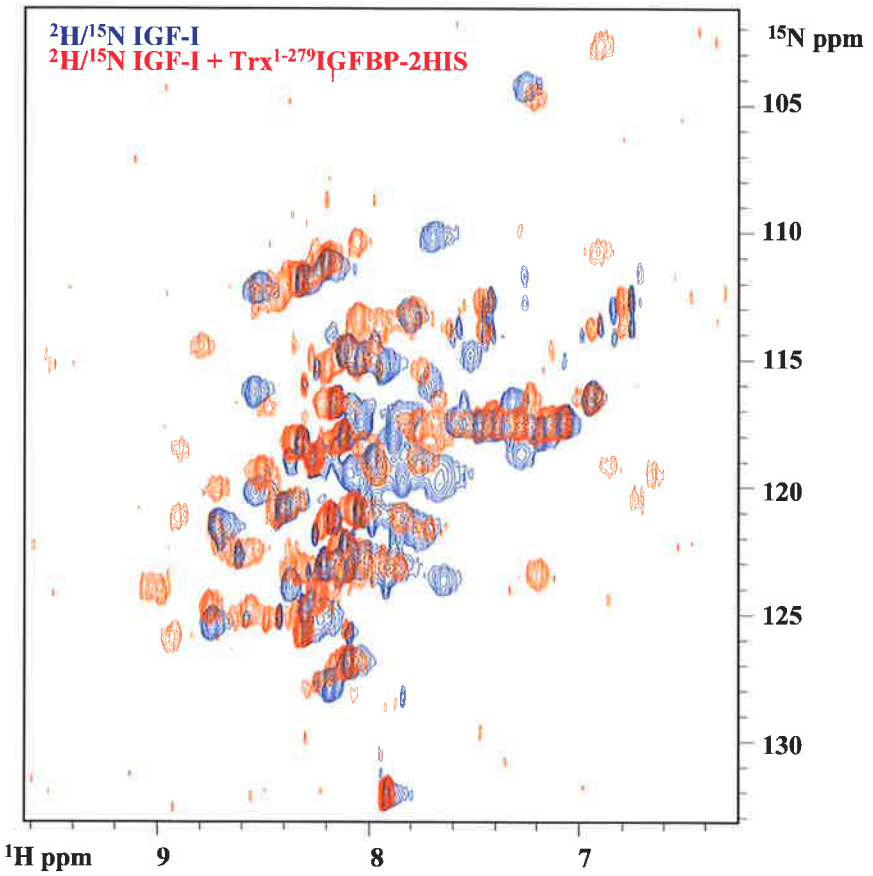

Figure 7.11 TROSY spectra of free IGF-I and IGF-I complexed to Trx$^{1-279}$IGFBP-2HIS
TROSY spectra of IGF-I were acquired at 600 MHz and 37 °C as described in Section 7.3.2. The spectra were derived from samples of free ligand at pH 5.1 (blue) or the complex at pH 4.8 (red). Spectra were referenced to an intrinsic peak at 0.15 ppm and overlaid for comparison using the XEASY program (Bartels *et al.*, 1995).

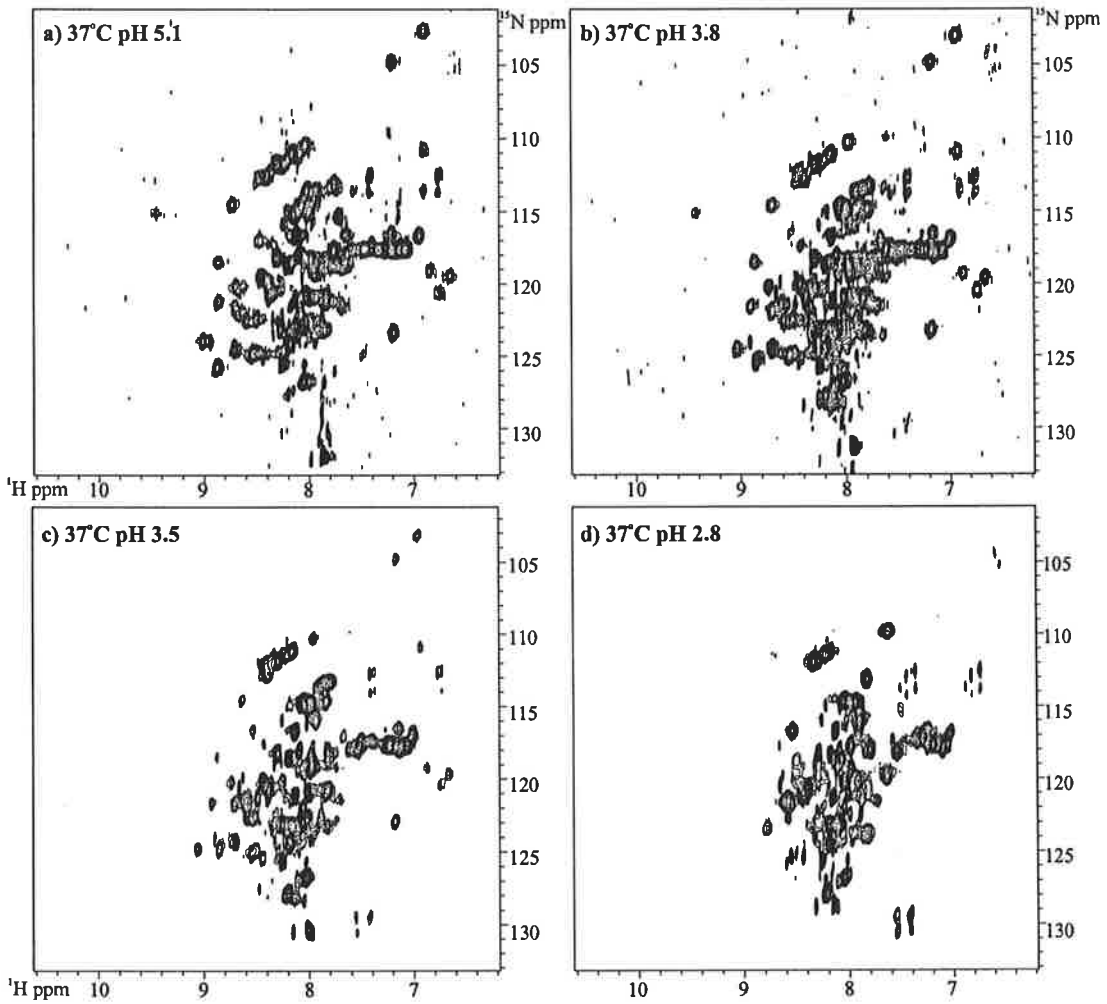

Figure 7.12 pH titration of $^{2}H/^{15}N$ IGF-I complexed to Trx^{1-279}IGFBP-2HIS
TROSY spectra of $^{2}H/^{15}N$ IGF-I complexed to Trx^{1-279}IGFBP-2HIS were acquired on a Bruker DRX-600 spectometer at 37°C and a) pH 5.1, b) pH 3.8, c) pH 3.5 and d) pH 2.8. Slow exchange between free and bound forms of IGF-I resulted in two resonances for each state. This figure was prepared in XEASY (Bartels *et al.*, 1995).

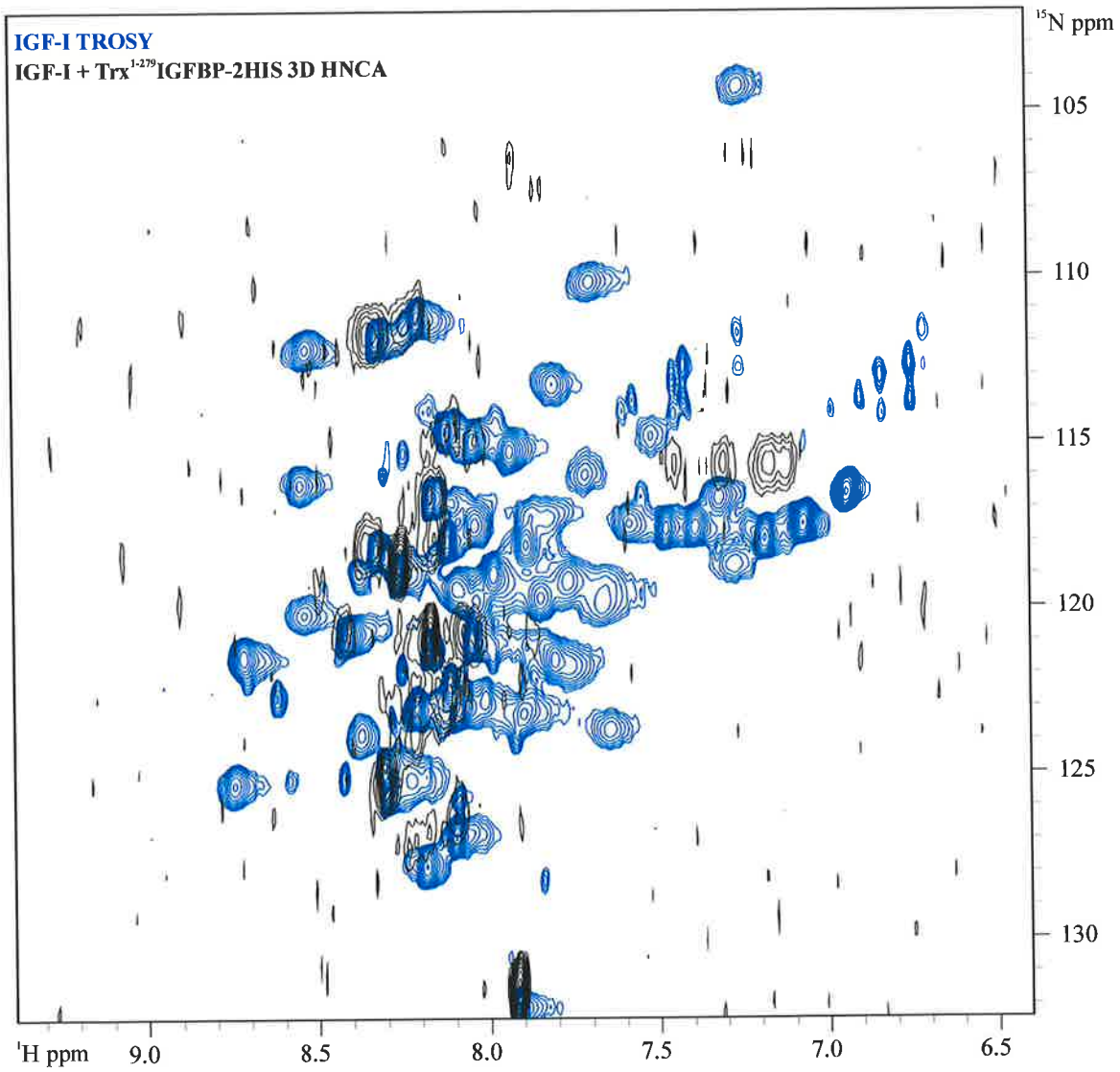

Figure 7.13 TROSY of free ligand overlaid with HNCA of IGF-I complexed with Trx^{1-279}IGFBP-2HIS

The TROSY spectrum of IGF-I acquired at 600 MHz, 37 °C and pH 5.0 (blue) has been overlaid with the 3D HNCA of $^{2}H/^{15}N/^{13}C$-IGF-I complexed to Trx^{1-279}IGFBP-2HIS acquired at 600 MHz, 37 °C pH 4.8 (black). The signal intensity of the HNCA is extremely weak and only the sharp well-resolved peaks are detected (as described in Section 7.4.3.1). This figure was prepared in XEASY (Bartels *et al.*, 1995).

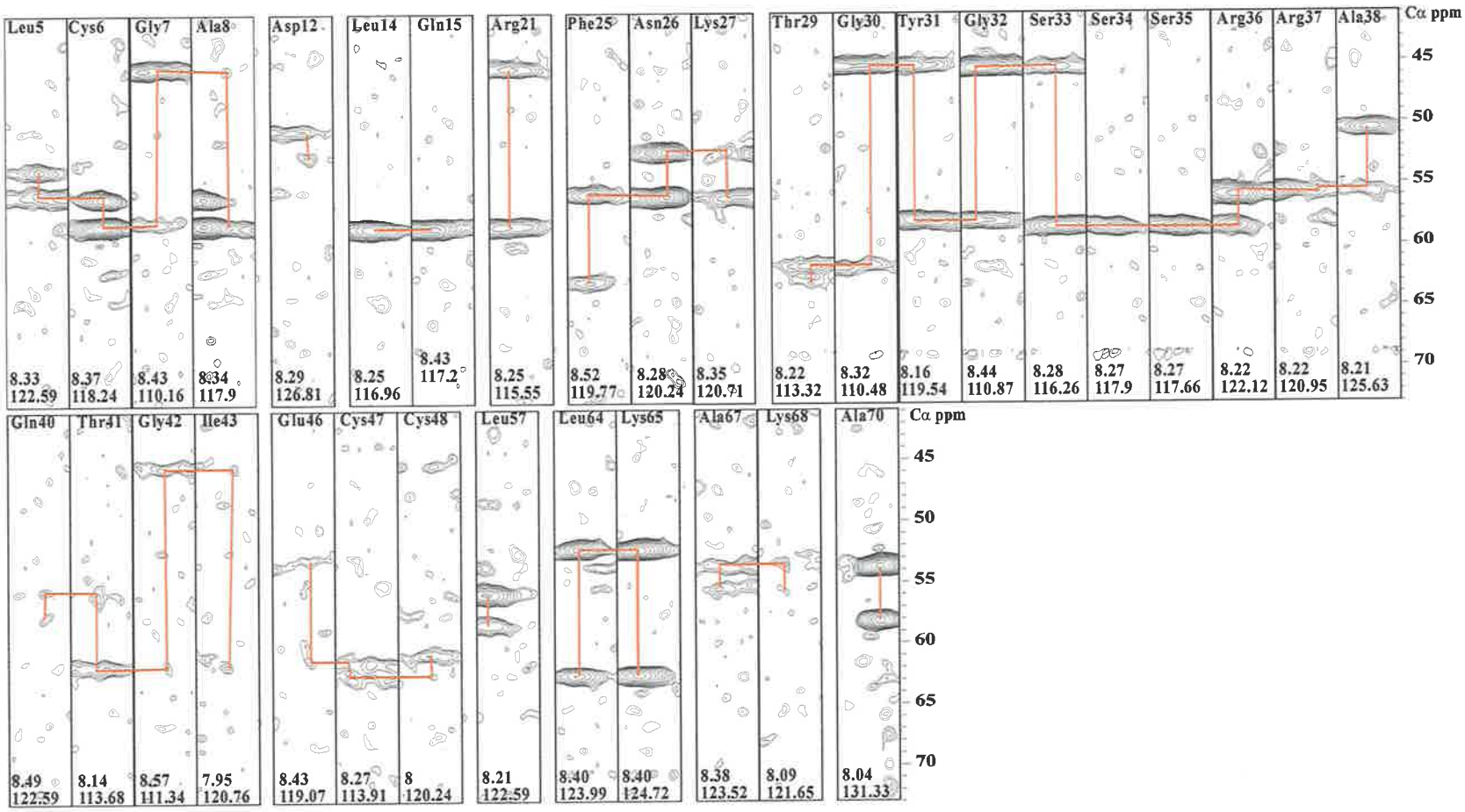

Figure 7.14 Strip plot of $^{2}H^{/15}N^{/13}C$ IGF-I complexed with Trx^{1-279}IGFBP-2HIS 3D HNCA experiment
Strip plot of $^{2}H^{/15}N^{/13}C$ IGF-I complexed to Trx^{1-279}IGFBP-2HIS. Three-dimensional HNCA data was acquired on a Bruker DRX-600 spectrometer at 37°C and pH 4.8. Data was processed in XWINNMR (Bruker) and analysed in XEASY (Bartels *et al.*, 1995). Strips are shown with cross peaks indicated by connecting red lines. Amino acid residues presented in each strip are indicated at the top of the strip. The ^{1}H and ^{15}N chemical shift values (ppm) are indicated at the bottom of the strips.

in Figure 7.13). Identified residues were generally perturbed by ≤ –0.1 ppm in the amide proton dimension and by 1 ppm in the nitrogen dimension (Figure 7.15). Of the assigned residues, Asn26 was perturbed most significantly in the amide proton dimension (-0.28 ppm) while Leu57 exhibited the largest chemical shift perturbation in the nitrogen dimension (2.5 ppm). These perturbations were still considered insignificant in comparison with residues that were perturbed considerably (> 0.3 ppm in the proton dimension and > 2.5 ppm in the nitrogen dimension).

In the absence of complete chemical shift assignments of the bound ligand, significantly perturbed resonance peaks were identified by comparison of the free and bound TROSY spectra (Figure 7.16). Several peaks were clearly perturbed upon addition of Trx^{1-279}IGFBP-2HIS including Glu3, Glu9, Leu10, Phe16, Val17, Cys18, Gly19, Asp20, Arg21, Gly22, Phe23, Ser34, Phe49, Ser51, Leu54, Glu58, Tyr60 and Cys61. Remaining unassigned residues include: Gly1, Pro2, Thr4, Val11, Tyr24, Pro28, Pro39, Val44, Asp45, Arg50, Cys52, Asp53, Arg55, Arg56, Met59, Pro63, Pro66 and Ser69.

Difficulties in assigning resonances for IGF-I complexed to IGFBP-1 were also experienced by Jansson and co-workers (1998), who only assigned resonances from Pro2, Glu3, Cys6, Gly7, Pro28-Gly42, Ser51, Leu54, Arg55, Glu58, Met59, Pro63-Ala70 (30 °C, pH 3.4). Interestingly, chemical shift perturbations of IGF-I upon binding of IGFBP-1 were only small compared to those observed in this study. Jansson *et al.*, (1998) defined significant chemical shifts as greater than 0.3 ppm for either of the C_α or C_β resonances and 0.15 ppm for the nitrogen resonances, which are comparable to those which were not significantly perturbed in the present study. The perturbed residues observed by Jansson and co-workers were Pro2, Arg3, Gly7, Gly19, Pro28-Gly30, Gly32, Arg36, Arg37, Gln40, Thr41, Pro63, Lys65, Pro66, Lys68-Ala70.

The largest IGF-I chemical shift perturbations reported by Jansson and co-workers, upon complexing with IGFBP-1, were observed for Ala70 (Δ^1H^N: -0.33, $\Delta^{15}N$ -3.69, $\Delta^{13}C_\alpha$ -2.11 ppm) and Gly7 (Δ^1H^N –0.23, $\Delta^{15}N$ -1.57, $\Delta^{13}C_\alpha$ -0.72 ppm). Interestingly, the two alternative

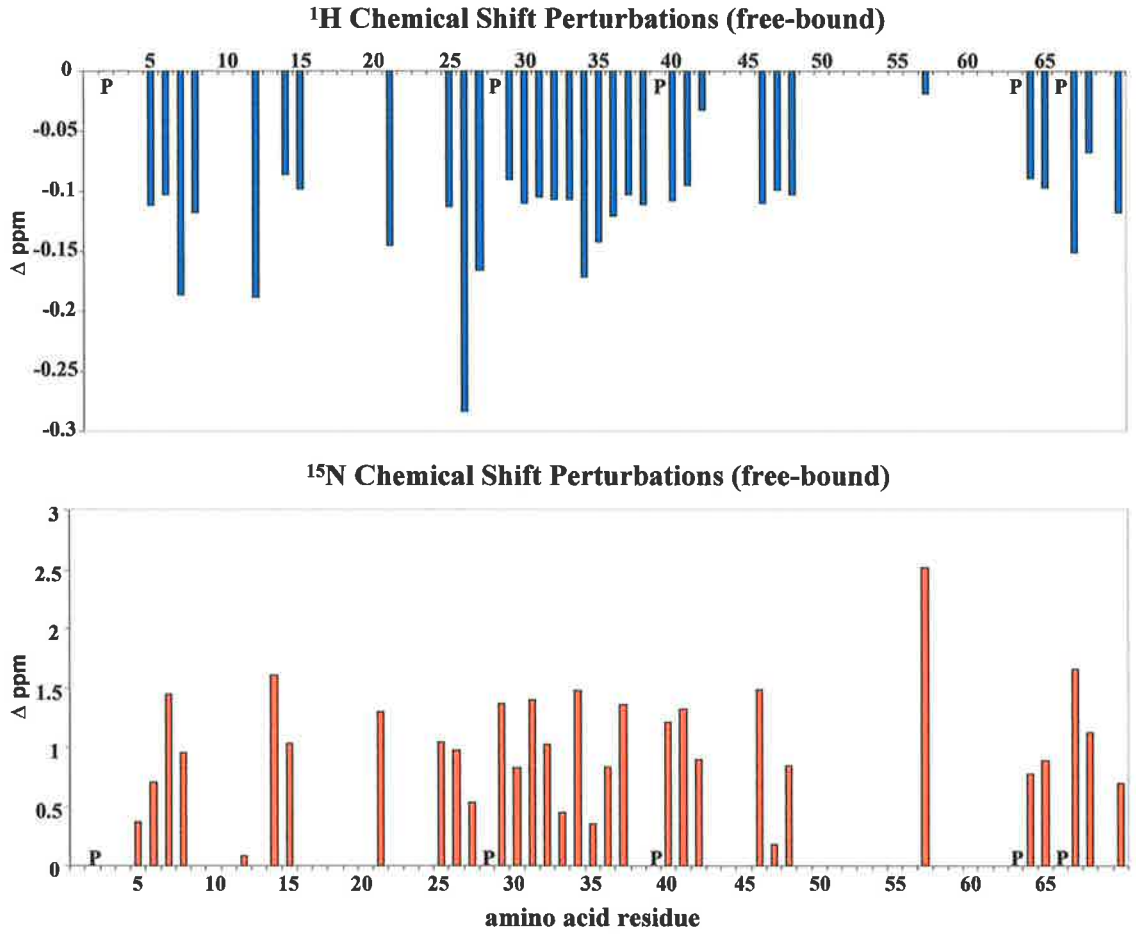

Figure 7.15 IGF-I residues which were perturbed insignificantly upon binding of Trx^{1-279}IGFBP-2HIS

The difference in chemical shift values (free ligand-bound ligand) of those residues defined as being perturbed insignificantly in this study are presented in the above graphs. Residues for which no bar exists could not be identified. Proline residues are indicated (P).

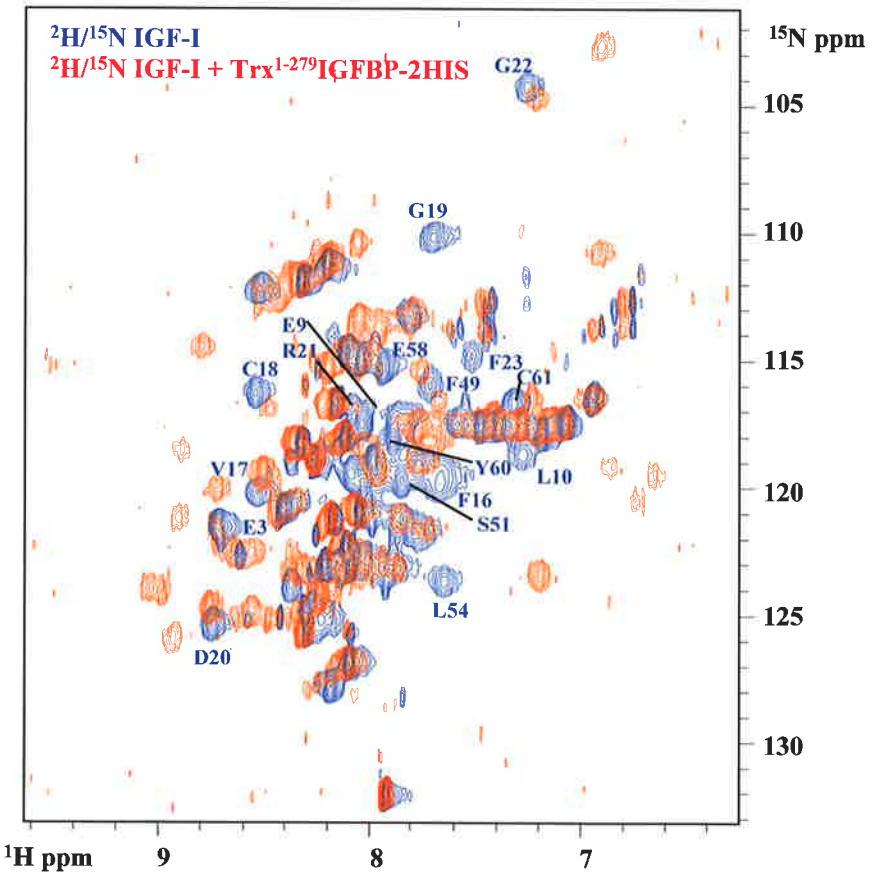

Figure 7.16 Identification of significantly perturbed IGF-I residues
IGF-I residues which were clearly perturbed upon complex formation with Trx$^{1-279}$IGFBP-2HIS are labelled based on assignments made for the free ligand from a 3D HNCA experiment as described in Section 7.3.3. Labels refer to resonances of free IGF-I. The figure was prepared in XEASY (Bartels *et al.*, 1995).

conformations of the C-terminal polypeptide Lys68-Ala70 were also observed by Jansson and coworkers for free IGF-I at 30 °C but not at 50 °C. Jansson and co-workers also reported perturbation of Gly7 and Ser51 upon the change in temperature from 30 °C to 50 °C. Perturbation of these residues was not observed under any pH or temperature investigated in this study. Aside from the chemical shift differences observed for Ala70 and Gly7, the chemical shift differences noted by Jansson and co-workers (1998) are very minor.

7.4.3.3 Chemical shift perturbations upon binding of Trx^{1-132}IGFBP-2 or $Trx^{136-279}$IGFBP-2HIS

Results reported previously in this thesis clearly show that both the amino- and carboxyl-terminal domains of IGFBP-2 need to be present and covalently attached to achieve high affinity binding of IGFs (also Carrick *et al.*, 2001). In an attempt to further define the essential differences between the amino-and carboxyl-terminal binding domains of IGFBPs, and to identify the specific IGF binding surfaces for each of these molecules, high resolution NMR spectra of IGF-I in complex with Trx^{1-132}IGFBP-2 (Figure 7.17) and $Trx^{136-279}$IGFBP-2HIS (Figure 7.18) were acquired.

Despite chemical shift perturbations observed upon complexing with $Trx^{136-279}$IGFBP-2HIS being much smaller than those caused upon binding of either Trx^{1-279}IGFBP-2HIS or Trx^{1-132}IGFBP-2, distinct chemical shift perturbations were observed (Figure 7.18). Comparison of the free ligand at comparable pH values suggests these perturbations are not due to pH differences. The amino acid residues that are perturbed upon binding of $Trx^{136-279}$IGFBP-2HIS are Gly19, Asp20, Gly22, Phe 23, Tyr24, Phe49 and Leu54. In addition to these residues, chemical shift resonances of the side chain amides have also been perturbed, suggesting involvement in the binding interaction (Figure 7.18).

The TROSY spectrum of IGF-I complexed to Trx^{1-132}IGFBP-2 displayed greater spectral dispersion and chemical shift perturbations than was observed upon binding of $Trx^{136-279}$IGFBP-2HIS. Interestingly, two resonances are observed for some residues, representing the free and bound states, which is indicative of the complex in slow exchange

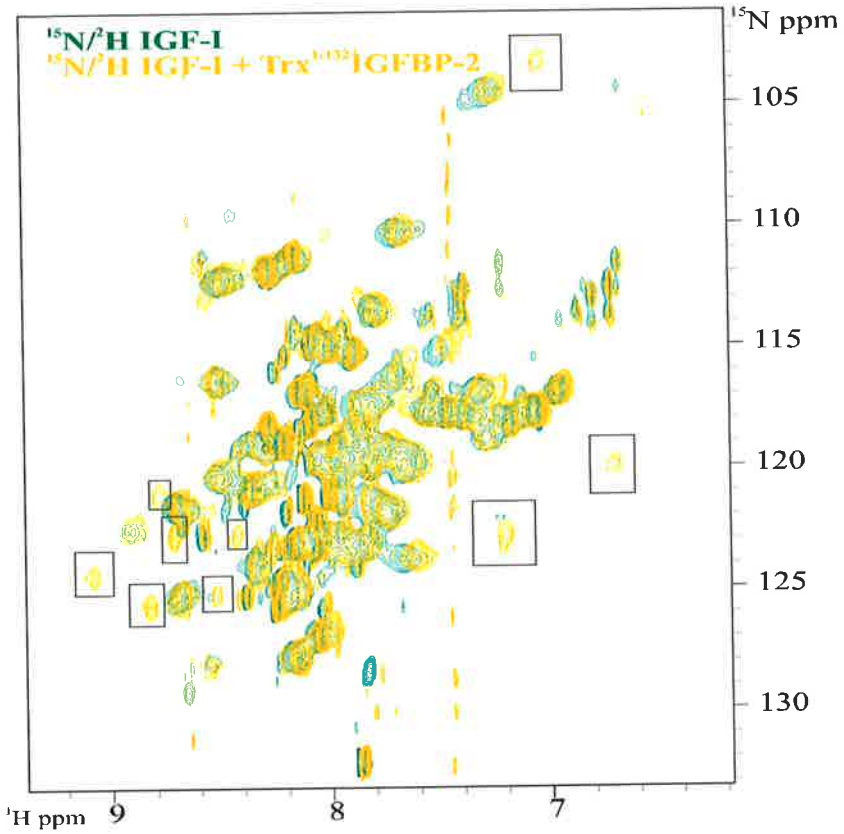

Figure 7.17 Comparison of Free ^{2}H/^{15}N IGF-I and Trx$^{1-132}$IGFBP-2 bound ^{2}H/^{15}N IGF-I
A TROSY spectrum of the free ligand was recorded at 600 MHz as described in Section 7.3.2 at pH 4.9 and 37 °C. The complex with Trx$^{1-132}$IGFBP-2 was formed as described in Section 7.3.1 and TROSY spectra recorded at pH 5.0 and 37 °C. Boxed peaks represent resonances that have been perturbed upon binding of Trx$^{1-279}$IGFBP-2HIS. This figure was prepared in XEASY (Bartels *et al.,* 1995).

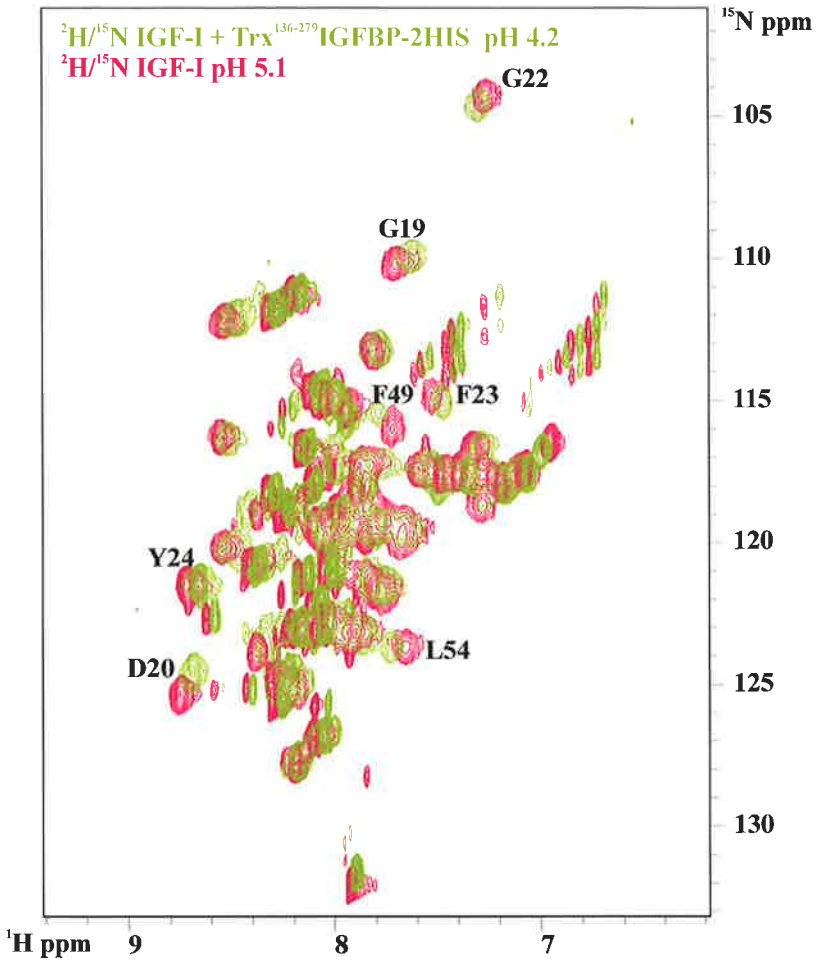

Figure 7.18 Chemical Shift Perturbations of IGF-I upon complex formation with Trx$^{136-279}$IGFBP-2HIS

TROSY spectra of free IGF-I (pink) and Trx$^{136-279}$IGFBP-2HIS complexed IGF-I (green) were recorded at 37 °C at 600 MHz. The free ligand was recorded at a pH value of 5.1 while the complex was recorded at both pH 4.8 and pH 4.2. Labelling refers to free resonances that have been perturbed upon complex formation. This figure was prepared in XEASY (Bartels *et al.*, 1995).

(Figure 7.17). This is despite the prediction that nearly 100 % of IGF ligand will form a complex with Trx^{1-132}IGFBP-2 based on biosensor affinities of 23 nM (Section 4.4.1). An estimate of the cross peak intensities of the (assumed) corresponding free and bound forms of the same residue suggests a 4:1 ratio of free to bound IGF-I. Spectra acquired at lower temperature (27 °C) did not influence the proportion of free and bound ligand and did not clarify the identity of the perturbed chemical shift resonances. Raising the temperature of the sample to 45 °C or decreasing the pH may potentially alter the dynamics of the interaction. In the absence of complete spectral assignments for IGF-I in complex with Trx^{1-279}IGFBP-2HIS however, interpretation of the chemical shifts of IGF-I perturbed upon binding of the amino-terminal fragment is difficult. Possibly, Gly22 and Leu54 are perturbed in IGF-I upon binding of Trx^{1-132}IGFBP-2 as indicated in Figure 7.17, but this needs to be confirmed. Consequently, identification of the residues perturbed upon binding of Trx^{1-132}IGFBP-2 has not been possible in this study.

7.4.3.4 Tertiary Model of IGF-I Residues Perturbed Upon Binding of Trx^{1-279}IGFBP-2HIS

The results from this study have been mapped onto a surface model of IGF-I (Sato *et al.*, 1992: PDB 1BQT) generated in MOLMOL (Koradi *et al.*, 1996) (Figure 7.19). The residues which were considered unperturbed upon analysis of the HNCA spectra are coloured blue (Leu5-Gly7, Asp12, Leu14-Gln15, Phe25-Lys27, Thr29-Ala38, Gln40-Ile43, Glu46-Cys48, Leu57, Leu64-Lys65, Ala67-Lys68 and Ala70). The residues that were clearly perturbed (but for which no chemical shift assignments could be made in the complex) are coloured pink (Glu3, Glu9, Leu10, Phe16, Val17, Cys18, Gly19, Asp20, Arg21, Gly22, Phe23, Ser34, Phe49, Ser51, Leu54, Glu58, Tyr60 and Cys61). The residues for which no assignments nor comment on their perturbations could be made are coloured in grey (Gly1, Pro2, Thr4, Val11, Tyr24, Pro28, Pro39, Val44, Asp45, Arg50, Cys52, Asp53, Arg55, Arg56, Met59, Pro63, Pro66 and Ser69).

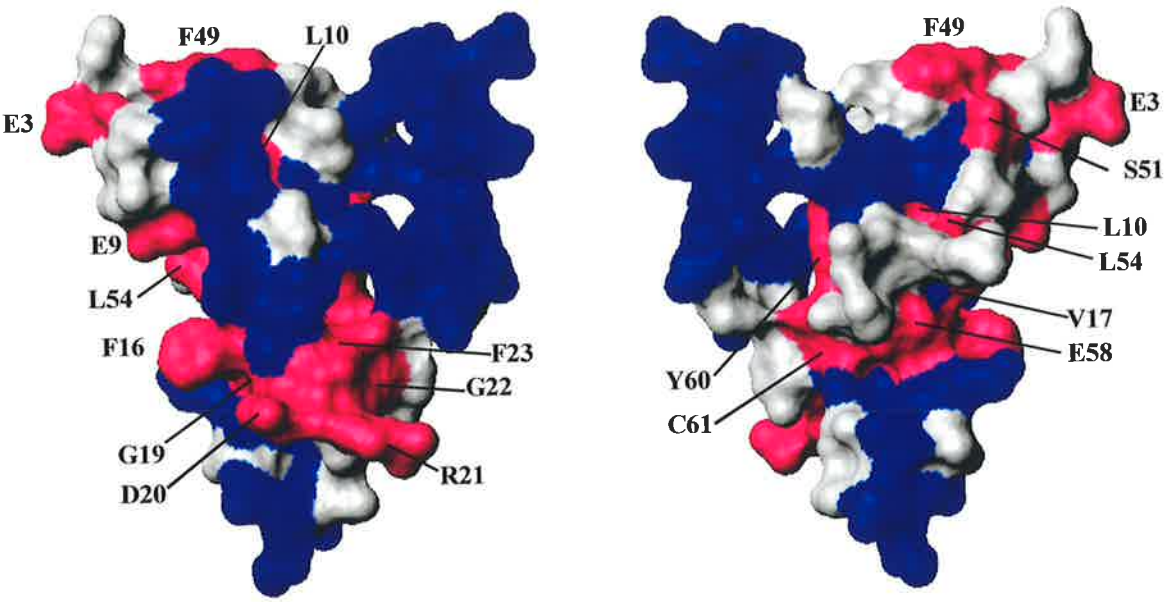

Figure 7.19 Surface representation of IGF-I with significantly perturbed residues highlighted

Results from the chemical shift analyses of IGF-I upon binding of Trx^{1-279}IGFBP-2 (as described in Section 7.4.3.4) are displayed on surface representations of the IGF-I molecule rotated 180° about the vertical axis. Significantly perturbed residues are coloured pink (viz: Glu3, Glu9, Leu10, Phe16, Val17, Cys18, Gly19, Asp20, Arg21, Gly22, Phe23, Phe49, Ser51, Leu54, Glu58, Tyr60 and Cys61). Residues which were not perturbed upon binding of Trx^{1-279}IGFBP-2HIS are coloured blue (viz: Leu5-Gly7, Asp12, Leu14-Gln15, Phe25-Lys27, Thr29-Ala38, Gln40-Ile43, Glu46-Cys48, Leu57, Leu64-Lys65, Ala67-Lys68 and Ala70). Residues which could not be identified are coloured grey (viz: Gly1, Pro2, Thr4, Val11, Tyr24, Pro28, Pro39, Val44, Asp45, Arg50, Cys52, Asp53, Arg55, Arg56, Met59, Pro63, Pro66 and Ser69). The IGF-I structures used in this figure were reported by Sato *et al.*, 1992. This figure was created using MOLMOL (Koradi *et al.*, 1996).

The residues of IGF-I, which are clearly perturbed upon binding of Trx^{1-279}IGFBP-2HIS (Figure 7.16) map to one region of the molecule. Residues that were reported to form the binding interface with mini-IGFBP-5 (Żesławski *et al.*, 2001) have also been seen here to be perturbed upon binding of IGFBP-2 (viz: Glu3, Phe16, Leu54). Additional residues were also perturbed upon binding of full-length IGFBP-2 including amino acid residues Glu9-Leu10, Val17-Phe23, Phe49, Ser51, Glu58 and Tyr60. These residues are located on the same face as the N-terminal binding interface for mini-IGFBP-5 and may comprise the binding interface for the C-terminal domain of IGFBP-2. Indeed, perturbations of IGF-I residues observed upon binding of $Trx^{136-279}$IGFBP-2HIS include Gly19, Asp20, Tyr24, Phe49 and Leu54. Interestingly, Leu54 was specifically reported to be part of the mini-IGFBP-5 interface (Żesławski *et al.*, 2001) but was perturbed upon binding of both Trx^{1-132}IGFBP-2 and $Trx^{136-279}$IGFBP-2HIS in TROSY spectra recorded in this study.

7.4.4 IDENTIFICATION OF IGF-II CHEMICAL SHIFT PERTURBATIONS UPON INTERACTION WITH TRX^{1-279}IGFBP-2HIS

7.4.4.1 IGF-II Chemical Shift Assignments

Spectra of IGF-II were less dispersed than for IGF-I containing a number of broad signals attributable to aggregation or conformational averaging (Figure 7.20). As reported by Torres and co-workers (1995), the presence of broad peaks present problems in the spectral analysis and assignment of chemical shifts resonances. IGF-II TROSY spectra were acquired at 37 °C pH 4.8 (Figure 7.20) and chemical shifts (Table 7.2) were assigned based on those published by Torres *et al.*, 1995 (27 °C pH 3.1). All chemical shifts for IGF-II were assigned values that were within 0.06 ppm of reported chemical shifts for the amide proton dimension (except for Leu8, at 0.09 ppm) and differed consistently by approximately -1.3 ppm in the nitrogen dimension (Figure 7.21 and Table 7.2). These variations in chemical shift assignments are consistent with TROSY spectra. Poor peak resolution was observed for residues such as Gly11, Leu13, Leu17, Val20, Arg30, Cys51 and Leu56. In addition to the 67 reported chemical

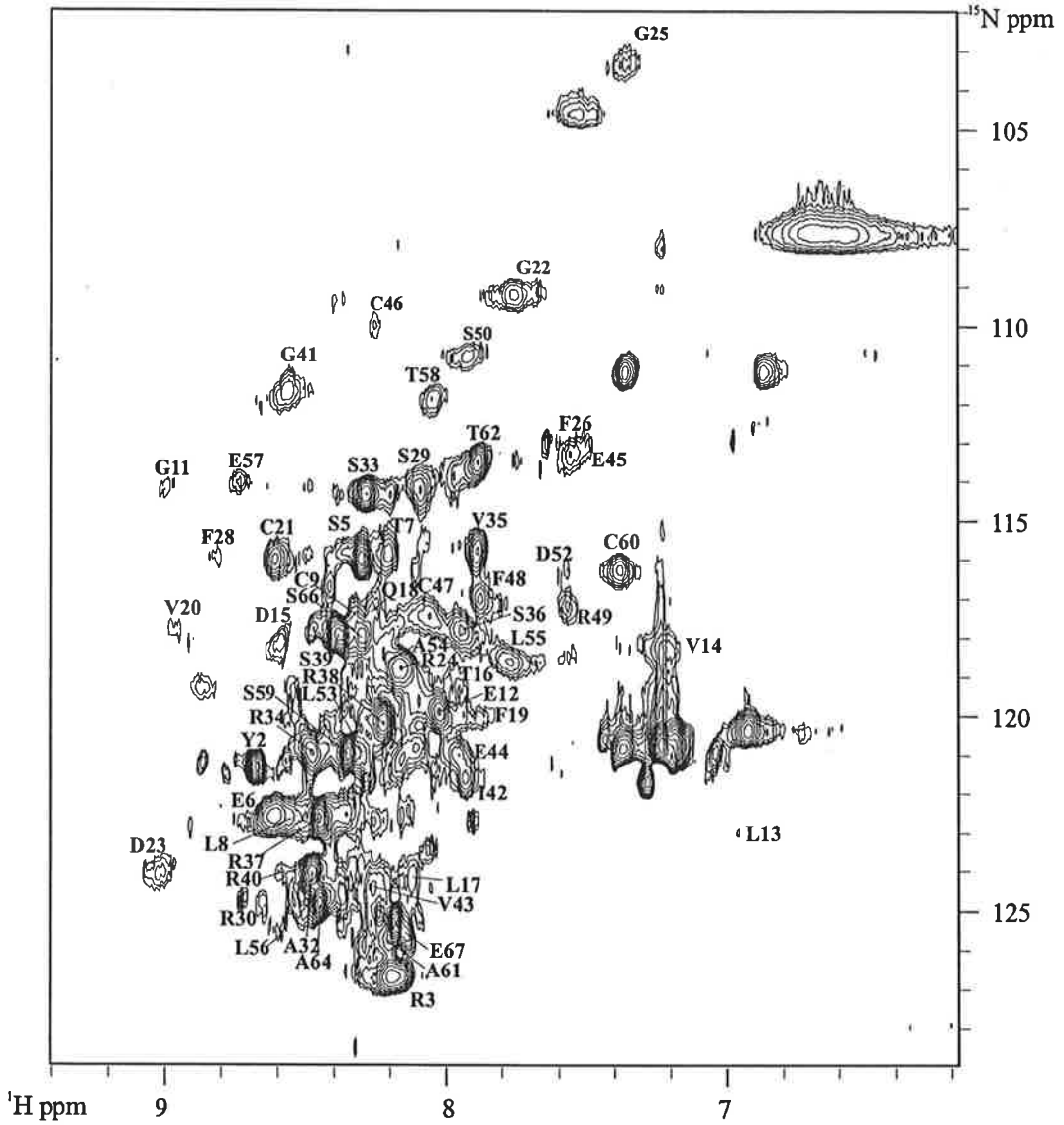

Figure 7.20 Labelled TROSY spectrum of ^{2}H/^{15}N IGF-II
Contour plot of an assigned 600 MHz 2D ^{1}H-^{15}N TROSY spectrum. Spectra were recorded on a 0.5 mM solution of partially deuterated ^{15}N-IGF-II in acetate buffer + 5 % D_2O at pH 4.8 and 37°C. Assignments were made based on those reported in the literature by Torres *et al.*, 1995. Additional unlabelled peaks are either side chain resonances or arise from contamination by the leader sequence. This figure was generated in XEASY (Bartels *et al.*, 1995).

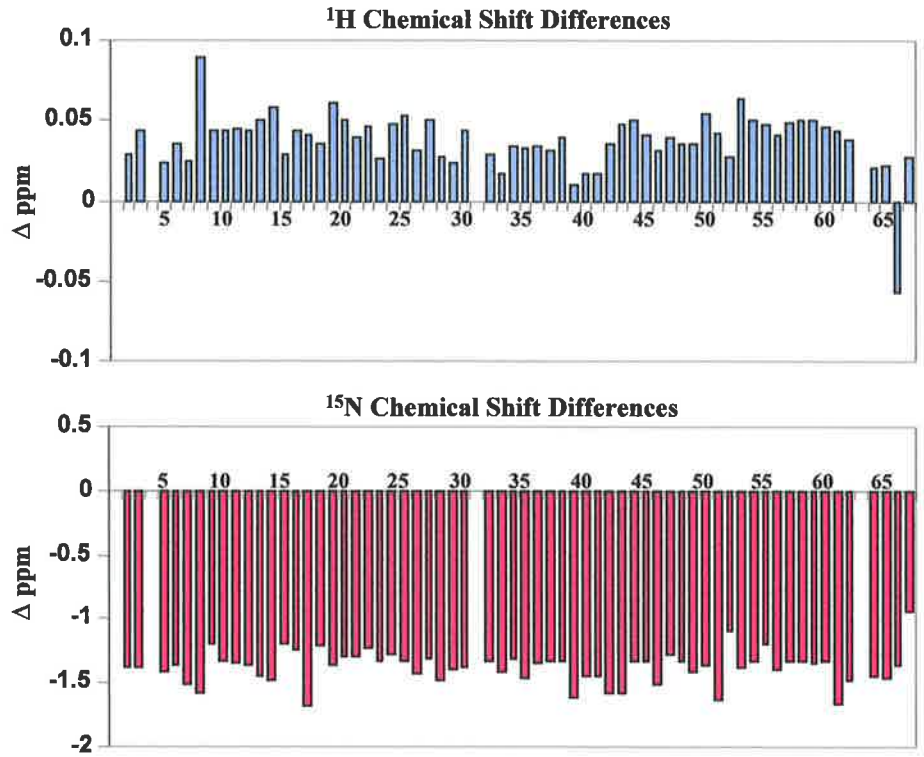

Figure 7.21 Comparison of IGF-II chemical shift assignments with values in the literature Variations in ^{1}H and ^{15}N chemical shift assignments for IGF-II compared with those published by Torres *et al.*, 1995 are presented as bar graphs. Graphs are plotted as the difference between chemical shift values derived in this study and values reported in the literature.

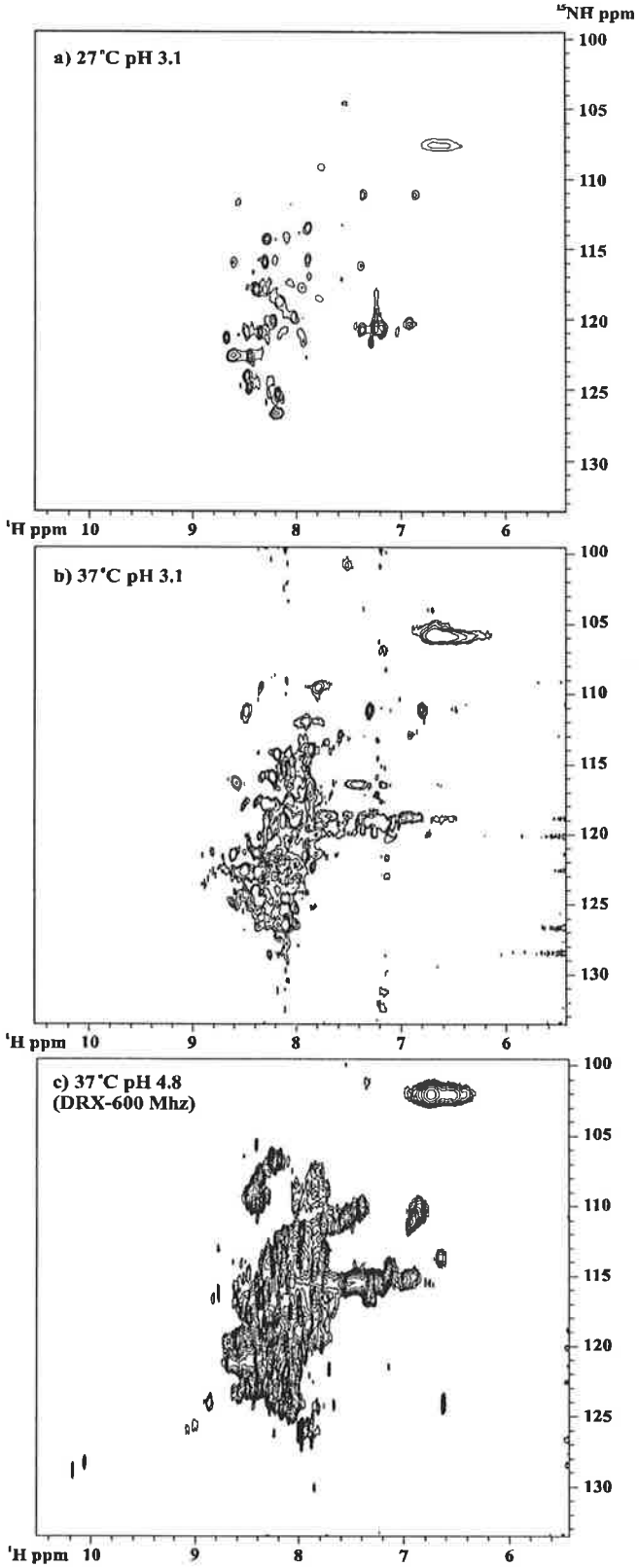

Figure 7.22 Temperature and pH titration of ^{15}N IGF-II
The spectral quality of ^{15}N IGF-II was compared in various HSQC experiments recorded at a) 27 °C pH 3.1, b) 37 °C pH 3.1 and c) 37 °C pH 4.8. HSQC spectra a) and b) were recorded at 500 MHz while spectrum c) was recorded at 600 MHz. This figure was made in XEASY (Bartels *et al.*, 1995).

TABLE 7.2 CHEMICAL SHIFT ASSIGNMENTS FOR IGF-II

Residue	Residue Name	^{1}H	^{15}N	Residue	Residue Name	^{1}H	^{15}N
1	Ala			35	Val	7.89	115.8
2	Tyr	8.68	121.3	36	Ser	7.94	117.8
3	Arg	8.19	126.7	37	Arg	8.45	122.7
4	Pro			38	Arg	8.22	120.1
5	Ser	8.30	116.0	39	Ser	8.39	117.9
6	Glu	8.61	122.6	40	Arg	8.60	124.0
7	Thr	8.21	115.9	41	Gly	8.57	111.7
8	Leu	8.56	122.6	42	Ile	7.94	121.6
9	Cys	8.32	117.4	43	Val	8.26	124.4
10	Gly	9.38	111.1	44	Glu	7.96	121.1
11	Gly	9.02	114.3	45	Glu	7.50	113.1
12	Glu	8.02	119.9	46	Cys	8.25	110.0
13	Leu	6.96	123.0	47	Cys	8.06	117.4
14	Val	7.31	118.2	48	Phe	7.88	117.0
15	Asp	8.59	118.2	49	Arg	7.57	117.2
16	The	7.94	119.4	50	Ser	7.93	110.8
17	Leu	8.12	124.2	51	Cys	10.04	120.9
18	Gln	8.27	117.3	52	Asp	7.58	116.2
19	Phe	7.88	120.1	53	Leu	8.27	121.5
20	Val	8.96	117.8	54	Ale	8.19	119.0
21	Cys	8.61	116.0	55	Leu	7.78	118.6
22	Gly	7.76	109.3	56	Leu	8.60	125.5
23	Asp	9.02	124.0	57	Glu	8.74	114.0
24	Arg	8.17	118.8	58	Thr	8.05	111.9
25	Gly	7.36	103.4	59	Tys	8.30	121.0
26	Phe	7.56	113.3	60	Cys	7.39	116.3
27	Tyr	8.87	119.3	61	Ala	8.21	125.7
28	Phe	8.82	115.9	62	Thr	7.89	113.5
29	Ser	8.09	114.2	63	Pro		
30	Arg	8.65	124.8	64	Ala	8.45	124.8
31	Pro			65	Lys	8.35	121.0
32	Ala	8.48	124.1	66	Ser	8.30	117.9
33	Ser	8.29	114.3	67	Glu	8.19	125.3
34	Arg	8.48	120.9				

*Assignments are based on those reported by Torres *et al.*, 1995. Data was acquired using a 0.5 mM sample of $^{2}H/^{15}N$-IGF-II at 600 MHz 37 °C, pH 4.8.

shifts, several other unidentified peaks were present in the spectra that correspond to amide side chains and resonances of the leader sequence.

The HSQC spectrum acquired at conditions conducive for complex formation (37 °C and pH 4.8) clearly varied from the spectrum acquired at pH 3.1 and 27 °C (Figure 7.22). In an attempt to translate chemical shift assignments between those reported by Torres and co-workers (1995) and those observed under conditions chosen for ligand binding (37 °C and pH 5.0), HSQC spectra of IGF-II were acquired at 37 °C and pH 3.1. Raising the temperature to 37 °C at 500 MHz however, resulted in broadening of the peaks and loss of peak definition (Figure 7.22). Additional weakening was expected upon further raising the pH.

7.4.4.2 Spectral Analysis of IGF-II Complexed to IGFBP-2

As observed for IGF-I, the chemical shift perturbations upon complex formation with Trx^{1-279}IGFBP-2HIS were large (Figure 7.23) and titration between the free and bound forms was not possible. Therefore assignments of free IGF-II could not be readily transferred to the spectra of complexed IGF-II. An ^{15}N-edited 2D NOESY of the complex was acquired to resolve spectral overlap and assist in the chemical shift assignment of complexed IGF-I. NOEs between overlapping proton resonances however, could not be resolved due to poor spectral resolution (results not shown). There was an improvement in dispersion of chemical shift resonances for IGF-II upon binding of Trx^{1-279}IGFBP-2HIS and interestingly, similarities between the complexed IGF-I and IGF-II spectra exist (Figure 7.24). Similar chemical shifts were observed for both complexed IGF-I and IGF-II at approximately 8.8-9 ppm and for the perturbed resonance at approximately (HN:N) 7 ppm:123 ppm in Figure 7.24. Likewise, the perturbed resonances observed for Gly19 and Gly22 of IGF-I are also present in the spectrum for corresponding residues of IGF-II. Consistent with mutagenesis studies in the literature, these results suggest similar amino acid residues of IGF-I and IGF-II are involved in binding IGFBP-2. Considering the modest preference of IGFBP-2 for IGF-II over IGF-I, it is

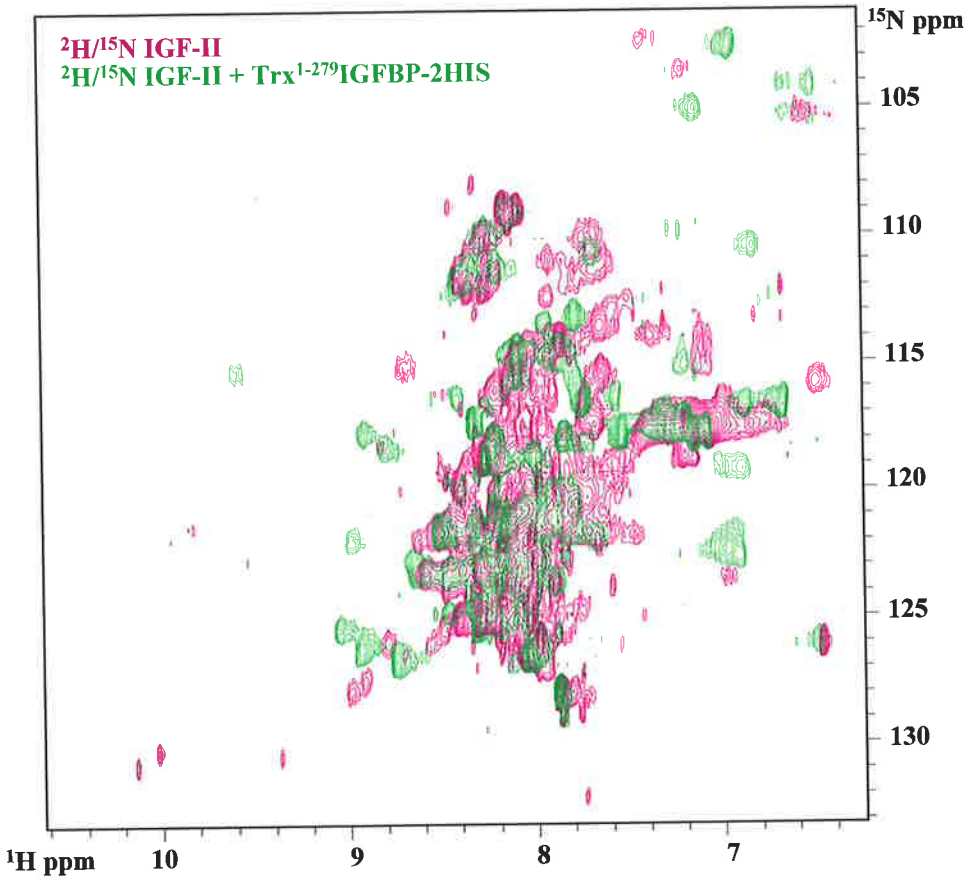

Figure 7.23 TROSY Spectra of Free IGF-II ligand and IGF-II complexed to Trx^{1-279}IGFBP2-HIS

TROSY spectra of IGF-II were acquired at 600 MHz and 37 °C as described in Section 7.3. The spectrum of the free ligand (magenta) was acquired at pH 5.1 while the complex (green) was acquired at pH 4.8. Spectra were referenced to an intrinsic peak at 0.15 ppm and overlayed for comparison. This figure was made in XEASY (Bartels *et al.*, 1995).

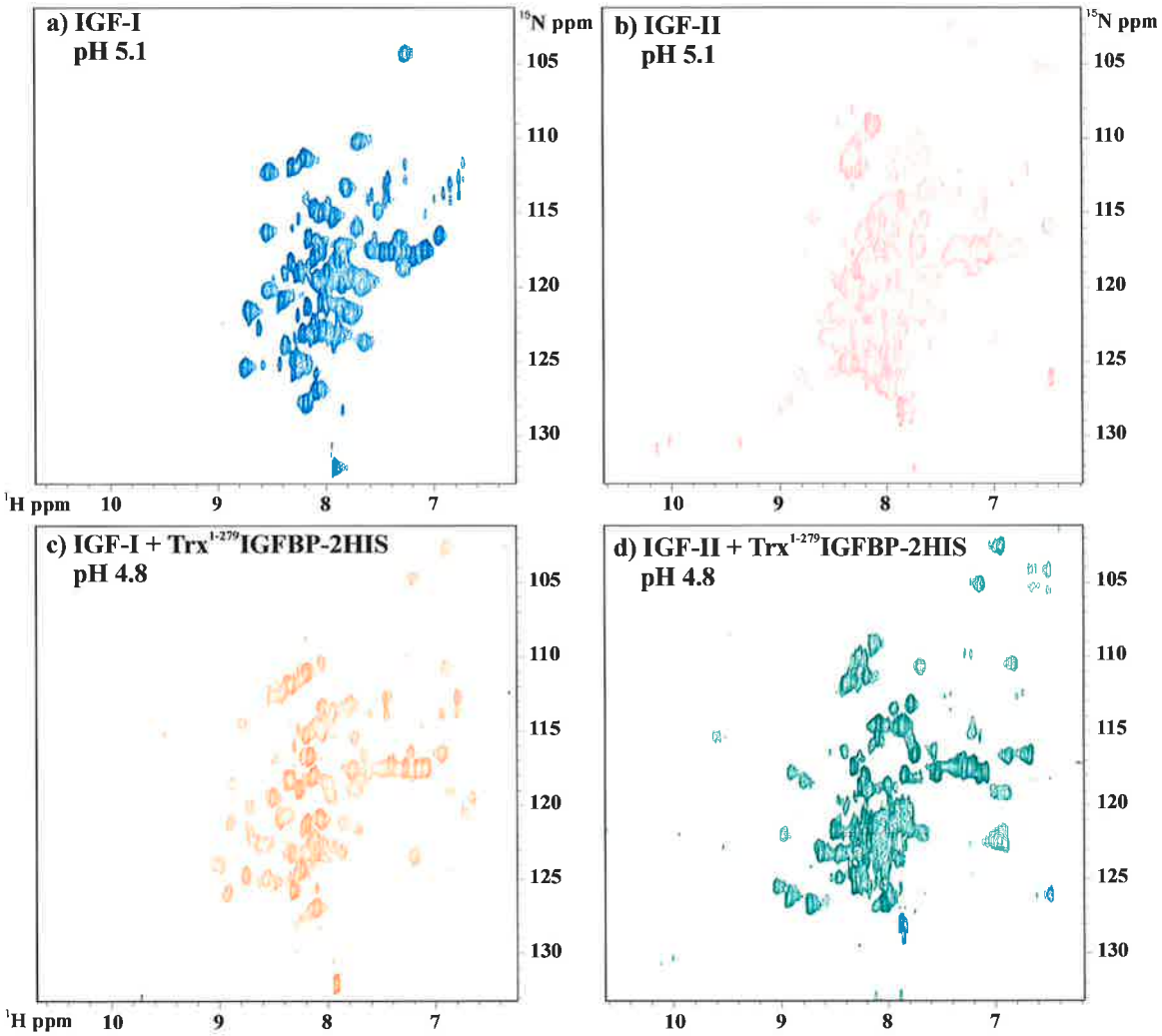

Figure 7.24 Comparison of the free and Trx$^{1-279}$IGFBP-2HIS bound spectra of IGF-I and IGF-II

TROSY spectra of free IGF-I (a) and IGF-II (b) are compared to spectra of IGF-I and IGF-II in complex with Trx$^{1-279}$IGFBP-2HIS (c and d, respectively) (see Figure 7.11 and Figure 7.23 for overlayed spectra of free and bound IGF-I and IGF-II, respectively). The spectral dispersion of IGF-II in complex with Trx$^{1-279}$IGFBP-2HIS is increased significantly compared to the free ligand and several similarities exist in the spectra of complexed ligands. This figure was generated in XEASY (Bartels *et al.*, 1995).

reasonable that the binding sites are largely similar. The specificity of IGFBPs for one IGF ligand over the other may indeed be attributable to the binding site on IGFBP itself. This may be particularly true for IGFBP-6, which exhibits significant preference for IGF-II.

The spectral resolution of IGF-II was not improved upon addition of Trx^{1-132}IGFBP-2 (Figure 7.25). Indeed, the increase in effective molecular weight of the sample resulted in broadened line widths and reduced spectral resolution as was seen for Trx^{1-279}IGFBP-2HIS. Consequently, a large number of chemical shift resonances for IGF-II were not observed and little information was derived from the TROSY spectrum.

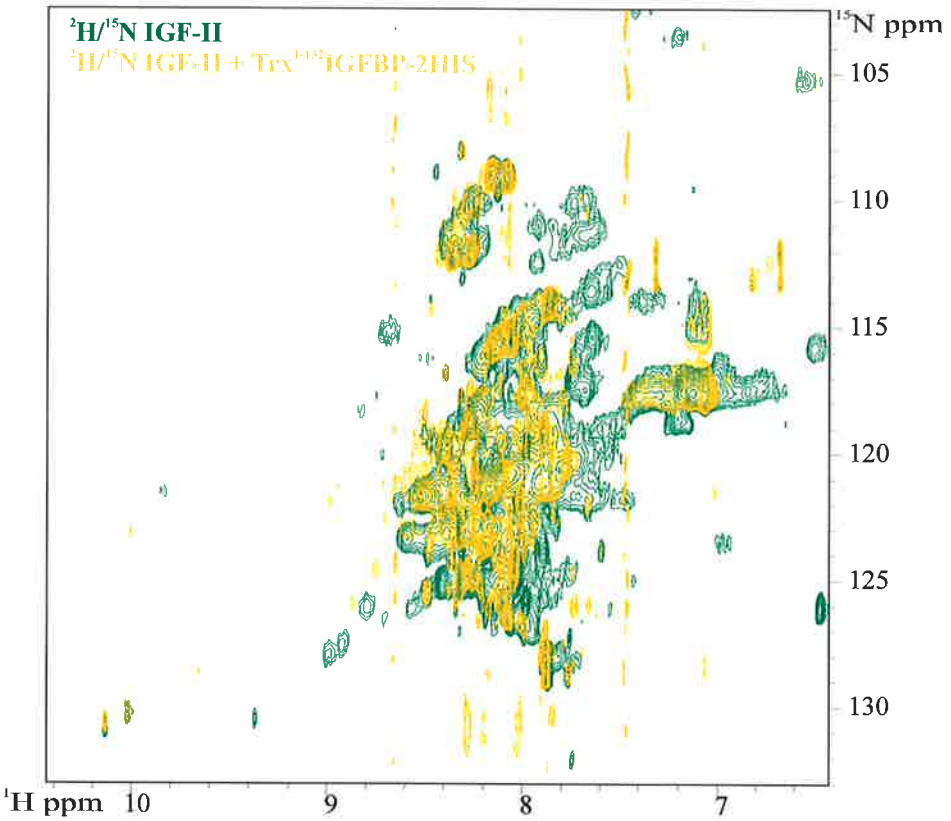

Figure 7.25 Comparison of free ^{2}H/^{15}N IGF-II and Trx$^{1-132}$IGFBP-2 bound ^{2}H/^{15}N IGF-II
A TROSY spectrum of the free ligand was recorded at 600 MHz as described in Section 7.3.2. at 37 °C, pH 4.9. The complex with Trx$^{1-132}$IGFBP-2 was formed as described in Section 7.3.1 and TROSY spectra recorded at 37 °C and pH 5.0. This figure was made in XEASY (Bartels *et al.*, 1995).

7.5 DISCUSSION

NMR has been used in this study in an attempt to define the intermolecular interface between ^{15}N- and ^{2}H/^{15}N-labelled IGF-I or IGF-II and unlabelled Trx$^{1-279}$IGFBP-2HIS. Chemical shift perturbations in IGF-I or IGF-II upon binding of Trx$^{1-279}$IGFBP-2HIS would identify residues involved directly in the binding interaction and those affected as a consequence of conformational changes in the molecule. Significant chemical shift perturbations for IGF-I upon Trx$^{1-279}$IGFBP-2HIS binding have been mapped to the surface of the IGF-I molecule (Figure 7.19) providing insight into the binding site for IGFBP-2.

Analysis of perturbations of IGF residues upon complex formation with IGFBP-2 relied on assignment of the chemical shift resonances of both free and bound ligand. Assignment of resonances however, was compromised by the lack of spectral dispersion and poor resolution due to broad line widths. Problems due to line broadening have been encountered previously in NMR studies of insulin (Kline and Justice, 1990; Hua and Weiss, 1991), IGF-I (Cooke *et al.*, 1991; Sato *et al.*, 1992) and IGF-II (Terasawa *et al.*, 1994; Torres *et al.*, 1995). Such line broadening is believed to be a consequence of conformational averaging which is further enhanced by the tendency of IGF-I, and even more so, IGF-II, to aggregate. In this study, deuteration of the ligand and the use of TROSY-based experiments improved spectral quality, particularly of the complexed ligand.

Significant chemical shift perturbations were observed for IGF-I upon complex formation with Trx$^{1-279}$IGFBP-2HIS. Indeed, the chemical shift perturbations observed in the present study were significantly greater than those reported by Jansson and co-workers for binding of IGFBP-1 (1998). It is possible that very little complex formed between IGF-I and IGFBP-1 at pH 3.4 and subsequent spectra were indicative of the free ligand. In the present study, BIAcore analysis of the binding interaction between IGF-I or IGF-II and IGFBP-2 was performed to determine the effect of pH on complex formation. As described in Section 5.4.5, the binding curve at pH 3.4 was atypical of the high-affinity binding interaction with IGFBP-2, dissociating more rapidly from IGF-I biosensor surfaces than at pH 4.4 or 5.4. Furthermore,

TROSY spectra of the complex at various pH values in this study indicated complexes dissociated between pH 3.5 and pH 2.8 (Figure 7.12).

Recently, crystal structures of IGF-I, either in complex with mini-IGFBP-5 (Żesławski *et al.*, 2001) or with a detergent, deoxy big CHAPS (Vajdos *et al.*, 2001) have been reported in the literature. The general fold of IGF-I reported from solution studies is preserved in the complexes. Although the structures are highly defined for most residues, large variations in structure were seen for residues 1-6, 62-67 and 31-40 which form a peripheral loop (Żesławski *et al.*, 2001). The N-terminal residues of IGF-I are well defined in the X-ray structure compared to the NMR structures, and may only become fixed upon complex formation (Żesławski *et al.*, 2001). Never the less, the chemical shift perturbations reported in the present study are unlikely to be due to large conformational changes but rather due to more localised changes in chemical shift environment.

Mutagenesis and chemical modification data in the literature and the present NMR study demonstrate that B- and A-domain residues of IGF are major determinants for the binding interaction with IGFBPs. IGF-I B-domain residues Glu3, Glu9 and Phe16 were significantly perturbed upon binding of Trx^{1-279}IGFBP-2HIS in this study and were also shown to make specific contact with amino acid residues Val49, Arg53, Arg59, Cys60, Leu61, Leu70 and Leu74 of mini-IGFBP-5 in the crystal complex (Żesławski *et al.*, 2001). Glu3 has been long considered critical for IGFBP binding (Bagley *et al.,* 1989) and when mutated in combination with Thr4, Gln15 and Phe16, IGFBP binding is reduced by more than 600-fold (Bayne *et al.*, 1989). Glu3 of IGF-I and Glu6 of IGF-II were also shown in this thesis to be important for binding of the amino-terminal domain of bIGFBP-2 and not to the carboxyl-terminal domain. Indeed, Glu3 was not perturbed significantly upon binding of $Trx^{136-279}$IGFBP-2HIS. Although Glu3 of IGF-I is directly involved in interactions with the N-terminal domain of IGFBPs, the amino-terminal tripeptide of IGF-I and hexapeptide of IGF-II are critically important for binding of the carboxyl-terminal domain of IGFBP-2 (Section 4.4.3, Carrick *et al.*, 2001, Ho and Baxter, 1997). This region therefore is clearly important for the structural integrity of the

complex for high-affinity interactions. Interestingly, Gln15 was not significantly perturbed in the present study and perturbation of Ala4 could not be determined unambiguously.

Additional B-domain residues were also clearly perturbed upon binding of Trx^{1-279}IGFBP-2HIS, including Leu10, Val17, Cys18, Gly19, Asp20, Arg21, Gly22 and Phe23. Dubaquie and Lowman (1999) reported amino acid residues Leu10 and Val17 were both involved in interactions with IGFBP-1 and IGFBP-3 while Jansson and co-workers (1998) reported perturbations only for Gly19. Interestingly, IGF-I B-domain residues Gly19, Asp20, Gly22, Phe23 and Tyr24 were also perturbed upon binding of $Trx^{136-279}$IGFBP-2HIS in the present study. Hence these residues may comprise the IGF binding interface for the highly conserved carboxyl-terminal domain of IGFBPs. Based on the results of Chapter 4, targeting IGF residues involved in binding through the C-terminal domain of IGFBP may influence the stability of the high affinity complex, subsequently releasing IGF for interaction with the receptor.

IGF-I A-domain residues Phe49, Arg50 and Ser51 are critically important for the IGFBP interaction (Cascieri *et al.*, 1989; Clemmons *et al.*, 1992; Oh *et al.*, 1993). Interestingly, the substitutions of 49, 50 and 51 selectively alter IGFBP-1 binding and not IGFBP-3 binding (Clemmons *et al.*, 1990). Discrete regions of the A-chain region of IGF-I therefore, may infer IGF binding specificity of IGFBP-1 and IGFBP-3 and possibly other IGFBPs. Indeed, chemical shift resonances for Phe49 and Ser51 were significantly perturbed upon binding of both Trx^{1-279}IGFBP-2HIS and $Trx^{136-279}$IGFBP-2HIS in the present heteronuclear NMR studies, however the resonance of Arg50 could not be identified. Curiously, these residues were not perturbed in NMR studies with IGFBP-1 (Jansson *et al.,* 1998). Residues Phe49 and Ser51 are both solvent exposed and therefore readily accessible for interaction with the IGFBP molecule. Interestingly though, these residues are located some distance from the rest of the putative binding interface for the carboxyl-terminal domain of IGFBP-2 (Gly19-Tyr24) and are located closer to the amino-terminal binding interface described by Kalus *et al.*(1998) (and inferred from the current data). Perturbation of Phe49 and Ser51 upon binding of $Trx^{136-279}$IGFBP-2HIS may therefore be the consequence of a change in chemical environment and not due to direct

interaction. The contribution of these residues for binding either the amino- or carboxyl-terminal domain of IGFBP-2 could be assessed in BIAcore studies using the IGF analogue Thr49, Ser50, Ile51 IGF-I (Cascieri *et al.*, 1989).

Leu54 of IGF-I was perturbed upon binding of and $Trx^{136-279}$IGFBP-2HIS (Figure 7.18). Leu54 of IGF-I makes direct contact with residues of mini-IGFBP-5 (Żesławski *et al.*, 2001) and is clearly involved in the binding interaction with both Trx^{1-279}IGFBP-2HIS (Figure 7.16) and Trx^{1-132}IGFBP-2 (Figure 7.17). Binding of the carboxyl-terminal domain of IGFBP-2 also induced a local change in environment of Leu54 that may or may not be a consequence of direct interaction. Interestingly, alanine substitution of Leu54 did not significantly affect IGFBP-1 binding (Dubaquie and Lowman, 1999) nor was Leu54 perturbed in NMR studies upon binding of IGFBP-1 (Jansson *et al.*, 1998). Leu54 therefore, may participate in binding IGFBP-2 but not IGFBP-1.

IGF tyrosine residues have been targeted previously in chemical modification studies of the IGFBP binding interaction. Only Tyr60 of IGF-I and Tyr59 of IGF-II were protected from iodination in the presence of IGFBP-2 (Moss *et al.*, 1991). The chemical shift resonance of Tyr60, but not Tyr31 of IGF-I, was perturbed significantly upon interacting with IGFBP-2 in the present NMR studies. Although Tyr60 was perturbed upon binding of Trx^{1-279}IGFBP-2HIS, it appears to be located in a region of the molecule not directly involved in binding IGFBPs. Indeed, Tyr60 is also important for receptor binding (Bayne *et al.*, 1990) and may be important for the structural integrity of the molecule. Furthermore, both the chemical modification data and the current study demonstrate that Tyr31 of IGF-I is not involved in IGFBP binding. Interestingly, Tyr24 was perturbed upon binding of the carboxyl-terminal fragment in this study, but could not be identified in spectra of the complex with Trx^{1-279}IGFBP-2HIS. Amino acid residues Gly19-Tyr24 are perturbed upon binding of $Trx^{136-279}$IGFBP-2HIS and possibly constitute the binding interface for the C-terminal fragment of IGFBP-2. Tyr24 of IGF-I is unlikely to make direct contact with the IGFBP based on mutagenesis studies; hence the reported chemical shift perturbation may be attributable solely to a change in chemical environment.

It appears from the present study that two distinct regions of IGF-I are significantly perturbed upon binding of IGFBP-2 (region 1: Glu3, Glu9, Leu10, Phe16, Val17, Cys18, Gly19, Asp20, Arg21, Gly22, Phe23 and region 2: Phe49, Ser 51, Leu54, Glu58, Tyr60 and Cys61). Dubaquie and Lowman (1999) identified two distinct regions of IGF-I that interact with IGFBP-1 and IGFBP-3, region 1 consists of Gly7, Leu10, Val11, Leu14, Phe25, Ile43 and Val44 while region 2 consists of Glu3, Thr4, Leu5, Phe16, Val17, and Leu54. In the crystal structure of IGF-I (Vajdos *et al.*, 2001) these regions are involved in detergent-mediated crystal packing which is entirely consistent with the observation that CHAPS blocks IGFBP-1 and –3 binding, but does not inhibit receptor binding.

IGFBP-2 binds both IGF-I and IGF-II with similar affinity and although the spectra for IGF-II are difficult to interpret, similarities exist with the spectrum of IGF-I (Figure 7.24). Furthermore, mutagenesis studies have implicated corresponding residues of both IGF-I and IGF-II in binding IGFBP (eg. IGF-I: Glu3, Phe16, Phe49-Ser51 and IGF-II: Glu6, Phe19, Phe48-Ser50). Therefore, it is possible that interface of IGF-I and IGF-II are similar for IGFBP-2, though it remains to be determined if distinct differences in IGF-I and IGF-II binding sites on IGFBP-2 also exist.

7.5.1 IMPLICATIONS FOR IGFBP BINDING

IGF-I residues Glu3, Glu9, Phe16 and Leu54 make direct contact with mini-IGFBP-5 (Żesławski *et al.*, 2001) and were also perturbed upon binding of Trx^{1-279}IGFBP-2HIS. The binding interface of mini-IGFBP-5 include residues Gly48, Val49, Tyr50, Arg59, Cys60, Leu61, Lys68, Pro69, Leu70, His71, Leu73 and Leu74 (Żesławski *et al.*, 2001), which are highly conserved across all IGFBPs. The strong sequence homology between mini-IGFBP-5 and the corresponding region of IGFBP-2 (amino acid residues 88-135), including conservation of disulfide-linkages, lends support to a common binding site on both the IGF ligand and the IGFBPs (Figure 6.4). A similar minimal IGF-binding fragment has also been identified for rIGFBP-4 (residues 52 to 92; Hashimoto *et al.*, 1997). In contrast, IGFBP-6 exhibits

preferential binding for IGF-II ligand and hence variations in either IGF or IGFBP binding sites are plausible. Analysis of both wildtype IGFBP-6 and an amino-terminal fragment of IGFBP-6 (residues 64-116) may provide insight into the differences in binding preferences exhibited by the IGFBPs.

Although sequence alignments of IGFBPs infer a common binding site, NMR experiments could be carried out to identify the specific regions of IGFBP-2 perturbed upon binding of unlabelled IGF-I and IGF-II ligands. Interpretation of chemical shift perturbations however would require resonance assignments for IGFBP-2. In the absence of such information, chemical tags (eg. fluorotryptophan labelling) could be used to obtain information regarding the perturbation of specific amino acid residues. For example, ^{19}F-labelling would enable the identification of aromatic residues involved in the binding interaction. Indeed, Tyr60 of IGFBP-2 and the corresponding Tyr50 of IGFBP-5 have been shown to be important for IGF binding (Hobba *et al.*, 1996: Kalus *et al.*, 1998). Differences observed between binding of IGF-I or IGF-II may provide insight into enhancing the selectivity of IGFBP-2 for one ligand over the other. Alternatively, if the same resonances on Trx$^{1-279}$IGFBP-2HIS were perturbed by IGF-I and IGF-II and by similar amounts, differing binding epitopes could be attributed to the different ligands. This approach has limitations, and certainly, it does not define the structure of either IGFBP or the complex. It does, however, provide valuable information regarding the residues perturbed upon complex formation, either due to direct contact or due to indirect conformational change. Such information is valuable in guiding the generation of site-specific mutations and for the design of binding mimics.

7.5.2 IMPLICATIONS FOR IGF RECEPTOR BINDING

IGF complexes with the IGFBPs and the type-1 IGF-receptor are mutually exclusive and evidence suggests this is due to overlapping binding sites on the IGF ligand. Indeed, Tyr60 of IGF-I was protected from iodination when complexed to either type-1 IGF-receptor (Maly & Lüthi, 1988) or IGFBP-2 (Moss *et al.*, 1991). Perturbation of Tyr60 in the present study clearly

implicated a change in chemical environment of this residue when in complex with IGFBP-2. Furthermore, epitope mapping of IGF-I identified three unique monoclonal antibody groups that interfered with both IGFBP and type-1 IGF receptor binding interactions (Manes *et al.*, 1999). Therefore, although the key residues involved in type-1 IGF-receptor and IGFBP binding are located on different faces of the IGF molecule, overlapping binding site residues may prevent simultaneous binding by IGFBPs and the type-1 receptor.

B-domain residues of IGF-I known to be important in type-1 receptor binding (viz: Phe-23, Tyr24 and Phe25 of IGF-I and Phe26, Tyr27 and Phe28 of IGF-II) (Cascieri *et al.*, 1988) overlap with residues which were significantly perturbed upon binding of Trx^{1-279}IGFBP-2HIS (viz: Phe16-Phe23). The extent of perturbation of Tyr24 of IGF-I could not be determined in the present study. In contrast, amino acid residues Phe25-Cys48 were not significantly perturbed upon binding of Trx^{1-279}IGFBP-2HIS. Leucine substitution of Tyr24 of IGF-I (Cascieri *et al.*, 1988) and Tyr27 of IGF-II (Sakano *et al.*, 1991) resulted in IGF analogues that retained only 1-5 % of their original type-1 IGF receptor binding affinity. While the Tyr24Leu mutation itself did not appear to affect IGFBP binding, when mutated in combination with Tyr60, the affinity for IGFBPs was reduced by half (Bayne *et al.*, 1990). In contrast, the individual IGF mutants Tyr31Ala Tyr60Leu and Tyr24Leu Tyr31Ala did not affect IGFBP binding (Bayne *et al.*, 1990). Certainly, it appears that this region of IGF-I contains information pertinent for both type-1 receptor and IGFBP binding.

C-domain residues of IGF-I, known to be important for type-1 receptor binding, were not perturbed upon binding of Trx^{1-279}IGFBP-2HIS. Tyr31 of IGF-I has been reported to be a critical determinant for IGF receptor binding and its solvent exposed location at the tip of the extension places it in an ideal location to interact with a receptor molecule. Replacement of IGF-I residues Pro28-Arg37 resulted in a 30-fold loss of affinity for the type-1 IGF receptor (Bayne *et al.*, 1989). Furthermore, both Arg36 and Arg37 were perturbed in NMR chemical shift analyses with IGFBP-1 (Jansson *et al.*, 1998) however were not significantly perturbed upon binding of Trx^{1-279}IGFBP-2HIS. Substitution of these residues therefore may be important

for the structural integrity of the molecule and indeed their surface exposed location lends itself to this theory.

The complex of IGF-I with mini-IGFBP-5 provided evidence for overlapping IGFBP and IGF receptor binding sites on the IGF molecule. In contrast to the complete inhibition of type-1 IGF receptor binding by an excess of IGFBP-5, incomplete inhibition of receptor binding was observed when mini-IGFBP-5 was in excess (Kalus *et al.*, 1998). Analysis of the structure of IGF-I, suggests the ligand will still be accessible to the receptor even when complexed to the truncated IGFBP-5 fragment. The C-terminal domain of IGFBP-5 appears to be essential for effective inhibition of receptor binding of IGF-I. The present study provides evidence to support this claim, as several of the residues of IGF-I perturbed by binding of $Trx^{136-279}$IGFBP-2HIS (viz: Phe 23 and Tyr24) are also important for receptor binding (Cascieri *et al.*, 1988).

7.6 CONCLUDING REMARKS

In summary, the IGFBP-2 binding determinants are localised in the B- and A-domains of IGF-I. Furthermore, the lack of involvement of the C-domain of IGF-I was confirmed in the present studies. Evidence for overlapping IGFBP and IGF receptor binding sites at the C-terminus of the B-domain of IGF-I was also presented. Our current analyses showed many differences from a previously published NMR study of the interaction between IGF-I and IGFBP-1 (Jansson *et al.*, 1998) and are more consistent with expectations from mutational studies. The present study has highlighted the value of NMR to probe the binding interface between IGF and IGFBP-2, but has also revealed some technical difficulties including aggregation and poor spectra resolution of the IGF molecules. A similar study is planned of the interactions of labelled IGF-I and IGF-II with IGFBP-6 (Professor R.Norton and Dr L. Bach) although the limitations reported in this chapter will need to be resolved before this is attempted. Ultimately, these studies will provide the basis for design of IGFBP agonists and antagonists for therapeutic applications.

CHAPTER 8

FINAL DISCUSSION

The importance of IGFBPs in modulating IGF availability and bioactivity is becoming increasingly more evident and clearly their biological roles extend beyond merely influencing IGF half-life in circulation or transporting IGFs to target tissues. Lack of information regarding the IGF binding mechanism of IGFBPs however, particularly at the molecular level, constitutes a considerable gap in the understanding of IGFBP function. Therefore the broad objective of this thesis was to increase the understanding of bIGFBP-2 structure and function relationships and to further delineate the binding sites on both IGF and IGFBP-2. Ultimately, novel information regarding the specific residues of IGF and IGFBP-2 involved in the binding interaction could be used for the design of specific binding mimics with either agonistic or antagonistic binding properties.

8.1 SUMMARY OF FINDINGS

As discussed in Section 1.7, at commencement of this study evidence suggested that both the amino- and carboxyl-terminal domains of IGFBPs participate in IGF-binding. Furthermore, there is a high degree of sequence homology throughout the IGFBP family in both the N- and C-terminal domains. Thus, the initial research goal was to identify the IGF binding site(s) of bIGFBP-2. The strategy involved generating discrete amino-terminal domains (amino acid residues 1-93, 1-104, 1-132 and 1-185) and carboxyl-terminal domains (amino acid residues 96-279, 136-279, 182-284) of bovine IGFBP-2 (bIGFBP-2).

Truncated forms of the native IGFBP-2 were recombinantly expressed from COS-1 cells for structural and functional analyses. This expression system provided reference bIGFBP-2 material that possessed binding affinities for IGF-I and IGF-II that were consistent with published values. Moreover, the COS-1 cells contained the machinery to express and correctly process truncated mutant analogues of bIGFBP-2. As the ability to detect IGF binding activity is largely dependent on methodology, BIAcore technology was used in this study to analyse the interactions between the amino- and carboxyl-terminal fragments of IGFBP-2 with

native IGF ligands and IGF analogues. Analysis of the binding properties of these truncations provided insightful knowledge into the high affinity binding interaction and has been published (Carrick *et al.*, 2001).

Both halves of bIGFBP-2 bind IGF-I and IGF-II in BIAcore studies, albeit with different affinities ($^{1-132}$IGFBP-2: K_D=36.3 nM and 51.8 nM; $^{136-279}$IGFBP-2HIS: K_D=23.8 nM and 16.3 nM respectively). The amino-terminal half appears to contain components responsible for fast association. In contrast, IGF binding by the carboxyl-terminal fragment results in a more stable complex as reflected by its K_D. Furthermore, des(1-3)IGF-I and des(1-6)IGF-II exhibited reduced binding affinity to $^{1-279}$IGFBP-2HIS, $^{1-132}$IGFBP-2 and $^{136-279}$IGFBP-2HIS biosensor surfaces compared with wildtype IGF. A charge reversal at positions 3 and 6 of IGF-I and IGF-II, respectively, affected binding interactions with the amino-terminal fragment and full-length bIGFBP-2 but not the carboxyl-terminal fragment. These results are consistent with a publication by Kalus and co-workers (1998), which localized a major binding epitope of IGF to residues 40-92 of hIGFBP-5. Furthermore, Ho and Baxter (1998) determined the amino hexapeptide of IGF-II was required for interaction with the C-terminal domain of IGFBP-2.

A second goal of this thesis was to further define the structure of the bIGFBP-2 molecule. To date, structure studies have been inhibited by molecular size constraints and the absence of a large-scale production system for IGFBP. NMR structural studies of bIGFBP-2 have only recently been contemplated, since an appropriate expression system capable of yielding large quantities of isotopically-labelled bIGFBP-2 was established in this study (Chapter 2). However, incorporation of an amino-terminal thioredoxin-tag increased the molecular weight of the fusion protein beyond the current spectral resolution, and removal of the fusion protein was relatively inefficient (yield of approximately 20 %). An alternative cleavage site therefore would be optimal for increased protein production. Screening a library of α-lytic proteases may potentially identify a unique cleavage site to separate $^{1-279}$IGFBP-2HIS from the Trx fusion partner, as has been described by Lien *et al.* (2001) for the removal of the porcine growth hormone 1-14 fusion partner from IGF-II.

Structure determination studies will ultimately provide a comprehensive insight into the molecular basis of the IGF·IGFBP binding interaction, making it possible to produce mutant binding proteins specific for a particular IGF for therapeutic applications. Structure determination techniques including NMR, X-ray crystallography and electron microscopy were undertaken in this study. Crystals of $^{1-279}$IGFBP-2HIS were obtained in this study, however they are presently too small for current X-ray diffraction technology. Similarly, low-resolution images prevented interpretation of electron microscopy data. NMR spectra of bIGFBP-2, though complex, were well-resolved and provided encouragement for continued NMR structural analysis. Analysis of full-length IGFBP-2 and its truncated N- and C-terminal fragments is continuing in parallel with structure determination of IGFBP-6 (Professor R. Norton, Professor J. Wallace and Associate Professor L. Bach).

In addition to structure determination, NMR was also used to investigate the specific residues of IGF involved in binding bIGFBP-2. This strategy had previously been used to define residues of IGF-I involved in binding IGFBP-1 (Jansson *et al.*, 1998). The residues of IGF-I that were significantly perturbed upon binding of Trx$^{1-279}$IGFBP-2HIS were Glu3, Glu9, Leu10, Phe16, Val17, Cys18, Gly19, Asp20, Arg21, Gly22, Phe23, Ser34, Phe49, Ser51, Leu54, Glu58, Tyr60 and Cys61. Residues of the C-domain of IGF-I were not perturbed in the presence of IGFBP-2 (Phe25-Cys48). It appears that residues Gly19, Asp20, Gly22, Phe 23, Tyr24, Phe49 and Leu54 are perturbed in the presence of the $^{136-279}$IGFBP-2HIS and potentially represent the binding site for this binding domain of IGFBP-2. Chemical shift analysis of the binding interaction between IGF-I and IGFBP-2 are consistent with mutagenesis studies in the literature. Furthermore, residues of IGF-I that made direct contact with mini-IGFBP-5 were also perturbed upon binding of IGFBP-2.

In conclusion, results from the present study have contributed to defining the IGF binding epitopes for IGFBP-2 and have attributed binding roles to the highly conserved amino- and carboxyl-terminal domains. BIAcore studies also provided insight into the orientation of the IGF and IGFBP-2 molecules in complex with each other.

8.2 FUTURE DIRECTIONS

The interaction between IGFs and IGFBPs is a complex one which researchers are only beginning to understand. The IGFBPs must bind IGFs with high affinity to maintain a latent reservoir, however they must also be highly labile under certain physiological conditions for rapid and controlled release of IGF. The mechanism(s) that underlie IGFBP-IGF interactions are complicated by the fact that both the amino- and carboxyl-terminal regions of IGFBPs are necessary for high affinity interactions with IGFs. Future studies therefore need to address the precise mechanisms of the IGF·IGFBP interaction and indeed progress toward the development of peptide mimics for therapeutic manipulation of the complex. A detailed knowledge of the tertiary structure of the complex will be essential to understanding function in molecular biology, structural biology and drug design.

8.2.1 STRUCTURE DETERMINATION

In addition to determining the mechanism by which the different binding proteins interact with the IGFs, the studies on the binding proteins would greatly benefit from more detailed structural knowledge. A solution structure for an N-terminal binding fragment of IGFBP-5 has only recently been published (Kalus *et al.*, 1998) and subsequently as a crystal structure in complex with IGF-I (Żesławski *et al.*, 2001). The structures of the central-linking domain and the highly conserved carboxyl-terminal region of IGFBPs remain elusive. Homology between IGFBPs and the thyroglobulin type-1 domain (Rechler, 1993; Guncar *et al.*, 1999) however, has allowed structural modelling of the C-terminal domain of IGFBP-2 (M. Lucic; PhD. Thesis, Adelaide University 2000), based on the X-ray crystal structure of the MHC class II-associated p41 Ii fragment (which had sequences typical of a thyroglobulin type-1 domain) (Guncar *et al.*, 1999). The known disulfide bond pattern of the C-terminal domain of IGFBP-2 (Forbes *et al.*, 1998) was maintained in the C-terminal domain model (M. Lucic; PhD

Thesis, Adelaide University 2000). This model therefore, provides a basis for interpretation of the effects of substitutions in the C-terminal region of IGFBP-2 on IGF binding and can be used to predict other amino acid residues that may be accessible for interacting with the IGFs.

Structure studies that are focused on the ligand have the advantage that they can be carried out over a short period of time. Information derived from these studies, however, is incomplete and the most valuable structural information is gained from high-resolution structures of the complex. Such studies provide the greatest insight into the nature of the binding pocket, which is essential for drug design. Information can then be used in the *de novo* design of analogues that are very different from the parent molecules. This might be accomplished by characterising the structural features of the binding site using algorithms such as CAVEAT (Lauri *et al.*, 1994), followed by 3D database search for compounds that have the proper functional groups and geometric properties for binding to this site. The complete 3D structure may also be useful to locate additional binding sites that would not be revealed in structural studies focussed on the ligand and may be used to explain differences in activity between structurally similar analogues.

Other parameters in addition to chemical shifts can also be monitored in NMR studies. Protection of backbone amides in the complex can be detected readily using hydrogen-deuterium exchange measurements (monitored by 2D HSQC spectra) while ^{15}N dynamics measurements can provide information on regions of the interacting proteins that become less flexible in the complex. Ehring (1999) demonstrated the effectiveness of hydrogen-deuterium exchange by analysing residues on IGF-I that interact with IGFBP-1. Participating backbone amide groups of IGF-I were identified by proteolysis and mass spectrometry (Ehring *et al*, 1999). On the other hand, ^{15}N relaxation experiments have been used to investigate the dynamic properties of mini-IGFBP-5 alone and in complex with IGF-I (Renner and Holak, 2001). Results showed that all but 11 unstructured flexible residues at the C-terminus of mini-IGFBP-5 remained rigid on the fast time scale. The dynamic properties of the residues involved in binding IGF varied, whereas differences in the rest of the protein were only due to slower rotational diffusion (Renner and Holak, 2001). NMR techniques can also be used to derive

information on the orientations of a large number of NH or CH bonds between interacting molecules. Dipolar couplings can be used to determine relative orientations of two molecules in the complex and to detect minor structural changes in free and bound states. Complementary to the structural information on regions of the ligand that bind to the receptor is the identification of the solvent-exposed portions of the ligand. Typically, this information could be used in the design of analogues that are modified at these sites to improve their physical properties without affecting their binding affinity (Fesik, 1991).

Evidence arising from this thesis and also by Kalus *et al.* (1998), suggest the amino-terminal domain of IGFBPs is responsible for rapid association while the C-terminal domain is essential to the stability of the high affinity complex. While, high affinity interactions are the culmination of numerous hydrophobic interactions, hydrogen bonds and electrostatic contacts, side-chain contacts can be essential for maintenance of a complex without facilitating complex formation. An example of this is the interface between growth hormone (hGH) and the growth hormone receptor (hGHbp) (reviewed by Wells, 1996). Alanine-scanning mutagenesis of the essential residues involved in the interaction generally increased rates of hGH dissociation from hGHbp, without affecting the rates of association (Wells, 1996). Indeed, a loss of stabilising interactions explains the rapid dissociation displayed by the amino-terminal fragments of IGFBP-2, which clearly requires covalent attachment to the carboxyl-terminal domain to establish the characteristic high-affinity interaction.

Various techniques including site directed mutagenesis, alanine screening and combinatorial chemistry are employed for mapping out the functional regions of proteins and small molecules. NMR has long been applied to these problems, with recent studies highlighting the utility of chemical shift analysis for the identification and design of high affinity ligands for proteins and for mapping intermolecular interfaces (Foster *et al.,* 1998). Recently, phage display techniques have been used to probe the binding interface between growth hormone and growth hormone receptor (Sidhu *et al.*, 2000). This approach provides invaluable information for selection of novel peptides.

8.2.2 DESIGN OF IGF AND IGFBP MIMICS

IGFBPs are strongly emerging as targets for indirect agonist drug design. Peptide antagonists of the interaction between IGFs and IGFBPs have recently been discovered by phage display analysis of peptide libraries (Lowman *et al.*, 1998) and by screening of chemical library collections (Liu *et al.*, 2001). Upon screening of phage-displayed libraries of small peptide ligands, Lowman and co-workers (1998) identified a 14 amino acid peptide that displaced IGF-I from human IGFBP-1. Interestingly, the peptide was specific for hIGFBP-1 and failed to interact with rIGFBP-1 and hIGFBP-3 at submillimolar concentrations. A detailed analysis of the structure of this peptide antagonist has provided important information regarding the features necessary for IGFBP-1 binding and structural integrity (Skelton *et al.*, 2001). In contrast, Liu and co-workers (2001) identified a non-peptide, organic molecule, NBI-31772, which displaced IGF-I from all six IGFBPs. The released IGF was biologically active. While NBI-31772 blocks the IGF·IGFBP interaction by binding IGFBPs with efficacy at low nanomolar concentrations, it is not specific for IGF-I or IGF-II. Also, it is not specific for any of the IGFBPs although it does exhibit varying activity toward each of the IGFBPs (IGFBP-2 and –4 > IGFBP-1, -3, and -5 > IGFBP-6) (Liu *et al.,* 2001). Discovery of an agonist specific for either IGF-I or IGF-II will be critical for treatment of particular disease states where only one of the IGF ligands is to be targeted.

Ligand agonists that interact specifically with the IGFBPs, but not the IGF receptors, to displace IGF-I from the IGF·IGFBP complex for treatment of diabetes and other IGF responsive diseases, have previously been reported in the literature. The IGF-I analogues [$Leu^{14,59,60}$ Ala^{31}]-IGF-I and [$Leu^{24}Ala^{31}$]-IGF-I interact specifically with the IGFBPs and do not bind the type 1 IGF receptor (Loddick *et al.*, 1998; Lowman *et al.*, 1998). Indeed, these analogues are neuroprotective in animal models of stroke and mimicked IGF-I activity on insulin secretion and blood glucose control in animal models of diabetes, respectively. The use of IGF analogues in human therapeutics however does not provide a distinct advantage over IGF-I because they remain relatively large peptides. Manufacture of such peptides is difficult and expensive, and

the value of their *in vivo* administration is reduced by rapid degradation and localisation difficulties. There is also a concern for the development of IGF as a therapeutic to treat different physiological states because of the association of high plasma levels of IGFs with cancers.

There is a significant advantage to identifying or designing small non-peptide ligands over exogenously applied IGF, which has the potential to cause hypoglycemia. Administration of a binding mimic that displaces free biologically active IGF from complexes with IGFBPs would be ideal for therapeutic application, in particular for the treatment of diabetes. Interestingly, the detergent that co-crystallised with IGF-I, deoxy big CHAPS, bound to IGF-I in a region of the surface known to be important for IGFBP interactions (K_D ~300 uM; Vajdos *et al.*, 2001). In fact, deoxy big CHAPS inhibited the binding of phage-displayed IGF-I to IGFBP-1 and IGFBP-3. Therefore, it may be possible to develop small molecule drugs which disrupt the IGF-I·IGFBP complex and thereby, as described by the authors above, release receptor active IGF-I from the inactive, systemic pool. Identification of agents capable of blocking the IGF·IGFBP interaction should be a priority of IGF research.

8.3 CONCLUSION

In conclusion, a comprehensive understanding of the binding determinants and tertiary structure of the IGF·IGFBP complex will enable development of specific IGF agonists and antagonists that mimic the binding epitope of IGFBPs. This would ultimately permit synthesis of molecules with different molecular frameworks but with spatially intact functional groups for therapeutic applications. These new molecules would be pharmacologically designed with increased specificity, improved resistance against catabolism and reduced toxicity. The residues to be targeted would be those identified in this and other studies as contributing most significantly to binding interactions with IGFs.

REFERENCES

Andress, D. L. and Birnbaum, R. S. (1992). Human osteoblast-derived insulin-like growth factor (IGF) binding protein-5 stimulates osteoblast mitogenesis and potentiates IGF action. *J Biol Chem* **267**(31): 22467-22472.

Andress, D.L. (1998). Insulin-like growth factor-binding protein-5 (IGFBP-5) stimulates phosphorylation of the IGFBP-5 receptor. *Am J Physiol* **274**(4 Pt 1): E744-50.

Andress, D.L., Loop, S.M., Zapf, J. and Kiefer, M.C. (1993). Carboxy-truncated insulin-like growth factor binding protein-5 stimulates mitogenesis in osteoblast-like cells. *Biochem Biophys Res Commun.* **195**(1): 25-30.

Arai, T., Busby, W., Jr. and Clemmons, D.R. (1996b). Binding of insulin-like growth factor (IGF) I or II to IGF-binding protein-2 enables it to bind to heparin and extracellular matrix. *Endocrinology* **137**(11): 4571-4575.

Arai, T., Clarke, J., Parker, A., Busby, W., Jr., Nam, T. and Clemmons, D.R. (1996a). Substitution of specific amino acids in insulin-like growth factor (IGF) binding protein-5 alters heparin binding and its change in affinity for IGF-I in response to heparin. *J Biol Chem* **271**(11): 6090-6106.

Arai, T., Parker, A., Busby, W. and Clemmons, D.R. (1994). Heparin, heparan sulfate, and dermatan sulfate regulate formation of the insulin-like growth factor-I and insulin-like growth factor-binding protein complexes. *J Biol Chem* **269**(32): 20388-20393.

Bach, L.A., Hsieh, S., Sakano, K.I., Fujiwara, H., Perdue, J.F. and Rechler, M.M. (1993). Binding of mutants of human insulin-like growth factor-II to insulin-like growth factor binding proteins 1-6. *J Biol Chem* **268**(13): 9246-9254.

Bach, L. A., Thotakura, N. R. and Rechler, M. M. (1992). Human insulin-like growth factor binding protein-6 is O-glycosylated. *Biochem. Biophys. Res. Commun.* **186**(1): 301-307.

Bagley, C.J., May, B.L., Szabo, L., McNamara, P.J., Ross, M., Francis, G.L., *et al.* (1989). A key functional role for the insulin-like growth factor-I amino-terminal pentapeptide. *Biochem J* **259**(3): 665-672.

Bairoch, A. (1991). PROSITE: a dictionary of sites and patterns in proteins. *Nucleic Acids Res* **19 Suppl**(11): 2241-2245.

Baker, J., Liu, J.P., Robertson, E.J. and Efstratiadis, A. (1993). Role of insulin-like growth factors in embryonic and postnatal growth. *Cell* **75**(1): 73-82.

Ballard, F.J., Francis, G.L., Ross, M., Bagley, C.J., May, B. and Wallace, J.C. (1987). Natural and synthetic forms of insulin-like growth factor-1 (IGF-1) and the potent derivative, destripeptide IGF-1: biological activities and receptor binding. *Biochem Biophys Res Commun* **149**(2): 398-404.

Bartels, C., Xia, T.H., Billeter, P., Guntert, P. and Wüthrich, K. (1995). The program XEASY for computer-supported NMR spectral analysis of biological macromolecules. *J Biomolecular NMR* **5**, 1-10.

Baserga, R., Resnicoff, M. and Dews, M. (1997). The IGF-I receptor and cancer. *Endocrine* **7**(1): 99-102.

Baxter, R.C. (1990). Glycosaminoglycans inhibit formation of the 140 kDa insulin-like growth factor-binding protein complex. *Biochem J* **271**(3): 773-777.

Baxter, R.C. (1994). Insulin-like growth factor binding proteins in the human circulation: a review. *Horm Res* **42**: 140-144.

Baxter, R.C. (2000). Insulin-like growth factor (IGF)-binding proteins: interactions with IGFs and intrinsic bioactivities. *Am J Physiol Endocrinol Metab* **278**(6): E967-76.

Baxter, R.C. and Firth, S.M. (1996). Modulation of human IGF binding protein-3 activity by structural modification. *Progress in Growth Factor Research.* **6(2-4):** 215-222.

Baxter, R.C. and Skriver, L. (1993). Altered ligand specificity of proteolysed insulin-like growth factor binding protein-3. *Biochem Biophys Res Commun* **196**(3): 1267-1273.

Bayne, M.L., Applebaum, J., Chicchi, G.G., Hayes, N.S., Green, B.G. and Cascieri, M.A. (1988). Structural analogs of human insulin-like growth factor-I with reduced affinity for serum binding proteins and the type-2 insulin-like growth factor receptor. *J Biol Chem* **263**(13): 6233-6239.

Bayne, M. L., Applebaum, J., Chicchi, G. G., Miller, R. E. and Cascieri, M. A. (1990). The roles of tyrosines 24, 31, and 60 in the high affinity binding of insulin-like growth factor-I to the type 1 insulin-like growth factor receptor. *J Biol Chem* **265**(26): 15648-15652.

Bayne, M. L., Applebaum, J., Underwood, D., Chicchi, G. G., Green, B. G., Hayes, N. S. and Cascieri, M. A. (1989). The C region of human insulin-like growth factor (IGF) I is required for high affinity binding to the type 1 IGF receptor. *J Biol Chem* **264**(19): 11004-11008.

Bentley, G., Dodson, E., Dodson, G., Hodgkin, D. and Mercola, D. (1976). Structure of insulin in 4-zinc insulin. *Nature* **261**(5556): 166-168.

Berman, H. M., Westbrook, J., Feng, Z., Gilliland, G., Bhat, T. N., Weissig, H., Shindyalov, I. N. and Bourne, P. E. (2000). The Protein Data Bank. *Nucleic Acids Res* **28**(1): 235-242.

Bicsak TA, Nakatani A, Shimonaka M, Malkowski M, Ling N. (1990). Insulin-like growth factor binding protein measurement: sodium dodecyl sulfate-stable complexes with insulin-like growth factor in serum prevent accurate assessment of total binding protein content by ligand blotting. *Anal Biochem.* **191**(1):75-79

Binkert, C., Lanwehr, J., Mary, J.-L., Schwander, J. and Heinrich, G. (1989). Cloning, sequence analysis and expression of a cDNA encoding a novel insulin-like growth factor binding protein-2 (IGFBP-2). *EMBO J.* **8**(9): 2497-2502.

Binoux, M. and Hossenlopp, P. (1988). Insulin-like growth factor (IGF) and IGF-binding proteins: comparison of human serum and lymph. *J. Clin. Endocrinol. Metab.* **67**(3): 509-514.

Binoux, M., Hossenlopp, P., Lassarre, C. and Segovia, B. (1991). Degradation of IGF binding protein-3 by proteases: Physiological implications. *Modern Concepts of Insulin Like Growth Factors.* E.M. Spencer, Editor. 329-336.

Blundell, T.L., Bedarkar, S. and Humbel, R.E. (1983). Tertiary structures, receptor binding, and antigenicity of insulin-like growth factors. *Fed Proc* **42**(9): 2592-2597.

Blundell, T.L., Bedarkar, S., Rinderknecht, E. and Humbel, R.E. (1978). Insulin-like growth factor: a model for tertiary structure accounting for immunoreactivity and receptor binding. *Proc Natl Acad Sci U S A* **75**(1): 180-184.

Booth, B.A., Boes, M. and Bar, R.S. (1996). IGFBP-3 proteolysis by plasmin, thrombin, serum: heparin binding, IGF binding, and structure of fragments. *Am J Physiol* **271**(3 Pt 1): E465-70.

Booth, B.A., Boes, M., Andress, D.L., Dake, B.L., Kiefer, M.C., Maack, C., *et al.* (1995). IGFBP-3 and IGFBP-5 association with endothelial cells: role of C-terminal heparin binding domain. *Growth Regul* **5**(1): 1-17.

Bork, P. (1993). The modular architecture of a new family of growth regulators related to connective tissue growth factor. *FEBS Lett* **327**: 125-130.

Bourner, M. J., Busby, W. H. J., Siegel, N. R., Krivi, G. G., McCusker, R. H. and Clemmons, D. R. (1992). Cloning and sequence determination of bovine insulin-like growth factor binding protein-2 (IGFBP-2): comparison of its structural and functional properties with IGFBP-1. *J. Cell. Biochem.* **48**(2): 215-226.

Bramani, S., Song, H., Beattie, J., Tonner, E., Flint, D.J. and Allan, G.J. (1999). Amino acids within the extracellular matrix (ECM) binding region (201-218) of rat insulin-like growth factor binding protein (IGFBP)-5 are important determinants in binding IGF-I. *J. Mol. Endocrinol.* **23**(1): 117-123.

Branden, C. and Tooze, J. (1991). Introduction to Protein Structure. *Garland Publishing, Inc.* NY and London.

Braulke, T. (1999). Type-2 IGF receptor: a multi-ligand binding protein. *Horm Metab Res* **31**(2-3): 242-246.

Brinkman, A., Kortleve, D.J., Schuller, A.G.P., Zwarthoff, E.C. and Drop, S.L.S. (1991a). Site-directed mutagenesis of the N-terminal region of IGF binding protein-1: analysis of IGF binding capability. *FEBS lett.* **291**(2): 264-268.

Brinkman, A., Kortleve, D.J., Zwarthoff, E.C. and Drop, S.L.S. (1991b). Mutations in the carboxyl-terminal part of insulin-like growth factor (IGF)-binding protein-1 result in dimer formation and loss of IGF binding capacity. *Mol Endocrinol* **5**(7): 987-994.

Brown, A. L. and Rechler, M. M. (1990). Cloning of the rat insulin-like growth factor-binding protein-2 gene and identification of a functional promoter lacking a TATA box. *Mol. Endocrinol.* **4**(12): 2039-2051.

Buck, M. A., Olah, T. A., Weitzmann, C. J., and Cooperman, B. S. (1989) Protein estimation by the product of integrated peak area and flow rate. *Analytical Biochemistry* **182,** 295-299.

Byun, D., Mohan, S., Kim, C., Suh, K., Yoo, M., Lee, H., *et al.* (2000). Studies on human pregnancy-induced insulin-like growth factor (IGF)-binding protein-4 proteases in serum: determination of IGF-II dependency and localization of cleavage site. *J Clin Endo Metab* **85**(1): 373-381.

Camacho-Hubner, C., Woods, K. A., Miraki-Moud, F., Clark, A. J. and Savage, M. O. (1999). Insulin-like growth factor-I deficiency caused by a partial deletion of the IGF-I gene: effects of rhIGF-I therapy. *Growth Horm. IGF Res.* **9**(Supp B): 47-52.

Canziani, G., Zhang, W., Cines, D., Rux, A., Willis, S., Cohen, G., Eisenberg, R. & Chaiken, I. (1999). Exploring biomolecular recognition using optical biosensors. *Methods* **19**, 253-269.
Cardin, A.D. and Weintraub, H.J. (1989). Molecular modeling of protein-glycosaminoglycan interactions. *Arteriosclerosis* **9**(1): 21-32.

Carr, J.M., Owens, J.A., Grant, P.A., Walton, P.E., Owens, P.C. and Wallace, J.C. (1995). Circulating insulin-like growth factors (IGFs), IGF-binding proteins (IGFBPs) and tissue mRNA levels of IGFBP-2 and IGFBP-4 in the ovine fetus. *J Endocrinol* **145**(3): 545-557.

Carrick FE, Forbes BE, Wallace JC. (2001). BIAcore analysis of bovine insulin-like growth factor (IGF)-binding protein-2 identifies major IGF binding site determinants in both the amino- and carboxyl-terminal domains. *J Biol Chem* **276**(29):27120-27128.

Cascieri, M. A., Saperstein, R., Hayes, N. S., Green, B. G., Chicchi, G. G., Applebaum, J. and Bayne, M. L. (1988). Serum half-life and biological activity of mutants of human insulin-like growth factor I which do not bind to serum binding proteins. *Endocrinology* **123**(1): 373-381.

Cascieri M.A., Chicchi G.G., Applebaum J., Green B.G., Hayes N.S., Bayne M.L. (1989) Structural analogs of human insulin-like growth factor (IGF) I with altered affinity for type 2 IGF receptors. *J Biol Chem* **264**: 2199-2202.

Ceda, G.P., Fielder, P.J., Henzel, W.J., Louie, A., Donovan, S.M., Hoffman, A.R., *et al.* (1991). Differential effects of insulin-like growth factor (IGF)-I and IGF-II on the expression of IGF binding proteins (IGFBPs) in a rat neuroblastoma cell line: isolation and characterization of two forms of IGFBP-4. *Endocrinology* **128**(6): 2815-2824.

Chelius, D., Baldwin, M. A., Lu, X. and Spencer, E. M. (2001). Expression, purification and characterization of the structure and disulfide linkages of insulin-like growth factor binding protein-4. *J Endocrinol* **168**(2): 283-296.

Chernausek, S.D., Smith, C.E., Duffin, K.L., Busby, W.H., Wright, G. and Clemmons, D.R. (1995). Proteolytic cleavage of insulin-like growth factor binding protein-4 (IGFBP-4): localization of cleavage site to non-homologous region of native IGFBP-4. *J Biol Chem* **270**(19): 11377-11382.

Clemmons, D. R., Busby, W. H., Winter, S. and Moralez, A. (1999). Complement 1s is an IGFBP-5 protease that is synthesized and secreted by fibroblasts and smooth muscle cells and regulates IGFBP-5 actions. *Growth Horm. IGF Res.* **9**(5): 317.

Clemmons, D.R., Cascieri, M.A., Camacho-Hubner, C., McCusker, R.H. and Bayne, M.L. (1990). Discrete alterations of the insulin-like growth factor I molecule which alter its affinity for insulin-like growth factor-binding proteins result in changes in bioactivity. *J Biol Chem* **265**(21): 12210-12216.

Clemmons, D.R., Dehoff, M.L., Busby, W.H., Bayne, M.L. and Cascieri, M.A. (1992). Competition for binding to insulin-like growth factor (IGF) binding protein-2, -3, -4, and -5 by the IGFs and IGF analogs. *Endocrinology* **131**(2): 890-895.

Clore, G.M. and Gronenborn, A.M. (1993). NMR of Proteins. *Boca Raton; CRC Press.*

Cohen (2000). Intracellular and Nuclear Interactions of IGFBPs. 4th International Workshop on IGF Binding Proteins, Terrigal, NSW, Australia, Churchill Livingstone.

Cohen, P., Graves, H.C.B., Peehl, D.M., Kamarei, M., Giudice, L.C. and Rosenfeld, R.G. (1992). Prostate-specific antigen (PSA) is an insulin-like growth factor binding protein-3 protease found in seminal plasma. *J Clin Endocrinol* **75**(4): 1046-1053.

Cohick, W.S. and Clemmons, D.R. (1993). The insulin-like growth factors. *Annu Rev Physiol* **55**: 131-153.

Conover, C. A. (1998). IGFBP regulation by proteases. In *Molecular mechanisms to regulate the activities of insulin-like growth factors.* (Takano, K., Hizuka, N. & Takahashi, S. I., eds.), pp. 107-114. Elsevier, Amsterdam.

Conover, C.A. (1991). Glycosylation of insulin-like growth factor binding protein-3 (IGFBP-3) is not required for potentiation of IGF-I action: evidence for processing of cell-bound IGFBP-3. *Endocrinology* **129**(6): 3259-3268.

Conover, C.A. and De Leon, D.D. (1994). Acid-activated insulin-like growth factor-binding protein-3 proteolysis in normal and transformed. *J Biol Chem* **269**(10): 7076-7080.

Conover, C.A. and Kiefer, M.C. (1993). Regulation and biological effect of endogenous insulin-like growth factor binding protein-5 in human osteoblastic cells. *J Clin Endocrinol Metab* **76**(5): 1153-1159.

Conover, C.A., Durham, S.K., Zapf, J., Masiarz, F.R. and Kiefer, M.C. (1995). Cleavage analysis of insulin-like growth factor (IGF)-dependent IGF-binding protein-4 proteolysis and expression of protease-resistant IGF-binding protein-4 mutants. *J Biol Chem* **270**(9): 4395-4400.

Conover, C.A., Kiefer, M.C. and Zapf, J. (1993). Posttranslational regulation of insulin-like growth factor binding protein-4 in normal and transformed human fibroblasts: insulin-like growth factor dependence and biological studies. *J Clin Invest* **91**(3): 1129-1137.

Cooke, R.M., Harvey, T.S. and Campbell, I.D. (1991). Solution structure of human insulin-like growth factor-I: a nuclear magnetic resonance and restrained molecular dynamics study. *Biochemistry* **30**(22): 5484-5491.

Coverley, J.A. and Baxter, R.C. (1997). Phosphorylation of insulin-like growth factor binding proteins. *Mol Cell Endocrinol* **128**(1-2): 1-5.

Craik, D. J. and Wilce, J. A. (1997). Studies of protein-ligand interactions by NMR. *Methods Mol Biol* **60**: 195-232.

de Pagter-Holthuizen, P., van Schaik, F.M., Verduijn, G.M., van Ommen, G.J., Bouma, B.N., Jansen, M., *et al.* (1986). Organization of the human genes for insulin-like growth factors I and II. *FEBS Lett* **195**(1-2): 179-184.

De Vroede, M.A., Rechler, M.M., Nissley, S.P., Joshi, S., Burke, G.T. and Katsoyannis, P.G. (1985). Hybrid molecules containing the B-domain of insulin-like growth factor-I are recognized by carrier proteins of the growth factor. *Proc Natl Acad Sci U.S.A* **82**: 3010-3014.

De Wolf, E., Gill, R., Geddes, S., Pitts, J., Wollmer, A. and Grotzinger, J. (1996). Solution structure of a mini IGF-1. *Protein Sci* **5**(11): 2193-2202.

Daughaday, W.H. and Rotwein, P. (1989). Insulin-like growth factors I and II. Peptide, messenger ribonucleic acid and gene structures, serum, and tissue concentrations. *Endocrinolo. Rev.* **10**, 68-91.

DeChiara, T.M., Efstratiadis, A. and Robertson, E.J. (1990). A growth-deficiency phenotype in heterozygous mice carrying an insulin-like growth factor-II gene disrupted by targeting. *Nature* **345**: 78-80.

D'Ercole, A.J., Stiles, A.D. and Underwood, L.E. (1984). Tissue concentrations of somatomedin C: further evidence for multiple sites of synthesis and paracrine or autocrine mechanisms of action. *Proc Natl Acad Sci U.S.A* **81**: 935-939.

Delhanty, P. J. and Han, V. K. (1992). The characterization and expression of ovine insulin-like growth factor-binding protein-2. *J. Mol. Endocrinol.* **9**(1): 31-38.

Diem, K. (1962). Documenta Giegy. Scientific Tables. Sixth Edition. *Giegy Pharmaceuticals.* Ardsley NY. Page 314.

Drake, B., Prater, C. B., Weisenhorn, A. L., Gould, S. A., Albrecht, T. R., Quate, C. F., Cannell, D. S., Hansma, H. G. and Hansma, P. K. (1989). Imaging crystals, polymers, and processes in water with the atomic force microscope. *Science* **243**(4898): 1586-1589.

Dubaquie`, Y. and Lowman, H.B. (1999). Total Alanine Scanning Mutagenesis of Insulin Like Growth Factor I (IGF-I) Identifies Differential Binding Epitopes for IGFBP-1 and IGFBP-3. *Biochemistry* **38**: 6386-6396.

Duan, C., Ding, J., Li, Q., Tsai, W. and Pozios, K. (1999). Insulin-like growth factor binding protein-2 is a growth inhibitory protein conserved in zebrafish. *Proc. Natl. Acac. Sci. U.S.A.* **96**(26): 15274-15279.

Durham, S.K., Riggs, B.L., Harris, S.A. and Conover, C.A. (1995). Alterations in insulin-like growth factor (IGF)-dependent IGF-binding protein-4 proteolysis in transformed osteoblastic cells. *Endocrinology* **136**(4): 1374-1380.

Dyson, H. J., Gippert, G. P., Case, D. A., Holmgren, A. and Wright, P. E. (1990). Three-dimensional solution structure of the reduced form of Escherichia coli thioredoxin determined by nuclear magnetic resonance spectroscopy. *Biochemistry* **29**(17): 4129-4136.

Dyson, H. J., Holmgren, A. and Wright, P. E. (1989). Assignment of the proton NMR spectrum of reduced and oxidized thioredoxin: sequence-specific assignments, secondary structure, and global fold. *Biochemistry* **28**(17): 7074-7087.

Edstrom, R. D., Meinke, M. H., Yang, X. R., Yang, R., Elings, V. and Evans, D. F. (1990). Direct visualization of phosphorylase-phosphorylase kinase complexes by scanning tunneling and atomic force microscopy. *Biophys J* **58**(6): 1437-1448.

Ehring, H. (1999). Hydrogen exchange/electrospray ionization mass spectrometry studies of structural features of proteins and protein/protein interactions. *Anal Biochem* **267**: 252-259.

Engh, R. A., Dieckmann, T., Bode, W., Auerswald, E. A., Turk, V., Huber, R. and Oschkinat, H. (1993). Conformational variability of chicken cystatin. Comparison of structures determined by X-ray diffraction and NMR spectroscopy. *J Mol Biol* **234**(4): 1060-1069.

Fesik, S. W. (1989) Approaches to drug design using NMR spectroscopy. In Perun, T.J and Propst, C.L. (Eds) *Computer aided drug design. Methods and Applications.* Marcel Dekker, NY pp 133-184.

Fesik, S. W. (1991). NMR studies of molecular complexes as a tool in drug design. *J Med Chem* **34**(10): 2937-2945.

Fesik, S.W. and Zuiderweg, E.R.P. (1988). Heteronuclear three dimensional NMR spectroscopy. A strategy for the simplification of homonuclear two dimensional NMR spectra. *J Mag Reson* **78**: 588-593.

Fesik, S.W., Luly, J.R., Erickson, J.W. and Abad, Z.C. (1988). Isotope-edited proton NMR study on the structure of a pepsin/inhibitor complex. *Biochemistry.* **27:** 8297-8301.

Firth, S.M. and Baxter, R.C. (1995). The role of glycosylation in the action of IGFBP-3. *Prog Growth Factor Res 1995+ADs* **6**(2-4): 223-229.

Firth, S.M. and Baxter, R.C. (1999). Characterisation of recombinant glycosylation variants of insulin-like growth factor binding protein-3. *J Endocrinol* **160**(3): 379-387.

Firth, S.M., Ganeshprasad, U. and Baxter, R.C. (1998). Structural determinants of ligand and cell surface binding of insulin-like growth factor-binding protein-3. *J Biol Chem* **273**(5): 2631-2638.

Forbes, B.E., Turner, D., Hodge, S.J., McNeil, K.A., Forsberg, G. and Wallace, J.C. (1998). Localization of an insulin-like growth factor (IGF) binding site of bovine IGF binding protein-2 using disulfide mapping and deletion mutation analysis of the C-terminal domain. *J Biol Chem* **273**(8): 4647-4652.

Foster, M. P., Wuttke, D. S., Clemens, K. R., Jahnke, W., Radhakrishnan, I., Tennant, L., Reymond, M., Chung, J. and Wright, P. E. (1998). Chemical shift as a probe of molecular interfaces: NMR studies of DNA binding by the three amino-terminal zinc finger domains from transcription factor IIIA. *J Biomol NMR* **12**(1): 51-71.

Fowlkes, J. and Freemark, M. (1992). Evidence for a novel insulin-like growth factor (IGF)-dependent protease regulating IGF-binding protein-4 in dermal fibroblasts. *Endocrinology* **131**(5): 2071-2076.

Fowlkes, J.L. and Serra, D.M. (1996). Characterization of glycosaminoglycan-binding domains present in insulin-like growth factor-binding protein-3. *J Biol Chem* **271**(25): 14676-14679.

Fowlkes, J.L., Thrailkill, K.M., George-Nascimento, C., Rosenberg, C.K. and Serra, D.M. (1997). Heparin-binding, highly basic regions within the thyroglobulin type-1 repeat of insulin-like growth factor (IGF)-binding proteins (IGFBPs) -3, -5, and -6 inhibit IGFBP-4 degradation. *Endocrinology* **138**(6): 2280-2285.

Francis, G.L., Aplin, S.E., Milner, S.J., McNeil, K.A., Ballard, F.J. and Wallace, J.C. (1993). Insulin-like growth factor (IGF)-II binding to IGF-binding proteins and IGF receptors is modified by deletion of the N-terminal hexapeptide or substitution of arginine for glutamate-6 in IGF-II. *Biochem J* **293**(3): 713-719.

Francis, G.L., Ross, M., Ballard, F.J., Milner, S.J., Senn, C., McNeil, K.A., *et al.* (1992). Novel recombinant fusion protein analogues of insulin-like growth factor (IGF)-I indicate the relative importance of IGF-binding protein and receptor binding for enhanced biological potency. *J. Mol Endocrinol* **8**: 213-223.

Francis, G.L., Upton, F.M., Ballard, F.J., McNeil, K.A. and Wallace, J.C. (1988). Insulin-like growth factors 1 and 2 in bovine colostrum. Sequences and biological activities compared with those of a potent truncated form. *Biochem J* **251**(1): 95-103.

Galanis M, Firth SM, Bond J, Nathanielsz A, Kortt AA, Hudson PJ, Baxter RC. (2001). Ligand-binding characteristics of recombinant amino- and carboxyl-terminal fragments of human insulin-like growth factor-binding protein-3. *J Endocrinol* **169**(1):123-133

Galiano, R.D., Zhao, L.L., Clemmons, D.R., Roth, S.I., Lin, X. and Mustoe, T.A. (1996). Interaction between the insulin-like growth factor family and the integrin receptor family in tissue repair processes. Evidence in a rabbit ear dermal ulcer model. *J Clin Invest* **98**(11): 2462-2468.

Gardner, K. H. and Kay, L. E. (1998). The use of ^{2}H, ^{13}C, ^{15}N multidimensional NMR to study the structure and dynamics of proteins. *Annu Rev Biophys Biomol Struct* **27**: 357-406.

Gill, R., Wallach, B., Verma, C., Urso, B., De Wolf, E., Grotzinger, J., Murray-Rust, J., Pitts, J., Wollmer, A., De Meyts, P. and Wood, S. (1996). Engineering the C-region of human insulin-like growth factor-1: implications for receptor binding. *Protein Eng* **9**(11): 1011-1019.

Gockerman, A. and Clemmons, D.R. (1995). Porcine aortic smooth muscle cells secrete a serine protease for insulin-like growth factor binding protein-2. *Circ Res* **76**(4): 514-521.

Goto, N. K. and Kay, L. E. (2000). New developments in isotope labeling strategies for protein solution NMR spectroscopy. *Curr Opin Struct Biol* **10**(5): 585-592.

Guler, H.P., Zapf, J., Schmid, C. and Froesch, E.R. (1989). Insulin-like growth factors-I and -II in healthy man. Estimations of half-lives and production rates. *Acta Endocrinol Copenh.* **121**(6): 753-758.

Guncar, G., Pungercic, G., Klemencic, I., Turk, V. and Turk, D. (1999). Crystal structure of MHC class II-associated p41 Ii fragment bound to cathepsin L reveals the structural basis for differentiation between cathepsins L and S. *Embo J* **18**(4): 793-803.

Hashimoto, R., Ono, M., Fujiwara, H., Higashihashi, N., Yoshida, M., Enjoh Kimura, T., *et al.* (1997). Binding sites and binding properties of binary and ternary complexes of insulin-like growth factor-II (IGF-II), IGF-binding protein-3, and acid-labile subunit. *J Biol Chem* **272**(44): 27936-27942.

Heding, A., Gill, R., Ogawa, Y., De Meyts, P. & Shymko, R. M. (1996). Biosensor measurement of the binding of insulin-like growth factors-I and -II and their analogues to the insulin-like growth factor-binding protein-3. *J Biol Chem* **271**(24), 13948-13952.

Helmerhorst, E. and Stokes, G.B. (1987). Self-association of insulin. Its pH dependence and effect of plasma. *Diabetes* **36**(3): 261-264.

Hendrickson, W.A. (1991) Determination of Macromolecular Structures from Anomalous Diffraction of Synchrotron Radiation. *Science* 254. 51-58.

Ho, P.J. and Baxter, R.C. (1997). Characterization of truncated insulin-like growth factor-binding protein-2 in human milk. *Endocrinology* **138**(9): 3811-3818.

Hobba, G.D., Forbes, B.E., Parkinson, E.J., Francis, G.L. and Wallace, J.C. (1996). The insulin-like growth factor (IGF) binding site of bovine insulin-like growth factor binding protein-2 (bIGFBP-2) probed by iodination. *J Biol Chem* **271**(48): 30529-30536.

Hobba, G.D., Lothgren, A., Holmberg, E., Forbes, B.E., Francis, G.L. and Wallace, J.C. (1998). Alanine screening mutagenesis establishes tyrosine 60 of bovine insulin-like growth factor binding protein-2 as a determinant of insulin-like growth factor binding. *J Biol Chem* **273**(31): 19691-19698.

Hober, S., Forsberg, G., Palm, G., Hartmanis, M. and Nilsson, B. (1992). Disulfide exchange folding of insulin-like growth factor I. *Biochemistry* **31**(6): 1749-1756.

Hodgkinson, S.C., Napier, J.R., Spencer, G.S. and Bass, J.J. (1994). Glycosaminoglycan binding characteristics of the insulin-like growth factor-binding proteins. *J Mol Endocrinol* **13**(1): 105-112.

Hoeck, W.G. and Mukku, V.R. (1994). Identification of the major sites of phosphorylation in IGF binding protein-3. *J Cell Biochem* **56**(2): 262-273.

Hoh and Hansma, 1992. Atomic force microscopy for high-resolution imaging in cell biology. *Trends in Cell Biology* **2**: 208-212.

Holly, J.M.P., Gunnell, D.J. and Davey Smith, G. (1999). Growth hormone, IGF-I and cancer. Less intervention to avoid cancer? More intervention to prevent cancer? *J Endocrinol* **162**: 321-330.

Holmgren, A., Soderberg, B. O., Eklund, H. and Branden, C. I. (1975). Three-dimensional structure of Escherichia coli thioredoxin-S2 to 2.8 A resolution. *Proc Natl Acad Sci U S A* **72**(6): 2305-2309.

Horney, M.J., Evangelista, C.A. and Rosenzweig, S.A. (2001). Synthesis and characterization of insulin-like growth factor-1 (IGF-1) photoprobes selective for the IGF binding proteins (IGFBPs): Photoaffinity labeling of the IGF-binding domain on IGFBP-2. *J Biol Chem* **276**(4): 2880-2889.

Hossenlopp, P., Seurin, D., Segovia-Quinson, B., Hardoiun, S. & Binoux, M. (1986). Analysis of serum insulin-like growth factor binding proteins using Western blotting: use of the method for titration of the binding proteins and competitive binding sites. *Anal Biochem* **154**, 138-143.

Howard, M. J. (1998). Protein NMR spectroscopy. *Curr Biol* **8**(10): R331-333.

Hua, Q. X. and Weiss, M. A. (1991). Comparative 2D NMR studies of human insulin and des-pentapeptide insulin: sequential resonance assignment and implications for protein dynamics and receptor recognition. *Biochemistry* **30**(22): 5505-5515.

Huhtala, M.L., Koistinen, R., Palomaki, P., Partanen, P., Bohn, H. and Seppala, M. (1986). Biologically active domain in somatomedin-binding protein. *Biochem Biophys Res Comm* **141**(1): 263-270.

Humbel, R.E. (1990). Insulin-like growth factors I and II. *Eur J Biochem* **190**(3): 445-62.

Hwa, V., Oh, Y. and Rosenfeld, R.G. (1999). The insulin-like growth factor-binding protein (IGFBP) superfamily. *Endocr Rev* **20**(6): 761-787.

Hynes, M.A., Van Wyk, J.J., Brooks, P.J., D'Ercole, A.J., Jansen, M. and Lund, P.K. (1987). Growth hormone dependence of somatomedin-C/insulin-like growth factor-I and insulin-like growth factor-II messenger ribonucleic acids. *Mol Endocrinol* **1**(3): 233-242.

Ikura, M., Krinks, M., Torchia, D. A. and Bax, A. (1990). An efficient NMR approach for obtaining sequence-specific resonance assignments of larger proteins based on multiple isotopic labeling. *FEBS Lett* **266**(1-2): 155-8.

Imai, Y., Busby, W.H., Jr., Smith, C.E., Clarke, J.B., Garmong, A.J., Horwitz, G.D., *et al.* (1997). Protease-resistant form of insulin-like growth factor-binding protein 5 is an inhibitor of insulin-like growth factor-I actions on porcine smooth muscle cells in culture. *J Clin Invest* **100**(10): 2596-2605.

Imai, Y., Moralez, A., Andag, U., Clarke, J.B., Busby, W.H., Jr. and Clemmons, D.R. (2000). Substitutions for hydrophobic amino acids in the N-terminal domains of IGFBP-3 and -5 markedly reduce IGF-I binding and alter their biologic actions. *J Biol Chem* **275**(24): 18188-18194.

Jansson, M., Andersson, G., Uhlen, M., Nilsson, B. and Kordel, J. (1998). The insulin-like growth factor (IGF) binding protein-1 binding epitope on IGF-I probed by heteronuclear NMR spectroscopy and mutational analysis. *J Biol Chem* **273**(38): 24701-24707.

Jansson, M., Uhlen, M. and Nilsson, B. (1997). Structural changes in insulin-like growth factor (IGF) -I mutant proteins affecting binding kinetic rates to IGF binding protein-1 and IGF-I receptor. *Biochemistry* **36**(14): 4108-4117.

Jeffrey, P.D., Milthorpe, B.K. and Nichol, L.W. (1976). Polymerization pattern of insulin at pH 7.0. *Biochemistry* **15**(21): 4660-4665.

Johannssen, W., Attwood, P. V., Wallace, J. C. and Keech, D. B. (1983). Localisation of the active site of pyruvate carboxylase by electron microscopic examination of avidin-enzyme complexes. *Eur J Biochem* **133**(1): 201-206.

Jones, J.I. and Clemmons, D.R. (1995). Insulin-like growth factors and their binding proteins: biological actions. *Endocr Rev* **16**(1): 3-34.

Jones, J.I., Busby, W.H.J., Wright, G., Smith, C.E., Kimack, N.M. and Clemmons, D.R. (1993c). Identification of the sites of phosphorylation in insulin-like growth factor binding protein-1: regulation of its affinity by phosphorylation of serine-101. *J Biol Chem* **268**(2): 1125-1131.

Jones, J.I., D'Ercole, A.J., Camacho-Hubner, C. and Clemmons, D.R. (1991). Phosphorylation of insulin-like growth factor (IGF)-binding protein-1 in cell culture and *in vivo*: effects on affinity for IGF-I. *Proc Natl Acad Sci U.S.A* **88**(17): 7481-7485.

Jones, J.I., Gockerman, A., Busby, W.H., Jr., Wright, G. and Clemmons, D.R. (1993a). Insulin-like growth factor binding protein 1 stimulates cell migration and binds to the alpha-5-beta-1 integrin by means of its Arg-Gly-Asp sequence. *Proc Natl Acad Sci U.S.A* **90**(22): 10553-10557.

Jones, J.I., Gockerman, A., Busby, W.H.J., Camacho Hubner, C. and Clemmons, D.R. (1993b). Extracellular matrix contains insulin-like growth factor binding protein-5: Potentiation of the effects of IGF-I. *J Cell Biol* **121**(3): 679-687.

Kalus, W., Zweckstetter, M., Renner, C., Sanchez, Y., Georgescu, J., Grol, M., *et al.* (1998). Structure of the IGF-binding domain of the insulin-like growth factor-binding protein-5 (IGFBP-5): implications for IGF and IGF-I receptor interactions. *EMBO J* **17**(22): 6558-6572.

Katti, S. K., LeMaster, D. M. and Eklund, H. (1990). Crystal structure of thioredoxin from Escherichia coli at 1.68 A resolution. *J Mol Biol* **212**(1): 167-184.

Khosla, S., Hassoun, A.A., Baker, B.K., Liu, F., Zein, N.N., Whyte, M.P., *et al.* (1998). Insulin-like growth factor system abnormalities in hepatitis C-associated osteosclerosis. Potential insights into increasing bone mass in adults. *J Clin Invest* **101**(10): 2165-2173.

Kim, H.S., Nagalla, S.R., Oh, Y., Wilson, E., Roberts Jr, C.T. and Rosenfeld, R.G. (1997). Identification of a family of low affinity insulin like growth factor binding proteins (IGFBPs): characterisation of connective tissue growth factor as a member of the IGFBP superfamily. *Proc Natl Acad Sci USA* **94**: 12981-12986.

King, R., Wells, J.R., Krieg, P., Snoswell, M., Brazier, J., Bagley, C.J., *et al.* (1992). Production and characterization of recombinant insulin-like growth factor-I (IGF-I) and potent analogues of IGF-I, with Gly or Arg substituted for Glu3, following their expression in Escherichia coli as fusion proteins. *J Mol Endocrinol* **8**(1): 29-41.

Kline, A. D. and Justice, R. M., Jr. (1990). Complete sequence-specific 1H NMR assignments for human insulin. *Biochemistry* **29**(12): 2906-2913.

Koradi, R., Billeter, M. and Wűthrich, K. (1996). MOLMOL: a program for display and analysis of macromolecular structures. *J Mol Graph* **14**(1): 51-55.

Kubler, B., Schrameck, U., Draeger, C., Forssman, W.G., Braulke, T. and Standker, L. (1999). Identification of circulating human IGFBP-3 fragments. *Growth Horm IGF Res* **9**(5): 362.

Kunkel, T.A. (1985). Rapid and efficient site-specific mutagenesis without phenotypic selection. *Proc Natl Acad Sci U S A* **82**(2): 488-492.

Laajoki, L.G., Francis, G.L., Wallace, J.C., Carver, J.A. and Keniry, M.A. (2000). Solution structure and backbone dynamics of Long-[Arg3]Insulin-like Growth Factor-I. *J Biol Chem* **275**: 10009-10015.

Laajoki, L. G., Milner, S. J., Francis, G. L., Carver, J. A., and Keniry, M. (1999) A. ^{1}H and ^{15}N assignments of Long-[L60]-IGF-I, an insulin-like growth factor I analogue. *J Biomol NMR* submitted. BMRB accession number 4278.

Lal, R. and John, S. A. (1994). Biological applications of atomic force microscopy. *Am J Physiol* **266**(1 Pt 1): C1-21.

Lalou, C., Lassarre, C. and Binoux, M. (1995). A proteolytic fragment of insulin-like growth factor (IGF) binding protein-3 that fails to bind IGF is a cell growth inhibitor. *Prog Growth Factor Res* **6**(2-4): 311-316.

Lalou, C., Sawamura, S., Segovia, B., Ogawa, Y. and Binoux, M. (1997). Proteolytic fragments of insulin-like growth factor binding protein-3: N-terminal sequences and relationships between structure and biological activity. *C R Acad Sci III* **320**(8): 621-628.

Landale, E.C., Strong, D.D., Mohan, S. and Baylink, D.J. (1995). Sequence comparison and predicted structure for the four exon-encoded regions of human insulin-like growth factor binding protein-4. *Growth Factors* **12**: 245-250.

Landwehr, J., Kaupmann, K., Heinrich, G. and Schwander, J. (1993). Cloning and characterization of the gene encoding murine insulin-like growth factor-binding protein-2, mIGFBP-2. *Gene* **124**(2): 281-286.

Lassarre, C. and Binoux, M. (1994). Insulin-like growth factor binding protein-3 is functionally altered in pregnancy plasma. *Endocrinology* **134**(3): 1254-1262.

Lauri, G. and Bartlett, P. A. (1994). CAVEAT: a program to facilitate the design of organic molecules. *J Comput Aided Mol Des* **8**(1): 51-66.

Lawrence, J.B., Oxvig, C., Overgaard, M.T., Sottrup-Jensen, L., Gleich, G.J., Hays, L.G., *et al.* (1999). The insulin-like growth factor (IGF)-dependent IGF binding protein-4 protease is pregnancy-associated plasma protein-A. *Proc Natl Acad Sci U.S.A* **96**: 3149-3153.

Leal, S.M., Huang, S.S. and Huang, J.S. (1999). Interactions of high affinity insulin-like growth factor-binding proteins with the type V transforming growth factor-beta receptor in mink lung epithelial cells. *J Biol Chem* **274**(10): 6711-6717.

Leal, S.M., Liu, Q., Huang, S.S. and Huang, J.S. (1997). The type V transforming growth factor beta receptor is the putative insulin-like growth factor-binding protein 3 receptor. *J Biol Chem* **272**(33): 20572-20576.

LeRoith, D., Baserga, R., Helman, L. and Roberts, C.T. (1995). Insulin-like growth factors and cancer. *Ann Intern Med* **122**(1): 54-59.

Li, W., Fawcett, J., Widmer, H.R., Fielder, P.J., Rabkin, R. and Keller, G.A. (1997). Nuclear transport of insulin-like growth factor-I and insulin-like growth factor binding protein-3 in opossum kidney cells. *Endocrinology* **138**(4): 1763-1766.

Lian, L.Y. and Roberts, G.C.K. (1993). Effects of chemical exchange on NMR spectra. In *NMR of macromolecules.* G.C.K Roberts, ed.: IRL Press at Oxford University Press). pp 153-182.

Lien, S., Milner, S. J., Graham, L. D., Wallace, J. C. and Francis, G. L. (2001). Linkers for improved cleavage of fusion proteins with an engineered alpha-lytic protease. *Biotechnol Bioeng* **74**(4): 335-343.

Liu, X. J., Xie, Q., Zhu, Y. F., Chen, C. and Ling, N. (2001). Identification of a nonpeptide ligand that releases bioactive insulin-like growth factor-i from its binding protein complex. *J Biol. Chem.* **276**(35): 32419-32422.

Loddick, S. A., Liu, X. J., Lu, Z. X., Liu, C., Behan, D. P., Chalmers, D. C., Foster, A. C., Vale, W. W., Ling, N. and De Souza, E. B. (1998). Displacement of insulin-like growth factors from their binding proteins as a potential treatment for stroke. *Proc Natl Acad Sci U S A* **95**(4): 1894-1898.

Liu B, Lee HY, Weinzimer SA, Powell DR, Clifford JL, Kurie JM, Cohen P. (2000). Direct functional interactions between insulin-like growth factor-binding protein-3 and retinoid X receptor-alpha regulate transcriptional signaling and apoptosis. *J. Biol. Chem.* **275**(43), 33607-33613.

Lowman, H. B., Chen, Y. M., Skelton, N. J., Mortensen, D. L., Tomlinson, E. E., Sadick, M. D., Robinson, I. C. and Clark, R. G. (1998). Molecular mimics of insulin-like growth factor 1 (IGF-1) for inhibiting IGF-1: IGF-binding protein interactions. *Biochemistry* **37**(25): 8870-8878.

Lucic, M. R. (2000). Characterisation of the Molecular Interactions between insulin-like growth factors and their binding proteins. *PhD. Thesis, Adelaide University.*

Lucic, M. R., Forbes, B. E., Grosvenor, S. E., Carr, J. M., Wallace, J. C. and Forsberg, G. (1998). Secretion in Escherichia coli and phage-display of recombinant insulin-like growth factor binding protein-2. *J Biotechnol* **61**(2): 95-108.

Lund, P.K., Moats-Staats, B.M., Hynes, M.A., Simmons, J.G., Jansen, M., D'Ercole, A.J., *et al.* (1986). Somatomedin-C/insulin-like growth factor-I and insulin-like growth factor-II mRNAs in rat fetal and adult tissues. *J Biol Chem* **261**(31): 14539-14544.

Macaulay, V.M. (1992). Insulin-like growth factors and cancer. *Br. J. Cancer* **65**: 311-320.
Magee, B.A., Shooter, G.K., Wallace, J.C. and Francis, G.L. (1999). Insulin-like growth factor-I and its binding proteins: a study of the binding interface using B-domain mutants. *Biochemistry* **38**(48): 15863-15870.

Magee, B. A., Shooter, G. K., Wallace, J. C. and Francis, G. L. (1999). Insulin-like growth factor I and its binding proteins: a study of the binding interface using B-domain analogues. *Biochemistry* **38**(48): 15863-15870.

Maile, L.A. and Holly, J.M.P. (1999). Insulin-like growth factor binding protein (IGFBP) proteolysis: occurrence, identification, role and regulation. *Growth Horm. IGF Res.* **9**(2): 85-95.

Maly, P. and Luthi, C. (1988). The binding sites of insulin-like growth factor I (IGF I) to type I IGF receptor and to a monoclonal antibody. Mapping by chemical modification of tyrosine residues. *J Biol Chem* **263**(15): 7068-7072.

Manes, S., Llorente, M., Lacalle, R.A., Gomez-Mouton, C., Kremer, L., Mira, E., *et al.* (1999). The matrix metalloproteinase-9 regulates the insulin-like growth factor-triggered autocrine response in DU-145 carcinoma cells. *J Biol Chem* **274**(11): 6935-6945.

Marinaro, J. A., Jamieson, G. P., Hogarth, P. M. & Bach, L. A. (1999). Differential dissociation kinetics explain the binding preference of insulin-like growth factor binding protein-6 for insulin-like growth factor-II over insulin-like growth factor-I. *FEBS lett.* **450**, 240-244.

Mayer, F., Wallace, J. C. and Keech, D. B. (1980). Further electron microscope studies on pyruvate carboxylase. *Eur J Biochem* **112**(2): 265-272.

McCusker, R. H., Cohick, W. S., Busby, W. H. and Clemmons, D. R. (1991). Evaluation of the developmental and nutritional changes in porcine insulin-like growth factor-binding protein-1 and -2 serum levels by immunoassay. *Endocrinology* **129(5):** 2631-2638.

Menouny, M., Binoux, M. and Babajko, S. (1997). Role of insulin-like growth factor binding protein-2 and its limited proteolysis in neuroblastoma cell proliferation: modulation by transforming growth factor-beta and retinoic acid. *Endocrinology* **138**(2): 683-690.

Milner, S.J., Francis, G.L., Wallace, J.C., Magee, B.A. and Ballard, F.J. (1995). Mutations in the B-domain of insulin-like growth factor-I influence the oxidative folding to yield products with modified biological properties. *Biochem J* **308**(Pt 3)(1-2): 865-871.

Moriyama S, Ayson FG, Kawauchi H. (2000). Growth regulation by insulin-like growth factor-I in fish. *Biosci Biotechnol Biochem* **64**(8):1553-1562. Review.

Moss, J.A., Francis, G.L., Ross, M., Wallace, J.C. and Ballard, F.J. (1991). Insulin-like growth factor (IGF)-I and IGF-II binding to an IGF binding protein. An investigation using chemical modification of tyrosine residues as a structural probe for the sites of interaction. *J Biol Chem* **266**(2): 909-914.

Muller, H.L., Oh, Y., Gargosky, S.E., Wilson, K.F., Lehrnbecher, T. and Rosenfeld, R.G. (1994). Insulin-like growth factor binding protein-3 concentrations and insulin-like growth factor binding protein-3 protease activity in sera of patients with malignant solid tumors or leukemia. *Pediatr Res* **35**(6): 720-724.

Nam, T.J., Busby, W.H., Jr. and Clemmons, D.R. (1994). Human fibroblasts secrete a serine protease that cleaves insulin-like growth factor-binding protein-5. *Endocrinology* **135**(4): 1385-1391.

Neumann, G.M. and Bach, L.A. (1999). The N-terminal disulfide linkages of human insulin-like growth factor-binding protein-6 (hIGFBP-6) and hIGFBP-1 are different as determined by mass spectrometry. *J Biol Chem* **274**(21): 14587-14594.

Neumann, G.M., Marinaro, J.A. and Bach, L.A. (1998). Identification of O-glycosylation sites and partial characterization of carbohydrate structure and disulfide linkages of human insulin-like growth factor binding protein-6. *Biochemistry* **37**(18): 6572-6585.

Nice, E. C. & Catimel, B. (1999). Instrumental biosensors: new perspectives for the analysis of biomolecular interactions. *BioEssays* **21**, 339-352.

Nissley, P. and Lopaczynski, W. (1991). Insulin-like growth factor receptors. *Growth Factors* **5**(1): 29-43.

Ocrant, I., Fay, C.T., Pham, H. and Rosenfeld, R. G. (1992). Not all insulin-like growth factor-binding proteins (IGFBPs) are detectable by western ligand blotting: case studies of PC12 pheochromocytoma and rat anterior pituitary IGFBPs and proteolyzed IGFBP-3. *Endocrinology* **131(1):** 221-227.

Oh, Y., Mueller, H.L., Lee, D.Y., Fielder, P.J. and Rosenfeld, R.G. (1993). Characterization of the affinities of insulin-like growth factor (IGF)-binding protein -1 to -4 for IGF-I, IGF-II, IGF-I/insulin hybrid, and IGF-I analogs. *Endocrinology* **132**(3): 1337-1344.

Oh, Y., Nagalla, S.R., Yamanaka, Y., Kim, H.-S., Wilson, E. and Rosenfeld, R.G. (1996). Synthesis and characterisation of insulin like growth factor binding protein (IGFBP-7). *J Biol Chem* **271**: 30322-30325.

Oh, Y., Yamanaka, Y., Kim, H.S., Vorwerk, P., Wilson, E., Hwa, V., *et al.* (1998). IGF-independent actions of IGFBPs. *Molecular mechanisms to regulate the activities of insulin-like growth factors.* K. Takano, N. Hizuka and S. I. Takahashi. Amsterdam, Elsevier: 125-133.

Okabe, E., Kajihara, J., Usami, Y. and Hirano, K. (1999). The cleavage site specificity of human prostate specific antigen for insulin-like growth factor binding protein-3. *FEBS lett.* **447**: 87-90.

Ooi, G.T. and Herington, A.C. (1988). The biological and structural characterization of specific serum binding proteins for the insulin-like growth factors. *J Endocrinol* **118**(1): 7-18.

Parker, A., Clarke, J.B., Busby, W.H. and Clemmons, D.R. (1996). Identification of the extracellular matrix binding sites for insulin-like growth factor-binding protein-5. *J Biol Chem* **271**(23): 13523-13529.

Perks, C.M., Newcomb, P.V., Norman, M.R. and Holly, J.M. (1999). Effect of insulin-like growth factor binding protein-1 on integrin signalling and the induction of apoptosis in human breast cancer cells. *J Mol Endocrinol* **22**(2): 141-150.

Pervushin, K., Riek, R., Wider, G. and Wűthrich, K. (1997). Attenuated T2 relaxation by mutual cancellation of dipole-dipole coupling and chemical shift anisotropy indicates an avenue to NMR structures of very large biological macromolecules in solution. *Proc Natl Acad Sci U S A* **94**(23): 12366-12371.

Peterkofsky, B., Gosiewska, A., Wilson, S. and Kim, Y.R. (1998). Phosphorylation of rat insulin-like growth factor binding protein-1 does not affect its biological properties. *Arch Biochem Biophys* **357**(1): 101-110.

Pintar, J., Schuller, A., Bradshaw, S., Cerro, C. and Grewal, A. (1998). Genetic disruption of IGF binding proteins. *Molecular mechanisms to regulate the activities of insulin-like growth factors.* K. Takano, N. Hizuka and S. I. Takahashi. Amsterdam, Elsevier: 65-70.

Pintar, J.E., Cerro, J.A. and Wood, T.L. (1996). Genetic approaches to the function of insulin-like growth factor-binding proteins during rodent development. *Horm Res* **45**(3-5): 172-177.

Pintar, J.E., Schuller, A. and Bradshaw, S. (1999). Combinatorial KOs of IGFBPs. *Growth Hor. IGF Res* **9**(5): 308.

Powell, D.R., Suwanichikul, A. and Cubbage, L. (1989). In: *Insulin-Like Growth Factor Binding Proteins.* (Drop S.L.S. and Hintz, R.L. Eds). Elsevier Amsterdam. 3-9.

Qin, X., Strong, D.D., Baylink, D.J. and Mohan, S. (1998). Structure-function analysis of the human insulin-like growth factor binding protein-4. *J Biol Chem* **273**(36): 23509-23516.

Rajah, R., Katz, L., Nunn, S., Solberg, P., Beers, T. and Cohen, P. (1995). Insulin-like growth factor binding protein (IGFBP) proteases: functional regulators of cell growth. *Prog Growth Factor Res* **6**(2-4): 273-284.

Rajah, R., Valentinis, B. and Cohen, P. (1997). Insulin-like growth factor (IGF)-binding protein-3 induces apoptosis and mediates the effects of transforming growth factor-beta1 on programmed cell death through a p53- and IGF-independent mechanism. *J Biol Chem* **272**(18): 12181-12188.

Rajaram, S., Baylink, D.J. and Mohan, S. (1997). Insulin-like growth factor-binding proteins in serum and other biological fluids: regulation and functions. *Endocr Rev* **18**(6): 801-831.

Ramos, A., Kelly, G., Hollingworth, D., Pastore, A. and Frenkiel, T. (2000). Mapping the interface of protein-nucleic acid complexes using cross saturation. *J Am Chem Soc.* **122**: 11311-11314.

Rathjen, P.D., S. Toth, A. Willis, J.K. Heath and A.G. Smith (1990). Differentiation inhibiting activity is produced in matrix-associated and diffusible forms that are generated by alternate promoter usage. *Cell* **62**(6): 1105-1114.

Rechler, M.M. (1993). Insulin-like growth factor binding proteins. *Vitam Horm* **47**: 1-114.

Rechler, M.M. (1997). Growth inhibition by insulin-like growth factor (IGF) binding protein-3-what's IGF got to do with it? [editorial]. *Endocrinology* **138**(7): 2645-2647.

Rees, C., Clemmons, D.R., Horvitz, G.D., Clarke, J.B. and Busby, W.H. (1998). A protease-resistant form of insulin-like growth factor (IGF) binding protein-4 inhibits IGF-1 actions. *Endocrinology* **139**(10): 4182-4188.

Renner, C. and Holak, T. (2001). NMR 15N relaxation of the insulin-like growth factor (IGF)-binding domain of IGF binding protein-5 (IGFBP-5) determined free in solution and in complex with IGF-II. *Eur J Biochem* **268**(4): 1058-1065.

Riek, R., Pervushin, K. and Wűthrich, K. (2000). TROSY and CRINEPT: NMR with large molecular and supramolecular structures in solution. *Trends Biochem Sci* **25**(10): 462-468.

Riek, R., Wider, G., Pervushin, K. and Wűthrich, K. (1999). Polarization transfer by cross-correlated relaxation in solution NMR with very large molecules. *Proc Natl Acad Sci U S A* **96**(9): 4918-4923.

Rinderknecht, E. and Humbel, R.E. (1978a). Primary structure of human insulin-like growth factor-II. *FEBS lett* **89**(2): 283-286.

Rinderknecht, E. and Humbel, R.E. (1978b). The amino acid sequence of human insulin-like growth factor-I and its structural homology with proinsulin. *J Biol Chem* **253**(8): 2769-2776.

Roberts EL, Shu N, Howard MJ, Broadhurst RW, Chapman-Smith A, Wallace JC, Morris T, Cronan JE Jr, Perham RN. (1999). Solution structures of apo and holo biotinyl domains from acetyl coenzyme A carboxylase of Escherichia coli determined by triple-resonance nuclear magnetic resonance spectroscopy. *Biochemistry* **38**(16):5045-5053.

Roden, L. D. & Myszka, D. G. (1996). Global analysis of macromolecular interaction measured on BIAcore. *Biochem Biophys Res Comm* **225**, 1073-1077.

Rohde, M., Lim, F. and Wallace, J. C. (1986). Pyruvate carboxylase from Saccharomyces cerevisiae. Quaternary structure, effects of allosteric ligands and binding of avidin. *Eur J Biochem* **156**(1): 15-22.

Rother, K. I. and Accili, D. (2000). Role of insulin receptors and IGF receptors in growth and development. *Pediatr Nephrol* **14**(7): 558-561.

Rotwein, P. (1991). Structure, evolution, expression and regulation of insulin-like growth factors I and II. *Growth Factors* **5**(1): 3-18.

Russo, V.C., Bach, L.A., Fosang, A.J., Baker, N.L. and Werther, G.A. (1997). Insulin-like growth factor binding protein-2 binds to cell surface proteoglycans in the rat brain olfactory bulb. *Endocrinology* **138**(11): 4858-4867.

Sakano, K., Enjoh, T., Numata, F., Fujiwara, H., Marumoto, Y., Higashihashi, N., *et al.* (1991). The design, expression, and characterization of human insulin-like growth factor-II (IGF-II) mutants specific for either the IGF-II/cation-independent mannose 6-phosphate receptor or IGF-I receptor. *J Biol Chem* **266**(31): 20626-20635.

Salahifar, H., Baxter, R.C. and Martin, J.L. (1997). Insulin-like growth factor binding protein (IGFBP)-3 protease activity secreted by MCF-7 breast cancer cells: inhibition by IGFs does not require IGF-IGFBP interaction. *Endocrinology* **138**(4): 1683-1690.

Salzmann, M., Pervushin, K., Wider, G., Senn, H. and Wüthrich, K. (1998). TROSY in triple-resonance experiments: new perspectives for sequential NMR assignment of large proteins. *Proc Natl Acad Sci U S A* **95**(23): 13585-13590.

Sambrook, J., E.F. Fritsch and T. Maniatis (1989). Molecular cloning: a laboratory manual. New York, Cold Spring Harbor Press.

Sanger, F., S. Nicklen and A.R. Coulson (1977). DNA sequencing with chain-terminating inhibitors. *Proc Natl Acad Sci U S A* **74**(12): 5463-5467.

Sara, V. R., Carlsson-Skwirut, C., Andersson, C., Hall, E., Sjogren, B., Holmgren, A. and Jornvall, H. (1986). Characterization of somatomedins from human fetal brain: identification of a variant from of insulin-like growth factor-I. *Proc. Natl. Acad. Sci. U.S.A.* **83**: 4904-4907.

Sato, A., Koyama, S., Yamada, H., Suzuki, S., Tamura, K., Kobayashi, M., *et al.* (2000). Three-dimensional solution structure of a disulfide bond isomer of the human insulin-like growth factor-I. *J Pept Res* **56**(4): 218-230.

Sato, A., Nishimura, S., Ohkubo, T., Kyogoku, Y., Koyama, S., Kobayashi, M., Yasuda, T. and Kobayashi, Y. (1992). 1H-NMR assignment and secondary structure of human insulin-like growth factor-I (IGF-I) in solution. *J Biochem* **111**(4): 529-36.

Sato, A., Nishimura, S., Ohkubo, T., Kyogoku, Y., Koyama, S., Kobayashi, M., *et al.* (1993). Three-dimensional structure of human insulin-like growth factor-I (IGF-I) determined by proton NMR and distance geometry. *Int J Pep Prot Res* **41**(5): 433-440.

Schedlich, L.J., Young, T.F., Firth, S.M. and Baxter, R.C. (1998). Insulin-like growth factor-binding protein (IGFBP)-3 and IGFBP-5 share a common nuclear transport pathway in T47D human breast carcinoma cells. *J Biol Chem* **273**(29): 18347-18352.

Schmid, C., Rutishauser, J., Schlapfer, I., Froesch, E. R. and Zapf, J. (1991). Intact but not truncated insulin-like growth factor binding protein-3 (IGFBP-3) blocks IGF I-induced stimulation of osteoblasts: control of IGF signalling to bone cells by IGFBP-3-specific proteolysis? *Biochemical and Biophysical Research Communications.* **179(1):** 579-585.

Schoen, T. J., Mazuruk, K., Waldbillig, R. J., Potts, J., Beebe, D. C., Chader, G. J. and Rodriguez, I. R. (1995). Cloning and characterization of a chick embryo cDNA and gene for IGF-binding protein-2. *J. Mol. Endocrinol.* **15**(1): 49-59.

Sepp-Lorenzino, L. (1998). Structure and function of the insulin-like growth factor-I receptor. *Breast Cancer Res Treat* **47**(3): 235-253.

Shalamanova L, Kubler B, Scharf JG, Braulke T. (2000). Ligand blotting: iodinated vs biotinylated IGF. *Growth Horm IGF Res* **10**(5):294.

Sidhu, S. S., Lowman, H. B., Cunningham, B. C. and Wells, J. A. (2000). Phage display for selection of novel binding peptides. *Methods Enzymol* **328**: 333-363.

Skelton, N. J., Chen, Y. M., Dubree, N., Quan, C., Jackson, D. Y., Cochran, A., Zobel, K., Deshayes, K., Baca, M., Pisabarro, M. T. and Lowman, H. B. (2001). Structure-function analysis of a phage display-derived peptide that binds to insulin-like growth factor binding protein 1. *Biochemistry* **40**(29): 8487-8498.

Sklenar, V., Piotto, M., Leppik, R. and Saudek, V. (1993). Gradient-tailored water suppression for ^{1}H-^{15}N HSQC experiments optimized to retain full sensitivity. *J. Magn. Reson. Ser. A* **102**: 241-245.

Smith, D. A. and Radford, S. E. (2000). Protein folding: pulling back the frontiers. *Curr Biol* **10**(18): R662-4.

Sohar, I., Sleat, D., Gong Liu, C., Ludwig, T. and Lobel, P. (1998). Mouse mutants lacking the cation-independent mannose 6-phosphate/insulin-like growth factor II receptor are impaired in lysosomal enzyme transport: comparison of cation-independent and cation-dependent mannose 6-phosphate receptor-deficient mice. *Biochem J* **330**(Pt 2): 903-908.

Sommer, A., Maack, C.A., Spratt, S.K., Mascarenhas, D., Tressel, T.J., Rhodes, E.T., *et al.* (1991). Molecular genetics and actions of recombinant insulin-like growth factor binding protein-3. *Modern Concepts of Insulin-like Growth Factors.* E. M. Spencer, Elsevier: 715-728.

Song, H., Beattie, J., Campbell, I.W. and Allan, G.J. (2000). Overlap of IGF- and heparin-binding sites in rat IGF-binding protein-5. *J Mol Endocrinol* **24**: 43-51.

Spencer, E.M. and Chan, K. (1995). A 3-dimensional model for the insulin-like growth factor binding proteins (IGFBPs); supporting evidence using the structural determinants of the IGF binding site on IGFBP-3. *Prog Growth Factor Res* **6**(2-4): 209-214.

Standker, L., Braulke, T., Mark, S., Mostafavi, H., Meyer, M., Honing, S., *et al.* (2000). Partial IGF affinity of circulating N- and C-terminal fragments of human insulin-like growth factor binding protein-4 (IGFBP-4) and the disulfide bonding pattern of the C-terminal IGFBP-4 domain. *Biochemistry* **39**: 5082-5088.

Standker, L., Mark, S., Mostafavi, H., Honing, S., Braulke, T. and Forssmann, W.G. (1999). Characterization of circulating fragments of human IGFBP-4. *Growth Horm IGF Res* **9**(5): 362.

Standker, L., Wobst, P., Mark, S. and Forssmann, W.G. (1998). Isolation and characterization of circulating 13 kDa C-terminal fragments of human insulin-like growth factor binding protein-5. *FEBS lett* **441**: 281-286.

Stone, M. J., Chandrasekhar, I., Holmgren, A., Wright, P.E. and Dyson, H.J. (1993). Comparison of backbone and tryptophan side-chain dynamics of reduced and oxidised *Escherichia coli* thioredoxin using ^{15}N NMR relaxation measurements. *Biochemistry* **32** 426-435.

Suikkari, A.M.B. and Baxter, R.C. (1991). Insulin-like growth factor (IGF) binding protein-3 in pregnancy serum binds native IGF-I but not iodo-IGF-I. *J-Clin-Endocrinol-Metab* **73**(6): 1377-1379.

Sun, Y., G. Hegamyer and N.H. Colburn (1993). PCR-direct sequencing of GC-rich region by inclusion of 10% DMSO: Application to C-jun. *Biotechniques* **15**(3): 372-374.

Szabo, L., Mottershead, D.G., Ballard, F.J. and Wallace, J.C. (1988). The bovine insulin-like growth factor (IGF) binding protein purified from conditioned medium requires the N-terminal tripeptide in IGF-1 for binding. *Biochem Biophys Res Commun* **151**(1): 207-214.

Terasawa, H., Kohda, D., Hatanaka, H., Nagata, K., Higashihashi, N., Fujiwara, H., *et al.* (1994). Solution structure of human insulin-like growth factor-II: recognition sites for receptors and binding proteins. *EMBO J* **13**(23): 5590-5597.

Thompson, J. D., Higgins, D. G. and Gibson, T. J. (1994). Clustal W: improving the sensitivity of progressive multiple sequence alignment through sequence weighting, position-specific gap penalties and weight matrix choice. *Nulceic Acids Res.* **22**(22): 4673-4680.

Thrailkill, K.M., Quarles, L.D., Nagase, H., Suzuki, K., Serra, D.M. and Fowlkes, J.L. (1995). Characterization of insulin-like growth factor-binding protein 5-degrading proteases produced throughout murine osteoblast differentiation. *Endocrinology* **136**(8): 3527-3533.

Torres, A.M., Forbes, B.E., Aplin, S.E., Wallace, J.C., Francis, G.L. and Norton, R.S. (1995). Solution structure of human insulin-like growth factor-II: Relationship to receptor and binding protein interactions. *J Mol Biol* **248**(2): 385-401.

Upton FZ, Francis GL, Ross M, Wallace JC, Ballard FJ. (1992) Production and characterization of recombinant chicken insulin-like growth factor-I from Escherichia coli. *J Mol Endocrinol* **9**(1):83-92.

Upton, F. Z., Szabo, L., Wallace, J. C. and Ballard, F. J. (1990). Characterization and cloning of a bovine insulin-like growth factor-binding protein. *J. Mol. Endocrinol.* **5**(1): 77-84.

Upton, Z., Francis, G.L., Chan, S.J., Steiner, D.F., Wallace, J.C. and Ballard, F.J. (1997). Evolution of insulin-like growth factor (IGF) function: production and characterization of recombinant hagfish IGF. *Gen Comp Endocrinol* **105**(1): 79-90.

Vajdos, F. F., Ultsch, M., Schaffer, M. L., Deshayes, K. D., Liu, J., Skelton, N. J. and de Vos, A. M. (2001). Crystal structure of human insulin-like growth factor-1: detergent binding inhibits binding protein interactions. *Biochemistry* **40**(37): 11022-11029.

Varadaraj, K. and D.M. Skinner (1994). Denaturants or cosolvents improve the specificity of PCR amplification of a G + C-rich DNA using genetically engineered DNA polymerases. *Gene* **140**(1): 1-5.

Varghese, J. N., Garrett, T. P., Colman, P. M., Chen, L., Hoj, P. B. and Fincher, G. B. (1994). Three-dimensional structures of two plant beta-glucan endohydrolases with distinct substrate specificities. *Proc Natl Acad Sci U S A* **91**(7): 2785-2789.

Varki, A. (1993). Biological roles of oligosaccharides: all of the theories are correct. *Glycobiology* **3**(2): 97-130.

Vorwerk, P., Yamanaka, Y., Spagnoli, A., Oh, Y. and Rosenfeld, R.G. (1998). Insulin and IGF binding by IGFBP-3 fragments derived from proteolysis, baculovirus expression and normal human urine. *J Clin Endocrinol Metab* **83**(4): 1392-1395.

Wallace, J.C., Bagley, C.J., May, B.L., Ross, M., Francis, G.L. and Ballard, J. (1989). The use of IGF analogs to determine ligand specificity of different IGF binding proteins. *Proceedings of International IGF-Binding Protein Workshop.* S. L. S. Drop and R. L. Hintz. Vancouver, Elsevier: 225-229.

Wang, J.F., Hampton, B., Mehlman, T., Burgess, W.H. and Rechler, M.M. (1988). Isolation of a biologically active fragment from the carboxyl-terminus of the fetal rat binding protein for insulin-like growth factors. *Biochem Biophys Res Comm* **157**(2): 718-726.

Ward, C. W., Garrett, T. P., McKern, N. M., Lou, M., Cosgrove, L. J., Sparrow, L. G., Frenkel, M. J., Hoyne, P. A., Elleman, T. C., Adams, T. E., Lovrecz, G. O., Lawrence, L. J. and Tulloch, P. A. (2001). The three dimensional structure of the type I insulin-like growth factor receptor. *Mol Pathol* **54**(3): 125-132.

Weisenhorn, A. L., Drake, B., Prater, C. B., Gould, S. A., Hansma, P. K., Ohnesorge, F., Egger, M., Heyn, S. P. and Gaub, H. E. (1990). Immobilized proteins in buffer imaged at molecular resolution by atomic force microscopy. *Biophys J* **58**(5): 1251-1258.

Wells, J. A. (1996). Binding in the growth hormone receptor complex. *Proc Natl Acad Sci U S A* **93**(1): 1-6.

Wider, G and Wűthrich, K. (1999). NMR spectroscopy of large molecules and multimolecular assemblies in solution. *Current Opinion in Structural Biology* **9**:594-601

Wishart, D. S., Bigam, C. G., Yao, J., Abildgaard, F., Dyson, H. J., Oldfield, E., Markley, J. L. and Sykes, B. D. (1995). 1H, 13C and 15N chemical shift referencing in biomolecular NMR. *J Biomol NMR* **6**(2): 135-140.

Wishart, D. S., Sykes, B. D. and Richards, F. M. (1992). The chemical shift index: a fast and simple method for the assignment of protein secondary structure through NMR spectroscopy. *Biochemistry* **31**(6): 1647-1651.

Wong, M., Fong, C. & Yang, M. (1999). Biosensor measurement of the interaction kinetics between insulin-like growth factors and their binding proteins. *Biochim. Biophys. Acta* **1432**, 293-301.

Won, W. and Powell-Braxton, L. (1998). Insulin-like growth factor gene targetting. Molecular mechanisms to regulate the activities of insulin-like growth factors. K. Takano, N. Hizuka and S. I. Takahashi. Amsterdam, Elsevier: 57-63.

Wood, T.L., Rogler, L., Streck, R.D., Cerro, J., Green, B., Grewal, A., *et al.* (1993). Targeted disruption of IGFBP-2 gene. *Growth Regul.* **3**(1): 5-8.

Wűthrich, K. (1995). NMR- this other method for protein and nucleic acid structure determination. *Acta crystal D* **51**, 549-570

Yu, H. and Rohan, T. (2000). Role of the insulin-like growth factor family in cancer development and progression. *J Natl Cancer Inst* **92**(18): 1472-1489.

Zadeh, S.M. and Binoux, M. (1997). The 16 kDa proteolytic fragment of insulin-like growth factor (IGF) binding protein-3 inhibits the mitogenic action of fibroblast growth factor on mouse fibroblasts with targeted disruption of the type-I IGF receptor gene. *Endocrinology* **138**(7): 3069-3072.

Zapf, J., Kiefer, M., Merryweather, J., Musiarz, F., Bauer, D., Born, W., Fischer, J. A. and Froesch, E. R. (1990). Isolation from adult human serum of four insulin-like growth factor (IGF) binding proteins and molecular cloning of one of them that is increased by IGF I administration and in extrapancreatic tumour hypoglycaemia. *J Biol Chem* **265(25):** 14892-14898.

Zapf, J., Born, W., Chang, J.Y., James, P., Froesch, E.R. and Fischer, J.A. (1988). Isolation and NH_2-terminal amino acid sequences of rat serum carrier proteins for insulin-like growth factors. *Biochem Biophys Res Commun* **156**(3): 1187-1194.

Żestawski, W., Beisel, H. G., Kamionka, M., Kalus, W., Engh, R. A., Huber, R., Lang, K. and Holak, T. A. (2001). The interaction of insulin-like growth factor-I with the N-terminal domain of IGFBP-5. *EMBO J* **20**(14): 3638-3644.

APPENDIX 1

BIACORE KINETIC MODELS USED TO EVALUATE THE INTERACTION BETWEEN BOVINE IGFBP-2 AND IGF

Fitting the experimental association and dissociation curves simultaneously using the BIAevaluation Software 3.0 derived kinetic data for the interaction between IGFs and IGFBPs. Models were fitted both globally across the data sets (simultaneously across the entire concentration series) (Roden and Myszka, 1996) and for each of the individual concentrations. Models used were the 1:1 Langmuir binding model and the two-state reaction (conformational change) model and are described below adapted from the BIAevaluation (version 3.0) manual and from M. Lucic, PhD. Thesis, 2000. All binding curves were corrected for background and bulk refractive index contribution by subtraction of the reference flow cells. And as such the bulk refractive index contribution has not been included in the models.

LANGMUIR 1:1 BINDING MODEL

-Used to describe a simple 1:1 binding interaction between an analyte and a ligand (Karlsson *et al.,* 1991).

$A + B \leftrightarrow AB$
Where total response = AB

DEFINITIONS

A	analyte (protein in solution)
[A]	concentration of analyte (M)
AB	complex formed between analyte and ligand
[AB]	concentration of the analyte-ligand complex (RU)
B	ligand (protein coupled to the sensor chip)
[B]	ligand concentration (RU), determined by Rmax - R
C	concentration of analyte (M)
ka	rate of analyte association with the ligand ($M^{-1}s^{-1}$)
kd	rate of analyte dissociation from the ligand (s^{-1})
R	response due to analyte binding (RU)
R_0	response (RU) at completion of analyte injection
Rmax	maximum analyte binding capacity (RU)

RATE EQUATION

This model is described by the following rate equation:

The net rate of complex formation = Complex formation - Complex decay

$$dAB/dt = (ka \,.\, [A] \,.\, [B] - kd \,.\, [AB])$$

$$dR/dt = ka \,.\, C \,.\, (Rmax - R) - kd \,.\, R$$

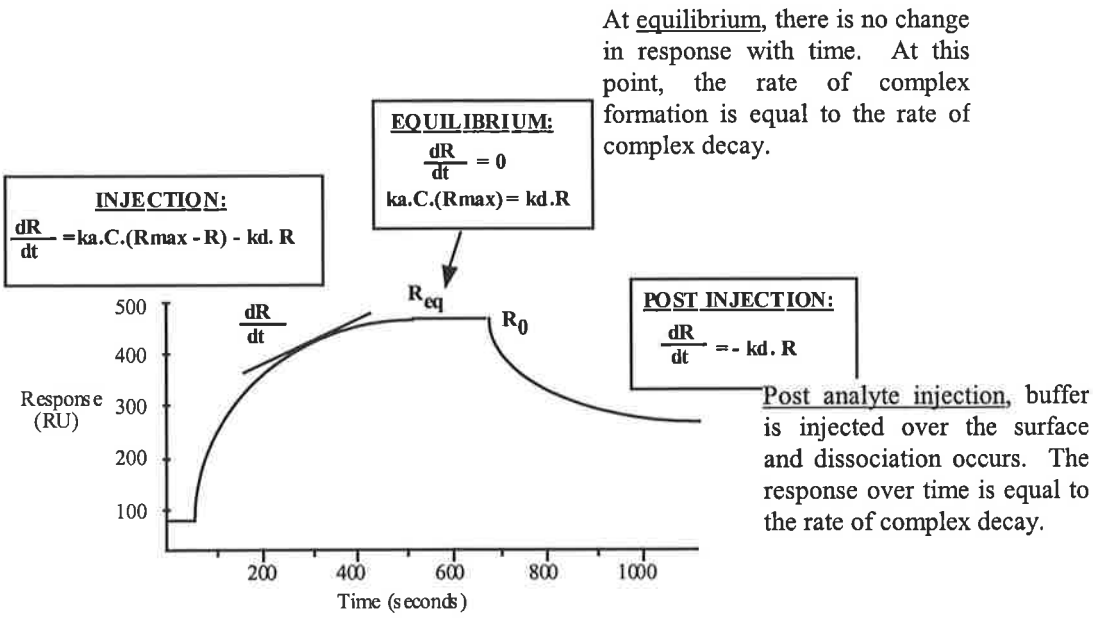

TWO-STATE REACTION (CONFORMATIONAL CHANGE)

-A 1:1 binding of an analyte to an immobilised ligand, followed by a conformational change in the complex (Karlsson and Falt, 1997). The complex AB undergoes a conformational change to AB*.

$A + B \leftrightarrow AB \leftrightarrow AB^*$

Where total response = AB + AB*

DEFINITIONS

A	analyte (protein in solution)
[A]	concentration of analyte (M)
B	ligand (protein coupled to the sensor chip)
[B]	ligand concentration (RU)
AB	complex formed between analyte and ligand
[AB]	concentration of the analyte-ligand complex (RU)
AB*	complex resulting from the conformational change of AB
[AB*]	concentration of the AB* complex (RU)
ka1	rate of analyte association with the ligand ($M^{-1}s^{-1}$)
ka2	rate of transition of AB to AB* (s^{-1})
kd1	rate of analyte dissociation from the ligand (s^{-1})
kd2	rate of transition of AB* to AB (s^{-1})

RATE EQUATIONS

This model is described by the following rate equations:

dAB/dt = (ka1.[A].[B] - kd1.[AB]) - (ka2.[AB] - kd2.[AB*])

dAB*/dt = (ka2.[AB] - kd2.[AB*])